FTIR spectroscopic study on the photocycle mechanism of Channelrhodopsins

D I S S E R T A T I O N
zur Erlangung des akademischen Grades

Doctor rerum naturalium
(Dr. rer. nat.)

eingereicht an der
Lebenswissenschaftlichen Fakultät der Humboldt-Universität zu Berlin

von
Diplom-Biologe Joel Christoph David Kaufmann

Präsidentin
der Humboldt-Universität zu Berlin

Prof. Dr.-ing. Dr. Sabine Kunst

Dekan der Lebenswissenschaftlichen Fakultät
der Humboldt-Universität zu Berlin

Prof. Dr. Bernhard Grimm

Gutachter/innen

1. Prof. Dr. Franz Bartl
2. Prof. Dr. Peter Hegemann
3. Prof. Dr. Peter Hildebrandt

Tag der mündlichen Prüfung: 05.12.2019

# Abstract

Channelrhodopsins (ChRs) are retinal binding membrane proteins found in single-cell algae. Photoisomerization of ChRs leads to formation of an ion channel. The resulting change in membrane voltage modulates flagellate motions allowing phototaxis and photophobic responses. Heterologously expressed in host cells, ChRs allow the evocation or suppression of changes in membrane potential with high spatio-temporal resolution – this method has become known as optogenetics.

Functional studies have raised questions concerning the molecular determinants for absorption, formation and closing of the ion channel and ion selectivity. It was the scope of this thesis to address these questions based on a comparison of the three different ChR variants C1C2, ReaChR (Red-activatable ChR) and Chrimson. C1C2 ($\lambda_{max} \approx 470$ nm) is a chimera of the *Chlamydomonas reinhardtii* ChRs *Cr*ChR1 and *Cr*ChR2. ReaChR ($\lambda_{max} \approx 520$ nm) is a variant of *Volvox carteri* ChR1 whose red-shifted absorption allows its use in deeper layers of organic tissue in optogenetic experiments. The even further red-shifted (*Cs*)Chrimson ($\lambda_{max} \approx 590$ nm) is a more distantly related ChR from *Chlamydomonas noctigama* with the N-terminal sequence from *Chloromonas subdivisa* ChR that is significantly more proton-selective. The photoreaction mechanism was investigated using FTIR (Fourier Transform Infrared) spectroscopy at room temperature and at cryostatic conditions. The results were complemented by UV-Vis spectroscopy and retinal extraction and subsequent HPLC (High Performance Liquid Chromatography) analysis.

As in most microbial rhodopsins, the retinal cofactor in ChRs is predominantly in 13-*trans*,15-*anti* conformation and bound to the protein by a retinal Schiff base (RSB) linkage to a lysine. Usually, the RSB is protonated in the dark ($RSBH^+$) stabilized by the counter-ion complex formed by a glutamate (counter-ion 1, Ci1) and an aspartate (counter-ion 2, Ci2). Photoreceptors are optimized to use photon energy to drive conformational changes of the protein backbone. Therefore, a fraction of the photon energy is stored by a transient distortion of the chromophore and separation of the charges in the active site by increased distance between the $RSBH^+$ and its counter-ions. In this thesis, it is shown that in ReaChR the transfer of the stored energy to the protein is largely affected by the Ci1 (Glu163) protonation state, being decelerated by protonated Ci1 due to an enhanced rigidity of the active site that stabilizes the distorted chromophore conformation. Instead, in Chrimson the chromophore

relaxes upon photoisomerization, hinting at an unusual distorted retinal geometry in the dark state, which is probably essential for its unprecedented bathochromic absorption.

In addition to single isomerization of 13-*trans*,15-*anti* retinal around the $C_{13}$=$C_{14}$ bond, double isomerization, which occurs around the $C_{13}$=$C_{14}$ and $C_{15}$=N bonds in parallel, can also take place and contributes to partial photocurrent inactivation, in particular during extended illumination. The resulting 13-*cis*,15-*syn* isomer is the non-conducting chromophore of a parallel photocycle that itself can be activated by isomerization around the $C_{13}$=$C_{14}$ bond. As observed in this thesis, the Ci1 protonation state in both ReaChR (Glu163) and Chrimson (Glu165) affects the efficiency of the competing photoreactions and enhancements of the double isomerization reaction by deprotonated Ci1 were observed in both receptors. Another factor that influences the stereoselectivity of the retinal binding pocket is $Asp^{DC}$ (Asp195 in C1C2), as its mutation to asparagine gives rise to isomers other then 13-*trans* retinal. $Asp^{DC}$ deprotonates in the photocycle of C1C2 and ReaChR while it is not conserved in Chrimson.

Formation of the ion-conducting state in C1C2 and ReaChR involves water influx into the ion channel which facilitates the transport of larger cations. As demonstrated in this thesis, the extent of water influx is reduced at acidic pH, indicating a narrower pore favoring $H^+$. Deprotonation of the central gate residue E3 (Glu129 in C1C2) leads to formation of a salt bridge in the middle of the pore that alters the ion selectivity of the channel as known from electrophysiological experiments. FTIR experiments indicate that the high proton selectivity of Chrimson that was revealed by electrophysiological characterization is due to a decisively reduced water influx into the channel during the photoreaction which favors conductance of protons over larger cations. One of the residues that determines the extent of water influx is the extracellular gate residue E4 (Glu139 in Chrimson) that together with Tyr159 forms an additional barrier against the influx of water molecules. Additionally, proton selectivity is presumably enhanced by deprotonation of Ci1 at acidic pH during formation of the conducting intermediate as deprotonated Ci1 stabilizes the $RSBH^+$, thereby creating a restriction site in the middle of the pore against the passage of larger cations.

# Zusammenfassung

Kanalrhodopsine (ChRs) sind Retinalproteine aus einzelligen Algen, deren lichtinduzierte Isomerisierungsreaktion die Bildung eines Ionenkanals zur Folge hat. Die daraus resultierenden Änderungen des Membranpotentials modulieren flagellare Bewegungsmuster und ermöglichen damit phototaktische bzw. photophobische Reaktionen. In der Optogenetik werden ChRs heterolog exprimiert, um mit hoher zeitlicher und räumlicher Auflösung das Membranpotential durch Licht zu modulieren.

Funktionsanalysen haben Fragen hinsichtlich der molekularen Grundlagen von Absorption, Bildung und Schließung des Ionenkanals sowie der Ionenselektivität aufgeworfen. In dieser Arbeit werden diese Fragen auf Grundlage dreier ChRs adressiert: C1C2, ReaChR (Red-activatable ChR, rot-aktivierbares ChR) und Chrimson. C1C2 ($\lambda_{max} \approx 470$ nm) ist eine Chimäre der *Chlamydomonas reinhardtii*-ChRs *Cr*ChR1 and *Cr*ChR2. ReaChR ($\lambda_{max} \approx 520$ nm) ist eine Variante von *Volvox carteri* ChR1, dessen Rotverschiebung eine optogenetische Verwendung in tieferen Gewebsschichten ermöglicht. Das noch weiter rotverschobene (*Cs*)Chrimson ($\lambda_{max} \approx 590$ nm) ist ein entfernter verwandtes ChR von *Chlamydomonas noctigama* mit der N-terminalen Sequenz von *Chloromonas subdivisa* ChR, welches eine höhere Protonenselektivität aufweist.

Der Mechanismus der Lichtreaktion wurde mittels FTIR (Fourier-Transform-Infrarot)-Spektroskopie unter Raumtemperatur- bzw. Kryobedingungen untersucht. Die Beobachtungen wurden durch UV-Vis-Spektroskopie sowie Retinalextraktionsexperimente mit anschließender HPLC-Messung (High Performance Liquid Chromatography, Hochleistungsflüssigchromatographie) ergänzt.

Wie in den meisten mikrobiellen Rhodopsinen liegt der Retinal-Kofaktor in ChRs hauptsächlich in 13-*trans*,15-*anti*-Konformation vor und ist über eine Retinal-Schiffbase (RSB) zu einer Lysinseitenkette an das Protein gebunden. Gewöhnlich ist die RSB im Dunkelzustand protoniert ($RSBH^+$) und wird durch den Gegenionkomplex stabilisiert, welcher von einem Glutamat (counter-ion 1 (Gegenion 1), Ci1) und einem Aspartat (counter-ion 2 (Gegenion 2), Ci2) gebildet wird. Lichtrezeptoren sind optimiert, um Lichtenergie zum Antreiben von Strukturänderungen zu nutzen. Zu diesem Zweck wird ein Teil der Lichtenergie durch eine Verdrillung des Chromophors sowie eine Ladungstrennung des $RSBH^+$-Gegenionkomplexes vorübergehend gespeichert. In der vorliegenden Arbeit wird gezeigt, dass in ReaChR der

Transfer der gespeicherten Energie zum Protein stark von dem Protonierungszustand von Ci1 (Glu163) abhängt, wobei protoniertes Ci1 den Transferprozess verlangsamt, indem es zu einer höheren Rigidität des $RSBH^+$-Gegenionkomplexes führt, welche die verdrillte Konformation des Chromophors stabilisiert. Bei Chrimson hingegen relaxiert der Chromophor nach Lichtaktivierung, was darauf hinweist, dass im Dunkelzustand eine verdrillte Geometrie des Kofaktors vorliegt. Vermutlich stellt dies einen wichtigen Faktor für die ungewöhnliche Rotverschiebung von Chrimson dar.

Parallel zu der Isomerisierungsreaktion von 13-*trans*,15-*anti*-Retinal um die $C_{13}$=$C_{14}$-Bindung findet eine simultane Isomerisierung um die $C_{13}$=$C_{14}$- und $C_{15}$=N-Bindung statt, die insbesondere bei längeren Belichtungszeiten zur partiellen Inaktivierung des Photostroms beiträgt. Das aus der Doppelisomerisierung resultierende 13-*cis*,15-*syn*-Isomer stellt den Dunkelzustand eines parallelen Photozyklus dar, der seinerseits durch Isomerisierung um die $C_{13}$=$C_{14}$-Bindung aktiviert werden kann. Hier wird gezeigt, dass der Protonierungszustand von Ci1 in ReaChR (Glu163) und Chrimson (Glu165) einen starken Einfluss auf die Effizienz der konkurrierenden Isomerisierungsreaktionen ausübt und deprotoniertes Ci1 die Effizienz der Doppelisomerisierung erhöht. Ein weiterer Faktor der Stereoselektivität der Retinalbindungstasche ist $Asp^{DC}$ (Asp195 in C1C2), was sich darin zeigt, dass die Mutation zu Asparagin den Anteil anderer Isomere zulasten von 13-*trans*-Retinal erhöht. $Asp^{DC}$ deprotoniert im Photozyklus von C1C2 und ReaChR, ist in Chrimson allerdings nicht konserviert.

In C1C2 und ReaChR beinhaltet die Bildung des ionenleitenden Intermediats den Einstrom von Wasser in den Ionenkanal, was den Transport größerer Ionen erleichtert. Wie hier gezeigt wird, ist bei saurem pH-Wert das Ausmaß des Wassereinstroms reduziert, was auf eine engere Pore hinweist. Die engere Porengeometrie begünstigt den Transport von Protonen. Die Deprotonierung von E3 (Glu129 in C1C2), einem Aminosäurerest im sogenannten Zentralen Tor, ermöglicht die Ausbildung einer Salzbrücke in der Mitte des ionenleitenden Kanals, welche gemäß elektrophysiologischer Messungen die Ionenselektivität moduliert. Die FTIR-Experimente ergeben, dass die hohe Protonenselektivität von Chrimson, welche durch elektrophysiologische Experimente gezeigt wurde, auf einen deutlich reduzierten Wassereinstrom während der Photoreaktion zurückzuführen ist, was den Transport von Protonen gegenüber größeren Kationen begünstigt. Eine der Aminosäuren, die das Ausmaß des Wassereinflusses reduziert, ist E4 (Glu139 in Chrimson), ein Aminosäurerest im

sogenannten Extrazellulären Tor; E4 bildet zusammen mit Tyr159 eine zusätzliche Barriere gegen den Wassereinstrom. Zusätzlich wird die höhere Protonenselektivität vermutlich dadurch verstärkt, dass bei niedrigem pH-Wert Ci1 während der Bildung des ionenleitenden Intermediats deprotoniert und in der deprotonierten Form die $RSBH^+$ stabilisiert; diese Wechselwirkung in der Mitte der Kanalpore bildet eine Barriere gegen den Transport größerer Kationen.

# List of publications

Published parts of this work:

Krause, B. S.; Grimm, C.; Kaufmann, J. C. D.; Schneider, F.; Sakmar, T. P.; Bartl, F. J.; Hegemann, P. Complex Photochemistry within the Green-Absorbing Channelrhodopsin ReaChR. *Biophys. J.* 2017, *112*, 1166–1175.

Kaufmann, J. C. D.; Krause, B. S.; Grimm, C.; Ritter, E.; Hegemann, P.; Bartl, F. J. Proton Transfer Reactions in the Red Light-Activatable Channelrhodopsin Variant ReaChR and Their Relevance for Its Function. *J. Biol. Chem.* 2017, *292* (34), 14205–14216

Krause, B. S.; Kaufmann, J. C. D.; Kuhne, J.; Vierock, J.; Huber, T.; Sakmar, T. P.; Gerwert, K.; Bartl, F. J.; Hegemann, P. Complex Tracking pore hydration in channelrhodopsin by site-directed infrared-active azido probes. *Biochemistry* 2019, 58 (9), 1275–1286

Manuscripts and other publications:

Kaufmann, J. C. D.; Krause, B. S.; Ritter, E.; Hegemann, P.; Bartl, F. J. Energy transfer from chromophore to protein is modulated by the protonation state of a glutamic acid in the active site of channelrhodopsin. Manuscript in preparation for resubmission.

Kaufmann, J. C. D.; Vierock, J.; Fischer, P.; Krause, B. S.; Hontani, Y.; Nguyen, T.B.T.; Kennis, J.; Hegemann, P.; Bartl, F. J. A unique gating mechanism is responsible for the high proton selectivity of the red-absorbing channelrhodopsin Chrimson. Manuscript in preparation.

Vierock, J., Kaufmann, J. C. D.; Krause, B. S.; Fischer, P.; Hontani, Y.; Nguyen, T.B.T.; Kennis, J.; Bartl, F. J.; Hegemann, P. Light adaptation in the red shifted channelrhodopsin Chrimson involves unprecedented bistability of two dark states. Manuscript in preparation.

Oppermann, J.; Fischer, P.; Silapetere, A.; Liepe, B.; Rodriguez-Rozada, S.; Flores-Uribe, J., Peter, E.; Keidel, A.; Vierock, J.; Kaufmann, J.; Broser, M.; Luck, M.; Bartl, F.; Hildebrandt, P.; Wiegert, J. S.; Béjà, O.; Hegemann, P.; Wietek, J. MerMAIDs: A novel family of metagenomically discovered, marine, anion-conducting and intensely desensitizing channelrhodopsins. *Nat. Commun.* 2019, 10, 3315–3327.

# Table of abbreviations

| | |
|---|---|
| 15-*anti* cycle | photocycle branch with the dark state in 13-*trans*, 15-*anti* conformation |
| 15-*syn* cycle | photocycle branch with the dark state in 13-*cis*, 15-*syn* conformation |
| ACR | anion-conducting channelrhodopsin |
| $Asp^{DC}$ | aspartate of the DC pair (Asp156 in *Cr*ChR2) |
| azF | *p*-azido-L-phenylalanine |
| BR | bacteriorhodopsin |
| C1C2 | chimera of *Cr*ChR1 and *Cr*ChR2 (introduced as C1C2) |
| *Ca*ChR1 | *Chlamydomonas augustae* channelrhodopsin-1 |
| ChR | channelrhodopsin |
| Ci1 | counter ion 1 to the $RSBH^+$ (Glu123 in *Cr*ChR2) |
| Ci2 | counter ion 2 to the $RSBH^+$ (Asp253 in *Cr*ChR2) |
| *Cr*ChR1 | *Chlamydomonas reinhardtii* ChR1 |
| *Cr*ChR2 | *Chlamydomonas reinhardtii* ChR2 |
| cryo-EM | cryo electron microscopy |
| *Cs*Chrimson | *Chlamydomonas noctigama* ChR with the N-terminal fragment from *Chloromonas subdivisa* ChR (referred to as 'Chrimson' in this thesis) |
| $Cys^{DC}$ | cysteine of the DC pair (Cys128 in *Cr*ChR2) |
| DDM | n-dodecyl *β*-D-maltoside |
| *Ds*ChR1 | *Dunaliella salina* ChR |
| E3 | glutamate of the central gate (Glu90 in *Cr*ChR2) |
| E4 | one of the glutamates of the extracellular gate (Glu82 in *Cr*ChR2) |

| | |
|---|---|
| EC | extracellular cavity |
| EPR | electron paramagnetic resonance |
| GPCR | G-protein coupled receptor |
| *Gt*ACR1 | *Guillardia theta* anion-conducting ChR1 |
| *Gt*ACR2 | *Guillardia theta* anion-conducting ChR2 |
| *Gt*CCR4 | *Guillardia theta* cation-conducting ChR4 |
| HEPES | 2-[4-(2-hydroxyethyl)piperazin-1-yl]ethanesulfonic acid |
| HOOP | hydrogen-out-of-plane |
| HPLC | High performance liquid chromatography |
| IC | intracellular cavity |
| $LN_2$ | liquid $N_2$ |
| $Lys^{CI}$ | lysine of the counter-ion complex (Lys93 in *Cr*ChR2) |
| MD | molecular dynamics |
| *Mv*ChR1 | *Mesostigma viride* ChR1 |
| n.d. | not detected |
| NMR | nuclear magnetic resonance |
| $Phe^{CI}$ | phenylalanine of the counter-ion complex (Phe135 in Chrimson) |
| PR | Proteorhodopsin |
| *Ps*ChR2 | *Platymonas subcordiformis* ChR2 |
| QM/MM | quantum mechanics/ molecular mechanics |
| ReaChR | Red-activatable ChR |
| RSB | retinal Schiff base |
| $RSBH^+$ | protonated retinal Schiff base |
| SNR | signal-to-noise ratio |
| SVD | singular value decomposition |

| | |
|---|---|
| TM | transmembrane helix |
| *Vc*ChR1 | *Volvox carteri* ChR1 |
| *Vc*ChR2 | *Volvox carteri* ChR2 |
| wt | wild type |
| XR | Xanthorhodopsin |

# Table of figures

# List of tables

# Table of contents

# 1 Introduction

## 1.1 Rhodopsins

Rhodopsins are photosensitive membrane proteins with seven transmembrane helices, whose light-sensing unit is a covalently bound retinal. Altering protein activity by light-induced isomerization of the retinal is a common principle of all rhodopsins. Rhodopsins found in multicellular animals are termed type 2 or metazoan rhodopsins, whereas rhodopsins from single-celled organisms are referred to as type 1 or microbial rhodopsins.[1] Type 1 and 2 rhodopsins differ significantly according to their mechanisms: Metazoan rhodopsins serve as photoreceptors in specialized photosensitive cells, such as rod cells in vertebrate eyes[2] or the rhabdomeric cells of compound eyes in non-vertebrates[3]. Microbial rhodopsins are described to serve as phototaxis receptors (sensory rhodopsin[4]), proton pumps (BR, bacteriorhodopsin[5]) or chloride ion pumps (halorhodopsin[6]). Channelrhodopsins (ChRs), the subject of this thesis, represent an additional class of microbial rhodopsins, *i.e.* light-gated ion channels.[7,8]

In general, rhodopsins serve the conversion of an optic into an electrochemical or biochemical signal. The latter is the case for metazoan rhodopsins: As a common principle of all G-protein-coupled receptors (GPCR), protein activation leads to conformational changes allowing for binding and subsequent activation of G-proteins (Fig. 1-1). Thereby, G-protein-mediated signaling cascades are initiated that eventually lead to cellular alterations, *e.*g. changes in the membrane potential and/or gene expression. Discovered more than 130 years ago[9–11], vertebrate rhodopsin has become a model protein for the GPCR protein family. This group is of great relevance in the treatment of a large number of diseases.[12] In microbial

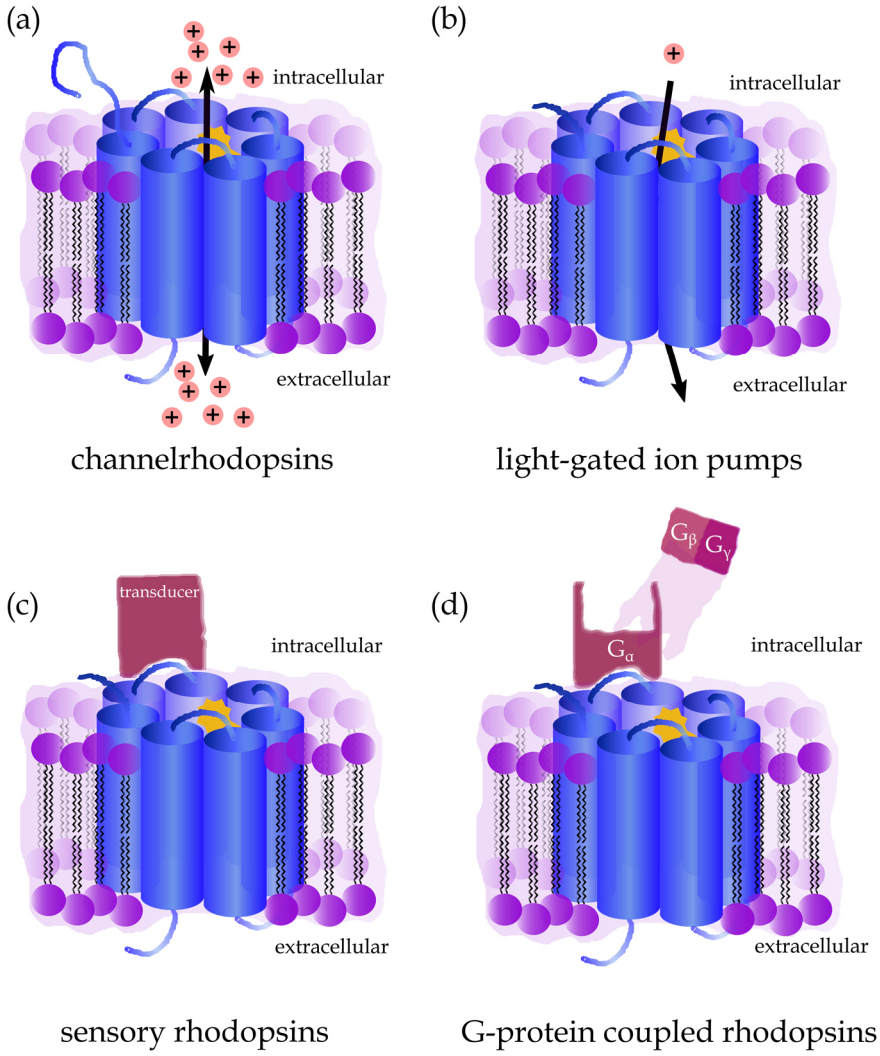


**Fig. 1-1** The working principles of microbial **(a)–(c)** and metazoan rhodopsins **(d)**. In sensory rhodopsins and G-protein coupled receptors, the light-induced conformational changes activate secondary messengers, while in light-gated channels and pumps, the light-induced conformational changes directly cause an ion current. In light-gated ion channels, direction of the photocurrent is mainly controlled by the electrochemical gradient, while it is unidirectional in light-gated ion pumps. Channels and pumps exist for both cations and anions.

rhodopsins, the photon signal is either converted to an electrochemical signal, as it is the case for light-triggered ion pumps and ion channels, or to a biochemical signal. In the latter case, light-activated proteins (sensory rhodopsins) interact with second messenger molecules that mediate intracellular signaling. The electrochemical output that is generated by light-triggered ion pumps and channels can serve spatio-temporal orientation as well as energy production as in the model protein bacteriorhodopsin (BR) whose discovery more than 40 years ago[13,14] represented the starting point for the exploration of the family of microbial rhodopsins.

## 1.2 Channelrhodopsins

Channelrhodopsins, found in the eye spot of single-cell algae, are membrane channels directly gated by light. The first ChRs characterized were channelrhodopsin-1[7] (*Cr*ChR1) and channelrhodopsin-2 from the *Chlamydomonas reinhardtii*[8] (*Cr*ChR2). Light-activation can alter the membrane potential of cells heterologously expressing ChRs. This is the key mechanism of optogenetics. In the following chapters, a detailed overview on the characteristics of ChRs with respect to structure, function and applications will be given.

### 1.2.1 Biological background

After *Cr*ChR1 and *Cr*ChR2 were identified as the photoreceptors in *Chlamydomonas reinhardtii*[7,8], a number of ChR variants was found in other algae within the *Chlamydomonas* genus[15] and other genera, such as *Volvox carteri*[16], *Mesostigma viride*[17] and *Platymonas subcordiformis*[18] (*Ps*ChR2). Long before the actual photoreceptors were discovered, the phototaxis of green algae had been subject to investigation.[19–21] Photosynthetic organisms have evolved systems to regulate their exposure to sunlight by phototactic or photophobic responses. For this purpose, the aquatic flagellated alga *Chlamydomonas reinhardtii* has developed a specialized organelle called the eyespot (Fig. 1-2) that consists of multiple layers of pigmented granules that are overlaid by the plasma membrane[22] and serve as antennae[23]. The overlaying membrane accumulates ChRs for light sensing. Light-triggered channel opening leads to a depolarization over the membrane of the eyespot. If light intensity is insufficient for depolarization, the current can be enforced by secondary voltage-gated channels.[22] The *Chlamydomonas reinhardtii* ChRs (*Cr*ChRs) conduct various cations ($H^+$ >> $Li^+$ > $Na^+$ > $K^+$ > $Ca^{2+}$ > $Mg^{2+}$).[8,24,25] The photocurrent, *i.e.* the current that is caused by light-induced channel opening, is comprised of multiple open states and typically decays within $10^0$–$10^2$ ms at continuous illumination. The light-induced depolarization over the eyespot region evokes an inward current in the flagellae region that modulates flagellate motion.[25–27] 10.000–120.000 ChRs are found in the eyespot of *Chlamydomonas reinhardtii*[25,28,29] with each channel transporting 10–100 charges per photocycle[30].

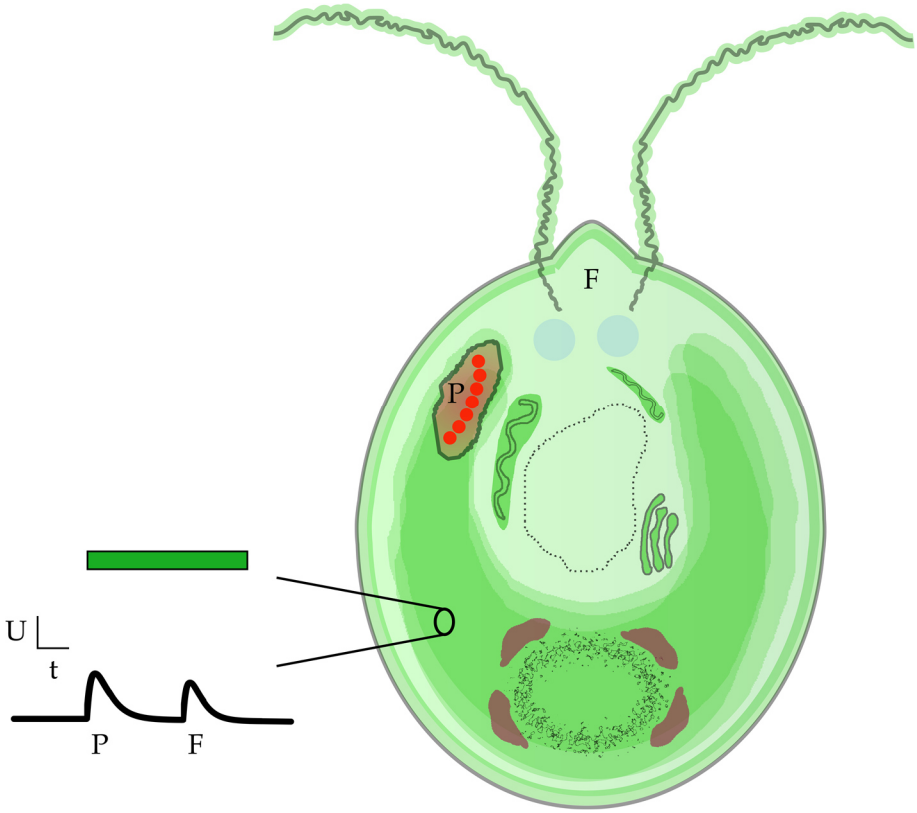


**Fig. 1-2** Scheme of *Chlamydomonas reinhardtii*. ChRs are tightly packed in the membrane of the eyespot. Light-triggered channel activation induces an inward ion current (*P*) that initiates opening of ion channels in the flagellate region (*F*). $Ca^{2+}$ influx modulates flagellate motion.

### 1.2.2 The family of channelrhodopsins

The first described ChRs are *Cr*ChR1 and *Cr*ChR2 from *Chlamydomonas reinhardtii*[7,8] whose discovery paved the way for the identification of numerous ChRs from other organisms (Fig. 1-3). In the eyespot, more *Cr*ChR1 proteins are found than *Cr*ChR2.[25,31] *Cr*ChR1 is red-shifted ($\lambda_{max}$ = 487 nm[7]) as compared to *Cr*ChR2 ($\lambda_{max}$ = 460 nm[8]). The absorption spectrum of *Cr*ChR1 is pH dependent in contrast to *Cr*ChR2. The light-induced photocurrents are smaller in *Cr*ChR1 and exhibit significantly less inactivation at continuous illumination.[24] A similar correlation of absorption maximum and photocurrent properties was described for other ChRs as well: *Volvox carteri* ChR1 *Vc*ChR1 ($\lambda_{max}$ = 536 nm[32,33]), *Chlamydomonas augustae* *Ca*ChR1 ($\lambda_{max}$ = 536 nm[34] and *Ds*ChR1 ($\lambda_{max}$ = 490 nm[16]) exhibit a red-shifted absorption as compared to *Cr*ChR2 along with reduced photocurrents and photocurrent inactivation. Inversely, *Platymonas subcordiformis* ChR2 *Ps*ChR2 ($\lambda_{max}$ = 444 nm) is *Cr*ChR2-like with blue-shifted absorption and large photocurrents.[18] Furthermore, it was proposed that green- but not blue-absorbing ChRs exhibit an

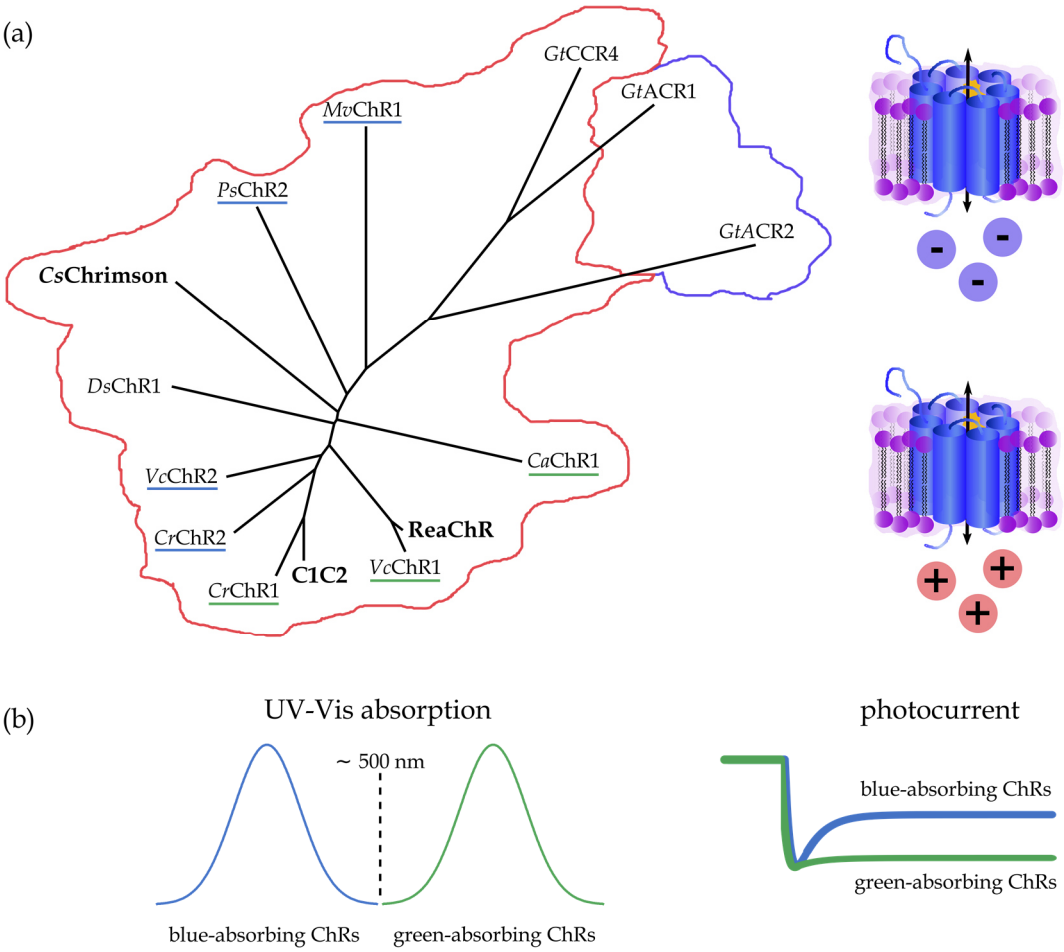


**Fig. 1-3** The ChR family. **(a)** Phylogenetic tree of selected ChRs calculated by Clustal Omega and the Simple Phylogeny tool provided by EMBL-EBI[227] and visualized with the Phylodendron server (version 0.8d). The family can be subdivided into cation-conducting (*red area*) and anion-conducting (*blue area*) ChRs. C1C2, *Cr*ChR1/2 chimera (pdb: 3ug9); *Ca*ChR1, *Chlamydomonas augustae* ChR1 (protein-ID: AER58220.1); *Cr*ChR1, *Chlamydomonas reinhardtii* ChR1 (protein-ID: AAL08946.1); *Cr*ChR2 (protein-ID: EDP06700.1); *Cs*Chrimson, construct of *Chlamydomonas noctigama* ChR with the N-terminal fragment from *Chloromonas subdivisa* (protein-ID: AIE89247.2); *Ds*ChR1, *Dunaliella salina* ChR1 (protein-ID: AGF84748.1); *Gt*ACR1, ACR1 (*Guillardia theta* Anion-Conducting Rhodopsin, protein-ID: AKN63094.1); *Gt*ACR2 (protein-ID: AKN63095.1); *Gt*CCR4 (*Guillardia theta* Cation-Conducting Rhodopsin, protein-ID: ARQ20888.1); *Mv*ChR1, *Mesostigma viride* ChR1 (protein-ID: AEI83869.1); *Ps*ChR2, *Platymonas subcordiformis* ChR2 (protein-ID: AGF84747.1); ReaChR, Red-Activatable ChR (protein-ID: AGT48260.1); *Vc*ChR1, *Volvox carteri* ChR1 (protein-ID: ABZ90901.1); *Vc*ChR2 (protein-ID: ABZ90903.1). ChRs investigated in this thesis are highlighted (*bold*). **(b)** The category of blue- and green-absorbing ChRs. It was proposed by Sineshchekov *et al.* 2013[35] that many ChRs can be assigned to either of these subgroups. The blue-absorbing *Cr*ChR2-like ChRs typically exhibit more significant photocurrent inactivation as compared to the green-absorbing *Cr*ChR1-like ChRs.[18,24,35]

outward-directed proton pumping activity, presumably conserved from a common ancestor with proton pumps.[35] This assumption is challenged by the observed proton pumping activity of *Cr*ChR2.[36,37] Although some evidence is provided to support the concept of two functionally different ChR groups, this categorization must be treated with caution and might only apply to a subgroup with large sequence homology. Stronger structural deviations yield different

functionalities: ChR1 from *Mesostigma viride* (*Mv*ChR1, $\lambda_{max}$ = 531 nm), in which the counter-ion complex to the $RSBH^+$ is significantly altered as compared to the above-mentioned ChRs, combines a red-shifted absorption with high photocurrents.[17] Drastic alterations in the binding pocket are found in Chrimson, which is the most red-shifted ChR described so far ($\lambda_{max}$ = 583 nm[38]) and still procudes strong photocurrents[39]. Further deviations in the active site of *Guillardia theta* ACRs shift the selectivity from cations to anions.[40]

In this thesis, three ChR variants were investigated: (1) the C1C2 chimera, (2) the red-activatable *Vc*ChR1 variant ReaChR and (3) the orange-absorbing Chrimson. The C1C2 chimera ($\lambda_{max} \approx$ 470 nm[24,41]) comprises the first five helices from *Cr*ChR1 and the last two helices from *Cr*ChR2.[41] While the pH dependence of its dark state absorption is more similar to *Cr*ChR1[24], the comparably strong photocurrent inactivation rather resembles *Cr*ChR2[41]. In the last years, the C1C2 chimera was in the spotlight of biophysical research on ChRs as it is the first ChR whose crystal structure was solved (by Kato *et al.* 2012[41]). So far, two FTIR- and one UV-Vis spectroscopic analysis of the C1C2 photocycle were published[42–44], along with several MD and QM/MM simulations based on C1C2 as template[45–48]. ReaChR (Red-activatable ChR) is an engineered variant of *Vc*ChR1 introduced by Lin *et al.* 2013[49], with the N-terminal region replaced by the respective *Cr*ChR1 sequence for better membrane trafficking[50] and TM6 exchanged for the respective sequence of *Vc*ChR2. The dark state absorption of ReaChR is pH dependent, reaching from 503 (pH 9) to 535 nm (pH 5).[51] Additionally, ReaChR can be efficiently activated by orange- and red-light to induce robust photocurrents.[49] Three mechanistic studies of the ReaChR photocycle were published with participation of the author.[51–53] (*Cs*)Chrimson is a construct of the natural red-shifted ChR ($\lambda_{max} \approx$ 590 nm[39,54]) discovered in *Chlamydomonas noctigama* by Klapoetke *et al.* 2014[38] and the N-terminal fragment from *Chloromonas subdivisa* ChR[39]. The promising combination of a bathochromically shifted absorption and large photocurrents makes Chrimson an interesting target for mechanistic characterization. To date, two publications issued the electrophysiological[39] and UV-Vis spectroscopic evaluation[54] of the Chrimson photocycle ('*Cs*' is omitted in the following).

### 1.2.3 Optogenetic application

The discovery and characterization of light-activated ion channels immediately promoted the idea of using them for manipulating electrochemical gradients across biological membranes.[7] It was demonstrated soon after that action potentials can either be directly evoked[55] or that the depolarization threshold can be reduced[56] by light-activation of ChRs embedded in neural membranes, giving birth to the new field of optogenetics[57]. ChRs have already been successfully applied as optogenetic tools in different organisms such as mice[58], *Drosophila melanogaster*[59] and *Caenorhabditis elegans*[60], and in different tissues such as retina[58,61], hippocampal neurons[56,62] and cardiac cells[63].

The choice of a suitable ChR variant depends on the actual requirements of the cellular system that is intended to be investigated. To achieve sufficient membrane depolarization, the ChR variant must be properly expressed. For that reason, modified variants are often used that provide better membrane trafficking (*e.g.* *Cr*ChR2-H134R). Depending on the intended activation and inactivation patterns, faster (*e.g.* *Cr*ChR2-E123T) or slower (*Cr*ChR2-C128T) variants can be selected.[22,64] It can also be advantageous to apply variants with altered ion selectivity such as the $Ca^{2+}$-selective Catch$^{+}$ variant that triggers the depletion of intracellular $Ca^{2+}$ stores.[33,65] Importantly, several anion-conducting ChR variants have been constructed or discovered, allowing the inhibition of action potentials.[40,66–68]

If a ChR variant is expressed in larger organisms, tissue scattering and absorption restrict the distance between light source and target cells that still allows protein activation. As the penetration depth of light is positively correlated with the wavelength, a higher maximum absorption of the variant is desirable.[69,70] The red-activatable channelrhodopsin variant (ReaChR) was designed for that purpose[49] and has already been applied in neurologic, cardiologic, and behavioral studies[59,61,63,71]. Chrimson is even more red-shifted so that it allows the independent activation of different target cells in combination with a blue-absorbing ChR.[38]

### 1.2.4 Structure

The first crystal structure of a ChR dark state was published in 2012.[41] C1C2 is a chimeric protein consisting primarily of *Cr*ChR1 with (i) helices 6 and 7 swapped to those of *Cr*ChR2 and (ii) a truncated C-terminal sequence. In 2017, the crystal structure of the *Cr*ChR2 dark state was released[72], followed recently by publication of the Chrimson dark state structure[73]. Additionally, structures of mutants of the C1C2 binding pocket[74] and the anion-conducting *Gt*ACR1[75] were published.

In the following, the main features of the crystal structures of *Cr*ChR2, C1C2 and Chrimson are discussed. Presumed structural alterations in the *Vc*ChR1 variant ReaChR that was investigated in this thesis along with C1C2 and Chrimson were derived from a sequence alignment with other ChRs (see Fig. S1) and highlighted in the respective sections.

In order to use a meaningful and economic nomenclature, key residues in this thesis are named according to their preserved position and/ or function. According to Schneider *et al.* 2015[22], the residues of the counter-ion complex to the protonated retinal Schiff base ($RSBH^+$) are termed Ci1 (Glu123 in *Cr*ChR2, add 39 to obtain the corresponding residue in C1C2, add 40 for ReaChR and 43 for Chrimson) and Ci2 (Asp253 in *Cr*ChR2) and the glutamates aligning the ion conduction pathway are termed E1–E5 (E1: Glu82, E2: Glu83, E3: Glu90, E4: Glu97, E5: Glu101 in *Cr*ChR2). The residues of the so-called DC pair, a functional module in the retinal binding pocket, are termed $Asp^{DC}$ and $Cys^{DC}$ in this thesis ($Asp^{DC}$: Asp156, $Cys^{DC}$: Cys128 in *Cr*ChR2). Note that $Asp^{DC}$ is not conserved in Chrimson (see Fig. S1). The lysine that forms the covalent bond to the $RSBH^+$ is termed $Lys^{RSB}$ (Lys257 in *Cr*ChR2) and the lysine found in the extended counter-ion complex is termed $Lys^{CI}$ (Lys93 in *Cr*ChR2). In Chrimson, a phenylalanine is found in this position instead ($Phe^{CI}$, Phe135).

### 1.2.4.1 General structure

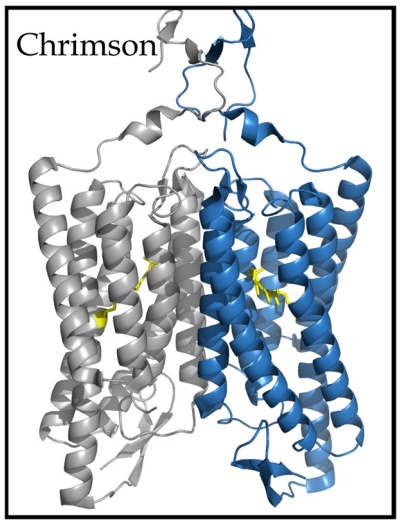


**Fig. 1-4** Dimeric structure of Chrimson (5ZIH). Structure was visualized with PyMol (Version 2.1.1.).

The general structure of ChRs is similar to other rhodopsins, comprising an extracellular N-terminus, seven transmembrane helices (TM) and an intracellular C-terminus (Fig. 1-4). The structures of *Cr*ChR2, C1C2 and Chrimson are all organized as dimers.[41,72,73] The monomers are connected by cystine bridges and hydrogen bonds. In the case of *Cr*ChR2, cystine bridges exist in the N-terminal region, while hydrogen bonds are formed in transmembrane helices 3, 4 and 5 (TM3, TM4, TM5). EPR spectroscopic measurements indicated that the dimers are tightly connected.[76,77] An oligomeric structure is not unusual for microbial rhodopsins, *e.g.* BR is organized as a trimer.[78] Notably, little is known about the interaction mechanism of the protomers. For *Cr*ChR2, small structural deviations between the protomers were reported, involving the distribution of water molecules.[72] Although the structures of *Cr*ChR2, C1C2 and Chrimson are essentially similar, TM2 and TM7 deviate by 2 and 2.5 Å on the extracellular and intracellular side, respectively, between Chrimson and the *Cr*ChRs.[73]

### 1.2.4.2 Active site

Fig. 1-5 shows the retinal binding pockets and active sites of *Cr*ChR2, C1C2 and Chrimson.[41,72,73] The retinal is bound to $Lys^{RSB}$ (lysine of the retinal Schiff base, Lys257 in *Cr*ChR2) by a Schiff base linkage.[41] Although not resolved in the ChR crystal structures, UV-Vis spectra of *Cr*ChR2, C1C2 and Chrimson suggest that the RSB is protonated in the dark state ($RSBH^+$) and that its N–$H^+$ bond points to the extracellular side, similar to BR.[78] The positive $RSBH^+$ charge is stabilized by the adjacent carboxylic amino acids Ci1 (counter-ion 1, Glu123 in *Cr*ChR2) and Ci2 (counter-ion 2, Asp253 in *Cr*ChR2) that together with a crystallized water molecule form the counter-ion complex (two waters were found in the Chrimson crystal structure[73]). Such $RSBH^+$-counter-ion complexes are typical features of rhodopsins

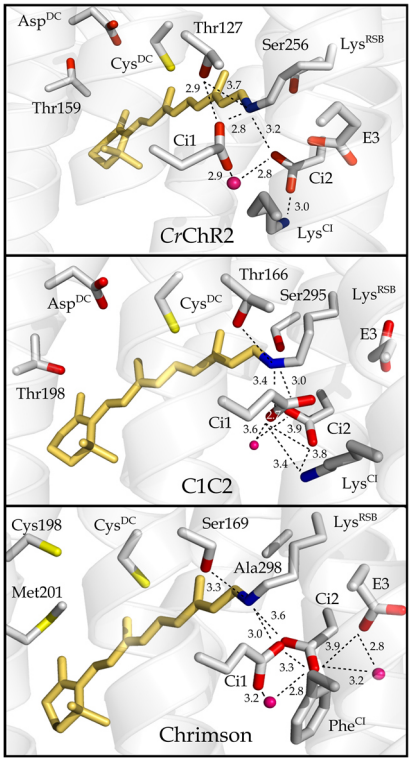


**Fig. 1-5** The binding pocket and active sites of *Cr*ChR2 (6EID, *above*), C1C2 (3UG9, *center*) and Chrimson (5ZIH, *below*). Distances are given in Å. Structures were visualized with PyMol (Version 2.1.1.).

in general. Light-induced alteration of the active site structure is most likely the key mechanism for channel opening. This is presumably achieved by an extended hydrogen bond network that involves amino acid residues and water molecules and connects the active site with the extracellular region.[72] A similar network is present in BR.[78] Probably, light-induced structural alterations of this network pave the way for the later pore formation in ChRs. The electrostatic stabilization of the positive charge residing at the $RSBH^+$ that is an important factor for the chromophore absorption spectrum, as described in detail in 1.2.5.2 (p. 20), is modulated by neighboring residues in the counter-ion complex. An important role was assigned to $Lys^{CI}$ (lysine of the counter-ion complex, Lys93 in *Cr*ChR2)[34] that stabilizes the anionic form of Ci1 in blue-absorbing ChRs such as *Cr*ChR2 and C1C2[34,79]. The *Cr*ChR2 structure reveals that $Lys^{CI}$ forms a hydrogen bond to Ci2 but not to Ci1, while in the C1C2 structure, $Lys^{CI}$ interacts with both counter-ions. Besides $Lys^{CI}$, two other residues are likely to affect the $pK_a$ of the counter-ions: The central gate residue E3 and the binding pocket residue Thr127 (in *Cr*ChR2). The latter forms a hydrogen bond to Ci1 as observed in the *Cr*ChR2 crystal structure and previously suggested by MD calculations.[45,80] A similar interaction is found in BR.[78] In both the *Cr*ChR2 and the C1C2 structures, Thr127 (Thr166 in C1C2) is in hydrogen bond distance to the $RSBH^+$, as well as the homologous Ser169 in Chrimson. These interactions suggest a direct link between the active site and residues aligned along the retinal polyene chain. As indicated by the multiple sequence alignment (see Fig. S1), in ReaChR Ser295 is exchanged for an alanine (Ala296).

Exchange of $Lys^{CI}$ for a phenylalanine in green- and orange-absorbing ChRs such as *Ca*ChR1 and Chrimson weakens the electrostatic stabilization of the $RSBH^+$ and thereby largely contributes to the bathochromic shift. Despite this exchange, the active site structure of Chrimson shows that both counter-ion residues are in close contact to the $RSBH^+$ as observed in blue-absorbing ChRs.[73]

Some distinctions exist between ChRs and BR with respect to the active site that might be decisive for the differences regarding protein function (proton pump BR vs. ion channels ChRs). In BR, the distance between the counter-ions and the $RSBH^+$ is increased, and the latter interacts directly with a water molecule instead. Furthermore, the BR active site retains a more rigid geometry due to tyrosine residues located close to Ci2.[78] Contrarily, QM/MM simulations of *Cr*ChR2 suggested a more flexible and heterogenous structure of the active site involving conformational substates with different hydrogen-bonding partners to the $RSBH^+$ (Ci1, Ci2 or $H_2O$).[48]

#### 1.2.4.3 Retinal binding pocket

In *Cr*ChR2 and C1C2, the binding pocket (Fig. 1-5) is built up by aromatic residues (Trp124, Phe178, Trp223, Phe226 and Phe230 in *Cr*ChR2) and the more polar residues Ser256, Thr127, $Cys^{DC}$, $Asp^{DC}$, Thr198 (according to the *Cr*ChR2 nomenclature) which are placed around the polyene chain and the $\beta$-ionone ring.[41] $Cys^{DC}$ and $Asp^{DC}$ (Cys and Asp of the DC gate[81] in retinal binding pocket, Cys128 and Asp156 in *Cr*ChR2) are crucial residues for channel closure and photocurrent inactivation as demonstrated by several studies on *Cr*ChR2[82–85] and commonly referred to as "DC pair" or "DC gate". In *Cr*ChR2, these residues interact indirectly via a water molecule as revealed by MD calculations[45,46] and the crystal structure[72] and thereby connect TM3 and TM4. In C1C2, a direct or indirect connection between $Cys^{DC}$ and $Asp^{DC}$ is not observed.[41] In Chrimson, the structure around the polyene chain is decisively altered involving replacements of Thr127 (Ser169), $Asp^{DC}$ (Cys198), Thr198 (Met201) and further residues present in the *Cr*ChRs.[73] In ReaChR, Thr198 is exchanged for a cysteine (Cys199).

### 1.2.4.4 Ion-conducting pathway and gating

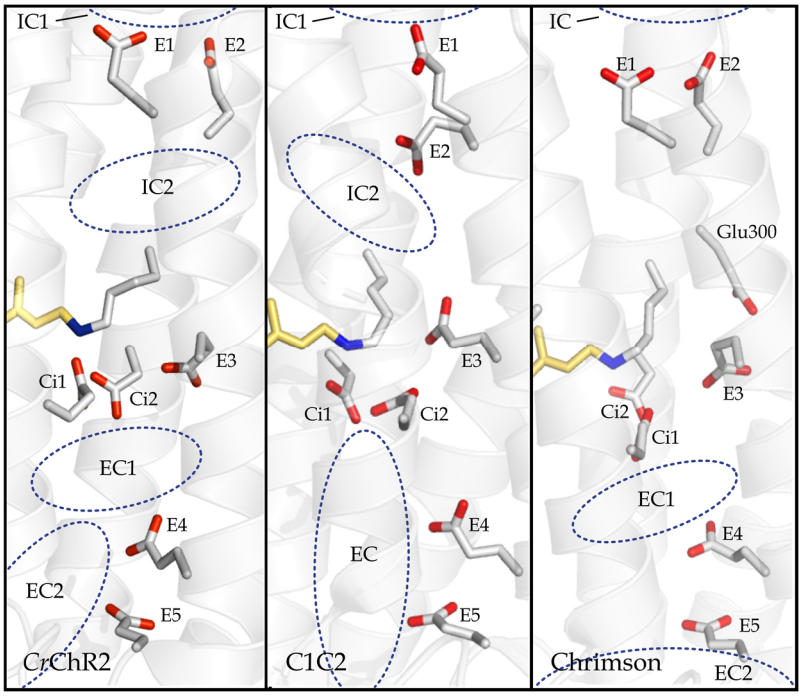


**Fig. 1-6** The putative ion-conducting pathway in *Cr*ChR2 (6EID, *left*), C1C2 (3UG9, *center*) and Chrimson (5ZIH, *right*) with 7–8 glutamates, respectively. Structures were visualized with PyMol (Version 2.1.1.). IC, intracellular cavity; EC, extracellular cavity.

In the ChR structures, large water-filled cavities are present in the extracellular half of the protein (EC), as opposed to smaller cavities in the intracellular half (IC).[41,72] In addition to Ci1 and Ci2, five glutamate residues are aligned along the putative ion-conducting pore named E1–E5 (Glu82, Glu83, Glu90, Glu97 and Glu101 in *Cr*ChR2, Fig. 1-6), with E1 located inner- and E5 located outermost.[22] In C1C2, the extracellular cavities are connected to a continuous pore already in the dark, restricted in the center of the protein by the central gate.[41] This is in contrast to *Cr*ChR2, in which two extracellular cavities are present that are separated by the outer gate.[72] The outer cavity is in contact with the medium, and the inner cavity is restricted by extracellular and central gate. The intracellular cavities are limited toward the extracellular side by the central gate and to the intracellular side by the intracellular gate.

The extracellular gate (EG, Fig. 1-7) in *Cr*ChR2 that represents the restriction site against the influx of external water molecules and ions in the dark is built up by the interaction of several residues connecting TM2, 3 and 7, involving E4, E5, Gln117 (Val156 in C1C2) and Arg120 (Arg159 in C1C2).[72] Among these, Arg120

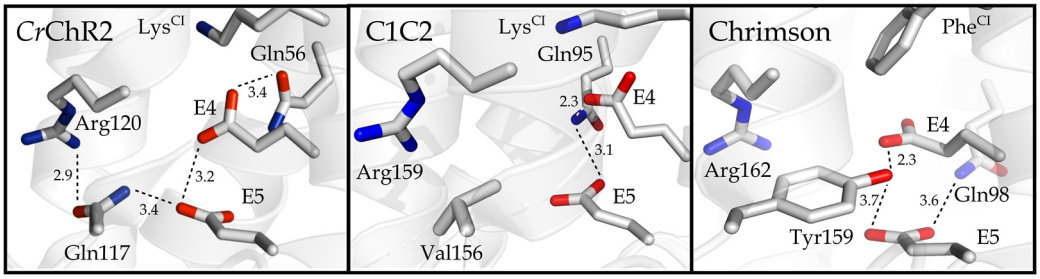


**Fig. 1-7** The extracellular gate in *Cr*ChR2 (6EID, *left*), C1C2 (3UG9, *center*) and Chrimson (5ZIH, *right*). Distances are given in Å. Structures were visualized with PyMol (Version 2.1.1.).

plays an outstanding role for gating as mutations abolish channel function.[34,41,86] In Chrimson, Gln117 is exchanged for a tyrosine (Tyr159) which increases the steric constriction of the EG in Chrimson as compared to *Cr*ChRs.[39] In Chrimson, E4 and E5 are decisive for the high $H^+$ selectivity with participation of Arg159.[39,73]

The central gate (CG, Fig. 1-8) in the *Cr*ChRs is formed by the counter-ions Ci1 and Ci2 along with $Lys^{Cl}$, E3, as well as a serine (Ser63 in *Cr*ChR2, Ser102 in C1C2) and an asparagine (Asn258 in *Cr*ChR2, Asn297 in C1C2). Electrophysiological investigations revealed a crucial role of the central gate for ion selectivity, in particular of E3.[67,86–89] Exchange of E3 for glutamine shifts ion selectivity from $H^+$ to $Na^+$ in both *Cr*ChR2 and ReaChR[52,88] but not in C1C2, in which the mutation led to a significantly reduced $Ca^{2+}$ and $K^+$ selectivity instead[41]. In *Cr*ChR2, mutation of E3 to histidine shifts the ion sensitivity from $Na^+$ to $H^+$[88,90] and replacement by positively charged arginine or lysine residues shifts the selectivity from cations to anions with far-reaching relevance for optogenetic applications[67]. *Cr*ChR2 and C1C2 differ with respect to the orientation of E3: In C1C2, its carboxylic side group is oriented toward the intracellular side, stabilized by hydrogen bonding to Asn297. Contrarily, in *Cr*ChR2 E3 is in an outward orientation and approaches the counter-ion complex. In Chrimson, the serine of the central gate is replaced by an

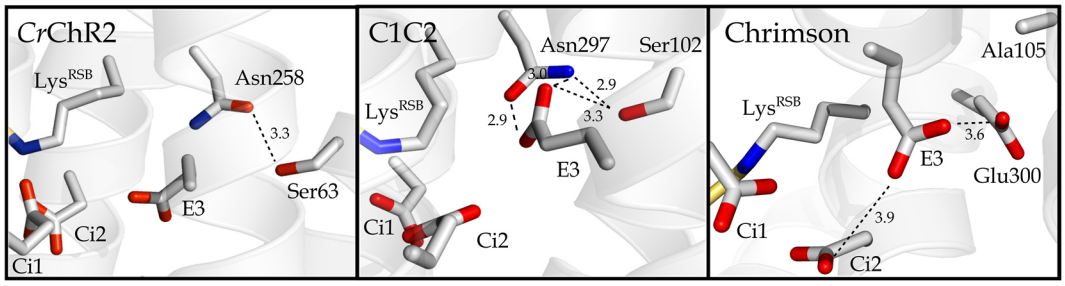


**Fig. 1-8** The central gate in *Cr*ChR2 (6EID, *left*), C1C2 (3UG9, *center*) and Chrimson (5ZIH, *right*). Distances are given in Å. Structures were visualized with PyMol (Version 2.1.1.).

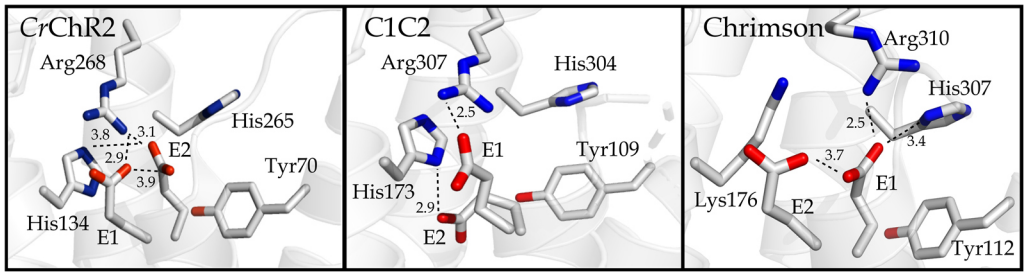


**Fig. 1-9** The intracellular gate in *Cr*ChR2 (6EID, *left*), C1C2 (3UG9, *center*) and Chrimson (5ZIH, *right*). Distances are given in Å. Structures were visualized with PyMol (Version 2.1.1.).

alanine and the asparagine by a glutamate, presumably resulting in an altered CG geometry. In both *Cr*ChR structures the intracellular gate (IG, Fig. 1-9) is formed by a tyrosine (Tyr70 in *Cr*ChR2, Tyr109 in C1C2), E1, E2, two histidines (His134/265 in *Cr*ChR2, His173/304 in C1C2) and an arginine (Arg268 in *Cr*ChR2, Arg307 in C1C2). The barrier against the influx of water and ions is probably achieved by interhelical salt bridges between E1, E2, His134 and Arg268. In Chrimson, His134 is exchanged for a lysine (Lys176) and E1 is oriented toward the cytoplasmic side.

## 1.2.5 Mechanism

ChRs allow the transformation of a light signal into an electrochemical signal. The absorbed photon energy triggers isomerization of the retinal cofactor. The resulting conformational changes in the active site lead to formation of the pre-conducting pore. Further structural alterations in the intracellular gate create an open channel. After channel closure, the dark state is restored via multiple pathways. This reaction chain is referred to as photocycle and in the following the underlying steps are discussed in detail.

### 1.2.5.1 Photocycle models

The electrophysiological characterization of many ChRs such as *Cr*ChR2[8,24,91], *Vc*ChR2[92], *Ps*ChR2[18] and *Gt*ACR2[40,68] heterologously expressed in host cells shows that the photocurrents evoked at continuous illumination conditions exhibit a larger transient current ($I_t$) and a smaller stationary current ($I_s$). This phenomenon is due to partial inactivation and was observed as well in the ChRs investigated in this thesis.[39,41,49] Notably, inactivation is reduced in more red-shifted ChRs such as *Ms*ChR1[17], *Gt*ACR1[68] and *Cr*ChR1[7,24,93]. Various models were considered to explain the photocurrent inactivation in ChRs.[92–95] In the following, two distinct models are presented involving either three states (model I) or four states (model II, Fig. 1-10). While model II was favored by most kinetic studies on ChRs[93–95], only one publication applied model I[94] and discarded it in favor of model II. For *Vc*ChR2, a combination of both models explained the photocurrents most accurately.[92]

According to model I[94], the ChR photocycle is sufficiently described by a closed state C, an open state O, and a desensitized closed state X (Fig. 1-10b). In the dark, ChR is 100 % in the C state. Illumination drives the C→O reaction with quantum efficiency $\varepsilon_{C\rightarrow O}$. A fraction $f_{O\rightarrow X}$ of O decays thermally to X with $\tau_{O\rightarrow X}$, and a second fraction $f_{O\rightarrow C}$ decays thermally to C with $\tau_{O\rightarrow C}$. Second illumination drives the X→O reaction with quantum efficiency $\varepsilon_{X\rightarrow O}$. If the quantum efficiency for formation of the open state O from the desensitized state X is smaller than the quantum efficiency for its formation from the closed state C ($\varepsilon_{X\rightarrow O} < \varepsilon_{C\rightarrow O}$) and channel closure is faster than the recovery of the closed state from the desensitized state

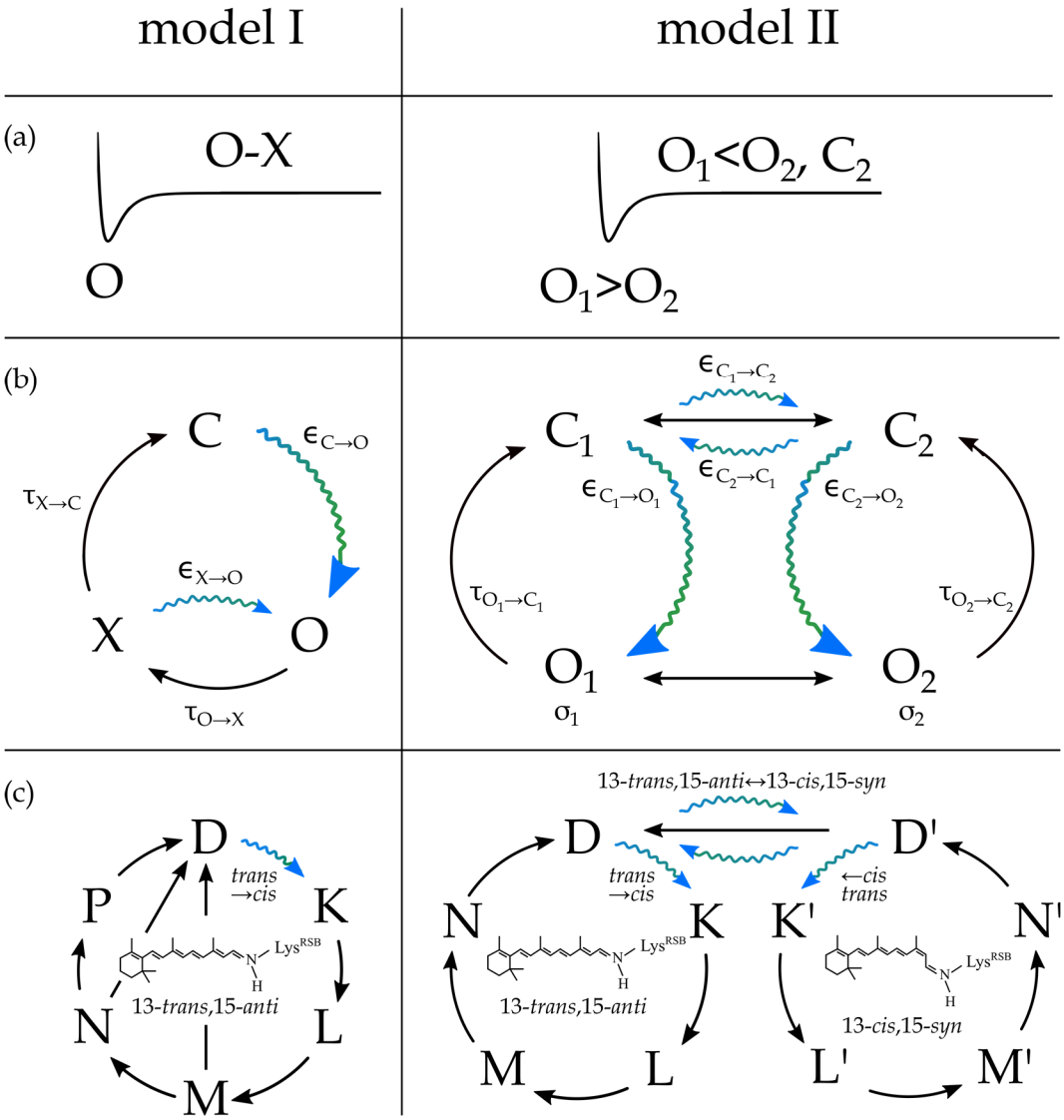


**Fig. 1-10** Function-derived photocycle models. In most ChRs, the photocurrent **(a)** comprises a transient current $I_t$ and a stationary current $I_s$. (**b**) According to model I, partial photocurrent inactivation at continuous illumination can be explained by accumulation of a long-lived desensitized state X, while according to model II it is described as the result of a second photocycle branch with a closed ($C_2$) and an open state ($O_2$) with reduced ion conductivity. (**c**) A spectroscopy-derived scheme that agrees with model I involves two different retinal isomers[104,105,176] as opposed to four different retinal isomers in model II[51,96,101].

($\tau_{O\rightarrow X} < \tau_{X\rightarrow C}$), X is accumulated at extended illumination resulting in a reduced photocurrent. In contrast, model II[93–95] assumes the coexistence of two closed states $C_1$ and $C_2$ in the dark from which two open states, $O_1$ and $O_2$, are induced with different conductivities $\sigma_1$ and $\sigma_2$ (Fig. 1-10b). Illumination drives the $C_1\rightarrow O_1$ reaction with quantum efficiency $\varepsilon_{C1\rightarrow O1}$ and the $C_2\rightarrow O_2$ reaction with quantum efficiency $\varepsilon_{C2\rightarrow O2}$. Recovery of the closed states occurs with $\tau_{O1\rightarrow C1}$ and $\tau_{O2\rightarrow C2}$. If (i) the conductivity $\sigma_2$ of the open state $O_2$ of the second photocycle branch is smaller than the conductivity $\sigma_1$ of the open state $O_1$ of the first photocycle branch ($\sigma_2 < \sigma_1$),

(ii) the quantum efficiency for formation of the open state is larger in the first photocycle branch ($\varepsilon_{C_2\rightarrow O_2} < \varepsilon_{C_1\rightarrow O_1}$) and channel closure is delayed in the second photocycle branch ($\tau_{C_2\rightarrow O_2} > \tau_{C_1\rightarrow O_1}$) $O_1$ dominates the initial photocurrent ($I_t$) while the relative contribution of the less-conductive $O_2$ is enhanced in $I_s$ (and $I_s < I_t$).

Of course, various modifications of these generalized schemes must be taken into consideration. Among these, light-induced and thermal conversion from $C_1$ to $C_2$, and *vice versa* should be highlighted as an important additional reaction pathway for model II, as recent measurements indicated the relevance of this reaction for the inactivation mechanism of *Cr*ChR2.[96–98] According to these concepts, under light the $C_1 \leftrightarrow C_2$ equilibrium is caused by the competing photoreactions, $C_1 \rightarrow C_2$ with quantum efficiency $\varepsilon_{C_1\rightarrow C_2}$, and $C_2 \rightarrow C_1$ with quantum efficiency $\varepsilon_{C_2\rightarrow C_1}$. In the dark, the equilibrium is due to thermal reactions, $C_1 \rightarrow C_2$ with $\tau_{C_1\rightarrow C_2}$ and $C_2 \rightarrow C_1$ with $\tau_{C_2\rightarrow C_1}$. If the quantum efficiency for formation of $C_2$ from $C_1$ is larger than the reverse reaction ($\varepsilon_{C_1\rightarrow C_2} > \varepsilon_{C_2\rightarrow C_1}$), continuous illumination additionally drives accumulation of $C_2$ and its less conductive open state $O_2$ and thereby contributes to channel inactivation as well.

The presence of two photoconvertible closed states in model II (Fig. 1-10b) implies the coexistence of multiple retinal isomers in ChRs that undergo different photoreactions and photocycles. Indeed, retinal isomer analysis by resonance Raman as well as retinal extraction and subsequent HPLC experiments indicate the coexistence of 13-*trans* and 13-*cis* retinal in the ChR dark state at a proportion of 70–80 : 20-30 %.[51,96,99,100] Similar to $BR_{548}$ (13-*cis*,15-*syn* retinal) and $BR_{568}$ (13-*trans*,15-*anti* retinal), these isomers also differ with respect to the conformation around the RSB $C_{15}$=N bond, with 13-*trans* retinal in 15-*anti* and 13-*cis* retinal in 15-*syn* conformation.[96,101] If these findings together with additional information on the photointermediates derived from UV-Vis spectroscopy are applied to photocycle model II (Fig. 1-10b), an extended photocycle model can be derived as exemplified in Fig. 1-10c: Here, 13-*trans*,15-*anti* is the cofactor of the predominant $C_1$ state, and 13-*cis*,15-*syn* the cofactor of the $C_2$ state. This concept, though, is challenged by NMR studies that revealed a 100 % 13-*trans*,15-*anti* initial dark state ($D_{IDA}$) obtained after long dark adaptation.[96,102] The most straightforward way to explain

the contradicting findings, is that at no-light conditions – realized in the NMR measurements – a pure 13-*trans*,15-*anti* dark state is present and that at low-light conditions – given in the resonance Raman and retinal extraction experiments – both, 13-*trans*,15-*anti* and 13-*cis*,15-*syn* are present.

Based on the assignment of $C_1$ and $C_2$ to 13-*trans*,15-*anti* and 13-*cis*,15-*syn* retinal chromophores, respectively, $O_1$ and $O_2$ are the photoproducts obtained by *trans*→*cis* (*cis*→*trans*) isomerization around the $C_{13}$=$C_{14}$ double bond, yielding 13-*cis*,15-*anti* (13-*trans*,15-*syn*) retinal. The $C_1$→$C_2$ photoreaction is due to $C_{13}$=$C_{14}$,$C_{15}$=N double isomerization.[97,98] As $C_1$ and $C_2$ and their photoproducts differ with respect to the conformation around the $C_{15}$=N bond, with $C_1$ in 15-*anti* and $C_2$ in a 15-*syn* conformation, the photocycles obtained from these closed states by single isomerization are in the following termed '15-*anti*' and '15-*syn*', respectively. While the 13-*trans*,15-*anti*→13-*cis*,15-*anti* isomerization of the 15-*anti* cycle is well characterized for ChRs by FTIR spectroscopy[31,42,99,100,103,104], it is more challenging to observe the 13-*cis*,15-*syn*→13-*trans*,15-*syn* photoreaction[98,105].

However, parallel photoreactions of 13-*trans*,15-*anti* and 13-*cis*,15-*syn* dark states are a common feature of microbial rhodopsins, observed in BR[106–110], sensory rhodopsins[79,111] and Archaerhodopsins[112,113] as well as Proteorhodopsin (PR)[114]. In BR, a thermal equilibrium between 13-*trans*,15-*anti* and 13-*cis*,15-*syn* retinal is established during dark adaptation[115], while light drives the retinal isomer ratio towards 13-*trans*,15-*anti*[116]. A decisive role for the 13-*trans*,15-*anti*↔13-*cis*,15-*syn* equilibrium in BR was assigned to the binding pocket residues Met145 and Tyr185.[110,117,118] Tyr185 that is located close to the BR active site influences the *anti*↔*syn* equilibrium by maintaining a twisted conformation of the $C_{14}$-$C_{15}$ bond.[118] Homologous residues to Met145 and Tyr185 in BR are not present in the ChRs investigated in this thesis with the exception of Chrimson in which a Tyr185-homologue is present (Tyr268). The actual determinants for the equilibrium between *syn*- and *anti*-cycle remain elusive for ChRs.

Usually, the photocycles or reaction sequences of photoreceptors are characterized by reaction intermediates that exhibit absorption spectra in the UV-Vis range different from the dark state. This concept applies to ChRs as well. However, most

photocycle models derived from UV-Vis spectroscopy do not consider the coexistence of parallel *anti* and *syn* photocycles as assignment of the photoproducts to either of these branches is challenging. The larger contribution of 13-*trans*,15-*anti* to the dark state suggests that the photoproducts are mainly in a 13-*cis*,15-*anti* conformation. Different nomenclatures exist for naming photointermediates. In this thesis, the intermediates are named according to the BR nomenclature (with the exception of the late intermediate 'P' that does not exist in BR). The common intermediates of ChRs are (with the alternative names for *Cr*ChR2 in brackets):

(1) A dark state D ($D_{470}$, D in *Cr*ChR2) adopting different retinal isomers at least at low-light conditions.
(2) The excited electronic state and additional transition states formed within $10^{-13}$–$10^{-10}$ s (no photoproduct names assigned).[44,119–121]
(3) The early photoproduct K ($P_{500}$, $P_1$ in *Cr*ChR2) that is red-shifted with respect to D and is formed within $10^{-12}$–$10^{-8}$ s.[31,44,92,122]
(4) The blue-shifted M intermediate ($P_{390}$, $P_2$ in *Cr*ChR2) that is formed from K within $10^{-6}$–$10^{-5}$ s.[31,44,104,122]
(5) The red-shifted N intermediate ($P_{520}$, $P_3$ in *Cr*ChR2) that is formed from M within $10^{-3}$–$10^{-2}$ s.[31,44,51,104,123] Ion conduction is partially assigned to the late M intermediate and mainly to N.[31,51,123]

Additionally, many spectroscopic photocycle models include a late P intermediate ($P_{480}$, $P_4$ in *Cr*ChR2) with a similar absorption spectrum but smaller extinction coefficient as D, formed from N within $10^{-2}$ s and decaying back to D within $10^{1}$ s.[31,52,96,104,105,123] More recently, P was interpreted as the dark state of a parallel photocycle branch, similar to $C_2$ and D' in Fig. 1-10 (p. 16).[98] In some ChRs[44,51], a slightly blue-shifted L intermediate was observed that is passed through in the K→M transition and present as well in the BR photocycle[124]. In the following, the characteristics of the ChR photocycle are discussed in detail.

### 1.2.5.2 The dark state

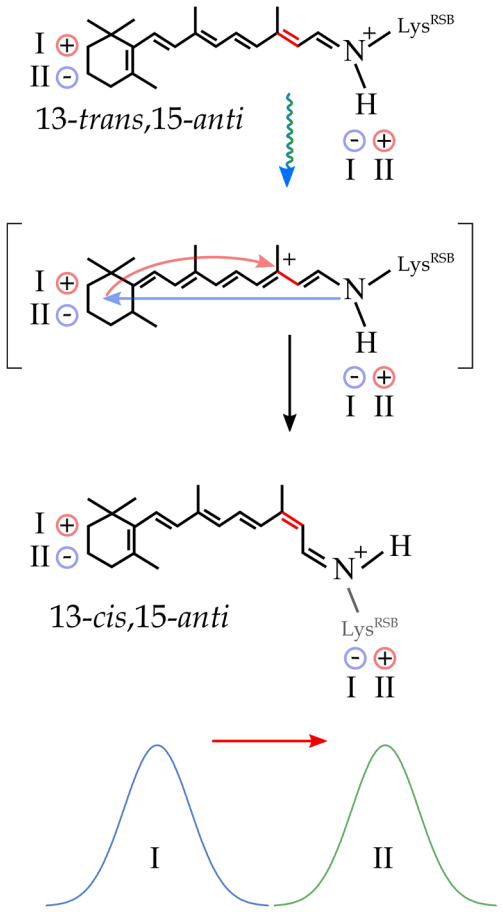


**Fig. 1-11** The mechanism of spectral tuning. Energy of the 13-*trans*,15-*anti* electronic ground state is lowered by stabilization of the positive charge at the $RSBH^+$ (I) and elevated by destabilization (II). Photoisomerization initiates charge translocation toward the *β*-ionone ring (*blue arrow*). Stabilization of this translocation by negative charges decreases the energy of the excited electronic state (II), while destabilization by positive charges leads to an increased energy (I). Modulations according to mechanism I lead to blue-shifted chromophores, while modulations according to mechanism II induce bathochromic shifts (*lower red arrow*). Upon progression of the photoreaction, the positive charge is transferred back toward the RSB (*upper red arrow*) and thereby transiently decreases the double bond character of the $C_{13}$=$C_{14}$ bond which is the prerequisite for 13-*trans*,15-*anti* →13-*cis*,15-*anti* isomerization.

Natural ChRs vary significantly with respect to their maximum absorption wavelength. By now, the range reaches from a maximum of the action spectrum at 436 nm (*Tetraselmis striata* channelrhodopsin) to 587 nm (*Chlamydomonas noctigama* channelrhodopsin).[22] The bathochromic shift with respect to free retinal ($\lambda_{max}$ ≈ 373–383 nm[125]) is due to (1) protonation of the retinal Schiff base by which the retinal cofactor is bound to the protein, and (2) interaction of the retinal with the chromophore binding pocket, *i.e.* by π-π stacking forces. Spectral tuning is mainly achieved by two factors (Fig. 1-11):

(1) Modulation of the positive charge residing at the $RSBH^+$ in the electronic ground state.

(2) Modulation of the translocation of the positive charge in the excited electronic state.

According to (1), electrostatic stabilization of the $RSBH^+$ in the ground state is mainly achieved by the counter-ion complex comprising Ci1, Ci2 and a water molecule (see Fig. 1-5, p. 10).[41,72,73] While Ci2 is considered as deprotonated in ChR dark states (based on its acceptor function for the $RSBH^+$ proton[104] and semi-empirical p$K_a$

calculations[41]), the protonation state of Ci1 differs: In blue-absorbing ChRs such as *Ps*ChR2, *Cr*ChR2 and C1C2, Ci1 is deprotonated[18,34,41,42] but protonated in green- and orange-absorbing ChRs such as *Ca*ChR1 and Chrimson[34,39,54,79]. The low p$K_a$ of Ci1 in blue-absorbing ChRs is largely due to electrostatic stabilization by the neighboring Lys$^{CI}$ while exchange of this residue by phenylalanine as in Chrimson results in a significant p$K_a$ increase.[34] Electrostatic stabilization of the positive charge of the RSBH$^+$ by the counter-ion complex increases the energy difference between ground state and excited state, which results in the hypsochromic absorption shift.[126] Accordingly, neutralization of the deprotonated Ci1 found in blue-absorbing ChRs by mutagenesis induces bathochromic shifts.[18,64,127] In contrast, mutations of the protonated Ci1 found in green- and orange-absorbing ChRs can even result in hypsochromic shifts[33,34,54], presumably due to the accumulation of water in the active site. Although little is known about the particular role of water for color tuning, water-mediated effects on chromophore absorption are described for other rhodopsins.[128] Similarly, ions residing in the active site could affect spectral absorption but were not resolved in the ChR crystal structures.[41,72] Another factor that is likely to affect the charge stabilization at the RSBH$^+$ is Ser295 in C1C2 (Ser256 in *Cr*ChR2, see Fig. 1-5, p. 10) that is exchanged for an alanine in both ReaChR and Chrimson (see Fig. S1). Besides local interactions, spectral shifts can be caused by long-range interactions as well. The ChR crystal structures revealed extended hydrogen bond networks connecting the active site with the extracellular side of the protein.[41,72] In the orange-absorbing Chrimson, alterations of such an interaction pattern by mutations of E4 and E5 that are located at the extracellular end of TM2 (see Fig. 1-7, p. 13) induced hypsochromic shifts[39], mostly by decreasing the p$K_a$ of Ci1. Similarly, mutation of Glu87 which is placed more than 20 Å away from the RSBH$^+$ induced a red-shift by 15 nm in *Cr*ChR1.[24]

Formation of the excited electronic state in rhodopsins involves translocation of the positive charge from the RSBH$^+$ toward the $\beta$-ionone ring.[129–131] During reversion of this charge transfer by backward movement of the positive electron density toward the RSB, the double bond character of the $C_{13}$=$C_{14}$ bond is transiently decreased which is the prerequisite for isomerization. Polar or

negatively charged residues located at the $\beta$-ionone ring stabilize the translocated positive charge, decrease the energy of the excited state and thereby contribute to the bathochromic shift. Accordingly, more nonpolar residues are found in the retinal binding pocket of blue-absorbing ChRs such as *Cr*ChR2 (Gly181, Phe189) and C1C2 (Gly220, Phe228) that are replaced by polar residues in green- or orange-absorbing ChRs such as *Vc*ChR1 (Ser176 and Tyr184) and Chrimson (Ser223 and Tyr231). Accordingly, S220G mutation in the C1V1 chimeric construct that comprises structural elements from *Cr*ChR1 and *Vc*ChR1 led to a spectral blue-shift[33], as well as M201T and S223G mutations in Chrimson[73] or T198G/ G202A in C1C2[74].

#### 1.2.5.3 The initial photoreaction

Light-induced isomerization of the retinal dark state is achieved by transition to the first excited electronic state ($S_1$). Vibrationally relaxed $S_1$ decays via two (or multiple) pathways either back to the dark state or to the isomerized photoproduct(s). Vibrational relaxation of the excited state to the first photoproduct occurs within 400 fs in *Cr*ChR2[122] and 100–110 fs in *Chlamydomonas augustae* ChR1 (*Ca*ChR1)[119,120]. The thermally relaxed photoproduct K is formed after 2.7 ps in *Cr*ChR2[121,122] and in a biphasic manner in *Ca*ChR1 with time constants of 500 fs and 5 ps[119] (only one time constant observed by Schnedermann *et al.* 2016[120]) and in Chrimson with time constants of 200 fs and 1.5 ps at alkaline pH[54]. On the basis of ultrafast FTIR measurements, it was proposed that the excess energy of the chromophore is efficiently transferred to the protein environment during thermal relaxation.[132]

As mentioned in the previous section, formation of the excited electronic state involves translocation of the positive charge residing at the $RSBH^+$.[129–131] It was reported based on investigations of *Cr*ChR2 and Chrimson that negatively charged Ci1 catalyzes the photoisomerization by stabilizing the positive charge near the $C_{13}$=$C_{14}$ bond, thus increasing its single bond character and facilitating isomerization.[54,121]

The K photoproduct is red-shifted with respect to the dark state. Studies on the corresponding intermediate in bovine rhodopsin, bathorhodopsin, explained this red-shift by a chromophore distortion and an increased distance between the $RSBH^+$ and its counter-ion.[133–135] In bovine rhodopsin, this chromophore distortion involves the dihedral angles of all double bonds of the polyene chain with the exception of the RSB-$C_{15}$=N bond.[134,135] As revealed by the crystal structure of its K intermediate, the distortion is more localized at the $C_{12}$–$C_{13}$=$C_{14}$ dihedral angle in BR.[136] Similarly, though, an increased distance from the $RSBH^+$ to the counter-ion complex is observed in BR that largely contributes to the bathochromic absorption shift of K.[136,137] Both, distortion of the chromophore geometry and weakening of the electrostatic stabilization of the $RSBH^+$ store energy from the initial photoreaction. In bovine rhodopsin, the free enthalpy of the K-like photoproduct is increased by ~ 147 kJ/ mol as compared to the dark state, thus > 60 % of photon energy is stored.[138] In BR, the free enthalpy change from D to K is ~ 67 kJ/ mol, indicating an energy storage of ~ 30 %.[139] For the metazoan rhodopsins, bovine and squid rhodopsin, it was shown that the relative contribution of the two mechanisms – chromophore distortion and weakening of electrostatic stabilization of the $RSBH^+$ – to the total energy storage is mediated by the active site environment.[135] In bovine rhodopsin, chromophore distortion accounts for 75 % of the stored energy as opposed to 17 % in squid rhodopsin.[135] This significant deviation was explained by a higher flexibility of the active site in squid rhodopsin. Other publications on the energy storage mechanism of bathorhodopsin report on contributions of chromophore distortion of 32 %[140], 51 %[141] and 60 %[142], respectively. In the K intermediate of BR, the contribution of charge separation to energy storage is presumably larger as compared to bathorhodopsin, accounting for ≥ 50 % of energy storage.[137,139,143]

Both, weakening of the $RSBH^+$-counter-ion interaction and chromophore distortion, can be tracked by vibrational spectroscopy. The electrostatic weakening during D→K transition leads to light-induced changes of $RSBH^+$-C=N stretching modes that are sensitive to stabilization of the positive charge, as observed in BR[144] and the ChRs *Cr*ChR2[132], C1C2[42], *Ca*ChR1[79] and *Gt*CCR4[145]. Chromophore distortion is reflected by hydrogen out-of-plane (HOOP-) vibrations arising

< 1000 $cm^{-1}$ in the FTIR spectrum. Strong HOOP bands are observed in the K-like intermediate of bovine rhodopsin[146], as well as the microbial rhodopsins BR and Xanthorhodopsin (XR)[147], as well as PR[148], *Anabaena* sensory rhodopsin[111], phoborhodopsin[149], or *Exiguobacterium sibiricum* rhodopsin[150]. In *Cr*ChR2 and *Gt*CCR4, the HOOP bands are comparably weak[31,145], while more pronounced in C1C2 and *Ca*ChR1[42,145,151], raising the question whether the concept of energy storage is applicable to ChRs as well.

In addition to changes of the chromophore, FTIR techniques allow the identification of light-induced changes in hydrogen-bonding and proton transfers based on changes in the C=O stretching modes of aspartic and glutamic acids (> 1690 $cm^{-1}$). Analysis of this region revealed that a hydrogen-bond between $Cys^{DC}$ and $Asp^{DC}$ (see Fig. 1-5, p. 10) is weakened in the D→K transition in *Cr*ChR2 and C1C2.[42,81] In *Ca*ChR1, a proton transfer from Ci1 to Ci2 was identified in the D→K reaction.[151]

#### 1.2.5.4 Channel opening

In *Cr*ChR2 and *Vc*ChR2, K is followed by two intermediates, M and N, that arise in the order of milliseconds.[31,82,92,104,123] In ReaChR and C1C2, an additional L intermediate was detected that precedes M.[44,51] L is blue-shifted as compared to the dark state.

In the following, the proton transport in BR is briefly reviewed based on crystallographic[78,136,152–154] and vibrational[155] investigations as the pumping mechanism is understood in great detail and served as an important template to understand the respective processes in ChRs. The formation of L in BR is explained by partial relaxation of the distorted chromophore around the dihedral $C_{12}$–$C_{13}$=$C_{14}$ bond occurring in the K→L transition and by a subsequent change of the angle between the $RSBH^+$ and the water molecule of the counter-ion complex, both processes contributing to the hypsochromic shift of L as compared to K. The structural rearrangements in the binding pocket pave the way for deprotonation of the $RSBH^+$ leading to formation of the blue-shifted M intermediate. The proton is transferred within the counter-ion complex via the water molecule to Asp85.

Due to this charge transfer, conformational stabilization of the RSB by a hydrogen bond network within the counter-ion complex is decisively weakened, allowing the RSB to rotate from the extracellular toward the intracellular side. This reorientation has important mechanistic relevance, achieving outward direction of the proton transfer and preventing RSB reprotonation by the proton acceptor group Asp85. The protonation state of Asp85 is coupled to the proton release group at the extracellular side via Arg82. This coupling raises the p$K_a$ of Asp85 and thereby also helps preventing proton transfer back to the RSB. Due to these alterations, a second pathway leads to reprotonation of the RSB, *i.e.* by Asp96. In the dark, Asp96 retains a high p$K_a$, is buried and in long distance to the RSB so that significant structural alterations are required to realize proton transfer. In the M→N transition, a proton-conducting pathway is formed between the donating Asp96 and the accepting RSB by reorientation of TM6 and reorganization of side groups in TM6 and TM7 allowing the influx of water molecules. Reprotonation of the RSB induces a bathochromic shift (N intermediate) and facilitates thermal back isomerization from 13-*cis*,15-*anti* to 13-*trans*,15-*anti* retinal in the N→O transition that additionally involves Asp96 reprotonation by the intracellular medium. The O state is red-shifted as compared to N, mainly due to the more planar chromophore geometry, and as well red-shifted as compared to the dark state. This can be explained by the weaker stabilization of the $RSBH^+$ due to still protonated Asp85. Recovery of the dark state involves deprotonation of Asp85 which is coupled to proton release to the extracellular side.

The above described proton pumping mechanism of BR might similarly apply to ChRs as well as electrophysiological investigations suggested that *Cr*ChR2 pumps protons to the extracellular side and that proton release occurs with N decay.[36,37] This observation, however, was challenged by Sineshchekov *et al.* 2013 who claimed that *Cr*ChR2 does not exhibit proton pumping activity, as well as *Mv*ChR1 and *Ps*ChR2, while proton pumping was observed in *Vc*ChR1, *Ca*ChR1 and *Ds*ChR1.[35] Based on their observations the authors developed the concept that ChRs can be separated into two groups: (1) blue-absorbing ChRs such as *Cr*ChR2 that do not exhibit proton pumping and produce high photocurrents, and (2) green-absorbing ChRs such as *Ca*ChR1 that do exhibit proton pumping and

produce small photocurrents. Most likely, the opposing observations concerning the proton pumping activity of *Cr*ChR2 are due to different measurement conditions. Accordingly, proton pumping might still be present in blue-absorbing ChRs but only reduced in comparison to green-absorbing ChRs.

More functionally relevant for the ChR function, though, is the presence of (an) ion-conducting state(s) in the late M and the N intermediate. The mechanistic research concerning formation of the ion-conducting state focused primarily on *Cr*ChR2. Although the mechanism is not fully understood yet, results from vibrational spectroscopy indicate that the process of pore formation can be separated into two steps: The first step involves formation of a continuous water-filled pore connecting the extracellular and intracellular cavities, driven by light-induced changes in the active site. The second step involves comparably small structural rearrangements at the inner gate.[47,101] As shown for *Cr*ChR2[31,101,103,104,156,157] and *Ca*ChR1[158,159], formation of the open state involves changes in the backbone structure that are significantly larger than in bacterial proton pumps such as BR[160,161] and proteorhodopsin (PR)[162,163], as well as the cyanobacterial light-driven pump from *Gloeobacter violaceus*[164]. These large structural changes were explained by helix hydration due to the influx of water molecules.[157] Furthermore, cryo-electron microscopic (cryo-EM) and electron paramagnetic resonance (EPR) spectroscopic measurements revealed movements of TM2, TM6 and TM7 during formation of the conducting state.[76,77,165] Based on a comparison of the kinetics of the M and N intermediates with the kinetics of the conducting state, channel opening in *Cr*ChR2 is realized within M and closure is linked with N decay.[123] Similar assumptions were made for ReaChR[51], while in *Ps*ChR2 the open state is largely identical with the N-like intermediate[166,167] as opposed to M as the conducting state in *Ca*ChR1[35].

The processes of M→N transition and formation of the ion-conducting state could be linked with proton dynamics of specific residues. However, most of these processes, reiterated in the following, are still under debate. FTIR spectroscopic measurements on *Cr*ChR2 revealed light-induced deprotonation of E3 (see Fig. 1-5, p. 10).[31,88] While Kuhne *et al.* 2015 proposed an early deprotonation of this

residue[47], *i.e.* prior to formation of the conducting state, Lórenz-Fonfría *et al.* 2013 assigned the deprotonation event to the late P intermediate ($P_{480}$) that succeeds the ion-conducting state[104]. Based on their FTIR spectroscopic measurements and corresponding MD simulations, Kuhne *et al.* 2015 developed a model for the first step of pore formation. According to this so-called E90-helix2-tilt (EHT) model[47], E3 (Glu90 in *Cr*ChR2) plays a crucial role in the formation of the ion-conducting pore: Light-induced retinal isomerization leads to a movement of the central gate residue Asn258 (TM7) with the number of hydrogen bonds to E3 (TM2) reduced from two to one. Subsequently, E3 flips toward the active site, then it deprotonates and forms a hydrogen bond to $Lys^{CI}$. This molecular rearrangement results in an outward tilt of helix 2 by 3.9 Å and allow water molecules to penetrate deeper into the channel. The tilt of TM2 caused by movement of E3 could accordingly displace residues within the inner gate (*e.g.* E1 and E2) and thereby lead to the actual channel opening. Movement of TM2 along with TM6 and TM7 was also demonstrated by cryo-EM and EPR measurements.[77,165] The MD simulation that led to the conclusions of the EHT-model was based on the C1C2 structure in which E3 forms a hydrogen bond to Asn258.[41] In contrast, the more recently released *Cr*ChR2 structure[72] revealed that E3 is oriented toward the active site already in the dark state (see Fig. 1-5, p. 10). This observation contradicts the assumed downward flip of E3, while it does not argue against the link of E3 deprotonation and water influx into the central gate. More recently, Kuhne *et al.* 2019 proposed that E3 deprotonation occurs exclusively in the 15-*syn* photocycle branch and not during the 15-*anti* cycle.[98]

A comparably better consensus within the ChR community exists concerning the acceptor group of the $RSBH^+$ during M formation: Ci2 is the primary proton acceptor in *Cr*ChR2, while Ci1 might act as a secondary acceptor with lower probability to receive the proton.[47,104] In *Ca*ChR1, however, Ci1 was described as the primary proton acceptor instead[35,151] and it was proposed that protonation of Ci1 is crucial for the enhanced proton pumping activity[35]. Very recently, it was suggested based on MD simulations that M state formation in *Cr*ChR2 involves an inward motion of the $RSBH^+$ similar to BR.[168]

FTIR spectroscopic measurements on *Cr*ChR2 and C1C2 revealed the light-induced deprotonation of $Asp^{DC}$.[43,104] Accumulation of M in the D156A mutant of *Cr*ChR2[82,84] as well as the correlation of FTIR bands assigned to $Asp^{DC}$ deprotonation with N decay[104] supported the identification of $Asp^{DC}$ as the proton donor for reprotonation of the RSB during M→N transition. Similar to Asp96 in BR, $Asp^{DC}$ is buried within the retinal binding pocket and in > 9 Å distance to the RSB. Thus, a proton transfer would require formation of a proton-conducting pathway. In addition to the long distance of the assumed donor-acceptor pair, the proton donor role of $Asp^{DC}$ is challenged by the fact that several $Asp^{DC}$ mutants in *Cr*ChR2 that abolish the carboxylic side group still maintain ion channel function.[52,67,83,85,169] In Chrimson, $Asp^{DC}$ is not conserved (Cys198, see Fig. 1-5, p. 10).

#### 1.2.5.5 Channel closure and dark state recovery

In contrast to ion pumps such as BR[170], PR[171–173], XR[174], Actinorhodopsin[175] or *Gloeobacter violaceus* rhodopsin[164] in which the dark state is restored << 1 s, ChRs comprise a late desensitized and non-conducting state that decays back to the dark state within $10^2$ s.[31,51,92,104,105,123] Such a long-lived desensitized state would represent a significant impairment for the performance of ion pumps given that usually only one proton is pumped per cycle. In contrast, 10–100 ions are transported by *Cr*ChRs per cycle.[30] Thus, desensitization might represent a mechanism to avoid damages at high light intensities that is not required in ion pumps. Desensitization is reflected by the photocurrent inactivation observed at continuous illumination conditions as discussed in detail in 1.2.5.1. (p. 15). To date, mainly two mechanisms are considered to explain the formation of the desensitized state:

(i) Transition of the conducting N state to a non-conducting P intermediate that slowly decays back to the dark state.[31,51,52,96,104,105,123] According to most photocycle models that include such an N→P transition, it involves isomerization from 13-*cis*,15-*anti* to 13-*trans*,15-*anti* retinal.

(ii) Retinal isomerization of the dark state D of the 15-*anti* cycle to the dark state D' of the 15-*syn* cycle by double isomerization from 13-*trans*,15-*anti* to 13-*cis*,15-*syn* that slowly decays back to D.[98]

Both of the proposed pathways could exist in parallel as well. Irrespective of the mechanism for P formation, a direct recovery pathway for D from N was described to occur within $10^{-2}$ s in *Cr*ChR2[98,105,176] and $10^{-1}$ s in C1C2[44]. The actual mechanism of ion channel closure is still under debate. It was shown that channel closing is mediated by the DC pair in *Cr*ChR2 as mutations decisively extended the life-time of the open state.[82,84,101,156,177] In ReaChR, only mutation of $Cys^{DC}$ but not $Asp^{DC}$ had a similar effect on the closing kinetics of the ion channel.[51,52] Furthermore, it was shown that channel closure is correlated with the dehydration of helices due to water efflux, supposedly on the intracellular side of the channel.[157] In Chrimson, channel closure was slowed down significantly by mutations of residues located in the center of the pore such as Glu300 (Asn in *Cr*ChRs), Ala105 (Ser in *Cr*ChRs), $Phe^{CI}$ (Lys in *Cr*ChRs) and Ci2 as well as the extracellular (E4) and the intracellular gate (E1 and E2, see Fig. 1-9, p. 14).[39]

### 1.2.5.6 Summary

The reviewed alterations in the ChR photocycle based on investigations of *Cr*ChR2[31,81,104,157], C1C2[42,43] and *Ca*ChR1[151,158] are summarized in Fig. 1-12. The controversially discussed dynamics of E3 were omitted for simplicity.

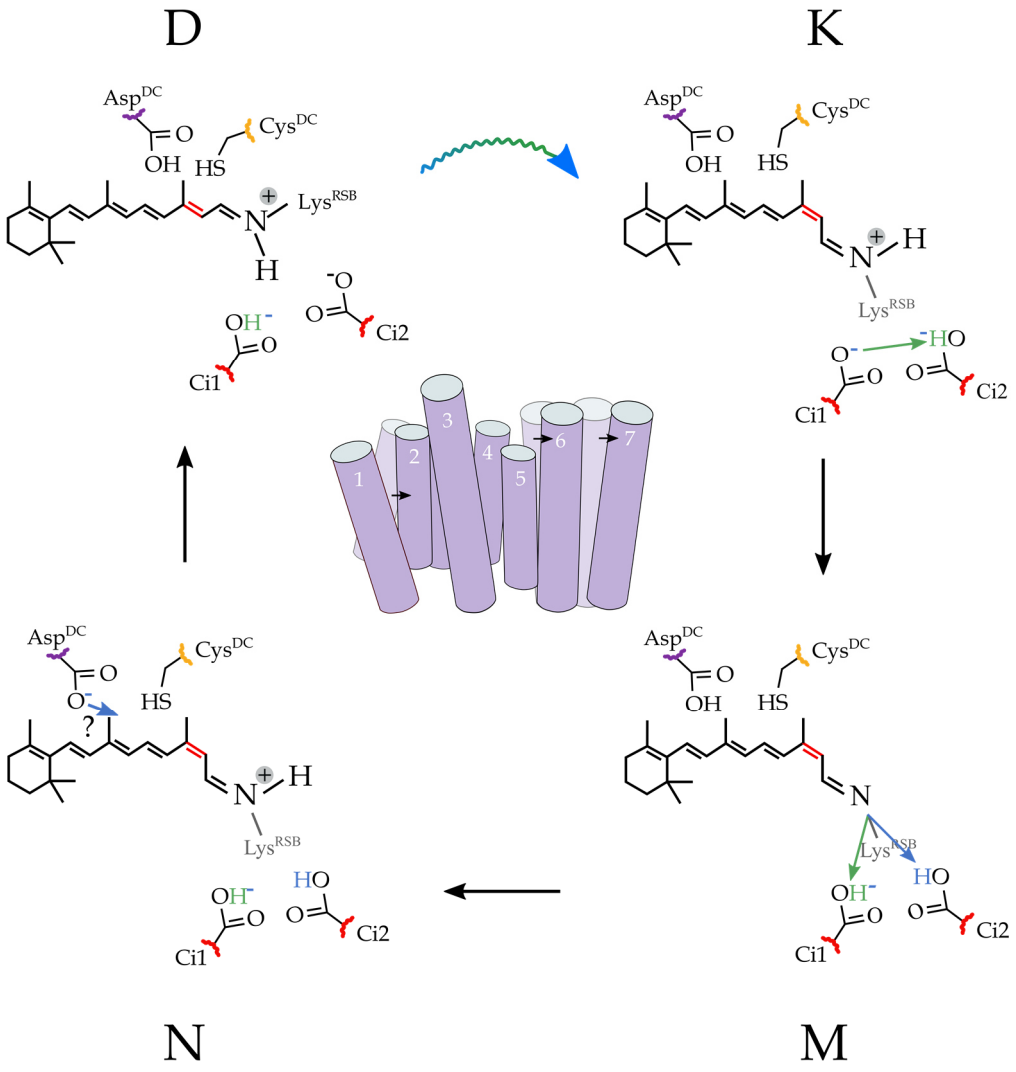


**Fig. 1-12** Molecular alterations in a simplified ChR photocycle. Some structural intermediates were omitted and only the 13-*trans*,15-*anti* branch was considered (discussed in 1.2.5.1, p. 15.) Light-triggered retinal isomerization leads to formation of K. In *Cr*ChR2 and C1C2, this transition involves weakening of an interaction between Asp$^{DC}$ and Cys$^{DC}$ (mediated by $H_2O$ in *Cr*ChR2[72], *blue dots*).[42,81] In *Ca*ChR1, a proton transfer occurs from Ci1 to Ci2 (*green arrow*).[151] Formation of M involves proton transfer from the RSBH$^+$ to the counter-ion complex. In *Cr*ChR2, Ci2 is considered as the primary proton acceptor (*blue arrow*)[104] as opposed to Ci1 in *Ca*ChR1 (*green arrow*).[158] During formation of M, larger backbone changes occur, involving motions of TM2, TM6 and TM7 that are linked with formation of the open state.[76,77,165] Reprotonation of the RSB leads to formation of N. Asp$^{DC}$ was proposed as proton donor in *Cr*ChR2 (*blue arrow*)[104], but this hypothesis is challenged by the long distance of the donor-acceptor pair and electrophysiological data on Asp$^{DC}$ mutants.[52,67,83,85,169] The proton transfer processes are reversed during dark state recovery. The controversially discussed dynamics of E3 were omitted for simplicity.

## 1.3 Motivation and objectives

In the last decade, numerous biophysical studies have made important contributions leading to a better mechanistic understanding of the effects seen in electrophysiological measurements on ChRs. The photocurrents themselves raise a number of questions concerning channel function:

- What are the factors for dark state absorption?
- How are the conducting states formed and closed?
- What are the factors determining ion selectivity?
- Which parallel photoreactions exist and how are they modulated?

The objective of this thesis was to expand the existing ideas that address these questions in the literature, by carrying out FTIR spectroscopic investigations of the ChR variants C1C2, ReaChR and Chrimson, complemented with UV-Vis spectroscopy and HPLC analysis. This thesis is structured such that the findings for each of the different ChR variants are compared in the general discussion (see chapter 4, p. 131) while more specific features are discussed separately, right after the results sections for C1C2, ReaChR and Chrimson (see 3.1, p. 47, 3.2, p. 61, and 3.3, p. 108, respectively).

Specific questions concerning C1C2:

- Is E3 deprotonated during the photocycle of C1C2?

Specific questions concerning ReaChR:

- What are the determinants for the pH dependency of the dark state?
- How does E3 affect the ion selectivity of the conducting state?
- What is the mechanism of photocycle branching?

Specific questions concerning Chrimson:

- What are the factors conferring its unprecedented red-shift?
- What are the determinants for the high proton selectivity?

# 2 Materials and methods

## 2.1 UV-Vis spectroscopy

### 2.1.1 Introduction

An electron in state $S_0$ with energy $E_0$ can be excited to state $S_1$ with energy $E_1$ by absorption of a photon that provides the required energy $\Delta E_{01} = E_1 - E_0 = h\nu$. Photon absorption requires a change in charge distribution from $S_0$ to $S_1$, characterized by the transition dipole moment $\overrightarrow{|M_{01}|}$. The probability for an electronic transition is proportional to $\overrightarrow{|M_{01}|}^2$ so that the transition is forbidden if $\overrightarrow{|M_{01}|} = 0$. Electron absorption processes of molecular orbitals and valence bonds typically occur within a wavelength range of ~ 180–750 nm ($\lambda = c/\nu$). This spectral region is divided into the ultraviolet (UV) range < 400 nm and the visible (Vis) range > 400 nm, defined by the wavelength dependence of human vision. The energy of the electron ($E_i$) is furthermore influenced by vibrational and rotational movements of the atom cores. Transitions between different vibronic states $S_{iv} \rightarrow S_{iv'}$ differ with respect to the required transition energies as indicated in the Jablonski diagram (Fig. 2-1). Accordingly, electronic transitions between different vibronic sublevels would lead to separate bands in a UV-Vis spectrum, but polar solvents such as water usually cause band broadening to a single apparent absorption band. In the rather nonpolar environment of a membrane protein, though, these vibrational sublevels are often observed.[96,105] Several pathways exist for an electron to return back from the excited state to the electronic ground state. One possibility is the emission of a photon, *i.e.* fluorescence. Another possibility is thermal conversion, *i.e.* dissipation of the absorbed light energy to the environment by evoking vibrations and/ or rotations. A third possibility is intersystem crossing, *i.e.* the radiationless transition from the excited state to an intermediate state ($T_1$ in Fig. 2-1) by spin reversal. The subsequent

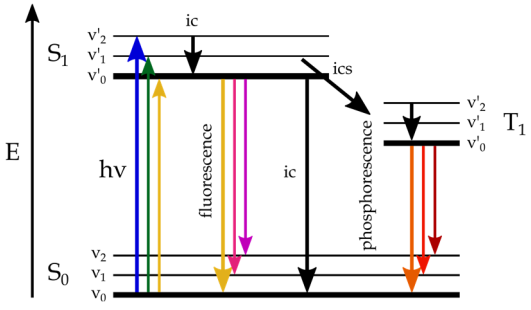


**Fig. 2-1** Jablonski diagram describing electronic transition by photon absorption. Relaxation to the electronic ground state $S_0$ is achieved by internal conversion (ic), fluorescence, intersystem crossing (ics) and phosphorescence. *Black arrows* indicate thermal transitions.

transition to the ground state by photon emission, *i.e.* phosphorescence, is slowed down as compared to the other transitions because the selection rule $\overrightarrow{|M_{01}|} > 0$ is violated and the probability is drastically decreased.

The most relevant electronic transitions for UV-Vis spectroscopy in proteins are $n \rightarrow \pi^*$, and $\pi \rightarrow \pi^*$. In proteins, suitable chromophores are peptide bonds and amino acid residues with a conjugated $\pi$ electron system such as tryptophane, tyrosine and phenylalanine. To obtain proteins suitable for light detection in the visible range, cofactors such as retinal are required that exhibit extended conjugated $\pi$ electron systems leading to an increased electronic ground state energy and a smaller transition energy.

### 2.1.2 Setup and methods

The UV-Vis spectroscopic measurements were performed with a Cary Bio 50 spectrometer (Varian Inc., Palo Alto, USA). Temperature was adjusted with the DN cryostat (Oxford Instruments, Abingdon, UK) placed into the spectrometer similar to Fig. 2-4 (p. 39). For illumination, a ring of LEDs was positioned around the aperture of the cryostat. Samples were prepared on a $BaF_2$ window by repeated drying under a nitrogen stream and subsequent rehydration. After preparation the sample was sealed with a second $BaF_2$ window. Until use the samples were stored at -40 °C. Between measurements samples were heated > 293 K to allow thermal relaxation. Light – dark difference spectra were calculated by subtraction of data recorded under illumination and the averaged data recorded prior to illumination in the dark. If required, data were corrected for baseline drifts using the “spoc” software package for GNU Octave developed by Dr. Eglof Ritter (Humboldt University Berlin).

# 2.2 FTIR spectroscopy

## 2.2.1 Introduction

Above ~ 800 nm wavelength – the upper limit of the UV-Vis region – photon energy is usually not sufficient to promote electronic transitions but instead provides energy for vibrational and rotational motions based on the selection rule $\overrightarrow{|M_{01}|} > 0$. The infrared region reaches from ~ 800 nm to ~ 1 mm wavelength and is divided further into different subregions. At usual temperatures on earth, heat radiation exhibits its highest intensity in the mid-infrared region (~ 3–50 µm) due to the excitation of molecular vibrations. In infrared spectroscopy, wavenumber $\tilde{\upsilon}$ [cm$^{-1}$] is typically used instead of wavelength $\lambda$ ($\tilde{\upsilon} = \lambda^{-1}$).

A linear (angled) molecule with N atoms has 3N – 5 (3N – 6) vibrational degrees of freedom. If $\overrightarrow{|M_{01}|} > 0$, these modes can be excited with infrared light providing $\Delta E = h\nu = E_{v1} - E_{v0}$. $\Delta E$ can be approximated by treating the vibrational mode as an harmonic oscillator:

$$\Delta E = \frac{h}{2\pi}\sqrt{k\mu^{-1}} \cdot \left(n + \frac{1}{2}\right)$$

with Planck`s constant h ($6.63 \cdot 10^{-34}$ Js), binding constant k, reduced mass $\mu = m_1 m_2/(m_1+m_2)$ and vibrational energy level n. The probability for vibrational transitions decreases with n. Nevertheless, overtones can interfere with fundamental frequencies of different oscillators, *e.g.* Fermi resonance, thereby challenging the assignment of vibrational modes.[178,179] The harmonic oscillator model shows that the vibrational frequency is positively correlated with k and negatively correlated with µ. The binding constant mainly depends on the bond strength (increasing from single to triple bonds) and the respective vibrational mode (*e.g.* stretching or bending mode). Furthermore, it is sensitive to the molecular environment. The amide I and amide II modes – vibrational modes of the peptide bonds highly relevant for infrared spectroscopy on proteins – can serve as an example: The amide I mode is mainly caused by C=O stretching (ν(C=O)) vibrations with minor contributions of out-of-phase CN stretching, CCN deformation and NH in-plane bending (Fig. 2-2). The amide II mode is primarily

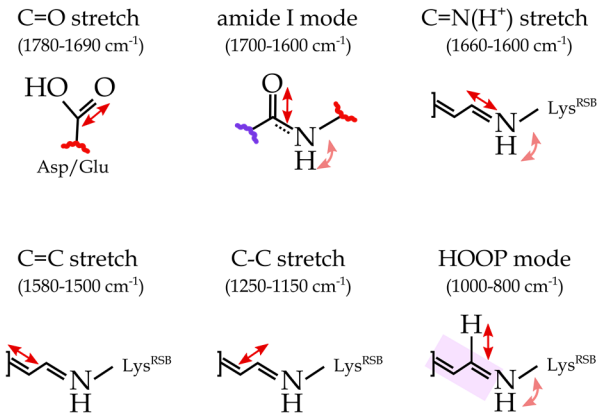


**Fig. 2-2** Important vibrational modes of retinal binding proteins used in FTIR difference spectroscopy.

an out-of-phase combination of the NH in-plane bending and the CN stretching vibration with minor contributions from the CO in-plane bending along with CC and NC stretching vibrations.[180] While amide I modes typically arise between 1700–1600 cm$^{-1}$, amide II modes are comparably downshifted to 1580–1480 cm$^{-1}$ according to the weaker bond strength. Amide I modes are highly sensitive to the secondary structure of proteins, because of altered hydrogen bonding of the peptide C=O groups.[180,181]

The activation of proteins coincides with structural changes involving the secondary structure as well as amino acid side groups. The overall structure, though, remains unaltered so that the activation-induced alterations are comparably small. For that reason, light ($I_l$)–dark ($I_d$) difference spectra (Fig. 2-3) are calculated to obtain the difference in absorption, $\Delta A$.

$$\Delta A = -\lg\left(\frac{I_l}{I_d}\right)$$

By this approach, small structural rearrangements become visible. The most important vibrational modes for this thesis are the above-mentioned amide I modes, the C=O stretching modes of aspartic and glutamic acids, the C=N(H$^+$) stretching mode of the RSBH$^+$, and the C=C and C–C stretching modes as well as the HOOP modes of the retinal cofactor (Fig. 2-2). The basic approach for obtaining information on the induced structural changes is exemplified for the C=O stretching mode of aspartic and glutamic acids (Fig. 2-3). These side groups are of particular interest for the infrared spectroscopy of proteins as the C=O stretching vibrations of protonated carboxylic groups arise in a spectral region (> 1690 cm$^{-1}$) that is not affected by other oscillators occurring in a protein.[182] Deprotonation of the carboxylic side group downshifts the vibrational frequency of the C=O stretch < 1500 cm$^{-1}$. If a COOH group deprotonates after activation, this will result in a negative mode in the spectral band region > 1690 cm$^{-1}$ and a positive mode < 1500

$cm^{-1}$ in the corresponding light – dark spectrum. Accordingly, protonation of a $COO^-$ group after activation will have the reverse effect. Hydrogen bonds typically lower the vibrational frequency of the C=O stretching mode by decreasing the C=O binding constant. Alterations of hydrogen bonds during a reaction are thus reflected by frequency changes, typically within the range of 1780 (no hydrogen bond) to 1690 $cm^{-1}$ (strong hydrogen bond(s)).[183] If the hydrogen bond(s) of a COOH group is (are) weakened after activation, this will result in one negative and one positive mode in the band region > 1690 $cm^{-1}$ of the corresponding light – dark spectrum, with the positive band at higher frequency. Accordingly, strengthening of the hydrogen bond(s) of a COOH group after activation will cause the opposite effect in this band area.

Usually, several COOH groups experience structural alterations within a reaction challenging the assignment of vibrational modes to distinct side groups. One possibility to improve assignability is the use of isotopes. Such experiments exploit the negative correlation of the vibrational energy with the mass of the oscillator. As an example, deuteration of an oscillator causes a frequency downshift of its vibrational modes. As H–D exchange requires transient proton release, deuteration typically occurs at polar O–H and N–H bonds such as in glutamic and aspartic acids. Furthermore, an oscillator can only be deuterated if it is in contact with the solution. Therefore, H–D exchange experiments can help to characterize the accessibility of oscillators to the solvent. The typical deuteration effect on the carboxylic group of an aspartic or glutamic acid is shown in Fig. 2-3. If the respective residue is in contact with the solvent and experiences H–D exchange, the corresponding vibrational mode will downshift, while a buried residue will not be affected. Deuteration effects can also be applied to characterize those vibrations occurring in the amide I region (1700–1600 $cm^{-1}$) that unlike the H–D insensitive amide I mode are H–D-sensitive.[182] To investigate oscillators other than polar X–H bonds, other isotope labels can be applied, *e.g.* $^{13}C$ and $^{15}N$. Most of the spectroscopic information on the dynamics of the retinal cofactor in BR was derived from the use of such labels by the fundamental research of Smith *et al.* 1984–85.[144,155,184] An enormous advantage of isotope labeling is the site-specificity that allows the precise assignment of a vibrational mode to a specific residue.

Another approach is the use of mutants that are introduced into the protein by site-directed mutagenesis. For example, removal of the carboxylic side group of aspartic and glutamic acids by mutation will abolish the corresponding C=O stretching modes if these are visible in the light – dark difference spectra. Of course, the specificity of mutations is limited and other vibrations are usually affected as well. Nevertheless, site-directed mutagenesis is the standard approach for the assignment of vibrational modes of amino acid residues and as well applied in this thesis.

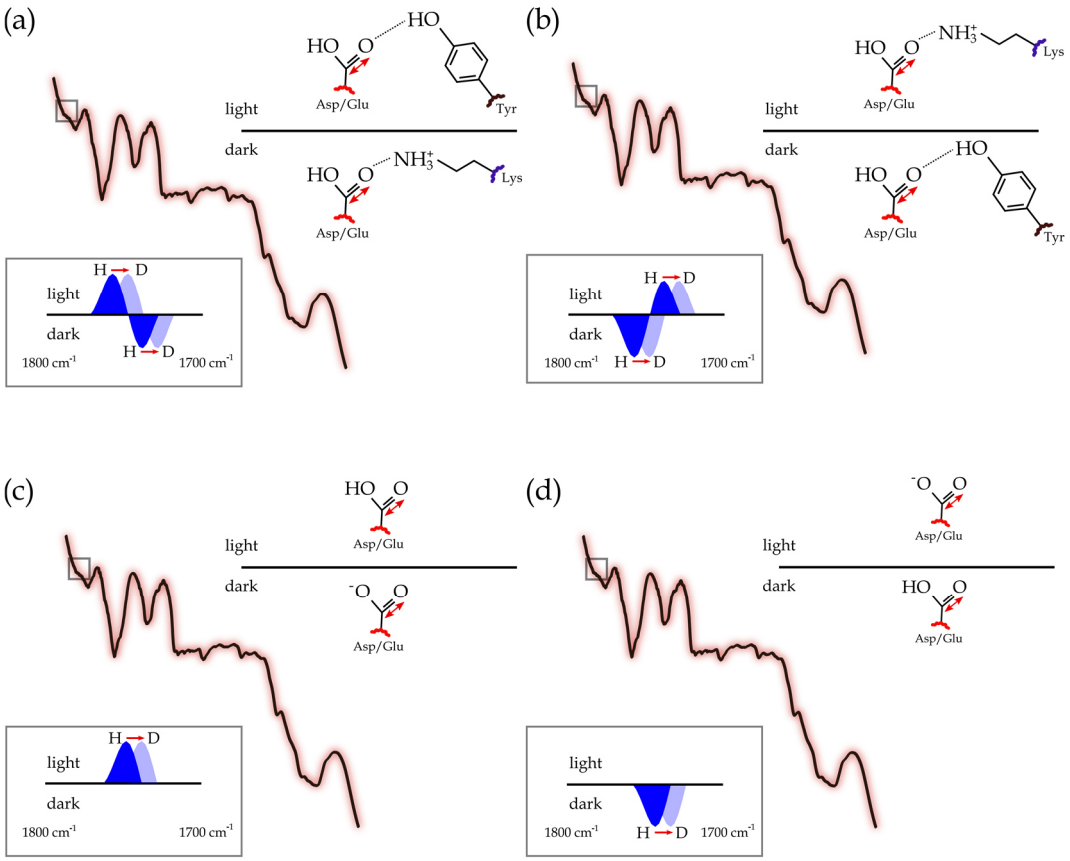


**Fig. 2-3** Manifestation of protonation changes in FTIR light – dark difference spectra calculated from transmission spectra. The C=O stretching vibration of aspartic and glutamic acids is observed in the region from 1780–1690 $cm^{-1}$, a spectral range with no further contribution of other vibrational modes typically arising in proteins. **(a)** Light-induced weakening of a hydrogen bond leads to a frequency upshift of the C=O vibration and a band pattern with an upshifted positive and a downshifted negative band in the difference spectrum. **(b)** Light-induced strengthening of a hydrogen bond has the opposite effect. **(c)** Light-induced protonation gives rise to a band in the C=O stretching region that was not observed in the dark and thus leads to a single positive band in the difference spectrum. **(d)** Light-induced deprotonation has the opposite effect. Furthermore, deuteration experiments can be applied to study water accessibility of the respective residues. If H–D sensitive, the bands typically undergo a spectral downshift (*light blue bands*).

Classical infrared techniques relied on dispersive elements to produce monochromatic light, requiring long recording times to obtain broad spectra. Fourier transform infrared (FTIR) spectroscopy allows significantly shorter recording times by using the Michelson interferometer (Fig. 2-4). In this compartment, the polychromatic light of the light source – in this thesis a globar was used for mid-infrared radiation – is split into two beams by a semitransparent mirror (beam splitter). One beam is directed to a stationary mirror and the other one to a mirror that moves back and forth with a constant frequency. The beams are reflected back to the beam splitter and interfere depending on the position of the moving mirror. After guided through the sample, the interferogram is collected by the detector. The interferogram obtained by polychromatic radiation is described by:

$$I(x) = \int_{-\infty}^{\infty} B(\tilde{v})\, cos(2\pi\tilde{v}x)\, dv$$

Herein, $I$ is the intensity at position $x$. The spectrum $B$ in dependence of the wavenumber $\tilde{v}$ is extracted by Fourier transformation:

$$B(\tilde{v}) = \int_{-\infty}^{\infty} I(x)\, cos(2\pi\tilde{v}x)\, dx$$

In practice, the maximum distance for the moving mirror is limited which leads to band broadening. Thus, the distance covered by the moving mirror correlates with spectral resolution. To correct for the limits defined by the interferometer, the interferogram is modified with truncation, *i.e.* limitation of the spectrum to

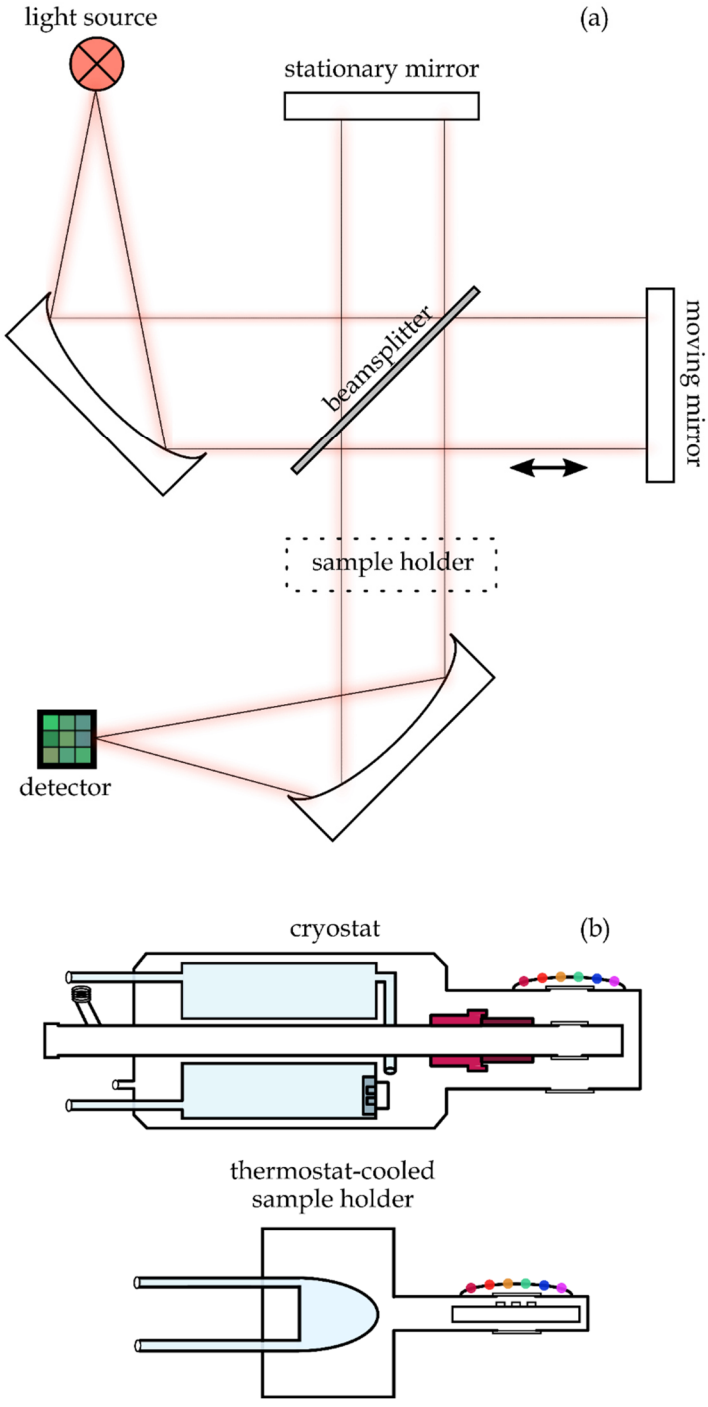


**Fig. 2-4** Setup for FTIR measurements. **(a)** Construction principle of an FTIR spectrometer with light source, Michelson interferometer and detector. **(b)** A sample holder can be placed into the beam path. In this thesis, a cryostat was used for measurements between 80–293 K and a thermostat-cooled sample holder for measurements at 293 K. Both sample holders were equipped with an LED ring placed around the aperture.

instrumental values from -L to L, and apodization by multiplying each value for $B(\tilde{\nu})$ that is < -L and > L by zero. The main advantages of FTIR over classical dispersive spectrometers are[185]:

(1) Jacquinot's advantage: With FTIR spectrometers, the use of slits can be avoided (being replaced by larger apertures). Thus, more light is guided through the sample, resulting in a better signal-to-noise ratio (SNR).
(2) Fellgett's advantage: FTIR allows the simultaneous recording of an entire spectrum so that significantly shorter recording times are required and the SNR is improved.
(3) Connes' advantage: The actual path difference between the stationary and the moving mirror is constantly read out by a HeNe laser so that the corresponding wavenumber is precisely determined leading to an improved spectral resolution.

### 2.2.2 Setup and methods

As described in[51,52] FTIR measurements were conducted using an ifs66v/s FTIR spectrometer (Bruker Optics, Karlsruhe, Germany). Only for measurements of the ReaChR wild type in $H_2O$ and $D_2O$ and the ReaChR-E163T mutant in $H_2O$ at pH 9 (pD 9.4) and 268 K (see Fig. 3-21, p. 83), a VERTEX 80v spectrometer (Bruker Optics) was used. Both spectrometers were equipped with an $LN_2$-cooled mercury cadmium telluride detector (Kolmar Technologies, Newburyport, USA). A 1850 $cm^{-1}$ optical cut-off filter was installed (with the exception of the measurements with the *p*-azido-L-phenylalanine (azF)-labelled ReaChR variants (see Fig. 3-19, p. 80) for which no filter was used). Spectra were recorded with a spectral resolution of 2 $cm^{-1}$. The FTIR measurements in this thesis were either conducted using a sample holder cooled by a thermostat (for measurements at 293.15 K) or the DN cryostat (for measurements from 80–293.2/293.3 K). For simplicity, the temperatures are rounded to the first pre-decimal position. Both thermostat and cryostat were equipped with an LED ring placed around the aperture, but the two setups differ with respect to the effective photon density at the sample. Sample preparation was conducted as described in 2.1.2 (p. 33). Samples prepared for use in the cryostat were stored at –40 °C between measurements, while the samples used in the thermostat-cooled sample holder were stored at 4 °C. As in UV-Vis spectroscopic measurements, samples investigated at cryostatic conditions were heated > 293 K between the measurements to allow thermal relaxation.

### 2.2.3 Data processing and analysis

#### 2.2.3.1 Basic data processing

If required, data were corrected for baseline drifts using the "spoc" software package (see 2.1.2, p. 33). Data averaging and smoothing as well as manual correction for baseline drifts were performed with the OPUS software (versions 6.0 and 6.5, Bruker Optics, Karlsruhe, Germany). Spectra were usually scaled to match the intensity of one of the prominent negative bands in the retinal fingerprint region of the reference spectrum at ~ 1230 $cm^{-1}$ and ~ 1200 $cm^{-1}$ that reflect depletion of the 13-*trans*,15-*anti* dark state.

#### 2.2.3.2 SVD, rotation procedure and global analysis

To evaluate the complexity of the underlying reaction, selected difference spectra were subjected to a singular value decomposition (SVD), followed by a rotation procedure and (if intended) a global analysis. These functions are implemented in the spoc software package. SVD is based on the concept that the original data matrix *M* consisting of spectra recorded at *n* times and *m* wavenumbers can be decomposed as follows[186]:

$$M = U \cdot S \cdot V^T$$

Here, the *m x m* matrix *U* contains the spectral and the *n x n* matrix $V^T$ the kinetic information. The *m x n* matrix *S* contains the singular values that reflect the significance of each component for *M*. The obtained data were then further processed using a rotation procedure introduced by Henry and Hofrichter 1992.[187] This procedure reduces the number of significant components by maximizing the autocorrelation function *C(V)* of *V* for some components, while reducing *C(V)* for others[186]:

$$C(V_i) = \sum_{j=1}^{n-1} V_{j,i} \cdot V_{j+1,i}$$

The results of the rotation procedure give a reliable estimate on the number of spectral components with distinct kinetics that contribute to *M*. In this thesis, this

evaluation method was used for investigating the reaction of ChRs to alternating illumination similar to Ritter *et al.* 2013.[101]

To obtain meaningful information on the actual kinetics of the underlying spectral components, data were further processed using a global analysis approach. Therefore, a second SVD was performed of the dataset obtained from the rotation procedure with a reduced number of components and the *V* matrix was fitted with a sum of exponential functions[186]:

$$T_{ij} = (1 - \exp(-k_i t_j)).$$

This fit yields time constants $k_i$ and amplitude *A*. Based on the fit, the so-called b-spectra given by the *B* matrix are obtained using the relation[186]:

$$M = B \cdot T^T.$$

*B* represents the spectral component described by a time constant $k_i$.

### 2.2.3.3 Determination of activation energy

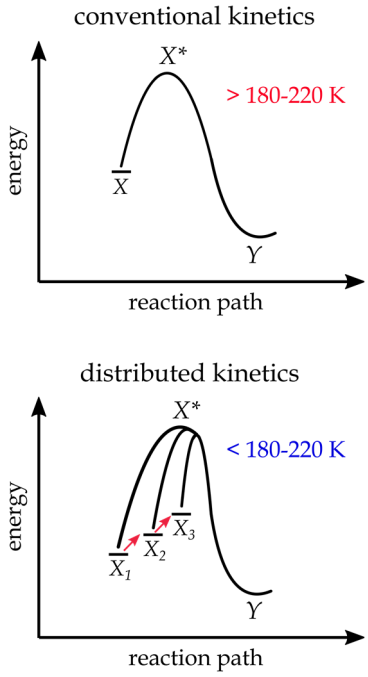


**Fig. 2-5** Reaction kinetics at ambient and cryo-temperatures. Below ~ 180–220 K, conformational substates of the educt with slightly different energy levels need to be considered for the determination of $E_a$.

The activation energy of a reaction is the energy that needs to be provided for a reaction to take place. According to transition state theory, a reaction $X \rightarrow Y$ with $\Delta G_{XY} < 0$ passes through a transition state $X^*$ with $\Delta G_{XX^*} > 0$. The Arrhenius equation describes $\Delta G_{XX^*}$ as activation energy $E_a$:

$$k = A \cdot \exp\left(\frac{-E_a}{RT}\right)$$

with a material-specific constant *A* and the gas constant *R* (≈ 8.31 J/ (mol·K). To obtain $E_a$, the time constant of the $X \rightarrow Y$ reaction needs to be determined at various temperatures. $E_a$ can then be directly yielded from the Arrhenius plot ($ln\, k$ vs. $T^{-1}$). Below a certain temperature between ~ 180–220 K, however, the different conformational substates $X_i$ (*e.g.* rotamers) contributing to *X* need to be taken

into consideration for the calculation of activation energies (Fig. 2-5). $\Delta G_{XiX(i+j)}$ is so small that the substates $X_i$ equilibrate to a single apparent state $X$ at temperatures $\gtrsim$ 220 K. To account for the parallel reactions $X_i \rightarrow Y$ at cryo-conditions, an empirical equation was introduced by Austin *et al.*[188]:

$$N(t) = (1 + \frac{t}{t_0})^{-n}$$

As parallel reactions $X_i \rightarrow Y$ will result in slightly different activation energies, an energy spectrum is obtained instead of a single $E_a$. The mean activation energy is given by the intercept on the ordinate of a plot of

$$RT \cdot ln(\frac{n}{t_0})$$

requiring the determination of $t_0$ and $n$ at various temperatures. This evaluation approach is based on the assumptions that (i) no reaction other than $X_i \rightarrow Y$ is observed and that (ii) $X_i \rightarrow Y$ is an irreversible reaction. In this thesis, the described method was used to evaluate the effect of the Ci1 protonation state on the chromophore relaxation of ReaChR so that $X_i$ is identical with the photoproduct with a distorted chromophore, while $Y$ represents the photoproduct with a relaxed chromophore (see 3.2.2.5, p. 70).

## 2.3 Retinal extraction and HPLC analysis

To analyze the isomeric composition of retinal binding proteins, the specific retention times of the different retinal isomers through a column can be exploited. Therefore, retinals must be extracted from the protein and then loaded into a high performance liquid chromatography (HPLC) device. Retinal extraction involves protein denaturation and subsequent dissolution of the retinal into the running buffer used for the HPLC run. For the experiments presented in this thesis, the following protocol was used as described in[51]: Chromophore extraction was achieved by addition of ice-cold ethanol. After 2 min, the extracted retinal was dissolved in heptane containing 6.5–7% diethyl ether (w/w). Prior to phase separation by centrifugation (1 min, 2000 rpm) the sample was incubated for 2 min. All working steps, except sample illumination, were conducted under dim red light and at room temperature. Separation of the retinal isomers in the heptane/ diethyl ether mixture was performed using an LC-20AD HPLC device (Shimadzu, Kyoto, Japan) equipped with a ReproSil 70 Si, 5 µm column (Dr. Maisch, Ammerbuch-Entringen, Germany). The chromatograms were corrected for baseline-drifts and the retinal isomer ratio was determined by band integration or fitting using the OPUS 6.5 software.

## 2.4 Biological samples

### 2.4.1 Molecular biology

Proteins were designed, expressed and purified by cooperation partners of the Hegemann group at the Humboldt University Berlin* and of the Institute of Medicinal physics and biophysics at Charité** Berlin.

C1C2 samples were provided by Katja Stehfest*, Christina Schnick* and Brian Bauer**. Sample preparation was performed according to Hontani *et al.* 2017[44] and Bruun *et al.* 2015[96]. C1C2 was expressed and purified from *P. pastoris* and stored in 20 mM TRIS-HCl containing 100 mM NaCl and 0.05 % (w/v) n-dodecyl β-D-maltoside (DDM) adjusted to pH 8.

ReaChR samples were provided by Benjamin Krause*, Thi Bich Thao Nguyen* and Anja Koch**. Samples used in FTIR experiments were either produced in HEK293 cells or in *P. pastoris* according to Krause *et al.* 2017[51] FTIR light – dark difference spectra of ReaChR-wt from HEK293 cells and *P. pastoris* did not exhibit distinct deviations (see Fig. S2). For retinal extraction and subsequent HPLC analysis only samples from *P. pastoris* were used. ReaChR *p*-azido-L-phenylalanine (azF) mutants were provided by Benjamin Krause* and produced according to Krause *et al.* 2019.[53] Samples were stored in Dulbecco's phosphate buffered saline (DPBS) buffer containing 0.03 % (w/v) DDM.

Chrimson samples were provided by Johannes Vierock* and Thi Bich Thao Nguyen*. Sample preparation was performed according to Vierock *et al.* 2017.[39] (*Cs*)Chrimson, a construct of *Chlamydomonas noctigama* ChR[38] and the N-terminal fragment from *Chloromonas subdivisa* ChR[39] (in the following termed 'Chrimson'), was expressed and purified from *P. pastoris* and stored either in 20 mM Citrate buffer containing 100 mM NaCl and 0.03 % (w/v) DDM adjusted to pH 5 or in 20 mM 2-[4-(2-hydroxyethyl)piperazin-1-yl]ethanesulfonic acid (HEPES) buffer containing 100 mM NaCl and 0.03 % (w/v) DDM adjusted to pH 6.5.

### 2.4.2 Buffer exchange

Repeated buffer exchange of stock solutions for pH or deuteration experiments was performed using centricons (GE Healthcare, Chalfont St Giles, UK) with > 2 buffer exchange steps. For deuteration, > 4 buffer exchange steps were carried out.

## 2.5 Further materials

### 2.5.1 Buffers

The buffers used in this thesis were provided by cooperation partners or prepared by the author with deionized water. For $D_2O$ buffers, pD was adjusted using DCl and/ or NaOD by assuming $pD = pH + 0.4$ according to [189,190].

(1) TRIS buffer: 20 mM TRIS-HCl, 100 mM NaCl. Used for measurements at pH 8 (C1C2) and pH 9 (ReaChR).
(2) DPBS buffer: 2.7 mM KCl, 136.9 mM NaCl, 10.0 mM $Na_2HPO_4$, 2.0 mM $KH_2PO_4$. Used for measurements at pH 7.4 (ReaChR). DPBS buffer in $D_2O$ (pD 7.8) was prepared with the same compounds with the exception of $D_2O$, leading to a slight contamination with hydrogen by $Na_2HPO_4$ and $KH_2PO_4$.
(3) HEPES buffer: 20 mM HEPES, 100 mM NaCl. Used for measurements at pH 6.5 (Chrimson).
(4) Citrate buffer: 20 mM citrate, 100 mM NaCl. Used for measurements at pH 4 (C1C2) and pH 5 (Chrimson, ReaChR). Citrate buffer in $D_2O$ was adjusted to pD 4.4 (C1C2) and pD 5.4 (Chrimson), respectively.

# 3 Results

## 3.1 The blue-absorbing C1C2 chimera

C1C2 is the first ChR of which a crystal structure was obtained.[41] The photocycle of C1C2 comprises photointermediates closely similar to those known from the best-studied ChR *Cr*ChR2 with intermediates K, M and N. In the D→K transition, $Asp^{DC}$ and probably E3 (see Fig. 1-5, p. 10) experience a weakening of their hydrogen bonds. E3 deprotonates prior to formation of M. In the M intermediate in which the $RSBH^+$ is deprotonated, major backbone rearrangements have occurred in conjunction with water influx during formation of the ion conducting pore. Formation of N involves deprotonation of $Asp^{DC}$ at pH 8, while it remains protonated at pH 4. Its mutation to asparagine has a strong impact on the isomeric composition of the chromophore, favoring the incorporation of isomers other than 13-*trans* retinal.

Key residues in chapter 3.1 (C1C2 nomenclature, see Fig. 1-5, p. 10)

Ci1, counter-ion 1 (Glu162); Ci2, counter-ion 2 (Asp292); E3, central gate residue Glu129; $Asp^{DC}$, binding pocket residue Asp195; $Lys^{CI}$, lysine of the extended counter-ion complex (Lys132)

### 3.1.1 The photocycle intermediates

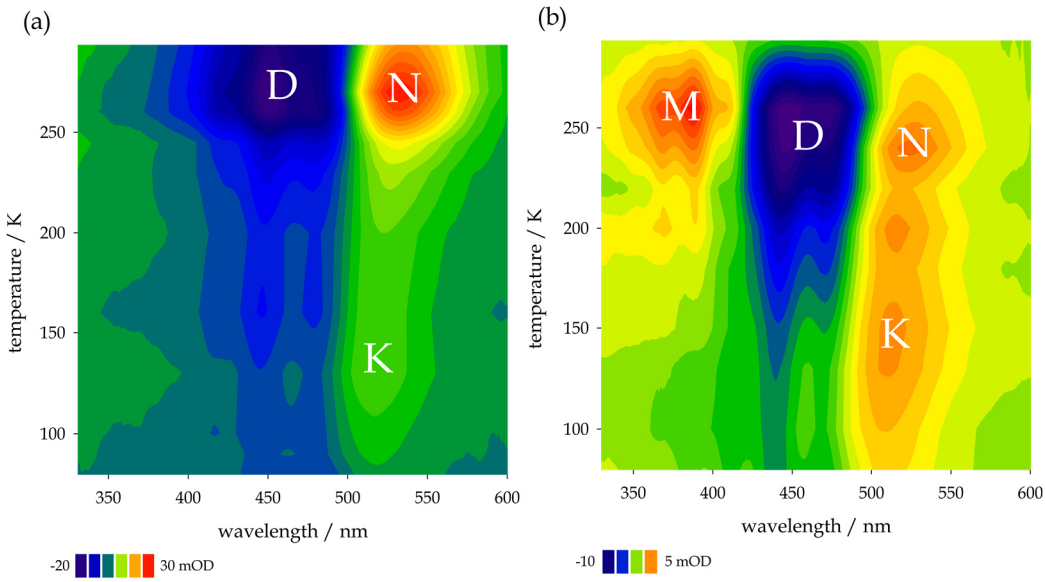


**Fig. 3-1** The photocycle of C1C2. UV-Vis light – dark difference spectra were recorded between 80 and 293 K at pH 4 (**a**) and pH 8 (**b**) yielding K, M and N intermediates at alkaline pH and K and N at acidic pH, hinting at a pH dependent equilibrium between M and N. Illuminations were conducted with blue LEDs ($\lambda_{max}$ ~ 471 nm) following ≥ 30 min in the dark at ≥ 293 K between measurements.

To investigate the photocycle of C1C2, UV-Vis difference spectra were recorded at pH 4 (Fig. 3-1a) and pH 8 (Fig. 3-1b) at different temperatures between 80 and 293 K. At both pH values, a red-shifted K intermediate is accumulated below 200 K. At temperatures above 200 K, both M and N are populated at pH 8, while no M is observed at pH 4, showing that M and N are in a pH dependent equilibrium as already described for *Cr*ChR2.[31] A recent model for the photocycle of C1C2 included (i) an L intermediate that precedes M, similar to ReaChR[51], and was not observed in the cryostatic measurements presented here, and (ii) an O state whose absorbance maximum is similar to D.[44]

| | $D_{app}$ (wild type) | $D_{app}$ (D195N) | $D_{IDA}$ (D195N) |
|---|---|---|---|
| 13-*cis* | 27.1 ± 1.4 | 31.7 ± 1.3 | 24.6 ± 2.1 |
| 11-*cis* | 1.2 ± 0.7 | 8.0 ± 1.1 | 9.9 ± 1.6 |
| 9-*cis* | n.d. | 10.1 ± 0.6 | 18.7 ± 2.5 |
| 7-*cis* | n.d. | n.d. | 3.0 ± 3.0 |
| 13-*trans* | 71.7 ± 1.4 | 49.8 ± 2.2 | 43.8 ± 5.0 |

**Tab. 1** Isomeric composition of the retinal in C1C2 wild type and the $Asp^{DC}$ mutant D195N at pH 8, revealed by retinal extraction and subsequent HPLC. Measurement conditions for $D_{app}$: 10 min blue light ($\lambda_{max}$ ~ 471 nm), 30 min dark. $D_{IDA}$: 10 min blue light ($\lambda_{max}$ ~ 471 nm), overnight in the dark. Equilibration was conducted at ambient temperature. HPLC runs are shown in Fig. S4.

Previous electrophysiological and spectroscopic investigations on ChRs suggested the presence of two parallel photocycles, with the retinal in 13-*trans*,15-*anti* (D) conformation in the dark state of the main branch as opposed to 13-*cis*,15-*syn* (D') in the side

branch.[51,96,101] While such a discrimination of main and side branch is not possible based on the static UV-Vis spectra in Fig. 3-1, it is supported by retinal extraction and subsequent HPLC analysis (Tab. 1). According to this analysis, $D_{app}$ (D + D') of the wild type contains 13-*trans* and 13-*cis* isomers in a ratio of roughly 70:30 similar to *Cr*ChR2 and *Ca*ChR1.[99,100] Interestingly, the amount of 13-*trans* is reduced to ~ 50 % in the $Asp^{DC}$ mutant D195N mutant in favor of 13-*cis*, 11-*cis* and 9-*cis* isomers. These distinctions are even more pronounced after dark adaptation overnight ($D_{IDA}$) with a further reduction of 13-*trans* and a significant increase of 9-*cis* retinal. A similarly strong effect on the isomeric composition was previously observed for the DC pair mutant *Cr*ChR2-C128T.[101]

### 3.1.2 The D→K transition

The early structural rearrangements following the initial photoreaction were investigated by FTIR difference spectroscopy at 80 K (Fig. 3-2). Bands at 1233(-), 1204(-) and 1190(+) $cm^{-1}$ in the spectrum of the wild type at pH 8 (Fig. 3-2a) reflect retinal isomerization of the 13-*trans*,15-*anti* dark state to the 13-*cis*,15-*anti* photoproduct.[42] The positive vibrational mode at 1190 $cm^{-1}$ is a typical feature of the early photoproduct in microbial rhodopsins and, in particular, indicates that the retinal is in 15-*anti* rather than 15-*syn* conformation.[144] The weakening of the $RSBH^+$ counter-ion interaction in the D→K transition is probably responsible for the pronounced band at 1662(-) $cm^{-1}$ that is assigned to the υ(C=$NH^+$) vibration of the $RSBH^+$.[42] In the υ(C=O) region (> 1690 $cm^{-1}$), vibrational modes reflect alterations of aspartic and glutamic acids (Fig. 3-2b). Two band patterns at

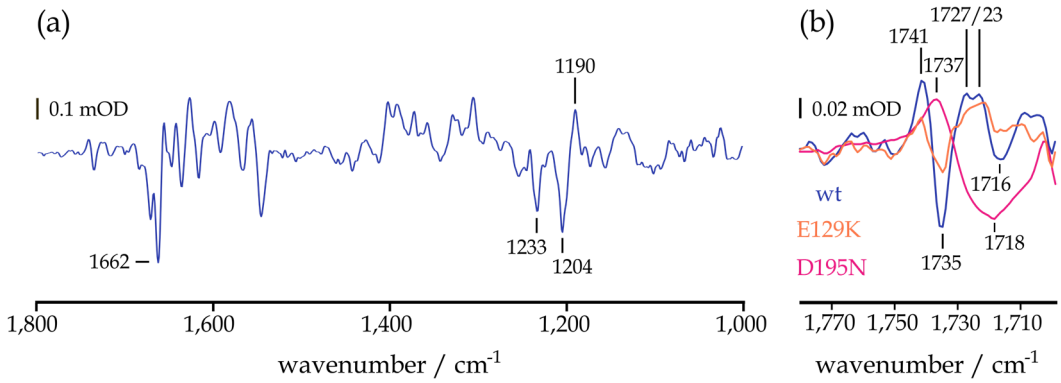


**Fig. 3-2** FTIR light – dark difference spectra at 80 K, trapping the D→K transition. **(a)** shows the difference spectrum of C1C2-wt at pH 8. **(b)** shows the υ(C=O) region of difference spectra of the wild type and mutants of E3 (E129K) and $Asp^{DC}$ (D195N). Illuminations were conducted with blue LEDs ($\lambda_{max}$ ~ 471 nm) following ≥ 30 min in the dark at ≥ 293 K. Spectra were scaled to bands in the retinal fingerprint region of the wild type difference spectrum (for details see 2.2.3.1, p. 41).

1741(+)/ 1735(-) and 1727/23(+)/ 1716(-) $cm^{-1}$ are seen. The first pattern is also observed in D→K spectra of *Cr*ChR2[31,81,103] and was assigned to a hydrogen bond change of $Asp^{DC}$.[42] Indeed, the band pattern is significantly altered in the $Asp^{DC}$ mutant, D195N, that instead gives rise to a positive vibrational band at 1737 $cm^{-1}$ and a broad negative band at 1718 $cm^{-1}$. This observation can be interpreted in two ways: (i) a frequency downshift of the pattern at 1741(+)/ 1735(-) $cm^{-1}$ and overlay with a pattern not affected by deuteration at 1727/23(+)/ 1716(-) $cm^{-1}$ or (ii) lack of the pattern at 1741(+)/ 1735(-) $cm^{-1}$ and rise of a new band pattern at 1737(+)/1718(-) $cm^{-1}$ due to unknown structural alterations in the $Asp^{DC}$ mutant. Only the second interpretation allows the assignment of the pattern at 1741(+)/ 1735(-) $cm^{-1}$ to a hydrogen bond change of $Asp^{DC}$ as the band pattern is vanished in the asparagine mutant Given the overall similarity of the D→K spectra between C1C2 and *Cr*ChR2[31,103], the second interpretation is favored. The comparably weaker band pattern at 1727/23(+)/ 1716(-) $cm^{-1}$ was observed only in some but not all K minus D difference spectra of *Cr*ChR2[81,103], presumably due to the small signal intensity. In the E129K mutant, the negative band at 1716 $cm^{-1}$ is reduced, while the positive counterpart is comparably less affected by the mutation, hinting at other oscillators also contributing to this band. Nevertheless, the mutational effect could support an assignment of the pattern at 1727/23(+)/ 1716(-) $cm^{-1}$ to a weakening in the hydrogen bond between E3 and an unknown bonding partner as proposed for *Cr*ChR2.[47]

## 3.1.3 Formation and decay of the ion-conducting state

### 3.1.3.1 pH dependence of photocycle transitions

The K intermediate is followed by M and N (see Fig. 3-1, p. 48). It was proposed that an L intermediate is present in C1C2 as well[44] but L might be obscured in the cryostatic measurements (see Fig. 3-1, p. 48) as presumably its absorption maximum is only slightly shifted with respect to D. For C1C2, formation of the open state was not assigned to a specific intermediate so far. In *Cr*ChR2, the open state is established within the late M intermediate and persists in N.[98,123,157] According to UV-Vis spectra obtained at 260 K, both M (387 nm) and N (529 nm) are accumulated at pH 8, as opposed to N only at pH 4 (533 nm, Fig. 3-3). The accumulation of N is reflected by a large positive band at 1535 $cm^{-1}$ based on the correlation of υ(C=C) vibrations with the UV-Vis absorption of the chromophore.[132,191] Accordingly, the bands at 1553/ 1551(-) $cm^{-1}$ at both pH values reflect depletion of the dark state that is blue-shifted as compared to N. Strong negative bands in the amide I region at 1662/ 1659 $cm^{-1}$ are well-known features

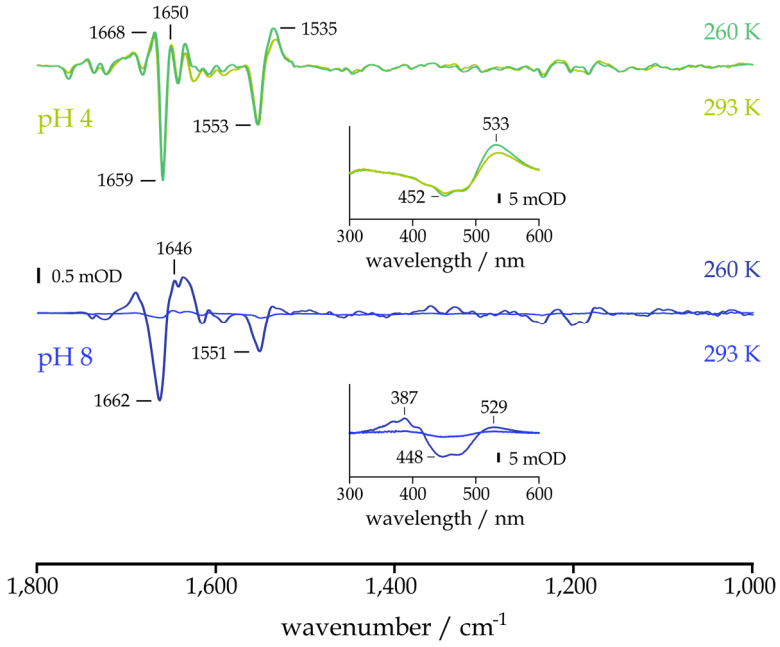


**Fig. 3-3** FTIR light – dark difference spectra of C1C2-wt at 260 K and 293 K and pH 4 and 8, respectively. The *insets* show light – dark UV-Vis difference spectra at the respective temperatures revealing that at 260 K and pH 4, N is accumulated (533 nm), and still present at 293 K. At 260 K and pH 8, M (387 nm) and N (529 nm) are both present, while only small light-induced transitions are observed at 293 K. Illumination was conducted with blue LEDs ($\lambda_{max}$ ~ 471 nm) following ≥ 30 min in the dark at ≥ 293 K. The spectrum at pH 4 and 260 K was scaled to retinal fingerprint bands of the spectrum at pH 8 and 260 K, and the spectrum at pH 4 and 293 K was multiplied by the same scaling factor. The spectrum at pH 8 and 293 K was not scaled and its significantly reduced intensity as compared to 260 K indicates that the photocycle is decisively faster at pH 8.

for formation of the ion-conducting state in *Cr*ChR2 or *Ca*ChR1[31,103,104,158] and were explained by helix hydration due to water influx in the open state conformation[157]. According to this concept, the positive bands at 1650/ 1646 $cm^{-1}$ reflect the altered vibrational frequencies of the hydrated helices in the putative conducting state, and the 4 $cm^{-1}$ frequency shift as well as the intensity difference hints at pH dependent alterations in the water content of the open pore. In addition, a positive band at 1668 $cm^{-1}$ is present at acidic pH that is not observed at pH 8, indicating further distinctions in the assumed open state conformation.

### 3.1.3.2 Protonation changes during formation of the open state

The open state FTIR difference spectra obtained at acidic and alkaline pH at 260 K (see Fig. 3-3, p. 51) exhibit different vibrational bands in the υ(C=O) region reporting on protonation changes of glutamic and aspartic acids. At pH 8 (Fig. 3-4a), two negative bands are present at 1738 and 1723 $cm^{-1}$. In *Cr*ChR2, the band at 1738(-) $cm^{-1}$ was assigned to deprotonation of $Asp^{DC}$.[104,192] This assignment is confirmed by the lack of this band in the $Asp^{DC}$ mutant D195N. Notably, in the spectra of this mutant the vibration at 1723(-) $cm^{-1}$ is vanished as well, similar to a previous FTIR spectroscopic investigation on $Asp^{DC}$.[43] The mode at 1723(-) $cm^{-1}$ is assigned to deprotonation of E3 as indicated by its lack in the E129K mutant without an additional effect on the band at 1738(-) $cm^{-1}$, similar to previous observations.[43] The effect of $Asp^{DC}$ mutation on the protonation dynamics of E3 hints at a difference between C1C2 and *Cr*ChR2, in which $Asp^{DC}$ neutralization (D156A) did not have an influence on the band of deprotonated E3.[104] At pH 4 (Fig. 3-4b), the band pattern is drastically altered with bands arising at 1764(-) and 1743(+) $cm^{-1}$. Upon H–D exchange, the mode at

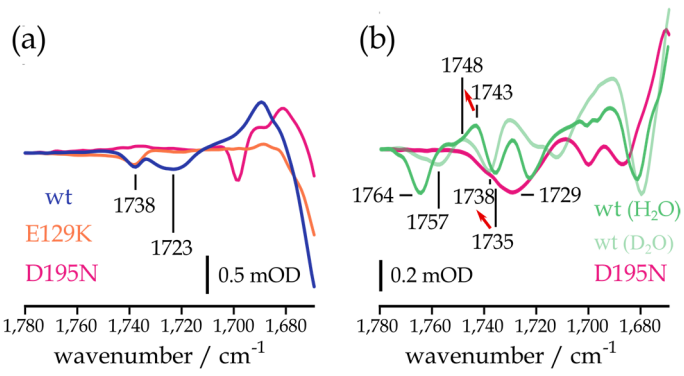


**Fig. 3-4** The υ(C=O) region of difference spectra of **(a)** C1C2 wild type and mutants of E3 (E129K) and $Asp^{DC}$ (D195N) at pH 8 and **(b)** C1C2 wild type in $H_2O$ and $D_2O$ and the D195N mutant at pH 4. Illumination was conducted with blue LEDs ($\lambda_{max}$ ~ 471 nm) at 260 K following ≥ 30 min in the dark at ≥ 293 K. Spectra were scaled to retinal fingerprint bands in the C1C2 wild type spectra in $H_2O$. *Red arrows* indicate frequency upshift in $D_2O$.

1764(-) $cm^{-1}$ is downshifted to 1757(-) $cm^{-1}$ indicating that this band represents deprotonation of a COOH group. Bands at 1743(+) and 1735(-) $cm^{-1}$ are moderately upshifted in $D_2O$ to 1748(+) and 1738(-) $cm^{-1}$. Such a frequency upshift in $D_2O$ is unusual, but was described before for $Asp^{DC}$ in *Cr*ChR2.[192] Thus, this effect supports the assignment of the 1743(+)/ 1735(-) $cm^{-1}$ band pattern to a light-induced weakening in the hydrogen bonding of $Asp^{DC}$, suggesting that unlike at pH 8 $Asp^{DC}$ does not deprotonate at pH 4. The band assignment is further confirmed by the fact that this band pattern is vanished in the $Asp^{DC}$ mutant that instead caused a pronounced negative band at 1729(-) $cm^{-1}$ and affected other bands as well.

### 3.1.3.3 Deprotonation dynamics of $Asp^{DC}$ and E3

In order to elucidate in which state of the photocycle $Asp^{DC}$ and E3 deprotonate, the following experimental approach was applied: A mixture of M and N was produced by blue illumination of the wild type at pH 8. Additional UV illumination was applied to deplete M and increase the contribution of N. Switching from UV to green reversed this effect, increasing M at the expense of N. The increase and decrease of N were tracked by the kinetics of the band at

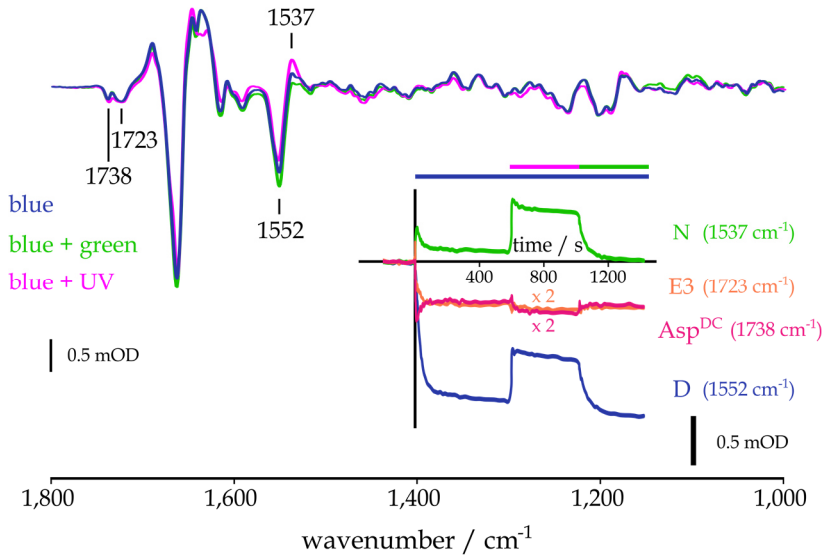


**Fig. 3-5** Deprotonation dynamics of $Asp^{DC}$ and E3 revealed by wavelength-dependent marker band kinetics. Blue light ($\lambda_{max}$ ~ 471 nm) was applied to the C1C2 wild type at pH 8 to induce a mixed state of M and N as shown in Fig. 3-3 (p. 51). Additional UV light ($\lambda_{max}$ ~ 405 nm) was used to remove M out of the mixed state and accumulate N, and green light ($\lambda_{max}$ ~ 529 nm) was applied for the inverse effect. The corresponding FTIR light – dark difference spectra are shown *above* and the marker band kinetics for D (1552 $cm^{-1}$), N (1537 $cm^{-1}$), $Asp^{DC}$ (1738 $cm^{-1}$) and E3 (1723 $cm^{-1}$) are shown *below*. Illuminations were conducted following ≥ 30 min in the dark at ≥ 293 K.

1537(+) $cm^{-1}$ and the dark state depletion by the band at 1552(-) $cm^{-1}$ based on the correlation of υ(C=C) vibrations with the UV-Vis absorption of the chromophore (Fig. 3-5).[132,191] The N marker band (1537(+) $cm^{-1}$), in contrast to D, runs through a transient peak after the beginning of blue illumination, is increased by simultaneous blue and UV illumination and decays to zero during simultaneous illumination with blue and green light. The marker band for $Asp^{DC}$ deprotonation (1738 $cm^{-1}$) follows this trend exhibiting a transient minimum during blue illumination and increased intensity during additional UV illumination. During combined blue and green illumination, intensity decreases again. The fact that the $Asp^{DC}$ marker does not decay to zero as the N marker band could be due to impaired reprotonation at 260 K. The correlation of $Asp^{DC}$ deprotonation with formation and decay of the N intermediate suggests that $Asp^{DC}$ deprotonates in the M→N transition, similar to *Cr*ChR2.[104] Contrarily, the marker band for E3 deprotonation (1723 $cm^{-1}$) correlates with the depletion kinetics of D and is hardly affected by additional UV or green illumination, suggesting that E3 deprotonation occurs in the K→M transition, similar to earlier assumptions for *Cr*ChR2 by Kuhne *et al.* 2015[47] that described a key role of this residue for formation of the ion-conducting pore.

More recently, though, Kuhne *et al.* 2019[98] proposed that deprotonation of E3 occurs in conjunction with a transition from the 13-*trans*,15-*anti* to the 13-*cis*,15-*syn* dark state. According to this concept, 13-*trans*,15-*anti* and 13-*cis*,15-*anti* conformations of the retinal would stabilize protonated E3, while 13-*cis*,15-*syn* along with its assumed photoproduct 13-*trans*,15-*syn* would stabilize deprotonated E3. If this concept held true for C1C2 as well, an impact of E3 mutation (E129K) on the 15-*anti*↔15-*syn* equilibrium could be assumed that should be reflected by alterations in the retinal fingerprint region between mutant and wild type spectrum. However, a comparison of the respective difference spectra shows that this is not the case (Fig. 3-6): The fingerprint bands at 1239(-), 1235(-), 1201(-) and 1188(-) $cm^{-1}$ are not significantly affected by mutation of E3 so that an effect on the 15-*anti*↔15-*syn* equilibrium is rather unlikely.

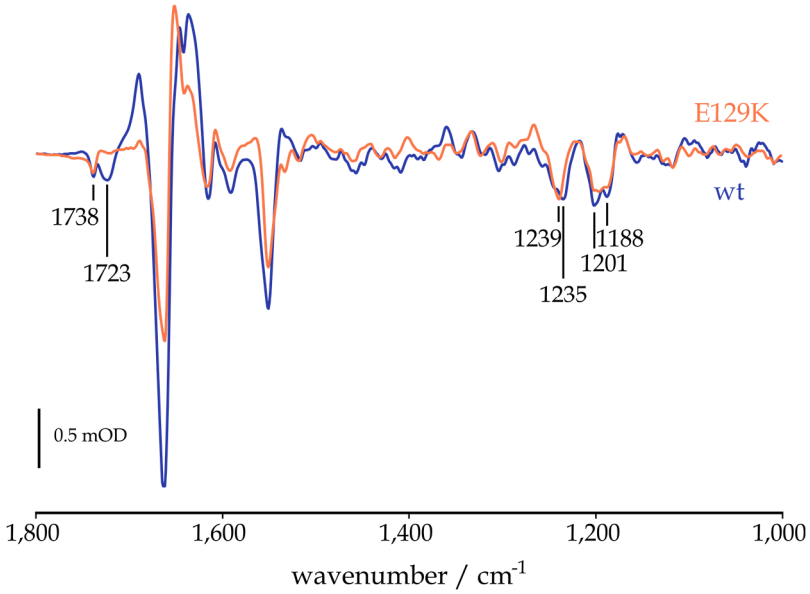


**Fig. 3-6** FTIR light – dark difference spectra of the C1C2 wild type and the E3 mutant E129K at 260 K and pH 8, revealing that the mutation does not have a strong effect on the retinal fingerprint region, supporting the concept that E3 deprotonates within the 15-*anti* cycle. Based on Fig. 3-4 (p. 52), the band at 1738 $cm^{-1}$ is assigned to deprotonation of $Asp^{DC}$ and the band at 1723 $cm^{-1}$ to deprotonation of E3. Illumination was conducted with blue LEDs ($\lambda_{max}$ ~ 471 nm) following ≥ 30 min in the dark at ≥ 293 K. Spectra were scaled to retinal fingerprint bands in the wt spectrum.

## 3.1.4 Discussion

### 3.1.4.1 Summary

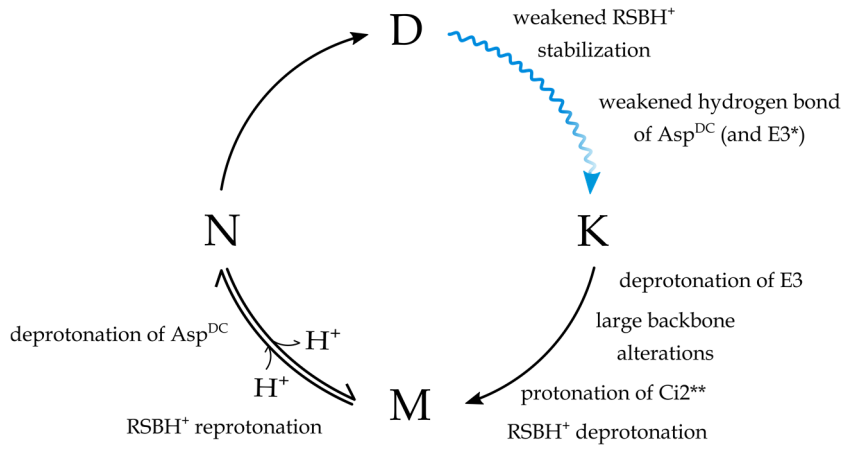


**Fig. 3-7** Simplified photocycle scheme of C1C2. The molecular alterations refer to the apparent photointermediates as it was not possible to distinguish between reactions specific for 15-*anti* and 15-*syn* retinal, respectively. *unclear result (see Fig. 3-2, p. 49). **not observed in this thesis, assumed as Ci2 is the primary proton acceptor in *Cr*ChR2.[104]

The presented photocycle model (Fig. 3-7) is largely based on the UV-Vis spectroscopic measurements at cryostatic conditions (see Fig. 3-1, p. 48). This scheme is a simplification as previous investigations on *Cr*ChR2 have revealed two photocycle branches with the retinal either in 15-*anti* or 15-*syn* conformation.[96,98,101] The HPLC data presented here (see Tab. 1, p. 48) support this concept since at low light conditions (dim-red light), a mixture of 13-*trans* and 13-*cis* retinal is formed in C1C2 as well.

As it was not possible to disentangle the specific photoreactions of either of the photocycle branches, the structural alterations and proton transfer processes refer to the apparent photocycle intermediates of both photocycles K, M, and N, shown in Fig. 3-7. However, the significantly larger contribution of the 15-*anti* photocycle branch to the observable photoreaction suggests that the structural alterations occur at least in the 15-*anti* cycle while it is unclear whether they occur in the 15-*syn* cycle as well. In the D→K transition, $Asp^{DC}$ (and probably E3) experience a weakening in hydrogen bond strength. E3 deprotonates in the K→M transition. Formation of the ion-conducting state involves large changes in the backbone structure that are presumably due to the influx of water molecules and are more intense at alkaline pH. Only small additional changes occur in the M→N

transition, involving the deprotonation of $Asp^{DC}$ at pH 8 that is blocked at pH 4. Mutation of $Asp^{DC}$ to asparagine had a strong effect on the isomeric composition.

#### 3.1.4.2 Deprotonation of E3 and formation of the ion-conducting state

The main structural alterations required for formation of the open state occur in the K→M transition, while only small additional changes take place in the transition from M to N (see Fig. 3-5, p. 53). In analogy to *Cr*ChR2, it is assumed that the late M intermediate in C1C2 is already conductive[123,157] and that the major backbone changes precede the opening of the ion channel[47,101,157].

A key role for channel formation in *Cr*ChR2 was earlier attributed to deprotonation of E3 (see Fig. 1-5, p. 10).[47] However, there is an ongoing debate at which stage of the photocycle this deprotonation event actually occurs. The main interpretations are:

(1) Deprotonation of E3 occurs in the early transitions of the 15-*anti* cycle, prior to formation of the conducting pore.[47]
(2) Deprotonation of E3 occurs during formation of the late P intermediate of the 15-*anti* cycle, after closure of the conducting pore.[104]
(3) Deprotonation of E3 occurs after the transition from 13-*trans*,15-*anti* to 13-*cis*,15-*syn* by retinal double isomerization.[97,98]

Concept (2) must be excluded for C1C2 as the deprotonation of E3 occurs before formation of M and N (see Fig. 3-5, p. 53). Concept (3) appears rather unlikely as the E3 mutant does not affect the isomeric composition of the light-adapted state as can be derived from the similarity of the retinal fingerprint region in the E3 mutant and the wild type (see Fig. 3-6, p. 55). If E3 deprotonation would specifically occur during or after the photoreaction from D to D′ as suggested by Kuhne *et al.* 2019[98] for *Cr*ChR2, preventing this process by mutation of E3 to lysine (E129K) would be expected to have a significant influence on the isomeric composition of the illuminated state. As this is not the case, it is more likely that in C1C2 E3 deprotonates in the K→M transition of the 15-*anti* cycle. Of course, this does not exclude the possibility that E3 deprotonates in the 15-*syn* cycle as well.

In order to understand why the deprotonation dynamics of E3 might differ between C1C2 (presumably deprotonating in both the 15-*anti* cycle and the 15-*syn* cycle) and *Cr*ChR2 (deprotonating exclusively in the 15-*syn* cycle[98]), the impact of E3 mutations on the photocurrents in both ChR variants should be considered: Kuhne *et al.* 2019[98] showed by electrophysiological measurements that E3 mutation (E90Q) in *Cr*ChR2 abolishes the conductance of the proton-selective open state of the 15-*syn* cycle ($P^*_{520}{}^{N}$) while only reducing the conductance of the late open state of the 15-*anti* cycle ($P_{520}{}^{N}$) which together with findings from FTIR spectroscopy and MD simulations led to the conclusion that E3 deprotonation occurs only in this branch of the photocycle. To the best of the author's knowledge, a similar electrophysiological analysis for C1C2 that would allow conclusions on the role of E3 for the different open states of the 15-*anti* and 15-*syn* cycles is not available. However, previous electrophysiological investigation hints at crucial differences of the role of E3 between *Cr*ChR2 and C1C2 as it showed that mutations of E3 in C1C2 (E129A and E129Q) significantly decreased the selectivity for $Ca^{2+}$ as compared to the wild type (and E129Q slightly decreased the selectivity for $K^+$), while they did not affect the proton selectivity[41] in contrast to the respective mutants in *Cr*ChR2[88]. Additionally, both E129A and E129Q resulted in moderately delayed off-kinetics of the photocurrents[41] as compared to the C1C2 wild type, while the E90Q mutant of *Cr*ChR2 decayed faster than the wild type at single-turnover conditions[98].

The different effects of E3 mutations in *Cr*ChR2 and C1C2 on ion selectivity could be the result of its different orientations: While protonated E3 is oriented toward the active site in the dark state of *Cr*ChR2, it instead forms a hydrogen bond to Asn258 in C1C2 (see Fig. 1-5, p. 10).[41,72] Presumably, the deprotonated E3 obtained after light activation forms a salt bridge in *Cr*ChR2 that establishes a narrow constriction site in the middle of the pore favoring the passage of protons over larger cations. Based on the dark state structure and MD simulations, $Lys^{CI}$ (see Fig. 1-5, p. 10) is the likely counter-ion to deprotonated E3 in *Cr*ChR2.[47,72] Contrarily, deprotonated E3 in C1C2 probably leads to a rather widened central gate geometry so that the passage of larger cations ($K^+$, $Ca^{2+}$) is facilitated.[41]

Deprotonation of E3 in C1C2 cannot be considered crucial for formation of the ion-conducting state, as the E3 mutants, E129A and E129Q, only moderately affected current amplitude and channel opening and closing kinetics.[41] An electrophysiological investigation of the E129K mutant is not available to the best of the author's knowledge, but it is expected to have similar consequences as the previously characterized E129R mutant as both mutations introduce positive charges to the central gate; C1C2-E129R exhibits decreased photocurrents as compared to the wild type and only partial $Cl^-$ conductivity[193] which is in contrast to the homologous mutation in *Cr*ChR2 that created an anion-selective channel with robust photocurrents.[67] This deviation gives a further hint at different roles of E3 in C1C2 and *Cr*ChR2.

A light-induced frequency downshift of the typical amide I modes in *Cr*ChR2 difference spectra from ~ 1660(-) to ~ 1645(+) $cm^{-1}$ was assigned to helix hydration during formation of the pre-conducting pore.[157] A similar frequency downshift is observed in C1C2 at alkaline pH. At acidic pH, though, the negative amide I band is significantly narrowed and a frequency upshift is observed with a band arising at 1668 $cm^{-1}$ (see Fig. 3-3, p. 51). Although further investigations are required to confirm this hypothesis, in particular by performing measurements in $H_2{}^{18}O$ as in the work of Lórenz-Fónfría *et al.* 2015[157], this observation implies that the water content in the open state depends on the pH with a significantly higher water content at alkaline pH. A possible explanation is that at acidic pH restriction sites against water influx could be – at least partially – maintained, while being abolished in the conducting state at alkaline pH. This would agree well with the fact that ChRs at acidic pH conduct more protons than at alkaline pH that - without hydration shell - are small enough to pass through a narrow restriction site.

#### 3.1.4.3 Deprotonation of $Asp^{DC}$

At pH 8, $Asp^{DC}$ deprotonates in the M→N transition (see Fig. 3-5, p. 53). This is similar to observations on *Cr*ChR2 that were the basis for the identification of $Asp^{DC}$ as the proton donor for reprotonation of the RSB.[104] The assumed proton donor function is challenged by the long distance (> 9 Å) between the presumed donor and acceptor groups[41,72] and by the fact that $Asp^{DC}$ mutants that abolished

the carboxylic side groups maintained robust ion channel function in several studies[52,67,83,85,169]. Nevertheless, the protonation state of $Asp^{DC}$ might affect the p$K_a$'s of the RSB and its counter-ions by a putative chromophore interaction network as characterized in 1.2.4.3. (p. 22), involving $Cys^{DC}$ and Thr166. By such an interaction, $Asp^{DC}$ could drive the reprotonation of the RSB in a more indirect fashion. Such a long-range effect of $Asp^{DC}$ becomes as well evident in the fact that the $Asp^{DC}$ mutant blocks E3 deprotonation or renders it deprotonated already in the dark (see Fig. 3-4, p. 52). Furthermore, $Asp^{DC}$ has a strong influence on the isomeric composition of the dark state, as the D195N mutant gave rise to isomers other than 13-*trans*-retinal (see Tab. 1, p. 48). It appears likely that this alteration is functionally relevant, but unfortunately, electrophysiological measurements are lacking to date. Given the overall high sequence homology of C1C2 to *Cr*ChR2, an unusual electrophysiological behavior of the D195N mutant can be expected: the respective mutant D156N in *Cr*ChR2 did not exhibit the typical photocurrent shape with a peak and a transient photocurrent.[82]

## 3.2 The red-activatable channelrhodopsin ReaChR

The *Vc*ChR1 variant ReaChR combines robust photocurrents with a bathochromically shifted absorption maximum rendering it a promising tool for optogenetic applications. The red-shifted absorption is partially caused by an increased p$K_a$ of Ci1 (see homologous residues of C1C2, Fig. 1-5, p. 10). The p$K_a$ of Ci1 is also relevant for the photoreaction: With deprotonated Ci1, the 13-*trans*,15-*anti*→13-*cis*,15-*syn* photoreaction by double isomerization that occurs in parallel to the single isomerization to 13-*cis*,15-*anti* retinal is enhanced as compared to the configuration with protonated Ci1. In the early K intermediate of the 13-*cis*,15-*anti* photoproduct, the chromophore is distorted, thereby storing energy of light absorption. Enhanced hydrogen bonding of protonated Ci1 stabilizes the distorted chromophore geometry by creating a more rigid active site, while it is comparably less stabilized in the configuration with deprotonated Ci1. E3 undergoes a hydrogen bond change in the D→K transition and deprotonates prior to formation of the conducting state. In the L→M transition, Ci2 receives the $RSBH^+$ proton. M decays via two pathways, M→N (main branch) and M→D (side branch). Side branching is achieved by a proton transfer from Ci2 back to the $RSBH^+$. $Asp^{DC}$ deprotonates in the M→N transition. Its mutation to asparagine has a strong impact on the isomeric composition of the chromophore, favoring the incorporation of isomers other than 13-*trans* retinal.

Key residues in chapter 3.2 (ReaChR nomenclature):

Ci1, counter-ion 1 (Glu163); Ci2, counter-ion 2 (Asp293); E3, central gate residue Glu130; $Asp^{DC}$, binding pocket residue Asp196; $Lys^{CI}$, lysine of the extended counter-ion complex, Lys133

### 3.2.1 The photocycle intermediates

Prior to the presentation of the data obtained by the author, relevant information on the photocycle of ReaChR by complementary methods is briefly reviewed based on Krause *et al.* 2017[51] and Kaufmann *et al.* 2017[52] and the Ph.D. dissertation by Benjamin Krause 2018[194]: Flash photolysis experiments revealed that the photocycle of ReaChR comprises the photointermediates K, L, $M_1$ and $M_2$, N and P. P was originally termed O[51,52] according to the BR nomenclature but considering its significantly slower decay kinetics (in the order of tens of seconds[51] as compared to O in BR that decays in the order of milliseconds[195]), a different terminology is used in this thesis, similar to Szundi *et al.* 2015.[166,167] After light-induced isomerization, K is formed within ns. K is followed by L, that is blue-shifted as compared to the dark state. L is present in the BR photocycle[144] and was recently observed in the photocycle of C1C2 as well[44]. Deprotonation of the $RSBH^+$ leads to formation of M. Due to its biexponential decay, two separate intermediates, $M_1$ and $M_2$, were assumed.[51] In the FTIR experiments presented in this thesis, $M_1$ and $M_2$ could not be distinguished and presumably both contribute to the M intermediate. Reprotonation of the RSB gives rise to the N intermediate. At physiological pH, N was not observed, presumably due to spectral overlap with the dark state. At acidic and alkaline pH, N is observed so that its formation is assumed for the wild type at pH 7.4 as well.[51] $M_2$ and N were identified as conducting states. N decays to the non-conducting P intermediate. The time

| | wt (pH 5) | wt (pH 9) | wt (pH 7.4) | E130Q (pH 7.4) | E163T (pH 7.4) | D293N (pH 7.4) | D196N (pH 7.4) |
|---|---|---|---|---|---|---|---|
| K→L | 1.72 µs | 391 ns | 1.01 µs | | 455 ns | 452 ns | |
| K→M | | | | 971 ns | | | 1.87 µs |
| L→M | 201 µs | 7.13 µs | 10.8 µs | | 18.8 µs | 245 µs | |
| M→M | | | | 8.69 µs | | | 87.1 µs |
| M→N | 570 ms | 5.49 ms | 6.54 ms | 10.4 ms | 8.54 ms | 12.7 ms | 263 ms |
| N→P | > 10 s | 101 ms | 151 ms | 92.3 ms | 16.7 ms | 22.9 ms | 4.42 s |
| P→D | | 6.25 s | > 10 s | 7.77 s | 2.99 s | 6.35 s | |

**Tab. 2** Half-life times of photocycle transitions of ReaChR wild type at pH 5, pH 7.4 and pH 9 and mutants of E3 (E130Q), Ci1 (E163T), Ci2 (D293N) and $Asp^{DC}$ (D196N) by Krause 2018[194], p. 133, 146, 149 and 152, obtained by fitting sequential reaction models to flash photolysis data. Note that the number of components was adjusted to the respective dataset and that only one M intermediate was considered, with the exception of E130Q and D196N, for which an M→M transition was included into the reaction scheme.

constants for photocycle transitions for the wild type at various pH conditions as well as for selected mutants are given in Tab. 2, derived from global analysis of flash photolysis experiments using a sequential reaction scheme (Krause 2018[194]). Note that the time constants for the wild type at pH 7.4 deviate from Kaufmann *et al*. 2017[52] with a half-life time of 6.54 ms for the M→N transition instead of 151 ms. Note as well that the applied fitting model involves only one M intermediate instead of $M_1$ and $M_2$, with the exception of E130Q and D196N, for which an M→M transition was included into the reaction scheme.

As a starting point for a detailed FTIR spectroscopic analysis, the photocycle of ReaChR was investigated at cryogenic conditions by UV-Vis spectroscopy for different temperatures between 80 and 293 K (Fig. 3-8a). The contour plot reveals that the K-state is accumulated < 200 K, whereas L is the dominant photoproduct > 200 K. Depletion of D is indicated by the negative absorption band. K and L are maximally populated at 150 and 240 K, respectively. The FTIR difference spectra recorded at the respective temperatures reflect changes concomitant with K and L formation, respectively Fig. 3-8b. While a detailed discussion will follow in later sections, two main aspects should be highlighted at this point: First, a pronounced hydrogen out-of-plane (HOOP) mode is observed at 968(+) $cm^{-1}$ in K that reflects

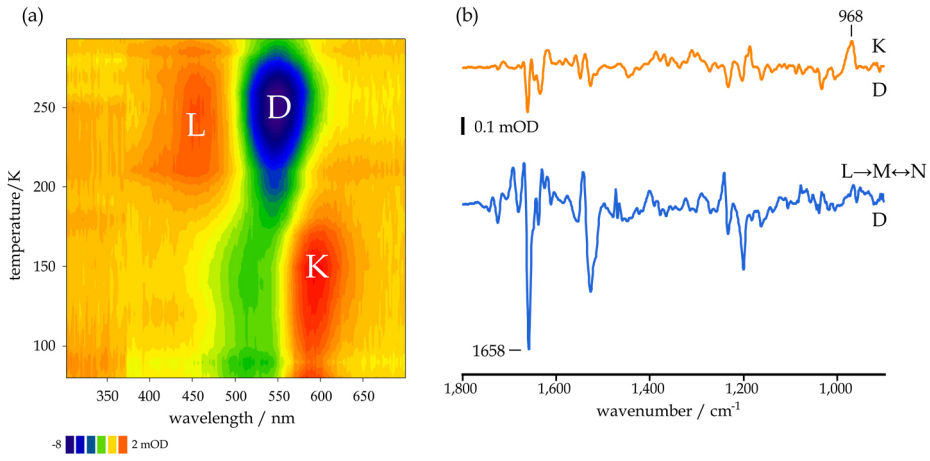


**Fig. 3-8** The photocycle of ReaChR. **(a)** UV-Vis light – dark difference spectra were recorded between 80 and 293 K, indicating the accumulation of two photoproducts, K and L, at continuous illumination conditions. **(b)** FTIR light – dark difference spectra recorded at 150 K and 240 K indicate the structural rearrangements occurring during formation of K and L in comparison with the dark state. FTIR spectroscopic investigation as presented in the following reveals that the steady state spectrum at 240 K contains contributions of M and N in addition to L (discussed in detail in 3.2.3.1, p. 74). Illuminations were conducted with green LEDs ($\lambda_{max}$ ~ 529 nm) following ≥ 30 min in the dark at ≥ 293 K between measurements. Spectra were scaled to the amide I region in absolute spectra.

a distorted chromophore.[144,196] The lack of this band in L indicates relaxation of the chromophore following K. Second, major backbone rearrangements occur in the K→L transition, as indicated by the strong band at 1658(-) $cm^{-1}$, reflecting preformation of the ion-conducting pore. Note that the spectrum at 240 K also contains contributions of the M and N intermediates as will be discussed in 3.2.3.1. (p. 74).

## 3.2.2 The D→K transition

### 3.2.2.1 pH dependent formation of the early K intermediate

In most rhodopsins, the first photoproduct that can be stabilized with $LN_2$-cooling at 80 K is a red-shifted K-like intermediate. In ReaChR at pH 7.4, K is maximally accumulated at 150 K (see Fig. 3-8a, p. 63) and comparably less pronounced at 80 K. In Fig. 3-9, FTIR difference spectra are shown for the wild type at pH 5, 7.4 and 9 at 80 K. In the υ(C=C) chromophore region (1580–1500 $cm^{-1}$), negative bands arise at 1527, 1528 and 1541 $cm^{-1}$ at pH 5, 7.4 and 9, respectively. These bands correlate with UV-Vis absorption (535 nm at pH 5, 527 nm at pH 7.4 and 503 nm at pH 9[51]) as demonstrated earlier for BR[191] and *Cr*ChR2[132]. The pH dependence of the UV-Vis absorption is due to a protonation change of Ci1 that exhibits a p$K_a$ of 7.6 in ReaChR, in contrast to 5.4 in C1C2.[a] The strong similarity of the υ(C=C) bands at pH 5 and pH 7.4 reflects that Ci1 is mainly protonated at pH 7.4. Note that the p$K_a$ obtained in solution[a] might slightly differ from the p$K_a$ in the FTIR sample, mainly due to changes in ionic strength during sample preparation (see 2.1.2., p. 33). This would explain why the positions of the dark state marker bands are largely identical between the samples at pH 5 and pH 7.4. Beyond that, most

[a] Data by Benjamin Krause, Humboldt University Berlin. Included in: Kaufmann *et al.* Energy transfer from chromophore to protein is modulated by the protonation state of a glutamic acid in the active site of channelrhodopsin. Manuscript in preparation for resubmission.

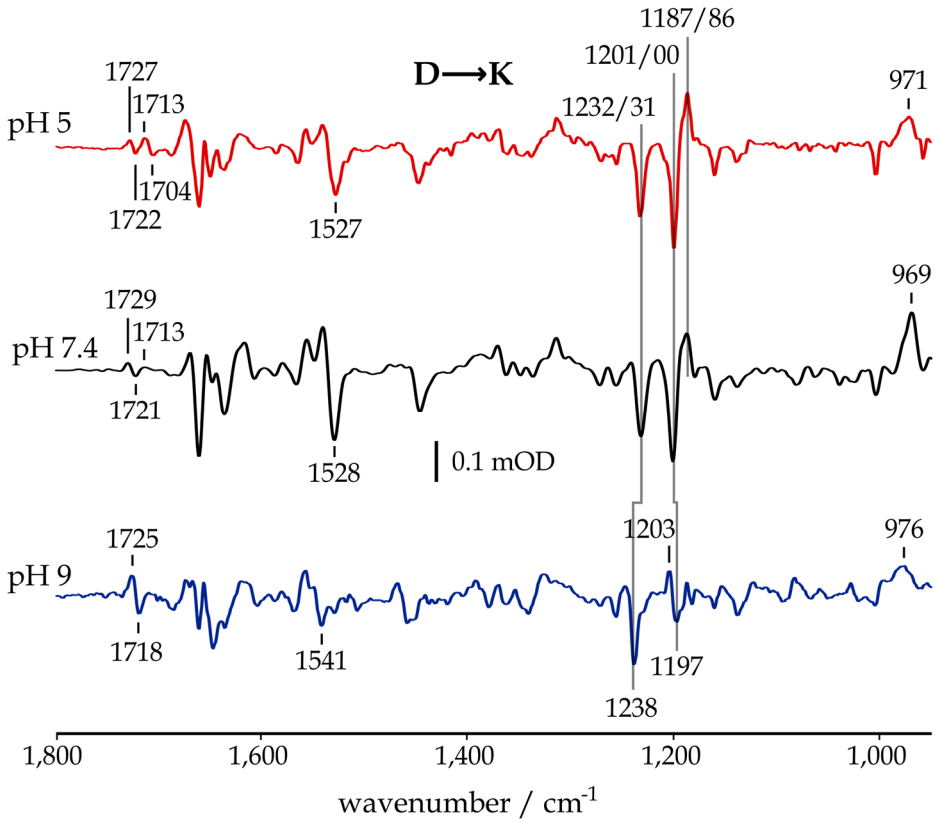


**Fig. 3-9** FTIR light – dark difference spectra of ReaChR-wt at pH 5, pH 7.4 and pH 9 recorded at 80 K, trapping the D→K transition (see Fig. 3-8, p. 63). Illuminations were conducted with green LEDs ($\lambda_{max}$ ~ 529 nm) following ≥ 30 min in the dark at ≥ 293 K. Spectra were scaled to retinal fingerprint bands of the difference spectrum at pH 7.4 (for details see 2.2.3.1, p. 41).

band features at pH 7.4 are similar to pH 5 and different to pH 9, hinting at a strong impact of Ci1 protonation on the spectra. Bands at 1232/31(-), 1201/00(-) and 1187/86(+) $cm^{-1}$, observed at physiological and acidic pH reflect *trans→cis* isomerization of a 13-*trans*,15-*anti* chromophore (D).[99] The positive band at 1187/86 $cm^{-1}$ is assigned to υ($C_{14}$–$C_{15}$) and υ($C_{10}$–$C_{11}$) vibrations of 13-*cis*,15-*anti*-retinal.[42,197,198] At pH 9, the band at 1232/31(-) $cm^{-1}$ is upshifted by 6 $cm^{-1}$ and the band at 1187/86(+) $cm^{-1}$ is not observed. The intensity of the band at 1197(-) $cm^{-1}$ is reduced, mostly due to an overlap with a positive band peaking at 1203(+) $cm^{-1}$. The strong alteration of the υ($C_{14}$–$C_{15}$) mode of the 13-*cis* photoproduct hints at a substantially different $RBSH^+$-counter-ion interaction in the configuration with deprotonated Ci1 as obtained at pH 9. Further pH effects on the chromophore geometry are observed in the HOOP band region with bands at 971 (pH 5), 969 (pH 7.4) and 976 $cm^{-1}$ (pH 9). The HOOP band region has the highest intensity at physiological pH and the weakest at high pH. In the υ(C=O) region (> 1690 $cm^{-1}$) that is indicative for vibrations of glutamic and aspartic amino acids, two band

patterns at 1727(+)/ 1722(-) and 1713(+)/ 1704(-) $cm^{-1}$ are present at pH 5. In the difference spectrum at pH 7.4, a vibrational band pattern at 1729(+)/ 1721(-) $cm^{-1}$ is seen along with a positive band at 1713 $cm^{-1}$. A negative band near 1704 $cm^{-1}$ is not clearly observed. At pH 9, only one band pattern at 1725(+)/ 1718(-) $cm^{-1}$ is present.

### 3.2.2.2 Hydrogen bond changes in the D→K transition

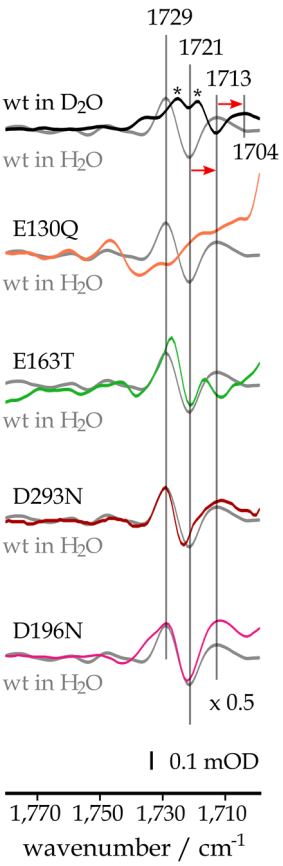


**Fig. 3-10** The υ(C=O) region of light – dark difference spectra of ReaChR-wt and mutants at pH 7.4 (pD 7.8) recorded at 80 K. Illumination was conducted with green LEDs ($\lambda_{max}$ ~ 529 nm) following ≥ 30 min in the dark at ≥ 293 K. Spectra were scaled to retinal fingerprint bands in the wild type spectrum in $H_2O$. *1725(+)/ 1719(+) $cm^{-1}$. *Red arrows* indicate frequency shifts in $D_2O$.

To characterize the bands arising in the υ(C=O) region, FTIR difference spectra of deuterated wild type and selected mutants were recorded at pH 7.4 and 80 K (Fig. 3-10). The band at 1721(-) $cm^{-1}$ observed in $H_2O$ is downshifted to 1713(-) $cm^{-1}$ after H–D exchange. Two additional positive bands arise at 1725 and 1719 $cm^{-1}$. These bands can be explained by an overlay of a positive band centered at around 1721 $cm^{-1}$ with the reduced negative vibration at 1721 $cm^{-1}$ that is observed in $H_2O$. This overlay is due to incomplete H–D exchange – also reflected by the reduced intensity of the negative band at 1713 $cm^{-1}$. The overlaid positive band at 1721 $cm^{-1}$ reflects downshift of the band at 1729 $cm^{-1}$ upon deuteration. The fact that both bands at 1729(+) and 1721(-) $cm^{-1}$ are downshifted in $D_2O$ to a similar extent suggests that they represent the same oscillator that undergoes a light-induced frequency upshift. This upshift suggests that the hydrogen bonding of the oscillator is weakened during the photoreaction.[183] The 1729(+)/ 1721(-) $cm^{-1}$ band pattern is not observed in the difference spectrum of the E130Q mutant, and therefore reflects an early hydrogen bond change of E3. In the D196N mutant this band pattern is increased. This could be due to a scaling error: scaling to bands in the fingerprint region is based on the assumption of a comparable dark state composition and photoreaction (for details see 2.2.3.2, p. 41). These conditions are

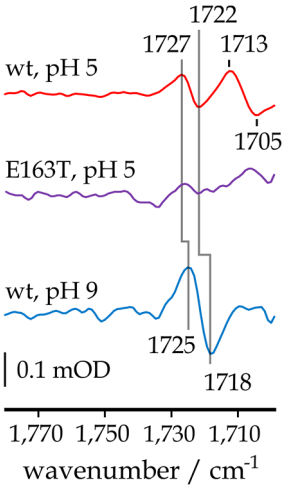


**Fig. 3-11** The υ(C=O) region of light – dark difference spectra of ReaChR-wt at pH 5 and 9 and the Ci1 mutant E163T at pH 5 recorded at 80 K. Illumination was conducted with green LEDs ($\lambda_{max}$ ~ 529 nm) following ≥ 30 min in the dark at ≥ 293 K ($\lambda_{max}$ ~ 529 nm). Spectra were scaled to retinal fingerprint bands in the wt spectrum at pH 9.

not given in the case of the D196N mutant as explained in detail later (see Tab. 3, p. 84). The positive band in the spectrum of the wild type at pH 7.4 at 1713 $cm^{-1}$ is downshifted by 9 $cm^{-1}$ in $D_2O$. This band pattern is most decisively altered by mutation of Ci1 (E163T) and E3 (E130Q). As E3 is already assigned to the vibrational pattern at 1729(+)/ 1721(-) $cm^{-1}$, the vibration at 1713 $cm^{-1}$ is most likely due to light-induced alteration of Ci1. A negative counterpart to this frequency is not clearly seen at pH 7.4. The band pattern is more clearly resolved in the spectrum of the wild type at pH 5, at which Ci1 is completely protonated, with distinct bands at 1713(+) and 1705(-) $cm^{-1}$ (Fig. 3-11). Given the lack of this band in the spectrum of the wild type at pH 9, at which Ci1 is deprotonated according to its p$K_a$ of 7.6 as well as in the spectrum of the Ci1 mutant E163T at pH 5, this band pattern can be unambiguously assigned to a hydrogen bond change of protonated Ci1. Given the active site structures of C1C2, *Cr*ChR2 and Chrimson (see Fig. 1-5, p. 10), the main candidates for the hydrogen bond partner of protonated Ci1 are the RSB nitrogen (as donor) and Ci2 (as acceptor).

### 3.2.2.3 Changes in the active site during the early D→K transition

The FTIR difference spectra at different pH conditions hint at a strong effect of the Ci1 protonation state on the retinal fingerprint region (see Fig. 3-9, p. 65). To confirm this hypothesis, the effect of Ci1 mutation for the D→K transition was investigated, along with mutations of other key residues (Fig. 3-12). Similar to the spectrum obtained at pH 9, Ci1 mutation (E163T) causes a frequency upshift of the retinal mode at 1231(-) $cm^{-1}$ observed in the wild type at pH 7.4 to 1236(-) $cm^{-1}$ and a reduction of the 1201(-)/ 1187(+) $cm^{-1}$ band pattern. This means that the υ($C_{14}$–$C_{15}$)/ υ($C_{10}$–$C_{11}$) vibration of the 13-*cis*,15-*anti* photoproduct is affected by both deprotonation and mutation of Ci1 in a similar fashion. Thus, the pH effect on these band features is not due to the additional charge provided by deprotonated

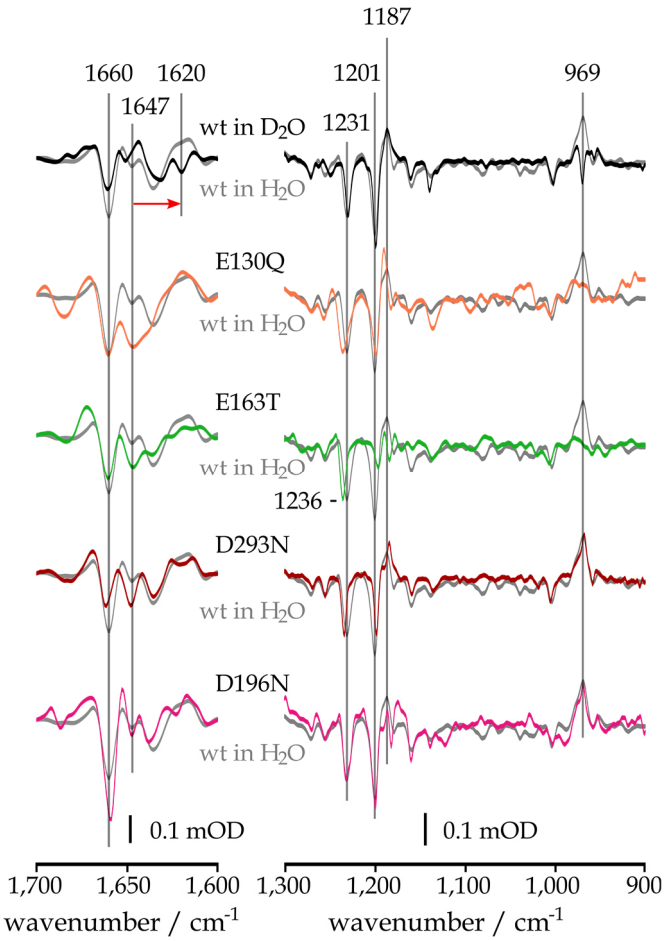


**Fig. 3-12** The amide I, υ(C–C) and HOOP region of light – dark difference spectra of ReaChR-wt and mutants at pH 7.4 (pD 7.8) recorded at 80 K. Illumination was conducted with green LEDs following ≥ 30 min in the dark at ≥ 293 K. Spectra were scaled to retinal fingerprint bands in the wild type spectrum in $H_2O$. *Red arrow* indicates shift in $D_2O$.

Ci1 at alkaline pH. Instead, both deprotonation and mutation of Ci1 must disturb an interaction that is present at conditions with protonated Ci1 in a similar fashion. Most likely, this is due to disruption of a hydrogen bond involving protonated Ci1. The similar consequences of Ci1 deprotonation and mutation are also reflected by the HOOP band region as Ci1 mutation as well as alkaline pH resulted in a reduced HOOP band. Mutation of E3 (E130Q) causes a similar reduction of the HOOP band vibration, presumably due to a decreased p$K_a$ of Ci1. A detailed analysis of the HOOP band region is conducted based on spectra recorded at 150 K (see Fig. 3-13, p. 69, and Fig. 3-14, p. 71). Light-induced structural alterations within the active site are also reflected by changes in the $RSBH^+$ υ(C=$NH^+$) vibration (Fig. 3-12).[199] In the wild type, two negative bands at 1660 and 1647 $cm^{-1}$ are observed that are reduced in $D_2O$. Additionally, a negative band arises at 1620 $cm^{-1}$ after H–D exchange. Notably, the band at 1647(-) $cm^{-1}$ is more pronounced in the mutants of the active site residues Ci1 and Ci2 and the neighboring E3. Both the absorption maximum of the UV-Vis spectrum and the H–D shift suggest an assignment of this band to the $RSBH^+$ vibration in the dark state. Its frequency of 1647 $cm^{-1}$ is similar to the respective mode in *Ca*ChR1 ($\lambda_{max}$ ≈ 519 nm[34], υ(C=$NH^+$) ≈ 1646 $cm^{-1}$ [79]) and rather different to the respective band in C1C2 ($\lambda_{max}$ ≈ 458 nm[24,200], υ(C=$NH^+$) ≈ 1665 $cm^{-1}$ [42]). The comparably low frequency

of the υ(C=NH⁺) vibration hints at a reduced stabilization of the positive charge located at the RSBH⁺ in the dark state, partially due to protonation of Ci1. The reduced electrostatic stabilization is the basis for the bathochromic shift of the UV-Vis spectrum.[201]

### 3.2.2.4 Changes in the active site during the late D→K transition

The effects of Ci1 deprotonation and mutation on the early photocycle indicate that at both conditions a hydrogen bond formed by the protonated Ci1 is disrupted. At 80 K, the HOOP bands were only weakly pronounced in the spectra of the wild type in $D_2O$ and the Ci1 mutant (see Fig. 3-12, p. 68). At 150 K, at which K is maximally populated (see Fig. 3-8, p. 63), these bands are more intense, allowing a more detailed analysis (Fig. 3-13). The HOOP band at pH 7.4 exhibits a maximum at 968 $cm^{-1}$ and a shoulder at ~ 976(+) $cm^{-1}$ and is composed of minimum three bands. H–D exchange gives rise to bands at 974(+), 963(+) and 953(+) $cm^{-1}$. The H–D sensi-tivity of the band at 953(+) $cm^{-1}$ suggests that it reflects the $C_{15}$-HOOP mode. This mode is typically deuteration-sensitive as it couples to N–H or N–D vibrations of the RSBH(D)⁺.[149] In BR, the $C_{15}$-HOOP band downshifts by 6 $cm^{-1}$ in $D_2O$[202], and by 7 $cm^{-1}$ in *Anabaena* sensory rhodopsin[111]. In C1C2 the strongest HOOP band peaks at 984(+) $cm^{-1}$ and downshifts by 9 $cm^{-1}$ in $D_2O$.[42] Ci1 mutation causes a significant reduction of the $C_{15}$-HOOP mode and the HOOP bands in general and leads to a frequency upshift by 12 $cm^{-1}$ to 980 $cm^{-1}$. As already observed at 80 K, the υ($C_{14}$–$C_{15}$) vibration of 13-*cis*,15-*anti*, reflected by the band at 1186(+) $cm^{-1}$, is reduced in the Ci1 mutant spectrum. The fact that E163T mutation and alkaline pH have similar effects on the $C_{15}$-sensitive bands in the fingerprint region supports the

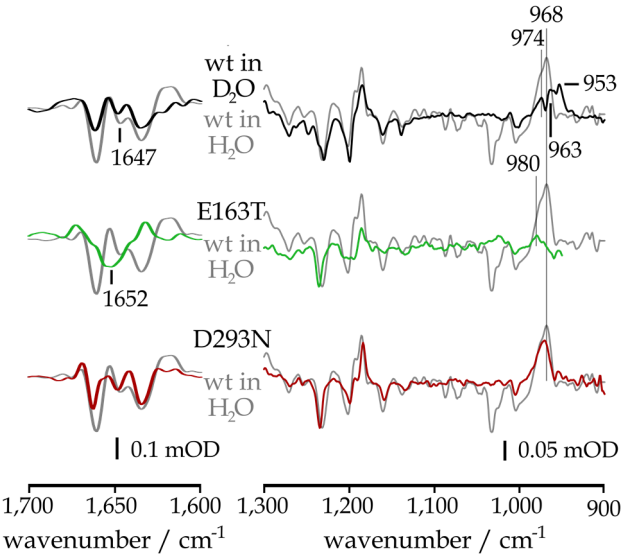


**Fig. 3-13** The amide I and υ(C–C) and HOOP region of light – dark difference spectra of ReaChR-wt and mutants at pH 7.4 (pD 7.8) recorded at 150 K. Illumination was conducted with green LEDs following ≥ 30 min in the dark at ≥ 293 K. Spectra were scaled to retinal fingerprint bands in the wt spectrum in $H_2O$.

hypothesis that at both conditions hydrogen bonding is affected that involves protonated Ci1 and is in short distance to $C_{15}$. Disruption or weakening of this hydrogen bonding influences the $RSBH^+$, as the υ(C=$NH^+$) band at 1647(-) $cm^{-1}$ is upshifted to 1652(-) $cm^{-1}$ in the Ci1 mutant.

#### 3.2.2.5 Energy transfer from chromophore to protein

Storage of the absorbed light energy in the chromophore is achieved by transient distortion of the retinal cofactor (strain energy) and/ or separation of the $RSBH^+$ counter-ion complex (electrostatic energy).[135,137,140,143] Chromophore distortions are reflected by HOOP bands.[203–205] In ReaChR, the HOOP bands appear to be dependent on the Ci1 protonation state, as they are reduced by both Ci1 deprotonation and mutation. However, this conclusion holds true only if the scaling to the retinal fingerprint region is correct. Scaling, though, is challenged by the fact that the vibrational modes used as reference are influenced by Ci1 deprotonation and mutation themselves. To overcome the scaling problem, the kinetics of HOOP band decay were investigated and the activation energy for chromophore relaxation was determined. As only those HOOP band dynamics are of interest that reflect the energy flow from the chromophore to the protein, further reactions, *e.g.* photocycle shortcuts involving retinal back isomerization, must be excluded. The strategy to avoid misinterpretation is exemplified in Fig. 3-14. At 80 K and both pH values, the retinal fingerprint bands in both the υ(C–C) and the HOOP region are reduced after light off (*green arrows*). This suggests that a back isomerization of the retinal takes place at this temperature (K→D) involving relaxation of the chromophore. In contrast, at 150 K and both pH conditions, only the HOOP bands decay after light off, while the υ(C–C) vibrations remain unchanged so that thermal back isomerization of the retinal is excluded. While at pH 9, chromophore relaxation is almost complete already at 150 K as reflected by the significantly reduced HOOP bands after ≥ 30 min in the dark, this process is significantly delayed at pH 5. At pH 5, HOOP band vibrations are still observed at 200 K, emphasizing the stabilizing effect of the Ci1 protonation state on the distorted chromophore conformation. At 200 K, a number of alterations occurs in the fingerprint region after ending the illumination, reflected by bands at 1263(-)/ 1254(+)/ 1179(+) $cm^{-1}$ and 1033(+)/ 1013(-) $cm^{-1}$. Following the concept of energy

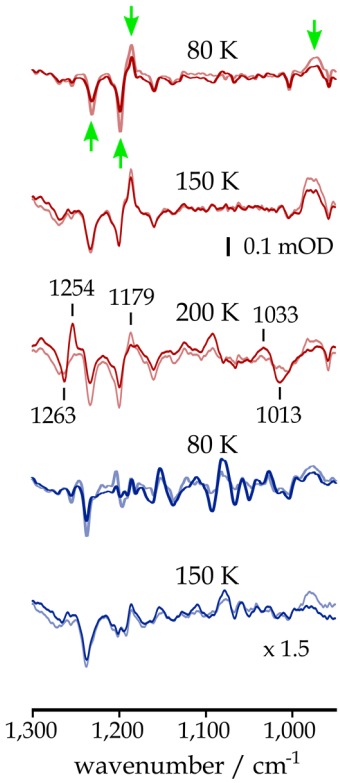


**Fig. 3-14** The υ(C–C) and HOOP region of light – dark difference spectra of ReaChR-wt at pH 5 and 9 recorded during (*light spectra*) and after (*dark spectra*) illumination with green LEDs ($\lambda_{max}$ ~ 529 nm) following ≥ 30 min in the dark at ≥ 293 K. At 80 K, K relaxes directly back to D as indicated by the reduction of υ(C–C) (*green arrows*) so that the respective decay kinetics were excluded from the calculation of $E_a$. Spectra were scaled to retinal fingerprint bands in the spectrum obtained during illumination at pH 5 at 150 K.

transfer from chromophore to protein, the reduction of HOOP bands should correlate with changes in protein vibrations. Such changes following chromophore relaxation are observed in the amide I region at both pH values (Fig. S5) but could not be assigned to distinct oscillators.

The approach for the determination of the activation energy $E_a$ for the chromophore relaxation (Fig. 3-15) is based on the distributed kinetics model introduced by Austin *et al.* 1975.[188] In short, this model takes into account that at cryogenic conditions different conformational substates (*e.g.* rotamers) are stabilized that are thermally averaged at temperatures typically > 180–220 K, yielding a single apparent state. While the activation energy for a reaction of the equilibrated state > 180–220 K can thus be determined without consideration of the conformational substates, temperatures < 180–220 K require their consideration. The respective kinetics can be fitted by the empirical equation $(1 + t/t_0)^{-n}$ that takes into account the different kinetics of the different conformational substates (see 2.2.3.3. for details, p. 42).

Within the observation time, the HOOP band decay is almost complete at 200 K at pH 5 (Fig. 3-15a) and at 165 K at pH 9 (Fig. 3-15b). Implementing the kinetic parameters $t_0$ and $-n$ into a plot of $RT \cdot \ln(n/t_0)$ vs. the temperature according to Austin *et al.* 1975[188] reveals the temperature dependence of the HOOP band decay (Fig. 3-15c). At pH 9, a linear dependence is observed and calculating the intercept on the ordinate of the interpolated linear function yields $E_a$ (pH 9) = 26.2 ± 1.5 kJ/ mol. Contrarily, at pH 5, a linear dependence is only observed for temperatures between 130 and 180 K. Based on the values within

the linear range, the activation energy for chromophore relaxation is $E_a$ (pH 5) = 35.7 ± 5.1 kJ/ mol. Discontinuity of the temperature dependence > 180 K can be explained in two ways: (1) HOOP band decay at temperatures > 180 K might be (partially) due to a K→D shunt reaction with different kinetics. A similar shunt reaction was observed in this temperature range for the L→D reaction in BR.[124] This suggestion is further supported by the reduced retinal fingerprint bands in the spectrum at 200 K after light off which are assigned to the 13-*trans*→13-*cis* photoreaction (see Fig. 3-14, p. 71). (2) HOOP band decay kinetics are likely to be influenced by a phase transition of the protein samples that usually occurs in this temperature range and is referred to as `glass transition´.[206,207]

The discontinuity of the temperature dependence aside, determination of $E_a$ revealed a strong influence of the Ci1 protonation state on the dynamics of energy transfer from the chromophore to the protein. This assumption is further supported by a comparison of the HOOP band decay kinetics of the wt at pH 5, 7.4 and 9 and the Ci1 and Ci2 mutants E163T and D293N at pH 7.4 (Fig.3-15 d). HOOP band decay kinetics at pH 7.4 ($k_{0.8}$ (time required to decline to 80 % of the initial HOOP band intensity in the light-induced steady state spectra) ≈ 299±16 s) are expectedly between those at pH 5 ($k_{0.8}$ ≈ 4522±73 s) and pH 9 ($k_{0.8}$ ≈ 29±2 s). Ci2 mutation (D293N) slows down the decay kinetics ($k_{0.8}$ ≈ 3508±90 s), while Ci1 mutation (E163T) accelerates HOOP band decay similar to pH 9 ($k_{0.8}$ ≈ 61±7 s). This finding is in agreement with the previous observations that deprotonation and mutation of Ci1 have similar consequences on the FTIR difference spectra. The best explanation for this finding is that stabilization of the distorted chromophore conformation at acidic pH is due to hydrogen bonding of protonated Ci1 (see Fig. 3-11, p. 67) that is disrupted or weakened by both Ci1 mutation and deprotonation.

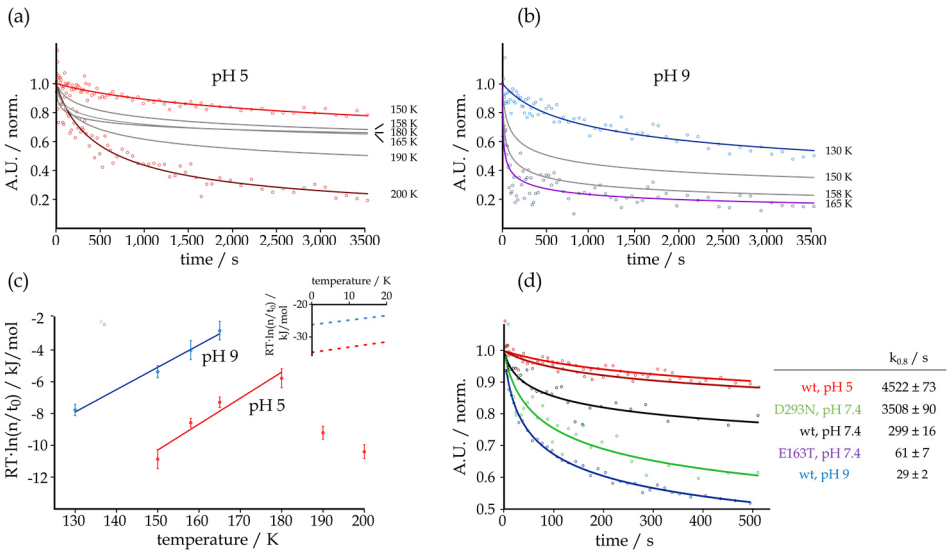


**Fig. 3-15** Estimation of the activation energy for energy transfer from chromophore to protein in dependence of the Ci1 protonation state. Decay kinetics of the HOOP bands of ReaChR wild type spectra at pH 5 **(a)** and pH 9 (**b**). Individual data points are shown only for the lowest and highest temperatures. Data were fitted using the empirical equation $(1+t/t_0)^{-n}$ introduced by Austin *et al.* 1975.[188] **(c)** Values for $RT \cdot \ln(n/t_0)$ obtained from the fits in **(a)** and **(b)** are plotted against the temperature. The intercept on the ordinate of the function obtained by linear interpolation (*inset*) is the mean activation energy of the energy transfer to the protein, with $E_a$ = 26.2 ± 1.5 kJ/mol at pH 9 and 35.7 ± 5.1 kJ/mol for the first release step at pH 5 (values for 190 and 200 K were excluded as explained in the text). **(d)** Decay kinetics of the HOOP bands from SVD-corrected spectra of the wild type at pH 5, 7.4 and 9, and the Ci1 mutant E163T and the Ci2 mutant D293N at pH 7.4 and 150 K. Data points were fitted using the empirical equation introduced by Austin *et al.* 1975.[188] The resulting $k_{0.8}$ values (time required to decline to 80 % of the initial HOOP band intensity) are summarized.

## 3.2.3 Formation of the ion-conducting state

### 3.2.3.1 Disentangling the photointermediates L, M and N

In the temperature range from 180–220 K, frozen protein samples undergo phase transitions.[206,207] Above this threshold, later photocycle intermediates can be stabilized. In the photocycle of ReaChR, K is succeeded by L, M and N. $M_2$ and N were identified as open states.[51] However, $M_1$ and $M_2$ could not be distinguished based on the FTIR spectroscopic data presented in this thesis and thus the following analysis refers to an apparent M intermediate instead. Based on the UV-Vis difference spectra recorded at cryo-conditions, L is accumulated above 200 K (see Fig. 3-8, p. 63). The contribution of N could not be evaluated based on the UV-Vis spectra as its absorption spectrum overlaps with the dark state absorption.[51] Generally, continuous illumination leads to mixed states comprised of multiple intermediates. The approach to disentangle the photointermediates was to change the equilibrium of the intermediates by adjusting experimental parameters such as temperature and equilibration time. This strategy, applied to ReaChR-wt at pH 5, pH 7.4 and pH 9, reveals two mixed states observed between 230 and 260 K, that differ with respect to selected marker bands (Fig. 3-16): Given the correlation of the υ(C=C) vibrations with UV-Vis absorption maxima[132,191], the vibrational band at 1547–43(+) $cm^{-1}$ is a marker band for formation of L, and the band at 1566/63(+) $cm^{-1}$ is a marker for formation of M (enlarged υ(C=C) region in Fig. S6). The assignment of the state 1 difference spectrum at pH 7.4 to M (in addition to L) is vague, as the marker band is small and only slightly more pronounced than in the state 2 difference spectrum (L and N). As shown in 3.2.3.2 (p. 76), the negative band at 1753/52 $cm^{-1}$ and the positive band at 1736/34 $cm^{-1}$ serve as marker bands for formation of N. According to these marker bands, the different states in Fig. 3-16 can be assigned to mixtures of the following photointermediates:

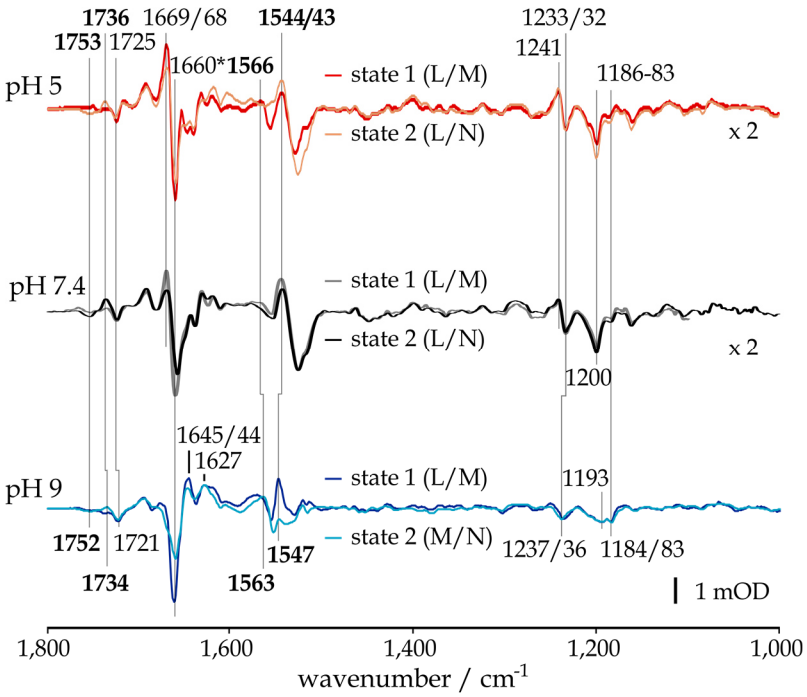


**Fig. 3-16** FTIR light – dark difference spectra of ReaChR wild type at pH 5, 7.4 and 9. The different intermediates were distinguished based on the marker bands discussed in the text (*bold* numbers). Measurement conditions: state 1 (pH 5) steady state at 230 K, state 2 (pH 5) steady state at 260 K; state 1 (pH 7.4) early spectra at 260 K, state 2 (pH 7.4) steady state at 260 K; state 1 (pH 9) early spectra at 260 K, state 2 (pH 9) steady state at 260 K. Illumination was conducted with green LEDs ($\lambda_{max}$ ~ 529 nm) following ≥ 30 min in the dark at ≥ 293 K. *Bands between 1660 and 1658 $cm^{-1}$. Spectra were scaled to retinal fingerprint bands in the state 1 difference spectrum at pH 9.

(1) state 1 (pH 5, pH 7.4): L and M

(2) state 2 (pH 5, pH 7.4): L and N

(3) state 1 (pH 9): L and M

(4) state 2 (pH 9): M and N

The most outstanding aspects of the mixed states are:

(i) In the υ(C=O) region in all states, a negative band arises between 1725 and 1721 $cm^{-1}$ that indicates deprotonation of a carboxylic side group. Considering the D→K transition spectra (see Fig. 3-10, p. 66), deprotonation of E3 is likely responsible for this vibration. Formation of state 2 involves additional proton transfer processes as indicated by the bands at 1753/52(-) and 1736/34(+) $cm^{-1}$.

(ii) Strong bands in the amide I region of state 1 indicate that larger backbone rearrangements occur already in the K→L transition, *i.e.* prior to formation of the ion-conducting state.[51] The band at 1660–1658 $cm^{-1}$ is a typical feature of the (pre-)conducting states of ChRs and was explained by helix

hydration due to water influx that causes a frequency downshift.[157] In agreement with this concept, positive vibrational bands arise at 1645/44 and 1627 $cm^{-1}$ at pH 9. In contrast, an upshifted positive band is detected at 1669/68 $cm^{-1}$ at pH 5 and 7.4, hinting at crucial distinctions concerning the open state structure at different pH conditions. From state 1 to state 2, the intensity of the backbone vibrational modes is reduced.

(iii) In the retinal fingerprint regions of both states, bleaching of the 13-*trans*,15-*anti* dark state is reflected by bands at 1237–32(-) and 1200–1193(-) $cm^{-1}$. Additionally, a negative band is observed between 1186 and 1183 $cm^{-1}$ that is strongly pronounced at pH 9 but weak at pH 7.4 and pH 5. For BR, a similar mode was assigned to a 13-*cis*,15-*syn*-retinal vibration.[79,99,109,111] For *Cr*ChR2, a similar band was instead assigned to the $\upsilon(C_{14}–C_{15})$ mode of 13-*trans*,15-*anti* retinal, indicative for isomerization around the $C_{15}$=N bond during retinal double isomerization from 13-*trans*,15-*anti* to 13-*cis*,15-*syn*.[97,98] Given the much closer relationship to *Cr*ChR2, the respective assignment to a 13-*trans*,15-*anti* retinal vibration is favored. At pH 5 and pH 7.4, a positive band arises at 1241 $cm^{-1}$ hinting at a transient change in chromophore geometry.

These observations raise questions concerning (1) protonation changes, (2) backbone changes, and (3) the photoreactions of different retinal isomers. These questions are addressed in the following.

#### 3.2.3.2 Protonation changes during formation of the ion-conducting state

In the $\upsilon$(C=O) region of the FTIR difference spectrum of state 2 at pH 7.4, *i.e.* the L/N mixed state, a band pattern at 1753(-)/ 1736(+)/ 1723(-) $cm^{-1}$ is observed that in the following is assigned to specific residues based on site-directed mutagenesis and H–D exchange (Fig. 3-17). The band at 1723 $cm^{-1}$ is absent only in the E3 mutant E130Q and undergoes an 8 $cm^{-1}$ downshift to 1715 $cm^{-1}$ in $D_2O$. As already observed at 80 K (see Fig. 3-10, p. 66), sample deuteration is incomplete leaving a residual band at 1723(-) $cm^{-1}$. However, the observation of a single band downshifting in $D_2O$ indicates deprotonation of the underlying residue.

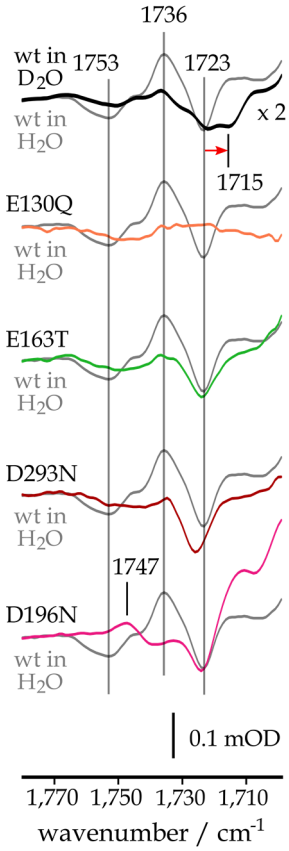


**Fig. 3-17** The υ(C=O) region of light – dark difference spectra of ReaChR-wt and mutants at pH 7.4 (pD 7.8) recorded at 260 K. Illumination was conducted with green LEDs ($\lambda_{max}$ ~ 529 nm) following ≥ 30 min in the dark at ≥ 293 K. Spectra were scaled to retinal fingerprint bands of the wt spectrum in $H_2O$. *Red arrow* indicates frequency shift in $D_2O$.

Accordingly, E3 deprotonates in the photocycle of ReaChR similar to observations in *Cr*ChR2.[47,88,104] The vibration at 1736(+) $cm^{-1}$ is affected by all mutants. It is reduced in the mutant spectra of Ci1 (E163T), Ci2 (D293N) and E3 and additionally upshifted to 1747(+) $cm^{-1}$ in the $Asp^{DC}$ mutant (D196N). As $Asp^{DC}$ mutation abolishes the band at 1753(-) $cm^{-1}$ as well, while observed in all other mutant spectra, this mode is assigned to deprotonation of $Asp^{DC}$. $Asp^{DC}$ was described as proton donor in *Cr*ChR2[104,192] mainly deduced from the drastic deceleration of M state decay ($\tau_{off}$ = 17 s) in the $Asp^{DC}$ mutant D156A[82] but challenged by the long distance to the RSB (> 9 Å) and the fact that several $Asp^{DC}$ mutants in *Cr*ChR2 that abolish the carboxylic side group still maintain ion channel function.[52,67,83,85,169] In ReaChR, $Asp^{DC}$ mutant D196N has a rather moderate effect on the M decay kinetics ($\tau_{off}$ ≈ 263 ms) as compared to the wild type ($\tau_{off}$ ≈ 6.54 ms, see Tab. 2, p. 62).

Considering the unambiguous assignment of the modes at 1723(-) and 1753(-) $cm^{-1}$, the band at 1736(+) $cm^{-1}$ is assigned to protonation of the counterions. This band is reduced but still observed in the spectra of both the Ci1 and Ci2 mutant. Ci1 is partially protonated at physiological pH, but its $pK_a$ is probably reduced < 5 if Ci2 is neutralized by mutation.[b] Accordingly, Ci1 can serve as proton acceptor if Ci2 is mutated. The primary proton acceptor group, though, is Ci2 as derived from flash photolysis experiments that revealed a significant retardation of M formation in the Ci2 mutant (see Tab. 2, p. 62). The frequency upshift of the Ci2 protonation band caused by $Asp^{DC}$ mutation reflects tight coupling between the distal ($Asp^{DC}$) and

[b] Data by Benjamin Krause, Humboldt University Berlin, included in: Kaufmann *et al.* Energy transfer from chromophore to protein is modulated by the protonation state of a glutamic acid in the active site of channelrhodopsin. Manuscript in preparation for resubmission.

the proximal side (Ci1) of the chromophore with respect to the $RSBH^+$, presumably achieved by modulation of the interaction between Thr167 and the $RSBH^+$ (see the homologue Thr166 in the C1C2 structure, Fig. 1-5, p. 10).[45,72,80] Notably, both vibrational modes at 1753(-) and 1736(+) $cm^{-1}$ are insensitive to H–D exchange. This can be interpreted as inaccessibility to bulk water, which – in view of the crystal structures[41,72] and earlier FTIR investigations[42] – is not unexpected for $Asp^{DC}$. However, Ci1 and Ci2 are clearly expected to be accessible to water molecules. The missing H–D shift of the respective band can again be explained by partial deuteration: While the Ci2-COOH mode is reduced in $D_2O$, the downshifted Ci2-COOD mode is cancelled out by the remains of the E3-COOH mode. Although this hypothesis can explain the observed unexpected H–D effects, it is unclear why deuteration was incomplete. As the deuteration procedure was repeated several times and worked well for both C1C2 and Chrimson, the possibility needs to be considered that in ReaChR distinct conformational substates exist that differ with respect to their water content.

#### 3.2.3.3 Structural changes during formation of the ion-conducting state

The amide I region shows strong pH dependence (see Fig. 3-16, p. 75). At physiological pH, a negative band is observed at 1658 $cm^{-1}$ and a positive band at 1669 $cm^{-1}$ (Fig. 3-18). The band at 1658(-) $cm^{-1}$ is reduced in $D_2O$ – different to the respective band in *Cr*ChR2[157] – and the 1669(+) $cm^{-1}$ band is upshifted by 4 $cm^{-1}$. As peptide bond oscillations are insensitive to H–D exchange, other vibrational modes must contribute to this band as well. The band pattern at 1669(+)/ 1658(-) $cm^{-1}$ was also observed at pH 5 but not at pH 9 (see Fig. 3-16, p. 75). The fact that a pronounced positive band at higher frequency was also observed in *Ca*ChR1[158], but not in *Cr*ChR2[157] hints at an impact of the Ci1 protonation state on the light-induced structural alterations of the protein backbone: In the configurations with protonated Ci1, such as ReaChR at pH 5 and (partially) at pH 7.4 as well as *Ca*ChR1, a frequency upshift of the α-helical dark state band occurs. This is in contrast to the frequency downshift observed in the configurations with deprotonated Ci1 such as ReaChR at pH 9 and *Cr*ChR2. In *Cr*ChR2, this frequency downshift from 1664(-) to 1648(+) $cm^{-1}$ was interpreted as hydration of helices due

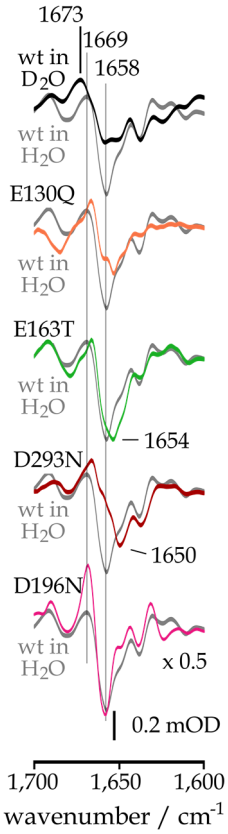


**Fig. 3-18** The amide I region of light – dark difference spectra of ReaChR wt and mutants at pH 7.4 (pD 7.8) recorded at 260 K. Illumination was conducted with green LEDs ($\lambda_{max}$ ~ 529 nm) following ≥ 30 min in the dark at ≥ 293 K. Spectra were scaled to retinal fingerprint bands of the wt spectrum in $H_2O$.

to water influx upon formation of the ion-conducting state.[157] If this concept could as well be applied to the observed frequency upshift at pH 5 and pH 7.4, it would hint at a different water content in the conducting states in dependence of the pH value and likely affected by the Ci1 protonation state. Ci1 mutation leads to a moderate 4 $cm^{-1}$ downshift of the 1658(-) $cm^{-1}$ band to 1654(-) $cm^{-1}$, while Ci2 mutation causes a more pronounced downshift by 8 $cm^{-1}$ to 1650(-) $cm^{-1}$. This downshift might be linked with the impaired function of the Ci2 mutant that is reflected by the drastically reduced ion conductance.[52] Mutation of E3 leads to a reduction of the 1658(-) $cm^{-1}$ band, which could either be explained by an effect of this mutation on the water content of the dark state or, alternatively, hint at a light-induced reorientation of the E3 peptide bond that is abolished in the mutant. $Asp^{DC}$ mutation results in a relative increase of the 1669(+) $cm^{-1}$ band as compared to the 1658(-) $cm^{-1}$ mode. Interpretation of the absolute band intensities in this mutant is particularly challenging since the retinal fingerprint region used for scaling is significantly altered in the $Asp^{DC}$ mutant. This phenomenon will be issued in section 3.2.3.4 (p. 82).

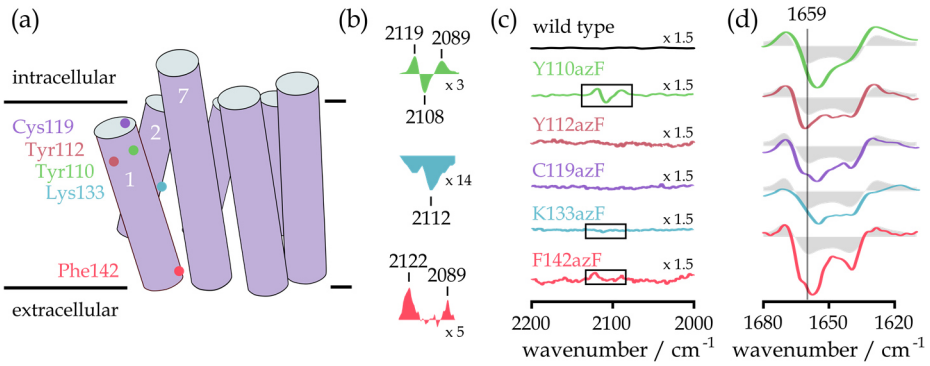


**Fig. 3-19** The implementation of azF labels into ReaChR for the local resolution of polarity changes. **(a)** Position of the labels in the protein. **(c)** The spectral window of the $\nu_{as}(N_3)$ mode of FTIR light – dark difference spectra of the unlabeled ReaChR-wt and azF mutants at pH 7.4 and 293 K (enlarged difference band patterns are shown in **(b)** for those azF mutant spectra that exhibited spectral differences). **(d)** The corresponding amide I region with the wild type spectrum in *gray*. Illumination was conducted with green LEDs ($\lambda_{max}$ ~ 529 nm) following ≥ 30 min in the dark at ≥ 293 K. Spectra were scaled to retinal fingerprint bands of the wild type spectrum. Scaling factors are given with respect to the spectra shown in (d). Note that while the wild type spectrum obtained at 293 K mainly represents formation of the inactive P intermediate with only minor contributions of the (pre-)conducting intermediates L, M and N as reflected by the reduced band at 1659(-) $cm^{-1}$ (for details see 3.2.4.1, p. 85), the azF mutant spectra presumably contain higher contributions of the intermediates preceding P as the band at ~ 1659(-) $cm^{-1}$ is significantly increased.

While the light-induced changes in the amide I region (Fig. 3-18) report on polarity changes of the entire protein during formation of the ion-conducting state, they do not provide information on the actual sites within the protein that experience these polarity changes. A better local resolution of the polarity changes occurring in the photocycle of ReaChR was possible by investigating variants labelled with *p*-azido-L-phenylalanine (azF) at several sites within the protein (Fig. 3-19a). The azF label exhibits a vibrational mode at ~ 2100 $cm^{-1}$ ($\nu_{as}(N_3)$) that due to the vibrational stark effect is sensitive towards its electrostatic environment.[208–210] Accordingly, changes in the electrostatics of the environment of the azF label due to light-induced structural alterations become evident in the FTIR difference spectra as frequency shifts at ~ 2100 $cm^{-1}$. The difference spectra in Fig. 3-19 were obtained at 293 K. In the ReaChR wild type, the inactive P intermediate is accumulated at this temperature with only minor contributions of the preceding intermediates L, M and N, which is reflected by the reduced amide I mode at 1659 $cm^{-1}$. This observation indicates that the backbone changes that led to the large amide I difference bands at 260 K (see Fig. 3-16, p. 75, and Fig. 3-18, p. 79) are largely reversed in P (for details see 3.2.4.1, p. 85). In the azF mutants, the contribution of

the preceding intermediates is presumably enhanced as can be derived from the increased amide I bands as compared to the wild type (Fig. 3-19d). In the spectral window for the $\nu_{as}(N_3)$ vibration (Fig. 3-19b and Fig. 3-19c), light-induced frequency shifts are observed in azF mutants with the azF label replacing (i) the inner gate residue Tyr110 (Y110azF, 2119(+)/ 2108(-)/ 2089(+) $cm^{-1}$), (ii) $Lys^{CI}$, which is located close to the counter-ion complex (K133azF, 2112(-) $cm^{-1}$), and (iii) Phe142, located in the extracellular region (F142azF, 2122(+)/ 2089(+) $cm^{-1}$). Contrarily, no shifts were detected in variants with the azF label replacing (i) Tyr112 (Y112azF) and (ii) Cys119 (C119azF) which are both found in the intracellular region. The most significant changes among all the labelled variants were observed in ReaChR-Y110azF with bands arising at 2108(-), 2119(+) and 2089(+) $cm^{-1}$. However, the interpretation of this pattern is challenged by the fact that a single negative band is found along with one upshifted and one downshifted positive band with similar intensities. This observation could be due to accidential Fermi resonance[178,179] or, instead, result from a broadening of the $\nu_{as}(N_3)$ band after light activation due to a higher variability of the electrostatic environment of the label as compared to the dark. According to the second explanatory approach, in some conformational substates of the light-activated state the label could experience an increased polarity in its environment that would lead to the upshifted band at 2119(+) $cm^{-1}$. Contrarily, in other conformational substates the label could experience a decreased polarity, resulting in the downshifted band at 2089(+) $cm^{-1}$.

The polarity changes of the azF label can be due to a light-induced rearrangement of salt bridges or hydrogen bonds, *e.g.* by water influx/ efflux near the labelling site. Given that formation of the ion-conducting pathway involves water influx[47,157], it appears likely that alterations in the hydrogen bonding to water molecules are at least partially responsible for the light-induced changes of the $\nu_{as}(N_3)$ band of Y110azF.

### 3.2.3.4 Alterations in the retinal isomer composition

The state 1 and state 2 spectra of ReaChR wild type at pH 9 (see Fig. 3-16, p. 75) exhibit a band in the retinal fingerprint region at 1184/83(-) $cm^{-1}$ that is assigned to the υ($C_{14}$–$C_{15}$) vibration of 13-*trans*,15-*anti* retinal and indicative for retinal double isomerization around the $C_{13}$=$C_{14}$ and $C_{15}$=N bonds.[97,98] This band is only weakly pronounced in the spectra obtained at pH 5 and pH 7.4 (see Fig. 3-16, p. 75), similar to the mutant spectra in Fig. 3-20, but the fact that the band is observed in all variants and at all applied pH conditions proves that it is not an artifact. Its assignment to the υ($C_{14}$–$C_{15}$) vibration of 13-*trans*,15-*anti* retinal is furthermore supported by the deuteration effect shown in Fig. 3-20: While a small band at 1184(-) $cm^{-1}$ is present in the wild type in $H_2O$, it is vanished in $D_2O$. Such a sensitivity to H–D exchange is expected for υ($C_{14}$–$C_{15}$) of 13-*trans*,15-*anti* due to moderate coupling to the $RSBH^+(D^+)$.[97,98] This is in contrast to υ($C_{10}$–$C_{11}$) of 13-*cis*,15-*syn* for which no sensitivity to H–D exchange is described.[110,111] The enhancement of the 13-*trans*,15-*anti*→13-*cis*,15-*syn* double isomerization at alkaline pH (see Fig. 3-16, p. 75) could either be due to the disruption or weakening of the hydrogen bonding of protonated Ci1 or, alternatively, be caused by the additional negative charge in the active site due to deprotonated Ci1. In Fig. 3-20, Ci1 mutation (E163T) does not lead to an increased band at 1184 (-) $cm^{-1}$. This suggests that the additional negative charge present at alkaline pH is decisive for the observed increase of this vibrational mode. In order to exclude the possibility that the enhancement of the band at 1184(-) $cm^{-1}$ at alkaline pH is the result of a more unspecific pH effect rather than more specifically due to the additional negative charge provided by deprotonated Ci1 to the active site, FTIR difference spectra of the wild type and the Ci1 mutant were recorded at pH 9 (Fig. 3-21). As expected, the band at 1184(-) $cm^{-1}$ is significantly reduced in the E163T mutant,

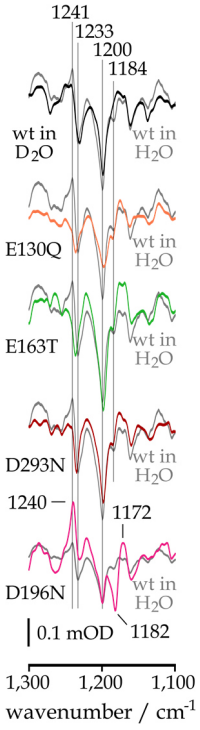


**Fig. 3-20** The υ(C–C) region of light – dark difference spectra of ReaChR-wt and mutants at pH 7.4 (pD 7.8) recorded at 260 K. Illumination was conducted with green LEDs ($\lambda_{max}$ ~ 529 nm) following ≥ 30 min in the dark at ≥ 293 K. Spectra were scaled to retinal fingerprint bands of the wt spectrum in $H_2O$.

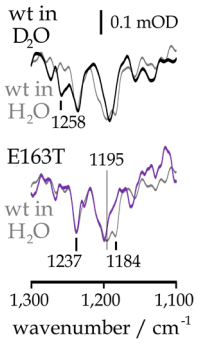


**Fig. 3-21** The υ(C–C) region of light – dark difference spectra of ReaChR-wt and the Ci1 mutant E163T at pH 9 (pD 9.4) recorded at 268 K. Illumination was conducted with green LEDs ($\lambda_{max}$ ~ 529 nm) following ≥ 30 min in the dark at ≥ 293 K. Spectra were scaled to retinal fingerprint bands of the wt spectrum in $H_2O$.

clearly showing that the increase of this band at alkaline pH is due to deprotonation of Ci1. Furthermore, the band at 1184(-) $cm^{-1}$ disappeared in $D_2O$ similar to pH 7.4 (see Fig. 3-20, p. 82) confirming the assignment to the υ($C_{14}$–$C_{15}$) vibration of 13-*trans*,15-*anti* retinal similar to *Cr*ChR2.[97,98] The presented results clearly demonstrate that the Ci1 protonation state modulates the efficiency of the 13-*trans*,15-*anti*→13-*cis*,15-*syn* retinal double isomerization.

The most astonishing changes in Fig. 3-20 (p. 82) are observed in the spectra of the $Asp^{DC}$ mutant. Here, a strong negative band arises at 1182(-) $cm^{-1}$ and positive modes are observed at 1240 and 1172 $cm^{-1}$. The band at 1240(+) $cm^{-1}$ is observed in the wild type as well but is lacking in the spectra of mutants of the extended counter-ion complex (E130Q, E163T and D293N). The vibrational band at 1182(-) $cm^{-1}$ could originate from retinal double isomerization from 13-*trans*,15-*anti* to 13-*cis*,15-*syn* and/or photoreactions within the 15-*syn* cycle as discussed previously.[98] If the differences in the retinal fingerprint region at alkaline pH and in the $Asp^{DC}$ mutant were exclusively due to an enhancement of the light-induced 13-*trans*,15-*anti*→13-*cis*,15-*syn* retinal double isomerization and not the result of a different isomeric composition of the dark state, retinal extraction and subsequent HPLC analysis of $D_{app}$ (obtained after 10–30 min in the dark) should not reveal significant differences in the 13-*cis* content with respect to the wild type at physiological and acidic pH. The analysis (Tab. 3) shows that, indeed, the 13-*cis* content of the wild type is not significantly pH dependent with values from 19–22 %. This strongly supports the finding from the FTIR difference spectra (see Fig. 3-16, p. 75, Fig. 3-20, p. 82, and Fig. 3-21, p. 83) that the 13-*trans*,15-*anti*→13-*cis*,15-*syn* reaction is enhanced at alkaline pH due to an increased quantum efficiency. The pH value, however, significantly affects the contribution of other retinal isomers to the apparent dark state as at pH 5 the 11-*cis* retinal

| | $D_{app}$ (wt, pH 5) | $D_{app}$ (wt, pH 9) | $D_{app}$ (wt, pH 7.4) | $D_{app}$ (D196N, pH 7.4) |
|---|---|---|---|---|
| 13-*cis* | 20.7 ± 0.0 | 18.7 ± 0.1 | 22.3 ± 0.0 | 32.2 ± 4.1 |
| 11-*cis* | 8.4 ± 1.2 | 2.7 ± 1.4 | n.d. | 8.6 ± 1.4 |
| 9-*cis* | 3.2 ± 0.2 | 4.4 ± 1.1 | n.d. | 6.9 ± 0.5 |
| 13-*trans* | 67.7 ± 1.3 | 73.7 ± 2.1 | 77.7 ± 0.0 | 52.2 ± 5.0 |

**Tab. 3** Retinal extraction and subsequent HPLC analysis of the ReaChR wild type at pH 5, 7.4 and 9 and the $Asp^{DC}$ mutant D196N at pH 7.4. $D_{app}$: 10 min green light ($\lambda_{max}$ ~ 529 nm), 30 min dark. In the case of the wild type at pH 7.4 only 10 min dark. Equilibration was conducted at ambient temperature. Spectra were corrected for baseline-drifts and bands were analyzed by fitting gaussians. Chromatograms are shown in Fig. S7.

content is increased at the expense of 13-*trans*. A similar pH effect on the isomeric composition was observed in XR.[114]

In contrast, the 13-*cis* content is substantially increased in the $Asp^{DC}$ mutant (by ~ 10 %). Together with increased amounts of 11-*cis* and 9-*cis*, this results in a clear reduction of 13-*trans* to ~ 50 %. Thus, $Asp^{DC}$ mutation causes significant alterations in the isomeric composition of the dark state. Considering the increased 13-*cis* content in the dark, it appears likely that the retinal fingerprint region in the D196N spectrum (see Fig. 3-20, p. 82) contains signals reflecting isomerization reactions within the 15-*syn* cycle that are more pronounced as compared to the wild type spectrum.

## 3.2.4 Recovery of the dark state

### 3.2.4.1 The long-lived desensitized state

According to several photocycle models for *Cr*ChR2, N ($P_3$ or $P_{520}$) proceeds to a late desensitized state P ($P_4$ or $P_{480}$) with a UV-Vis absorption similar to the dark state[31,96,101,104,123,176] and some of these models additionally included a direct transition from N to D[105,176]. Contrarily, a recent publication on *Cr*ChR2 stated that N relaxes to D completely and that desensitization observed at continuous illumination is due to accumulation of the dark state D' of the 15-*syn* photocycle branch and its photoproducts.[98] For ReaChR, UV-Vis spectroscopic and electrophysiological characterization revealed the formation of a desensitized state that was termed O[51,52] and in this thesis is referred to as 'P' (because the corresponding O intermediate in BR decays in the order of milliseconds[195]). FTIR difference spectra recorded at 293 K represent a mixed state with a large

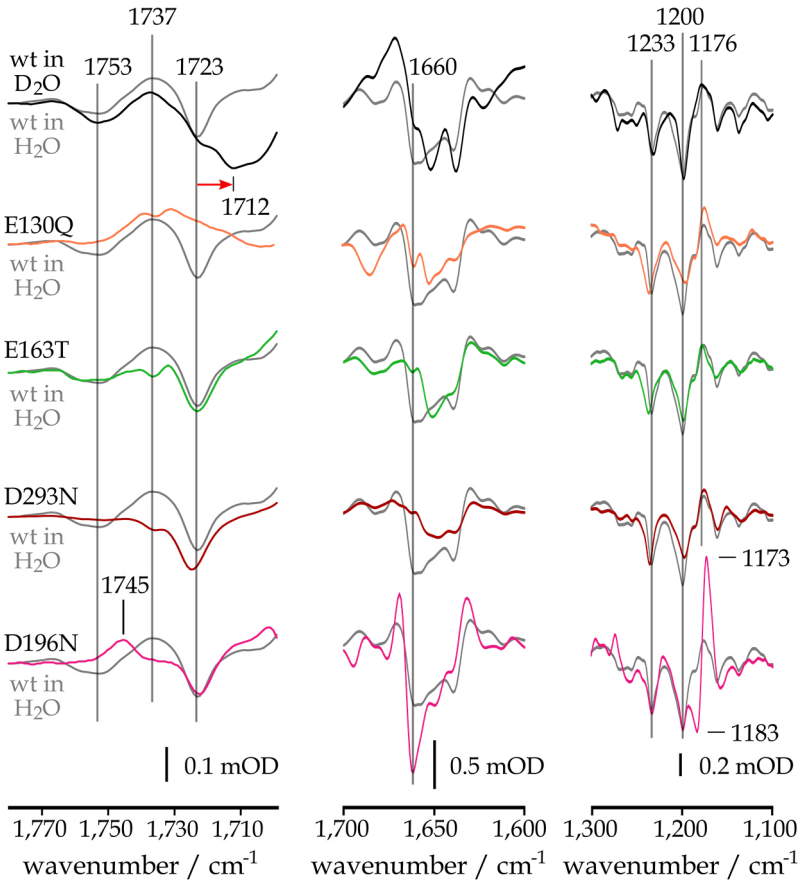


**Fig. 3-22** FTIR light – dark difference spectra of ReaChR-wt and mutants at pH 7.4 (pD 7.8) recorded at 293 K. Illumination was conducted with green LEDs ($\lambda_{max}$ ~ 529 nm). Spectra were scaled to retinal fingerprint bands of the wt spectrum in $H_2O$. R*ed arrow* indicates shift in $D_2O$.

contribution of P, given its slower decay kinetics ($\tau_{off}$ > 10 s, see Tab. 2, p. 62) as compared to the preceding intermediates L, M and N (Fig. 3-22). In comparison to the spectra at 260 K (see 3.2.3, p. 74), in which the contribution of the intermediates preceding P was higher, several aspects need to be highlighted:

(1) In the υ(C=O) region (Fig. 3-22, *left column*), the band at 1753(-) $cm^{-1}$ that was assigned to deprotonation of $Asp^{DC}$ is clearly reduced in the mutants of E3 (E130Q) and Ci2 (D293N), indicating that these mutations affect the reprotonation of $Asp^{DC}$. The band at 1737(+) $cm^{-1}$ that was assigned to the protonation of Ci2 is vanished in mutations of Ci1 (E163T) and Ci2. This shows that the deprotonation dynamics of this residue are affected by mutations within the counter-ion complex. In the E3 mutant, however, two band maxima are observed in this region, while no band was observed at 260 K. Given the shape of this double band pattern, it is most likely the result of an overlap of the positive band that reflects protonation of Ci2 as observed in the wild type with a band peaking at around 1738(-) $cm^{-1}$. Such a negative band is also present in the Ci1 and Ci2 mutant spectra but could not be assigned based on the ReaChR mutants investigated in this thesis.

(2) In the amide I region (Fig. 3-22, *central column*), the band at 1660(-) $cm^{-1}$ is clearly reduced, with the exception of the $Asp^{DC}$ mutant (D196N). The reduction of this band suggests that the major backbone changes occurring during formation of the ion-conducting state are largely reversed already in P, similar to observations on *Cr*ChR2.[104] Its decrease in the mutant spectra of the active site residues Ci1 and Ci2 and the central gate residue E3 furthermore indicates that the residual structural alterations in P are partially due to persisting reorientation of these residues. The comparably large band at 1660(-) $cm^{-1}$ in the $Asp^{DC}$ mutant spectrum reflects the fact that the N intermediate is accumulated in this mutant (although the channel closing kinetics are only moderately prolonged, $\tau_{off}$ = 132 ms as compared to $\tau_{off}$ = 202 ms in the wild type[52]), while a P intermediate was not observed.[52]

(3) In the υ(C–C) region (Fig. 3-22, *right column*), the band pattern at 1233(-)/ 1200(-) $cm^{-1}$ implies that depletion of the 13-*trans*,15-*anti* retinal dark state

persists in P. This raises the question whether retinal back isomerization has already occurred as suggested for the corresponding P intermediate in *Cr*ChR2[31,105,176] or whether the retinal in P is instead still predominantly in 13-*cis*,15-*anti* conformation in ReaChR. As a third possibility, P could be identical with the D' state with a retinal in 13-*cis*,15-*syn* conformation as it is the case for *Cr*ChR2.[98]

#### 3.2.4.2 Photocycle branching

Based on UV-Vis spectroscopic measurements it was shown that two recovery pathways exist in ReaChR, M→D and P→D[52], similar to the N→D and P→D transitions previously reported for *Cr*ChR2[105,176]. In order to shed light on the mechanism of this branching, the dark state recovery of the mixed state at 293 K was investigated (Fig. 3-23).

Therefore, the spectra associated with thermal decay of the mixed state at 293 K were evaluated with SVD and rotational analysis (Fig. 3-23a). The reduced dataset was fitted by a global fit routine with a biexponential function. As the obtained time constants deviated significantly between different measurements, they are only rough estimates for the real decay kinetics. Additionally, the maximum time resolution was 1 s, so that the time constant obtained for the fast transition is particularly uncertain. The two spectral components differ with respect to a number of spectral features summarized in the following. For the fast transition spectrum ($\tau_{off} \approx 1.3$ s) the following spectral aspects are highlighted:

(1) The reversion of large backbone changes is reflected by the band at 1661(+) $cm^{-1}$.
(2) Recovery of the dark state chromophore is indicated by the band at 1526(+) $cm^{-1}$. Coexistence of a band at 1551(+) $cm^{-1}$ points to a complex dark state being restored in the fast transition. Based on the correlation of υ(C=C) vibrations with UV-Vis absorption maxima[132,191], the underlying dark state is comparably blue-shifted. It could thus represent the 13-*cis*,15-

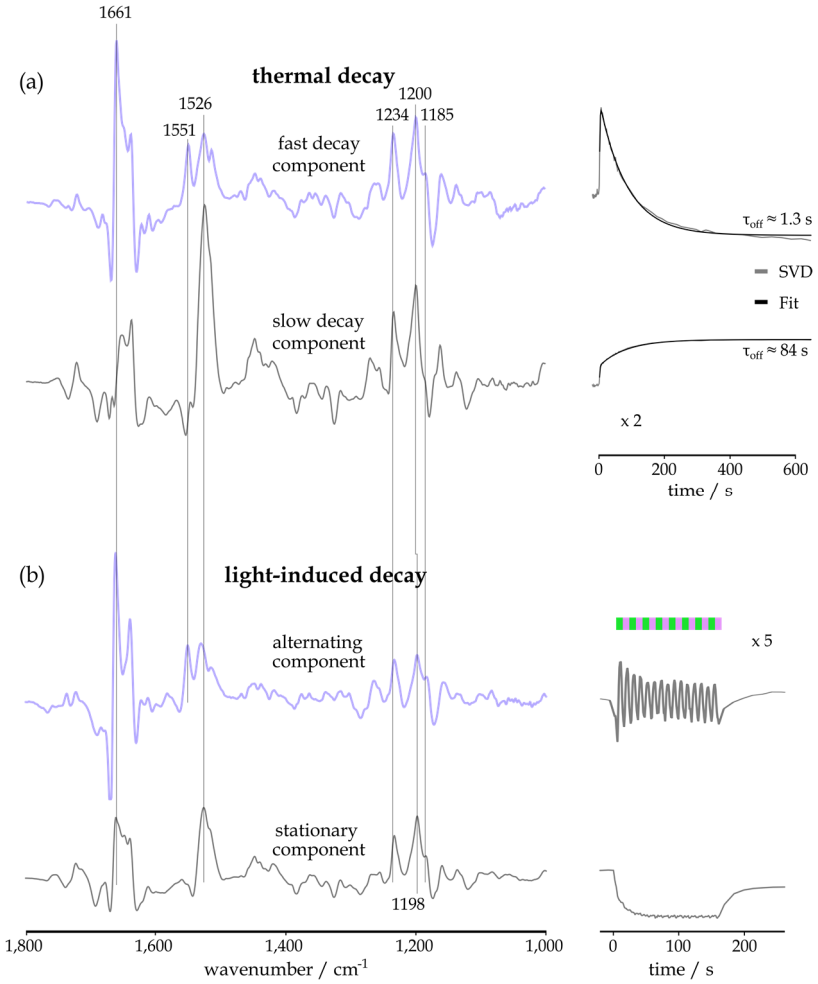


**Fig. 3-23** Dark state recovery of the ReaChR wild type at pH 7.4 and 293 K. **(a)** Spectral components associated with the decay of the light – dark difference spectrum (*left*) and the corresponding kinetics (*right*) revealed by SVD and a rotational analysis and fitted by a global fit using a biexponential function ($R^2 > 0.99$). Illumination was conducted with green LEDs ($\lambda_{max}$ ~ 529 nm). **(b)** Alternating illumination of the wild type at pH 7.4 and 293 K with green ($\lambda_{max}$ ~ 529 nm) and UV ($\lambda_{max}$ ~ 405 nm) LEDs. Data evaluation was performed with SVD and rotational analysis. Shown are the steady state component and the component sensitive to alternating illumination with spectra (*left*) and corresponding kinetics (*right*). Other components were omitted for simplicity. Absorbance is given in arbitrary units. Spectra were scaled to retinal fingerprint bands. Note that the obtained time constants can only be considered as rough estimates for the order of magnitude, in particular the time constant for the fast transition ($\tau_{off} \approx 1.3$ s), as the maximum time resolution of the experiment was 1 s.

*syn* dark state (D′) in analogy to $BR_{548}$ (13-*cis*,15-*syn*) that is blue-shifted as compared to $BR_{568}$ (13-*trans*,15-*anti*).[108,191,211,212]

(3) Back isomerization to 13-*trans*,15-*anti* is reflected by the bands at 1234(-) and 1200(+) $cm^{-1}$. Coexistence of a band at 1185(+) $cm^{-1}$ indicates that the presumed 13-*trans*,15-*anti*→13-*cis*,15-*syn* double isomerization[98] is reversed in the fast transition as well (for details on the assignment of this band see 3.2.3.4, p. 82).

Considering these spectral properties, the fast decay component is largely similar to the L, M and N intermediates (see Fig. 3-16, p. 75). Spectral features noticeable in the slow transition ($\tau_{off} \approx 84$ s) are:

(1) The vibrational bands in the amide I region are reduced, hinting at the decay of a non-conductive state (along with the slow kinetics).

(2) Recovery of the dark state chromophore as indicated by the band at 1526(+) $cm^{-1}$ is not accompanied by a pronounced additional mode as observed in the fast recovery component at 1551(+) $cm^{-1}$.

(3) The retinal fingerprint region is largely similar to the fast transition spectrum with strong positive bands at 1234 and 1200 $cm^{-1}$. The band at 1185 $cm^{-1}$ is not observed that was described as a marker for formation of 13-*trans*,15-*syn* retinal and used to identify the late desensitized state ($P_{480}$) in *Cr*ChR2 as the dark state D′ of the 15-*syn* photocycle branch[98]. This implies that the slow P→D transition in ReaChR involves back isomerization from 13-*cis*,15-*anti* to 13-*trans*,15-*anti* retinal rather than the transition of a 15-*syn* photointermediate. This is not only in contrast to the model by Kuhne *et al.* 2019[98] but also contradicts previous assumptions by Lórenz-Fonfría *et al.* 2015[105] and Saita *et al.* 2018[176] who stated that the retinal in the long-lived desensitized state was in 13-*trans*,15-*anti* conformation like the dark state. To underline this argument, the enlarged retinal fingerprint regions of ReaChR wt spectra at pH 7.4 from Fig. 3-16 (p. 75) and Fig. 3-23 are shown in Fig. 3-24. While the marker at 1185–83(-) $cm^{-1}$ for isomerization from 13-*trans*,15-*anti* to 13-*cis*,15-*syn* retinal[98] (applicability of this assignment to ReaChR is supported by its sensitivity to $D_2O$, see Fig. 3-20,

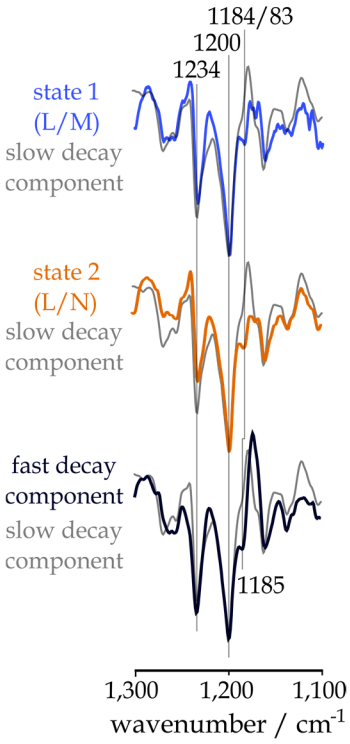


**Fig. 3-24** The υ(C–C) region of light – dark difference spectra of ReaChR-wt at pH 7.4. The state 1 and 2 spectra are taken from Fig. 3-16 (p. 75) and the fast and slow decay component spectra from Fig. 3-23a (p. 88). Illumination was conducted with green LEDs ($\lambda_{max}$ ~ 529 nm) following ≥ 30 min in the dark at ≥ 293 K. Spectra were scaled to retinal fingerprint bands of the slow transition spectrum.

p. 82, and Fig. 3-21, p. 83) is present in the state 1 (L/M) and state 2 (L/N) spectra as well as in the fast photocycle transition spectrum, it is lacking in the slow transition spectrum.

Based on the time constants obtained from single turnover UV-Vis spectroscopic experiments (see Tab. 2, p. 62[51,52]), the slow decay component is largely identical with the P intermediate. The fast decay component presumably reflects recovery of the dark state from the intermediates that precede P. Thus, several relaxation pathways exist in ReaChR, as similarly proposed for *Cr*ChR2.[105,176]

Now, the question is yet to be answered at which stage of the photocycle (L, M or N) the fast transition actually occurs: An L→D transition should be reflected by depletion of the L-marker band at ~ 1543 $cm^{-1}$. The M-marker band should arise at ~ 1560 $cm^{-1}$ but was only weakly pronounced at 260 K (see Fig. 3-16, p. 75). For N, a marker band in the υ(C=C) region could not be identified. Due to the lack of a well-defined marker band, a different approach was chosen to identify the photointermediate that shortcuts to the dark state (Fig. 3-23b): Similar to an FTIR spectroscopic study of the C128T mutant in *Cr*ChR2[101], an illumination protocol with alternating light was applied and analyzed by a combination of SVD and a rotational procedure[186,187]. Green light induces a P-rich spectrum with further contributions of L, M and N. UV light drives the photoreaction of M and removes it out of the light-induced steady state. The analysis revealed a stationary component that mainly reflects the formation of P and an alternating component that reflects the formation and decay of M, depending on the illumination wavelength: Positive bands are induced by UV light and report on the dark state recovery (M→D transition), while negative bands refer to the green light induced M intermediate (D→M transition). Evidently, the alternating component obtained by this illumination protocol strongly resembles the fast decay component (*e.g.* considering the strong amide I band at 1661 $cm^{-1}$ and the assumed υ(C=C) mode at 1551 $cm^{-1}$) , while the stationary component fits the slow decay component obtained from the analysis of thermal decay (Fig. 3-23a). The resemblance of thermal and light-induced decay spectra allows the conclusion that the photocycle branching occurs in the M intermediate, and that the M→D and M→N transitions

occur in parallel, as already demonstrated by UV-Vis flash photolysis data of ReaChR.[52]

### 3.2.4.3 Reversion of protonation changes

In order to characterize the actual molecular determinants of this bifurcation event, distinctions in the spectra associated with the M→D and P→D transitions, respectively, need to be considered. Strong deviations are found in the υ(C=O) region (Fig. 3-25). Difference spectra of both thermal and light-induced M→D transition exhibit a band pattern at ~ 1766(-)/ 1757(+) $cm^{-1}$ that was already observed in the state 1 spectrum (see Fig. 3-16, p. 75) and reflects a hydrogen bond change of protonated $Asp^{DC}$. In addition to the D196N mutant spectra (see Fig. 3-17, p. 77, and Fig. 3-22, p. 85), assignment of this vibration to $Asp^{DC}$ is further backed up by the $Cys^{DC}$ mutant spectra in $H_2O$ and $D_2O$ that do not exhibit this band pattern as well. $Cys^{DC}$ mutation leads to a long-lived M state from which the dark state is only slowly recovered within thousands of seconds[51], similar to *Cr*ChR2[82,101]. The lack of the band pattern at ~ 1766(-)/ 1757(+) $cm^{-1}$ in the C168S mutant suggests that $Cys^{DC}$ is the hydrogen bond partner of $Asp^{DC}$ as reported for *Cr*ChR2.[81] In P, $Asp^{DC}$ is deprotonated and reprotonates in the P→D transition as reflected by the band at 1753(+) $cm^{-1}$. The second difference between the M→D and P→D transition spectra refers to the vibrational bands at around 1738 $cm^{-1}$: In the P→D transition, Ci2 releases the proton it received from the $RSBH^+$ during M state formation, reflected by the band at 1738(-) $cm^{-1}$. This similarly occurs in the M→D transition. The respective band, though, is partially overlaid by an additional band at around 1738(+) $cm^{-1}$ that

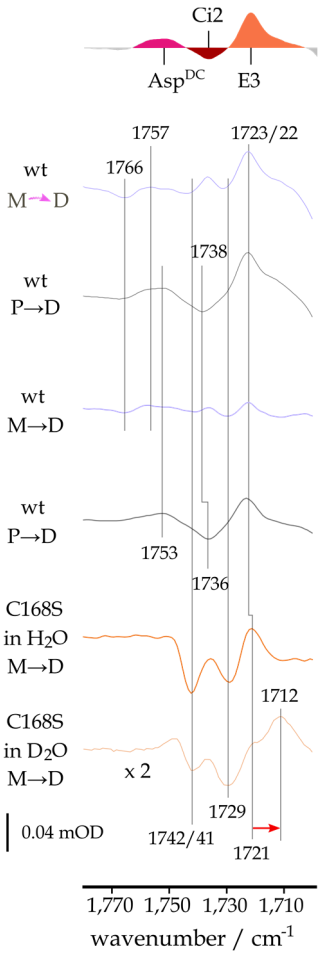


**Fig. 3-25** The υ(C=O) region of difference spectra of ReaChR-wt at pH 7.4 from Fig. 3-23 (thermal and light-induced decay spectra, p. 88), and of dark – light spectra of the $Cys^{DC}$ mutant C168S in $H_2O$ and $D_2O$ at pH 7.4 and 293 K (pD 7.8) after illumination with green LEDs ($\lambda_{max}$ ~ 529 nm). Spectra were scaled to retinal fingerprint bands in the spectrum of the C168S mutant in $D_2O$. The *red arrow* indicates a frequency shift in $D_2O$.

presumably reflects reprotonation of an unknown residue. This overlay leads to a split of the apparent band reflecting protonation of Ci2, leading to maxima at 1742(-) and 1729(-) $cm^{-1}$. The fact that Ci2 deprotonates in the M→D transition makes it a suitable donor for reprotonation of the RSB. This assumption is further supported by the fact that other possible donor groups (aspartic and glutamic acids) that would be reflected by additional negative modes are not present in the υ(C=O) region. All spectra, however, exhibit a band at 1723–21(+) $cm^{-1}$ (and 1712 $cm^{-1}$ in the $Cys^{DC}$ mutant in $D_2O$) that is due to reprotonation of E3. Thus, during both M→D and P→D transition the proton transfers involving Ci2 and E3 are reversed, while deprotonation of $Asp^{DC}$ occurs only in the M→N transition after the photocycle bifurcation.

## 3.2.5 Discussion

### 3.2.5.1 Summary

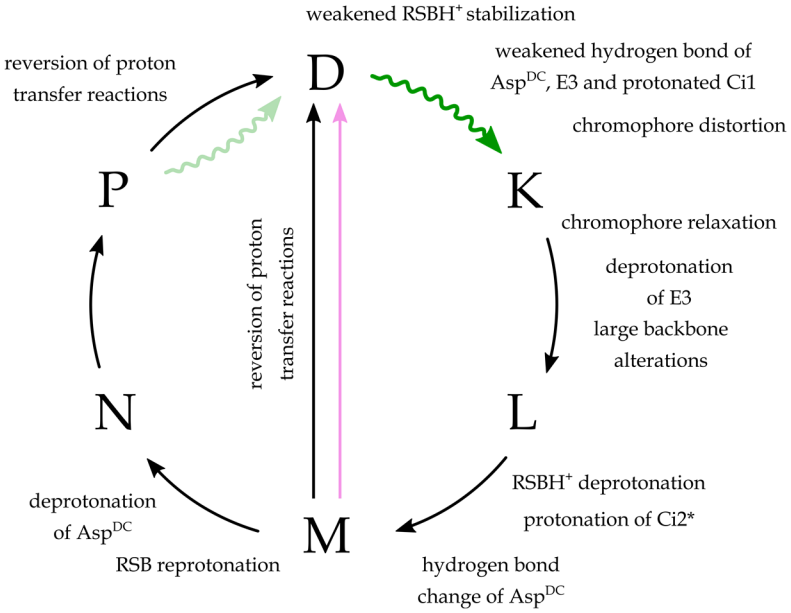


**Fig. 3-26** The photocycle dynamics of ReaChR with respect to the apparent intermediates D, K, L, M, N and P. A two-branched photocycle scheme comprising the 15-*anti* and 15-*syn* branch as presented in Krause *et al.* 2017[51] and introduced in 1.2.5.1 (p. 15) was omitted, as it was not possible to distinguish between intermediates of the 15-*anti* and the 15-*syn* photocycle branch, respectively, based on the FTIR spectroscopic data. Similarly, the distinction between $M_1$ and $M_2$ as included in the photocycle scheme of ReaChR in Krause *et al.* 2017[51] was omitted, as it was not possible to discriminate these intermediates. In addition to the M→N reaction, a transition from M to D was observed (see Fig. 3-23, p. 88). A photoreaction of the late desensitized P intermediate must be assumed in order to explain the observation from electrophysiological experiments that ReaChR is not trapped in a non-conducting photointermediate at continuous illumination but instead a stationary photocurrent is maintained.[51,52] *based on time-resolved UV-Vis spectra.[52]

The structural alterations and proton transfer processes characterized in Fig. 3-26 refer to apparent photocycle intermediates, as it was not possible to disentangle the specific photoreactions of either of the photocycle branches. However, the significantly larger contribution of the 15-*anti* photocycle branch to the observable photoreaction considering the isomeric composition of the apparent dark state (see Tab. 3, p. 84), implies that the structural alterations can at least be assigned to this photocycle branch (along with further evidence from FTIR spectroscopic data as discussed in particular for the proton dynamics of E3, see 3.2.5.3, p. 97).

In the D→K transition, E3 experiences a weakening in hydrogen bonding and hydrogen bonding involving protonated Ci1 is weakened as well. In the K→L transition, the light energy stored in the distorted chromophore conformation is released by relaxation and induces minor structural changes. The relaxation

process depends on the Ci1 protonation state, being delayed by the enhanced hydrogen bonding of Ci1. In the L intermediate, E3 deprotonates and large backbone alterations occur that are likely due to water influx into the intracellular half channel. In the L→M transition, the $RSBH^+$ proton is transferred to Ci2[52] and hydrogen bonding of $Asp^{DC}$ is weakened. From M, a photocycle branching occurs. While a fraction undergoes M→D transition, another fraction proceeds via N further to the long-lived P intermediate. $Asp^{DC}$ might play a role in photocycle bifurcation as it remains protonated in the M→D transition but deprotonates in the M→N transition. The bifurcation event furthermore depends on Ci2 which presumably serves as proton donor for reprotonation of the RSB in the M→D transition.

While the recent publication by Kuhne *et al.* 2019[98] proposed based on the analysis of the retinal fingerprint region in FTIR spectra that the cofactor in the late desensitized state in *Cr*ChR2 ($P_{480}$) is in 13-*cis*,15-*syn* conformation, application of the same band assignments to the dark state recovery spectra of ReaChR (see Fig. 3-23, p. 88) strongly implies that the retinal in P is mainly in 13-*cis*,15-*anti* conformation. Following this argument, a light-induced P→D transition (13-*cis*,15-*anti*→13-*trans*,15-*anti*) needs to be included in the photocycle scheme (Fig. 3-26) in order to explain the observation that ReaChR is not trapped in a non-conductive state (P) at continuous illumination similar to the recently discovered MerMAID ChRs[213] but instead maintains a stationary photocurrent.[51,52]

#### 3.2.5.2 Energy transfer from chromophore to proteins

FTIR spectroscopic investigation of the early phototransitions in the photocycle of ReaChR revealed a significant distortion of the chromophore after light activation as reflected by intense HOOP bands[203–205] (see Fig. 3-13, p. 69, and Fig. 3-14, p. 71). Chromophore distortion is one of the main mechanisms of energy storage in rhodopsins along with transient displacement of the charges of the counter-ion complex.[135,137,140,143] The observations that (i) the overall extent of chromophore distortion was reduced (see Fig. 3-13, p. 69, and Fig. 3-14, p. 71) and (ii) the dynamics of chromophore relaxation reflected by HOOP band decay (Fig. 3-15, p. 73) were strongly accelerated by both deprotonation of Ci1 and its mutation to

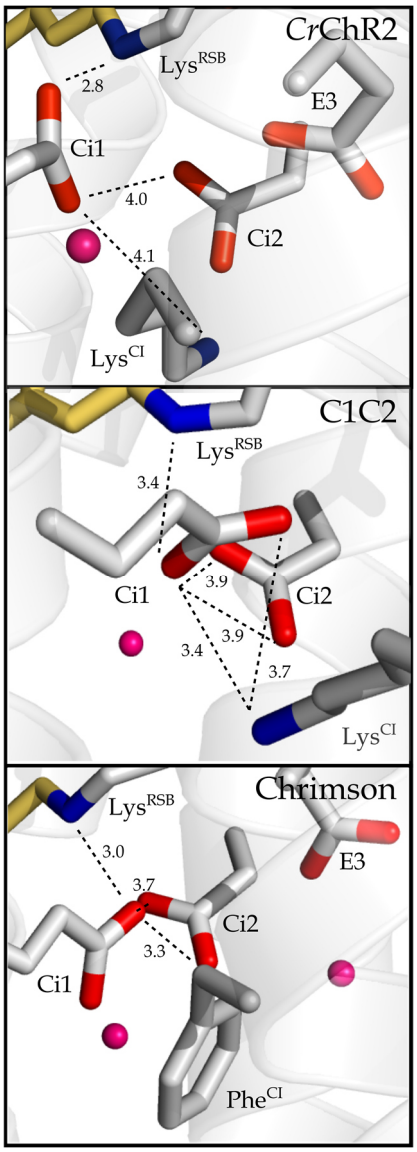


**Fig. 3-27** The active sites of *Cr*ChR2 (6EID, *above*), C1C2 (3UG9, *center*) and Chrimson (5ZIH, *below*). The Chrimson structure suggests that the Ci1-Ci2 interaction is enhanced with protonated Ci1. The *Cr*ChR2 and C1C2 structures imply that $Lys^{RSB}$ and $Lys^{CI}$ compete for salt bridge formation to deprotonated Ci1. Distances are given in Å. Structures were visualized with PyMol (Version 2.1.1.).

threonine indicate that specific interactions of protonated Ci1 stabilize the distorted chromophore conformation and delay release of the strain energy. Direct proof for hydrogen bonding of protonated Ci1 is given by FTIR difference spectra obtained at 80 K, as transient weakening of this hydrogen bonding caused a difference band pattern in the υ(C=O) region (see Fig. 3-11, p. 67). The frequencies of this band pattern (1713(+)/ 1705(-) $cm^{-1}$) report on strong hydrogen bonding of protonated Ci1 in the dark that possibly involves multiple partners and is weakened (although still strong) after illumination.[183] Likely candidates are the $RSBH^+$ (as hydrogen bond donor) and Ci2 (as hydrogen bond acceptor). It is also possible that different hydrogen bonding patterns exist in parallel in conformational substates as indicated by QM/MM simulations on *Cr*ChR2.[48]

Ci1 and the $RSBH^+$ are in hydrogen bond distance in *Cr*ChR2, C1C2 and Chrimson (Fig. 3-27).[41,72,73] The Ci1-Ci2 distance is larger in C1C2 (3.9 Å) and *Cr*ChR2 (4.0 Å) and smaller in Chrimson (3.3 Å). This indicates that in C1C2 and *Cr*ChR2 no hydrogen bond is formed between Ci1 and Ci2 as both counter-ions are deprotonated (according to $pK_a$(Ci1) < 4 in *Cr*ChR2[24d] and 5.4 in C1C2[cd]), while in Chrimson hydrogen bonding between Ci1 and Ci2 exists because Ci1 is protonated

[c] Data by Benjamin Krause, Humboldt University Berlin. Included in: Kaufmann *et al.* Energy transfer from chromophore to protein is modulated by the protonation state of a glutamic acid in the active site of channelrhodopsin. Manuscript in preparation for resubmission.

[d] pH conditions during crystallization: pH 5.2–5.6 in *Cr*ChR2[24], pH 6.0 in C1C2[41]

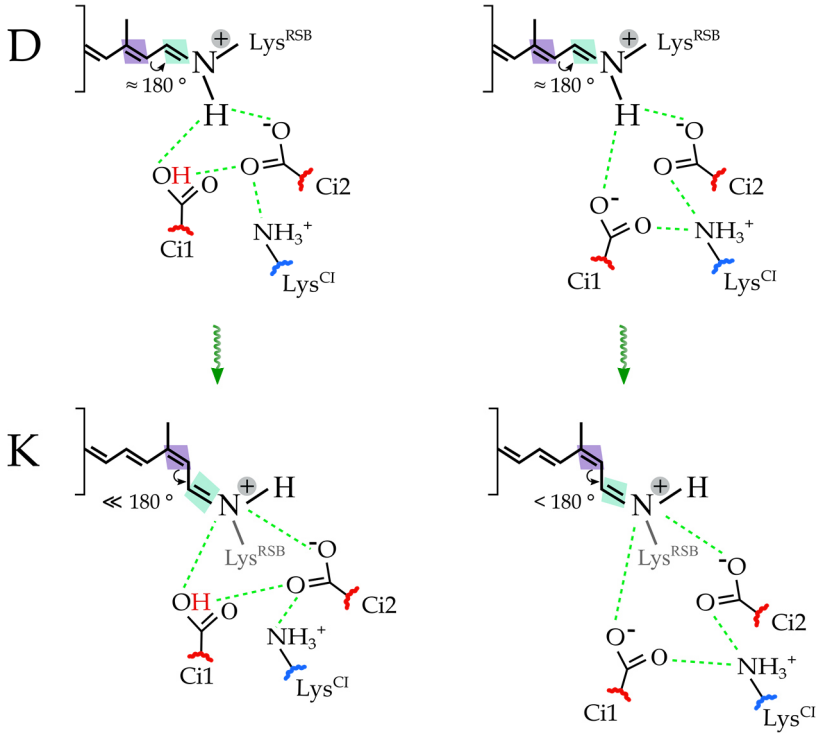


**Fig. 3-28** The role of the Ci1 protonation state for energy transfer from chromophore to protein. The dark state absorption is tuned by the Ci1 protonation state as deprotonated Ci1 *(upper row, right column)* leads to a better electrostatic stabilization of the RSBH+ and thereby to a hypsochromic shift. In the dark state configuration with protonated Ci1 **(***upper row***,** *left column***),** hydrogen bonding is enhanced as compared to deprotonated Ci1 (*upper row, right column*). This probably results in a larger rigidity of the active site that leads to stabilization of the distorted chromophore conformation after light activation (*lower row, left column*). In contrast, the higher flexibility of the active site with deprotonated Ci1 allows a comparably faster release of the strain energy (*lower row, right column*).

(according to p$K_a$(Ci1) 7.4–8.1[54e]). Formation of strong hydrogen bonds in the active site with protonated Ci1 probably increases the rigidity and thus might stabilize the distorted chromophore conformation in the K intermediate. Accordingly, the active site could gain flexibility with deprotonated Ci1 due to weakened hydrogen bonding. This could explain the accelerated energy transfer to the protein (see Fig. 3-15, p. 73). In addition to the weakened hydrogen bonding of deprotonated Ci1, it might also change ist orientation as compared to protonated Ci1 due to a stronger interaction with Lys$^{CI}$. In C1C2 that likely is the better template for the ReaChR structure as compared to *Cr*ChR2 given (i) the higher sequence identity (76.7 as compared to 63.3 %, calculated with ExPASy[214]) and (ii) the increased p$K_a$ of Ci1 (5.4[f] vs. < 4 in *Cr*ChR2[24] which renders it more

[e] pH condition during crystallization: pH 5–7[54]

[f] Data by Benjamin Krause, Humboldt University Berlin. Included in: Kaufmann *et al.* Energy transfer from chromophore to protein is modulated by the protonation state of a glutamic acid in the active site of channelrhodopsin. Manuscript in preparation for resubmission.

similar to ReaChR (7.6[f])), deprotonated Ci1 is relatively close to $Lys^{CI}$ with distances of 3.4 and 3.7 Å (see Fig. 3-27, p. 95). In *Cr*ChR2, though, Ci1 and $Lys^{CI}$ are more distant (6.1 and 4.1 Å). This picture is reversed for the Ci1-$RSBH^+$ interaction as it is stronger in *Cr*ChR2 (2.8 Å) as compared to C1C2 (3.4 Å). This suggests that the nitrogens of the $RSBH^+$ and $Lys^{CI}$ compete for salt bridge formation to deprotonated Ci1. Thus, deprotonated Ci1 in the active site of ReaChR could interact more strongly with $Lys^{CI}$ and thereby increase the flexibility near the $RSBH^+$ allowing faster chromophore relaxation along with a faster energy transfer to the protein. The accelerated energy transfer with deprotonated Ci1 is reflected by the lower activation energy for HOOP band decay with ($E_a$ = 26.2 ± 1.5 kJ/ mol) in comparison to the configuration with protonated Ci1 ($E_a$ = 35.7 ± 5.1 kJ/ mol, see Fig. 3-15, p. 73). As chromophore relaxation is expected to lead to a comparable blue-shift of the absorption spectrum, the elevated activation energy for release of the strain energy in protonated Ci1 is also the most suitable explanation for the delayed K→L transition at pH 5 ($\tau \approx 1.72$ µs) as compared to pH 9 ($\tau \approx 391$ ns) and the Ci1 mutant ($\tau \approx 455$ ns) deduced from time-resolved UV-Vis spectroscopic measurements at single turnover conditions (see Tab. 2, p. 62).[51,52] A similar effect was observed in PR with 8 µs at pH 5 and 4 µs at pH 9[215] and a similar p$K_a$ of Ci1 (p$K_a$(Ci1) ≈ 7[171,172,216]). An effect of the electrostatic interaction in the counter-ion complex on the extent of chromophore distortion can also be derived from studies on BR and bovine rhodopsin. In bovine rhodopsin in which only one counter-ion (Glu113) to the $RSBH^+$ is present (more similar to ReaChR with protonated Ci1), chromophore distortion is the dominant mechanism of energy storage.[135,142] Contrarily, in BR in which two counter-ions exist (Asp85 and Asp212, more similar to ReaChR with deprotonated Ci1) charge separation is comparably more relevant for energy storage.[137,139,143]

#### 3.2.5.3 Formation of the ion-conducting state

The K intermediate is followed by L, $M_1$, $M_2$ and N.[51] In the FTIR spectroscopic experiments presented in this thesis, a discrimination between $M_1$ and $M_2$ was not possible, so that the data interpretation is based on the assumption of an apparent M state (as in the photocycle model in Fig. 3-26, p. 93). Component analysis of flash photolysis experiments revealed that the decay of M cannot be described by a

simple M→N reaction scheme since a fraction of M shortcuts to D.[52] The largest structural rearrangements occur in the K→L transition (see Fig. 3-16, p. 75). The changes observed in the amide I region, mainly hinting at alterations of the backbone structure, depend strongly on the pH value. At alkaline pH, the backbone changes are largely reminiscent of FTIR difference spectra of *Cr*ChR2 with a similar vibrational band pattern at 1660/59(-)/ 1645/44(+) $cm^{-1}$ that was explained by helix hydration due to the influx of water molecules into the intracellular half-channel.[157] The analysis of time-resolved FTIR spectra of azF-labelled ReaChR variants proved this concept of water influx as these difference bands in the amide I region tallied the time course of difference bands in the azido stretch region (~ 2100 $cm^{-1}$) that are indicative of local polarity changes.[53] In contrast, the band shifts in the amide I region of alkaline samples are inverted at acidic pH with bands arising at 1660/59(-) and 1668(+) $cm^{-1}$, pointing to significant differences in the structure of the (pre-)conducting states in dependence of the pH value. Considering the inverse correlation of the α-helical amide I mode frequency with the degree of hydration[157], this hints at pH dependent deviations in the water content of the conducting states. Although further investigations are required for a more detailed characterization of this pH effect, this deviation agrees well with the fact that at lower pH the channel predominantly conducts protons that in comparison with larger ions can pass through a narrower pore without hydration shell.

While the amide I bands can serve as markers for global hydration changes occurring during the photoreaction, they do not provide information on the actual sites within the protein that experience these changes. A better spatial resolution could be achieved by the introduction of the *p*-azido-L-phenylalanine (azF) label at different positions within the presumed ion-conducting pathway. Polarity changes of the label environment can be due to alterations of (i) the local electrostatic field or (ii) the local water solvation or (iii) they can arise from altered hydrogen-bonding of the label. As the vibrational modes of azido labels are assumed to be only weakly affected by electric fields[217,218], frequency shifts of the azF label at ~ 2100 $cm^{-1}$ (see Fig. 3-19, p. 80) are most likely due to changes in local water solvation or in hydrogen bonding. The absence of a difference signal in this band region in the azF mutants Y112azF and C119azF indicates that they do not

experience hydration changes during the photoreaction, which supports homology models that localize these residues at the C-terminal end of TM1[53], so that they are solvent-exposed already in the dark. The presence of small difference signals in the F142azF and the K133azF mutants hints at only moderate hydration changes during the photoreaction, which could be explained by a more polar microenvironment of these labeling sites already in the dark.[53] The complex band pattern of the inner gate Y110azF mutant with one up- (2119(+) $cm^{-1}$) and one downshifted (2089(+) $cm^{-1}$) band arising from a single negative band (2108(-) $cm^{-1}$) hints at an increased variability of the environment at this position after light activation rather than a total change in polarity. However, in the time-resolved FTIR spectrum of the Y110azF mutant obtained after laser excitation that presumably reflects the conducting state, the band at 2119(+) $cm^{-1}$ was more pronounced than the band at 2090(+) $cm^{-1}$ so that a net increase in polarity can be assumed during presence of the ion-conducting pore.[53] Such a behaviour is in line with the influx of water into the inner gate during formation of the ion-conducting state. This is supported by the crystal structures of C1C2[41], *Cr*ChR2[72] and Chrimson[73] according to which the inner gate (see Fig. 1-6, p. 12) is largely dehydrated in the dark.

The spectral analysis of the υ(C=O) region (see Fig. 3-17, p. 77) indicates that the structural rearrangements in the K→L transition are linked with deprotonation of E3, similar to previous suggestions for *Cr*ChR2 by Kuhne *et al.* 2015[47]. However, Kuhne *et al.* 2019[98] proposed that E3 is deprotonated only in the 15-*syn* cycle and not in the 15-*anti* cycle. If this concept was applicable to ReaChR as well, the hydrogen bond change of E3 would be associated with formation of the 15-*syn* dark state D′ rather than a photoproduct of the 15-*anti* cycle. For *Cr*ChR2, this concept was derived from electrophysiological experiments that revealed a strong effect of E3 mutation (E90Q) on the open state of the 15-*syn* cycle ($P^*_{520^N}$). $P^*_{520^N}$ is a highly proton-selective conducting state that accumulates at continuous illumination due to its slow decay kinetics as compared to the open states of the 15-*anti* cycle and thus contributes largely to the stationary current. In *Cr*ChR2-E90Q, the stationary photocurrent is significantly reduced.[98] To the best of the author's knowledge, a comparable electrophysiological investigation that allows the discrimination of the open states of the 15-*anti* and 15-*syn* cycle does not

exist for ReaChR. However, previous electrophysiological experiments[52] showed that while E3 mutation in ReaChR (E130Q) reduces the proton selectivity similar to *Cr*ChR2-E90Q[98,219], it had no significant effect on the decay kinetics of the conducting state, in contrast to *Cr*ChR2-E90Q at single turnover illumination conditions[98]. More generally, the overall contribution of the 15-*syn* photocycle to the stationary spectra appears to be reduced in ReaChR as compared to *Cr*ChR2 (with the exception of ReaChR at pH 9) as can be concluded from the reduced intensity of the respective marker band for formation of 15-*syn* retinal at ~ 1185(-) $cm^{-1}$ in the P state spectrum (see Fig. 3-24, p. 89). This is in stark contrast to the observed increase of this band in the $P_{480}$ spectrum (D' of the 15-*syn* cycle) in *Cr*ChR2.[98] As a conclusion, it is more likely that the concept by Kuhne *et al.* 2019[98] is not applicable to ReaChR so that E3 does not only deprotonate in the 15-*syn* cycle but also deprotonates in the 15-*anti* cycle.

While on the basis of FTIR spectroscopic experiments, E3 deprotonation can only be assigned more vaguely to the K→M transition (see Fig. 3-16, p. 75), the complete lack of L in the UV-Vis flash photolysis experiments of E130Q[52] suggests its deprotonation more precisely in the K→L transition. Accordingly, the weakening of the hydrogen bonding of E3 in the D→K transition (see Fig. 3-10, p. 66) paves the way for its subsequent deprotonation in K→L. A key role for the (pre-)formation of the ion conducting pore was previously assumed for E3 in *Cr*ChR2 and described in the E90-helix2-tilt (EHT model[47]) that comprises the following mechanistic steps: (1) In the dark state, E3 forms a hydrogen bond to Asn258 and is thus oriented toward the intracellular side. (2) Retinal isomerization leads to a weakening of the hydrogen bond between E3 and Asn258 by causing a displacement of $Lys^{RSB}$. (3) E3 deprotonates and flips toward the extracellular side forming a salt bridge to $Lys^{CI}$. (4) This process opens the central gate and allows the influx of water molecules into the intracellular half-channel. However, the *Cr*ChR2 crystal structure revealed that the starting condition used for the MD calculations that was the basis of this model was incorrect: in contrast to C1C2 that was used as the template for the respective model, E3 is oriented towards the counter-ion complex in the *Cr*ChR2 dark state (see Fig. 1-5, p. 10). Albeit these contradiction, it is likely that the correlation of E3 deprotonation and water influx still holds true as it was derived based on the presumably correct starting condition

with E3 oriented towards the counter-ion complex as in the *Cr*ChR2 dark state structure. Additionally, the correlation between water influx and E3 deprotonation is supported by the reduced amide I vibrations in the E130Q mutant (see Fig. 3-18, p. 79). An enhanced electrostatic stabilization of the $RSBH^+$ by deprotonated E3 could furthermore explain the blue-shift in UV-Vis absorption with respect to the dark state that occurs during formation of L and is completely absent in the E3 mutant E130Q.[52] More challenging, though, is to explain the selectivity filter function of E3. In the E130Q mutant, the ion selectivity is shifted from protons to $Na^+$,[52] similar to *Cr*ChR2[88,98]. In *Cr*ChR2, replacement by aspartate hardly affects ion selectivity at all, while neutralization by glutamine or alanine shifts the selectivity toward $Na^+$[88] and exchange for lysine or arginine creates $Cl^-$-conducting channels[67]. Thus, the negative charge provided by deprotonated E3 in the open state is an important determinant for the high proton selectivity. This is presumably achieved by the formation of a salt bridge, presumably to $Lys^{CI}$ as proposed by Kuhne *et al.* 2015 based on MD calculations.[47] Such a salt bridge could form a barrier against the passage of larger cations and favor the influx of protons.

While large structural rearrangements occur during formation of L, only small further changes are required to establish the open state (see Fig. 3-15, p. 75). These changes involve a proton transfer from the $RSBH^+$ to Ci2 as derived from UV-Vis experiments[52], similar to *Cr*ChR2[104] but different to *Ca*ChR1[158]. This process leads to the formation of M. Ci2 remains protonated in the N intermediate. Electrophysiological measurements indicate a key role of Ci2 for formation of the conducting state as Ci2 mutation (D293N) resulted in a drastic reduction of the channel current[52], similarly observed in C1C2[41] and *Cr*ChR2[104]. The FTIR mutant spectra suggest that this is mainly due to a large mutational effect on the dark state conformation (see Fig. 3-18, p. 79) that might lead to the influx of water molecules already in the dark, thereby producing a leaky ion channel.

#### 3.2.5.4 Photocycle branching

Time-resolved UV-Vis spectroscopy revealed that two decay pathways for the M intermediate exist: a faster M→N and a slower M→D transition.[52] N proceeds to P from which the dark state is recovered in a slow process ($\tau_{off}$ in the order of tens of seconds[52]). Thus, two pathways exist for recovery of the dark state, *i.e.* M→D and

P→D. Both decay spectra exhibit the characteristic bands of 13-*trans*,15-*anti* retinal at 1234 and 1200 $cm^{-1}$ (see Fig. 3-23, p. 88, and Fig. 3-24, p. 89). An additional fingerprint band at 1185 $cm^{-1}$ that was characterized as a marker for isomerization around the C=N bond arising during double isomerization from 13-*trans*,15-*anti* to 13-*cis*,15-*syn* retinal[98] is only weakly pronounced at pH 7.4 as well as pH 5 (see Fig. 3-16, p. 75, and Fig. 3-23, p. 88) – a remarkable difference to the spectra at pH 9 which is addressed in the upcoming section. However, this suggests that the retinals in both decaying intermediates, M and P, are predominantly in 13-*cis*,15-*anti* conformation (along with minor contributions of 15-*syn* retinal as reflected by the band at 1185 $cm^{-1}$). This is in contrast to previous assumptions for *Cr*ChR2; it was suggested by several publications that the P intermediate adopts 13-*trans*,15-*anti* retinal as the dark state so that back isomerization occurs already in the N→P transition.[31,105,176] More recently, it was proposed instead that the long-lived desensitized state in *Cr*ChR2 is largely identical with the dark state D′ of the 15-*syn* cycle with the retinal in 13-*cis*,15-*syn* conformation.[98] In either case, existence of a long-lived desensitized closed state, P or D′, that can be re-activated by light with lower probability as compared to the initial dark state, D, is necessary to explain partial photocurrent inactivation at extended illumination times (see Fig. 1-10, p. 16). Thus, if P in ReaChR at both physiological and acidic pH predominantly adopts 13-*cis*,15-*anti* retinal which is strongly indicated by the retinal fingerprint region, two photons would be required to re-initiate the photocycle (P→D (hν) and D→K (hν), see Fig. 3-26, p. 93), as previously discussed by Ritter *et al.* 2008.[31]

It appears that the photocycle branching that starts from M[52] (see Fig. 3-23, p. 88) depends on the $Asp^{DC}$ protonation state: $Asp^{DC}$ remains protonated in the fraction that undergoes the M→D shortcut and deprotonates in the fraction that proceeds to the N intermediate instead (see Fig. 3-25, p. 91). In the M→D transition, the proton donor for reprotonation of the $RSBH^+$ is Ci2, which serves as the acceptor group during formation of M.[52] This proton transfer creates a charge distribution in the active site similar to the dark state ($RSBH^+$ protonated, Ci2 deprotonated) which is the prerequisite for retinal back isomerization in this pathway and in line with the theoretical calculations on thermal reactions of the retinal chromophore

by Tavan *et al.* 1985.[220] UV-Vis flash photolysis experiments support a crucial role of Ci2 for the photocycle bifurcation, as the M→D reaction is enhanced in the Ci1 mutant E163T that presumably decreases the p$K_a$ of Ci2 and thus enforces proton release from Ci2 to the $RSBH^+$.[52] Contrarily, the M→D reaction is weakened in the Ci2 mutant D293N.[52] This neutralizing mutation renders Ci1 the acceptor group for the RSB proton, but most likely Ci1 still retains a higher p$K_a$ than Ci2 due to the molecular surrounding that determines its p$K_a$ of 7.6[g] in the wild type and thus proton release to the RSB is decelerated.

While releasing its proton in the M→D reaction, Ci2 remains protonated in the faster M→N transition until its deprotonation in the P→D back reaction (see Fig. 3-25, p. 91). The kinetics of the M→N transition is significantly affected by $Asp^{DC}$ mutation (D196N) that leads to a delay by factor ~ 40 (see Tab. 2, p. 62). In contrast, in the corresponding D156A mutant of *Cr*ChR2 an M→N transition was not described and the M decay was delayed by factor ~ 9000.[82] Based on this significant effect, $Asp^{DC}$ was described as the proton donor for reprotonation of the RSB in *Cr*ChR2.[104] This conclusion is challenged by the long distance between $Asp^{DC}$ and the $RSBH^+$ (> 9 Å) and the fact that several $Asp^{DC}$ mutants in *Cr*ChR2 that abolish the carboxylic side group still maintain ion channel function.[52,67,83,85,169] Possibly, these contradictions could be resolved if a more indirect influence of $Asp^{DC}$ on the active site was considered; depending on its protonation state, $Asp^{DC}$ could alter the p$K_a$ values of the $RSBH^+$ and its counter-ions. Such wide-range effects are implied by the frequency upshift of the υ(C=O) vibration of Ci2 caused by mutation of $Asp^{DC}$ (see Fig. 3-17, p. 77) as well as the accelerated reprotonation of $Asp^{DC}$ by the counter-ion mutations (see Fig. 3-22, p. 85). Considering the comparably weaker effect of $Asp^{DC}$ mutation on the kinetics of M decay as compared to *Cr*ChR2[82], this assumed long-range influence of $Asp^{DC}$ on the active site and its indirect role for reprotonation of the RSB are less dominant in ReaChR. This could help to explain the mechanism of the photocycle bifurcation as illustrated in Fig. 3-29: If $Asp^{DC}$ remains protonated, the M intermediate is

[g] Data by Benjamin Krause, Humboldt University Berlin. Included in: Kaufmann *et al.* Energy transfer from chromophore to protein is modulated by the protonation state of a glutamic acid in the active site of channelrhodopsin. Manuscript in preparation for resubmission.

comparable stable ($\tau_{off}$(M→D) in the order of seconds[52] as compared to $\tau_{off}$(M→N) ~ 6.5 ms (see Tab. 2, p. 62)) and slowly decays directly to D as Ci2 releases its proton for reprotonation to the RSB and thereby lowers the energy barrier for the back reaction. Contrarily, if $Asp^{DC}$ deprotonates, reprotonation of the $RSBH^+$ is accelerated by a long-range effect of deprotonated $Asp^{DC}$ on the active site, and thereby deprotonation of Ci2 prior to decay of the P intermediate is prevented.

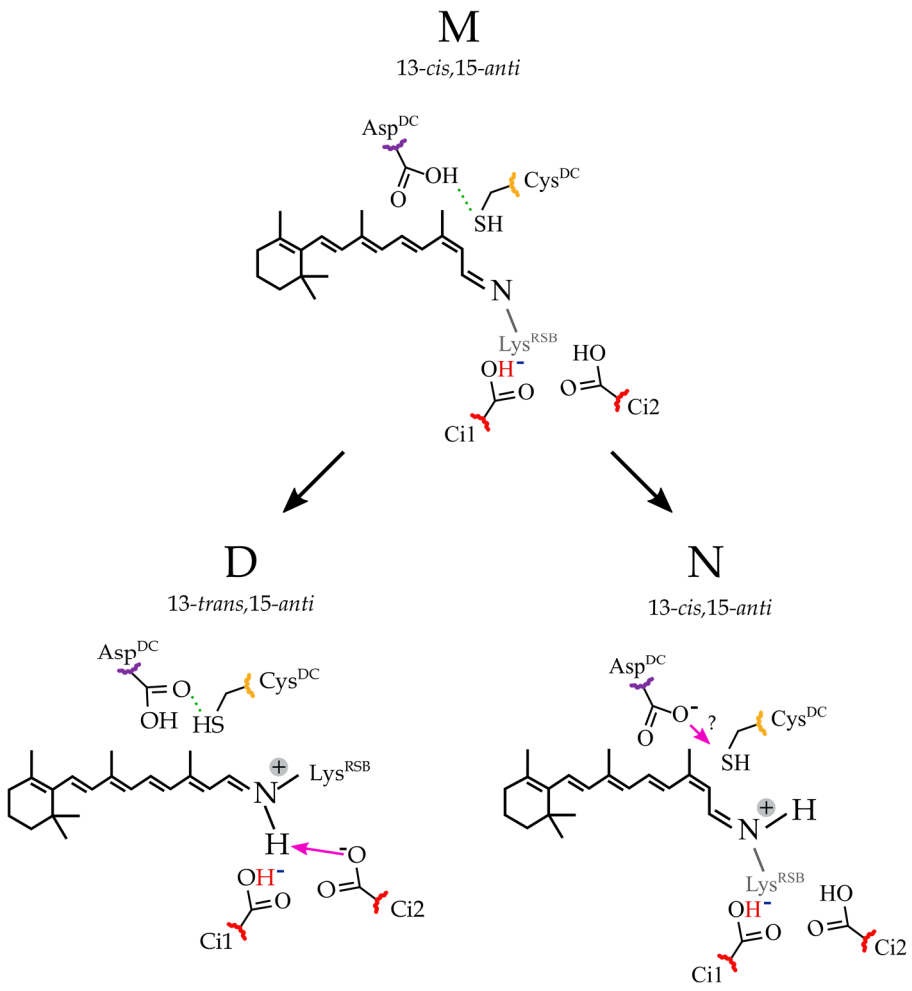


**Fig. 3-29** The photocycle bifurcation mechanism in ReaChR. From M, a photocycle branching occurs: In the M→D shortcut reaction, $Asp^{DC}$ remains protonated and Ci2 donates its proton for reprotonation of the RSB so that a charge distribution in the active site similar to the dark state is achieved. Contrarily, in the M→N reaction, $Asp^{DC}$ deprotonates which in an indirect fashion catalyzes reprotonation of the RSB while Ci2 remains protonated. From N, the photocycle proceeds to the closed P state from which the dark state is recovered. The *red* hydrogen and the *blue* negative charge at Ci1 shall illustrate its different protonation states.

#### 3.2.5.5 Parallel photocycles

According to NMR studies, the initial dark state ($D_{IDA}$) that is obtained during long dark adaptation periods adopts 100 % 13-*trans*,15-*anti* retinal.[96,102] However, a pure 13-*trans*,15-*anti* dark state has never been observed in ChRs based on HPLC analyses of extracted retinals.[51,99–101] In order to resolve this contradiction, it can be assumed that an equilibrium of 13-*trans*,15-*anti* and 13-*cis*,15-*syn* is present at least at low light conditions. As demonstrated by Bruun *et al.* 2015[96], the light-induced double isomerization from 13-*trans*,15-*anti* (D) to 13-*cis*,15-*syn* (D′) plays a crucial role in the formation of this equilibrium and presumably contributes to the partial photocurrent inactivation at continuous illumination. Additionally, photocycles are initiated from both D and D′ by isomerization around the $C_{13}$=$C_{14}$ bond and it is assumed that the ion-conducting state of the 15-*syn* cycle is less-conductive as compared to the conducting state of the 15-*anti* cycle so that its increased contribution at extended illumination contributes to the partial photocurrent inactivation as well (see 1.2.5.1 for details, p. 15).

Mutation of the binding pocket residue $Asp^{DC}$ (D196N) has a strong effect on the ratio of the parallel photocycles by affecting both the dark state and the photointermediates. The isomeric composition of the dark state is altered with a significant reduction of 13-*trans* in favor of 13-*cis*, 11-*cis* and 9-*cis* (see Tab. 3, p. 84) and the photoreactions are more complex as indicated by the strong vibrational band at 1182(-) $cm^{-1}$ that is only weakly pronounced in the wild type (see Fig. 3-20, p. 82). The higher contribution of retinal isomers other than 13-*trans* to the D196N dark state could help to explain the observation from electrophysiological measurements that ReaChR-D196N mutation changes the typical shape of the wild type photocurrent by abolishing the peak current[52], similar to the D156A mutant in *Cr*ChR2[82]. According to Kuhne *et al.* 2019[98], partial photocurrent inactivation that leads to the stationary current in electrophysiological measurements at continuous illumination reflects equilibration of the open and closed states of the 15-*anti* and 15-*syn* photocycles of *Cr*ChR2. Considering their decay kinetics, the conducting states of the 15-*anti* cycle ($P_{390b}^{M2}$ and $P_{520}^{N}$, $\tau_{off} \approx 30$ ms[98]) contribute more to the transient current while the conducting state of the 15-*syn* cycle ($P^{*}_{520}{}^{N}$, $\tau_{off} \approx 250$ ms[98]) contributes more to the stationary current. The lower initial

concentration of 13-*trans*,15-*anti* retinal in the $Asp^{DC}$ mutant D196N as compared to the wild type that is implied by the HPLC analysis (see Tab. 3, p. 84) could reduce the contribution of the open state of the 15-*anti* cycle and thus vanish the transient current.

In addition to $Asp^{DC}$ mutation, the isomeric composition of the dark state is affected by the Ci1 protonation state with an increased contribution of 11-*cis* at the expense of 13-*trans* in the configuration with protonated Ci1 (derived from the isomeric composition of the wild type at pH 5, see Tab. 3, p. 84). A similar pH effect was observed in XR, in which low pH increased the contribution of 9-*cis* retinal.[114] In addition to this effect, the Ci1 protonation state also has a strong influence on the efficiency of the competing photoisomerization reactions: In the configuration with deprotonated Ci1, the 13-*trans*,15-*anti*→13-*cis*,15-*syn* retinal double isomerization is enhanced as compared to protonated Ci1 (see Fig. 3-16, p. 75, and Fig. 3-21, p. 83). This observation could be explained by a direct influence of the additional negative charge of deprotonated Ci1 on the stereoselectivity of the photoreaction by modulation of the energy landscape of the excited electronic state. Although pump-probe measurements in the ps time regime are required to confirm this possible explanation, the hypothetic catalytic effect of deprotonated Ci1 on the stereoselectivity of the photoreaction is briefly described (Fig. 3-30): Translocation of the positive charge residing at the $RSBH^+$ toward the *β*-ionone ring upon photon absorption is a key mechanism of photoisomerization in rhodopsins.[129–131,221] In BR, it leads to formation of the blue-shifted excited electronic state, I.[221] Subsequently, the positive charge is transferred backwards in the direction of the RSB which transiently increases the single bond character of the $C_{13}$=$C_{14}$ bond. This step that coincides with a spectral red-shift is referred to as J intermediate in BR and the prerequisite for *trans*→*cis* isomerization.[221] It was shown based on neutralizing mutations of the counter-ions in BR that the negative charge provided by the counter-ions is essential for an efficient electrostatic stabilization of the positive charge in the $C_{13}$=$C_{14}$ bond.[129,222] Similar observations were made by Scholz *et al.* 2012 who showed that the negative charge provided by deprotonated Ci1 catalyzes isomerization around the $C_{13}$=$C_{14}$ bond in *Cr*ChR2.[121] Notably, evaluation of their data obtained by femtosecond time-resolved

spectroscopy revealed a second photoproduct at pH 7.4 (at which Ci1 is deprotonated in *Cr*ChR2) that was observed neither at pH 4 (at which Ci1 is probably largely protonated) nor in the E123T mutant.[121] This observation hints at a parallel photoreaction taking place at physiological pH, presumably 13-*trans*,15-*anti*→13-*cis*,15-*syn*[98], similar to the assumption for ReaChR. Likely, deprotonated Ci1 helps focusing the positive charge in the J-like intermediate in both the $C_{13}$=$C_{14}$ and the $C_{15}$=N bond, thus increasing their single bond character and increasing the probability for 13-*trans*,15-*anti*→13-*cis*,15-*syn* double isomerization.

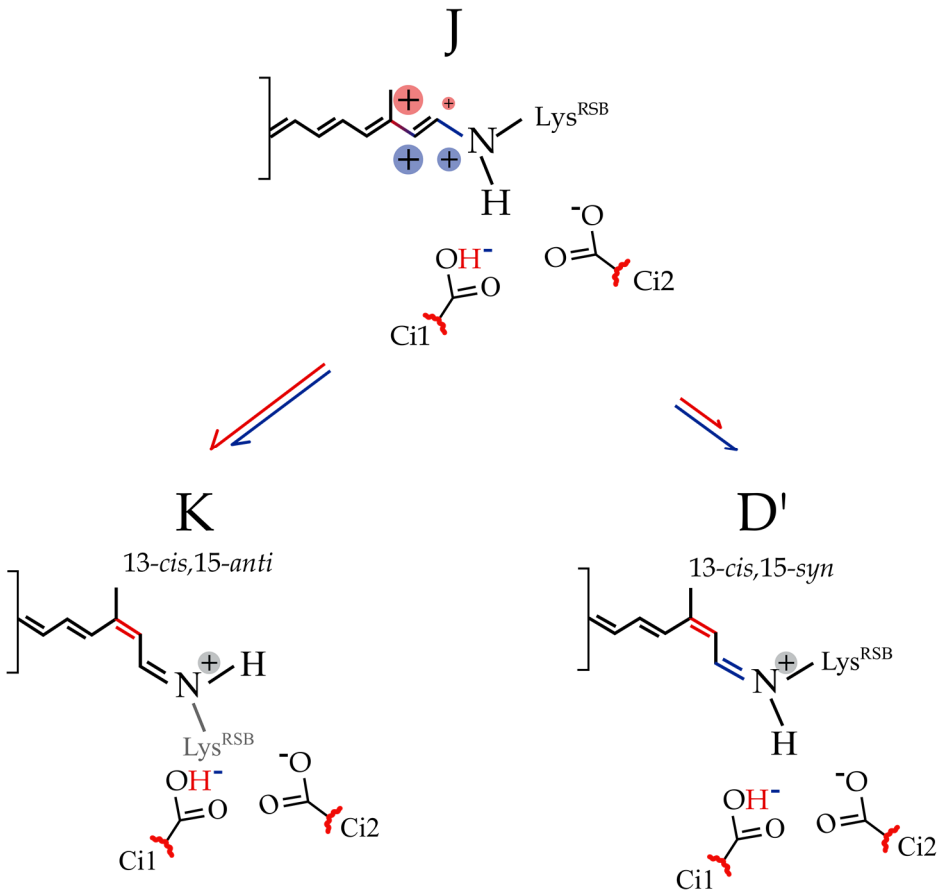


**Fig. 3-30** Possible reaction model for the effect of the Ci1 protonation state on the competing photoisomerization reactions 13-*trans*,15-*anti*→13-*cis*,15-*anti* (D→K transition) and 13-*trans*,15-*anti*→13-*cis*,15-*syn* (D→D′ transition). In ReaChR with deprotonated Ci1, the D→D′ transition is enhanced as compared to protonated Ci1. Photon absorption leads to a translocation of the positive charge from the $RSBH^+$ toward the *β*-ionone ring. Subsequent backward movement of the positive charge toward the RSB leads to a transient negative electron density near $C_{13}$=$C_{14}$ and presumably $C_{15}$=N that increases the single bond character of these bonds and thereby promotes isomerization. In BR, the respective intermediate is termed J.[221] The catalytic effect of deprotonated Ci1 for the 13-*trans*,15-*anti*→13-*cis*,15-*syn* double isomerization reaction could then be explained by a relatively stronger electrostatic stabilization of the negative electron density at $C_{15}$=N as compared to protonated Ci1 which would increase the probability for simultaneous rotation around the $C_{13}$=$C_{14}$ and $C_{15}$=N bonds as required for formation of 13-*cis*,15-*syn* retinal (D′).

## 3.3 The orange-absorbing ChR Chrimson

(*Cs*)Chrimson is a proton-selective ChR from *Chlamydomonas noctigama* with the N-terminal sequence from *Chloromonas subdivisa* ChR that exhibits an unprecedented red-shifted absorption maximum ($\lambda_{max}$ ~ 590 nm) and is thus a promising tool for optogenetic applications as it allows deeper tissue penetration. Factors for this unusual bathochromic shift are the protonation of Ci1 (see Fig. 1-5, p. 10) and an extraordinary distortion of the chromophore in the dark. Light activation of Chrimson at acidic pH leads to relaxation of the distorted chromophore and to deprotonation of Ci1, establishing a blue-shifted conducting intermediate, termed L. The backbone changes occurring upon formation of L are significantly smaller as compared to other ChRs, suggesting a barrier to water molecules at the extra- and intracellular gates. In the external gate, this barrier that is decisive for the high proton selectivity of Chrimson is due to a restriction site involving E4 (see Fig. 1-7, p. 13). Remarkably, the p$K_a$'s of E4 and Ci1 are coupled by a long-range interaction as neutralization of E4 leads to deprotonation of Ci1. Through this p$K_a$ coupling, channel gating is rather delocalized along the ion-conducting pore in contrast to the role of the central gate of the blue-absorbing *Cr*ChR2. Formation of L is due to 13-*trans*,15-*anti*→13-*cis*,15-*anti* isomerization. At continuous illumination with orange or red light, an additional non-conductive blue-shifted state is formed that is thermally stable but can be photoconverted to the dark state by green light. Its formation is most likely due to retinal double isomerization from 13-*trans*,15-*anti* to 13-*cis*,15-*syn* so that it represents the D′ state of Chrimson.

Key residues in chapter 3.3 (see Fig. 1-5, p. 10, and Fig. 1-7, p. 13):

Ci1, counter-ion 1 (Glu165); Ci2, counter-ion 2 (Asp295); E3, central gate residue Glu132; E4, extracellular gate residue, Glu139; $Phe^{CI}$, residue of the extended counter-ion complex, Phe135

## 3.3.1 The photocycle intermediates

### 3.3.1.1 Temperature-resolved UV-Vis measurements

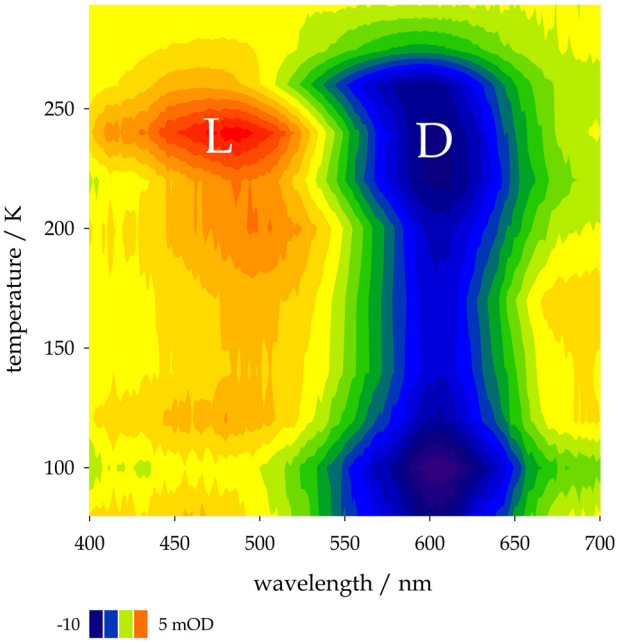


**Fig. 3-31** UV-Vis light – dark difference spectra of the Chrimson wild type at pH 5, recorded between 80 and 293 K, revealing formation of the L intermediate upon illumination with orange LEDs ($\lambda_{max}$ ~ 594 nm) following ≥ 30 min in the dark at ≥ 293 K between measurements.

To investigate the photocycle of Chrimson, UV-Vis difference spectra were recorded at pH 5 in the temperature range from 80 to 293 K (Fig. 3-31). At this pH value, Ci1 is protonated[54] and exhibits an absorption maximum at ~ 590 nm[39,54]. Accordingly, the photoreaction was induced by orange light ($\lambda_{max}$ ~ 594 nm). Dark state bleaching is reflected by a negative absorption band at around 600 nm (D). A positive band arises at around 490 nm (L) with maximum intensity at 240 K. Based on its hypsochromic absorption shift with respect to the dark state, this intermediate is termed L in the following in analogy to BR. The static UV-Vis measurements conducted at cryogenic conditions for Chrimson at pH 5 must be complemented by the time-resolved experiments by Urmann *et al.* 2017[54]: Here, UV-Vis flash photolysis experiments of Chrimson at pH 6 (yielding protonated Ci1) revealed a blue-shifted photoproduct L as observed in Fig. 3-31. Its biphasic decay ($\tau_{1off}$ = 23 ms and $\tau_{2off}$ = 115 ms) agreed well with the biphasic decay kinetics of the photocurrent so that L was identified as the conducting state.[h] Prior to L, a K-like intermediate absorbing at ~ 680 nm is formed.[54]

At pH 9.5 (yielding deprotonated Ci1), the flash photolysis experiments reported by Urmann *et al.* 2017.[54] revealed an early K intermediate ($\lambda_{max}$ ~ 640 nm), followed

[h] Confirmed by Johannes Vierock, Humboldt University Berlin. Included in: Kaufmann *et al.* A unique gating mechanism is responsible for the high proton selectivity of the red-absorbing channelrhodopsin Chrimson. Manuscript in preparation.

by an M intermediate, while L was not observed. The M state is followed by N ($\lambda_{max}$ ~ 640 nm). In comparison to the photocycle at acidic pH, the dark state recovery is slow (the slowest spectral component of the photoproduct is not recovered within the observation time of 10 s).[54] The fact that neither K nor D′ are observed in the difference spectra obtained at cryo-conditions (Fig. 3-31) can be explained by light scattering due to freezing of the protein sample which significantly lowers the SNR.

### 3.3.1.2 Recovery of the dark state

At the illumination conditions used in the temperature-resolved UV-Vis experiments, the L intermediate was maximally accumulated at 240 K (see Fig. 3-31, p. 109). In Fig. 3-32a, the UV-Vis light – dark steady state spectra from 220–275 K corrected for background noise by SVD (for details see 2.2.3, p. 41) are shown. The spectra at 220 and 240 K exhibit maxima at ~ 487 nm and thus represent formation of the L intermediate. With increasing temperature, though, the maximum absorption is downshifted to ~ 478 nm. The corresponding kinetics of the bands at 478 and 598 nm at 275 K are shown in Fig. 3-32b. Orange light induces a blue-shifted difference spectrum. This shift is increased by additional or exclusive red illumination and reduced by green illumination. After light off, the absorption at 598 nm increases and a plateau is formed that persists during the

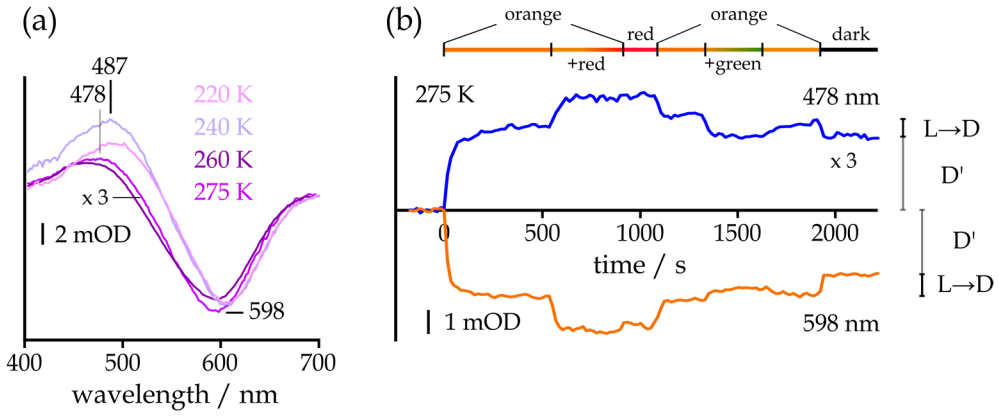


**Fig. 3-32** Dark state recovery and wavelength dependence of Chrimson-wt at pH 5. **(a)** UV-Vis light – dark difference spectra between 220–275 K after illumination with orange LEDs ($\lambda_{max}$ ~ 594 nm) following ≥ 30 min in the dark at ≥ 293 K between measurements. L is maximally accumulated at 240 K and the difference band is blue-shifted > 240 K. **(b)** Kinetic traces of the maximum absorption bands observed at 275 K at 478 and 598 nm. After light-off, the intensity of both marker bands is partially reduced, reflecting the fast L→D transition. A large fraction remains stable in the dark indicating the presence of a long-lived intermediate (D′). Along with orange LEDs, green ($\lambda_{max}$ ~ 523 nm) and red ($\lambda_{max}$ ~ 633 nm) LEDs were used.

observation time. The kinetics at 478 nm largely mirror the kinetics at 598 nm. The temporal course after light-off suggests that in addition to the fast L→D transition, a fraction of the blue-shifted photoproduct is thermally stable and is referred to as D′ in the following. Such a state was not observed at the single-turnover conditions in the flash photolysis experiments by Urmann *et al.* 2017.[54], indicating that it is the result of a photoreaction with reduced quantum efficiency.[i] Considering the fast decay kinetics of the photocurrents[39,54], D′ is a closed state.

### 3.3.2 The early photointermediates

In the early photoreaction, the K intermediate is formed, absorbing maximally at ~ 680 nm. Additionally, the D' state ($\lambda_{max}$ = 478 nm) observed in Fig. 3-32 (p. 110) should be formed at 80 K although it was not observed in transient UV-Vis

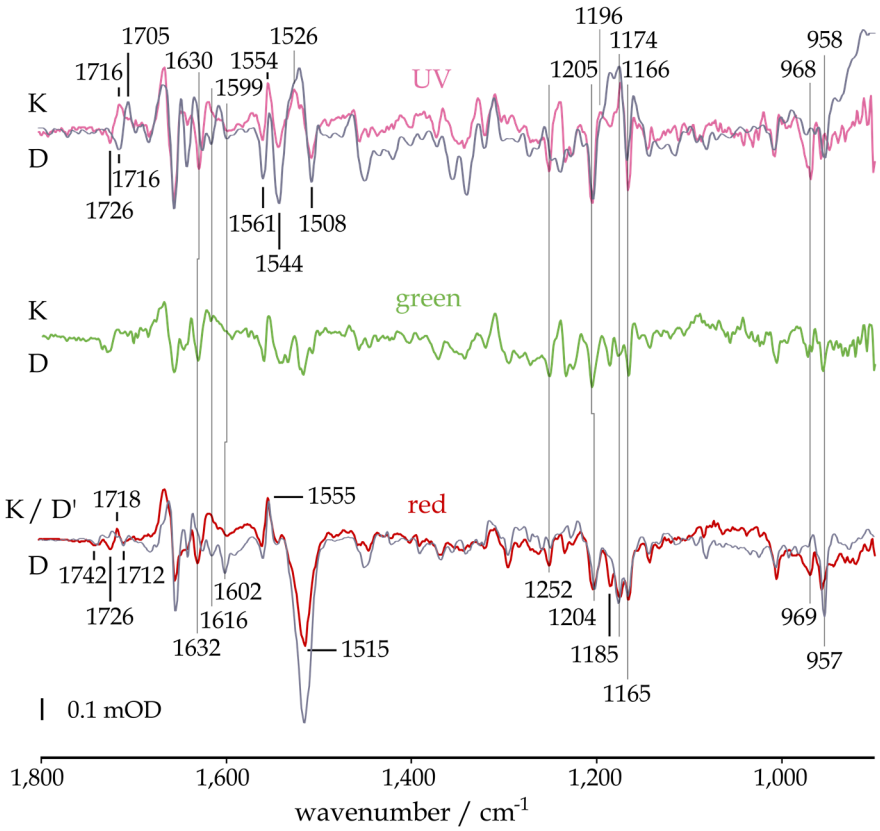


**Fig. 3-33** FTIR light – dark difference spectra of Chrimson-wt at pH 5 recorded at 80 K with UV ($\lambda_{max}$ ~ 405 nm), green ($\lambda_{max}$ ~ 523 nm) and red ($\lambda_{max}$ ~ 633 nm) illumination following ≥ 5 min in the dark at ≥ 293 K in $H_2O$ (*colored*) and $D_2O$ (*gray*). UV and green light mainly trap the D→K transition, while red light accumulates both K and D′. Spectra were scaled to retinal fingerprint bands in the spectrum obtained in $H_2O$ after red illumination (for details see 2.2.3.1, p. 41).

[i] Confirmed by Johannes Vierock, Humboldt University Berlin. Included in: Vierock, Kaufmann *et al.* Light adaptation in the red shifted channelrhodopsin Chrimson involves unprecedented bistability of two dark states. Manuscript in preparation.

spectra[54], possibly due to low SNR. In order to test whether both K and D' are formed in Chrimson at pH 5 at 80 K, different illumination wavelengths were applied to induce the photoreaction. Continuous red illumination is expected to favor the formation of D′ at the expense of K because of a red light-induced K→D back reaction, while green illumination is assumed to have the inverse effect by inducing a D′→D back reaction. As the resulting light – dark difference spectrum obtained by green illumination has a low SNR (Fig. 3-33, *middle spectrum*), illumination with UV light was additionally performed and yielded a better SNR. The following spectral analysis therefore focuses on the difference spectra obtained by UV (*upper spectrum*) and red (*lower spectrum*) illumination, respectively.

The large negative band at 1515 $cm^{-1}$ after red illumination reflects the υ(C=C) vibrations of the dark state chromophore and correlates well with the absorption maximum at ~ 590 nm. The correlation between retinal υ(C=C) modes and UV-Vis absorption is a well-known feature of rhodopsins.[132,191] UV illumination gives rise to three negative bands at 1561, 1544 and 1508 $cm^{-1}$ that would accordingly correlate with dark states absorbing UV, blue and red light, respectively. However, it needs to be taken into account that amide II modes contribute as well to this region impairing the assignment of photoproducts especially in the early intermediates, similar to *Cr*ChR2 and C1C2.[31,103,132] In both the UV and the red light induced difference spectra, a vibrational band at 1555/54(+) $cm^{-1}$ is present that might reflect the blue-shifted retinal υ(C=C) modes of D′ that might partially be formed as well upon UV illumination. Additionally, UV light gives rise to a band at 1526(+) $cm^{-1}$ that presumably reflects formation of K.

In the retinal fingerprint region, two negative bands at 1205/04 and 1166/65 $cm^{-1}$, both largely insensitive to H–D exchange, are present in both the red and the UV light induced spectra and hint at the depletion of a 13-*trans*,15-*anti* chromophore.[110] The band at 1166/65(-) $cm^{-1}$ presumably reflects the $\upsilon(C_{10}–C_{11})$ vibration of 13-*trans* retinal[144] and is not observed in *Cr*ChR2[31,103,151] and C1C2[42] but present in the green-absorbing *Ca*ChR1[158] and ReaChR[51], as well as BR[147], implying differences in the chromophore geometry around the $C_{10}–C_{11}$ bond between Chrimson and *Cr*ChR2

that could be relevant for the bathochromic absorption shift. At both illumination conditions but more emphasized after UV illumination, two additional H–D sensitive negative bands are present at 1252 and 1234/33 $cm^{-1}$. A mode similar to the band at 1252(-) $cm^{-1}$ was observed in BR and assigned to a $\upsilon(C_{12}–C_{13}+C_{14}–C_{15})$ vibration coupled with the $RSBH^+$.[105] Due to coupling to the $RSBH^+$, this vibration is sensitive to deuteration.[42] In other ChRs, a pronounced negative band was observed between 1240–1230 $cm^{-1}$.[42,51,104,151] The fact that the band at 1252(-) $cm^{-1}$ is decisively reduced and that no further pronounced band is observed in this range gives another hint at differences in the chromophore structure of the Chrimson dark state in comparison with other ChRs. Two bands at 1196(+) and 1174(+) $cm^{-1}$ in the UV light induced difference spectrum reflect formation of the photoproduct. In other ChRs, usually a single intense mode is observed instead, arising between 1196 and 1185 $cm^{-1}$.[31,42,51,103,151]

In contrast to UV illumination, red light causes the depletion of two additional bands at 1185(-) and 1174(-) $cm^{-1}$. In several microbial rhodopsins, a band at around 1185(-) $cm^{-1}$ was assigned to the 13-*cis*,15-*syn*→13-*trans*,15-*syn* photoreaction of a 13-*cis*,15-*syn* retinal dark state.[79,99,109,111,114] In BR, this band was assigned to the $\upsilon(C_{10}–C_{11})$ vibration of 13-*cis*,15-*syn*.[155] Recent findings for *Cr*ChR2, though, suggest an assignment of this band to the $\upsilon(C_{14}–C_{15})$ mode of 13-*trans*,15-*anti* retinal that is depleted by retinal double isomerization to 13-*cis*,15-*syn*.[98] The band is vanished after H–D exchange, but the upshifted oscillator cannot be identified. H–D sensitivity is typical for $\upsilon(C_{14}–C_{15})$ vibrations coupling to the $RSBH(D)^+$.[155] Accordingly, the band most likely indicates that a 13-*trans*,15-*anti*→13-*cis*,15-*syn* photoreaction is responsible for the formation of D′. Positive bands similar to the modes at 1196(+) and 1174(+) $cm^{-1}$ observed after UV illumination are not seen in the red light induced spectrum. This could be due to an overlap with the negative bands formed in this vibrational range.

| | $D_{app}$ | $D_{app}$ |
|---|---|---|
| 13-*cis* | 22.7 ± 0.8 | 20.3 ± 0.9 |
| 11-*cis* | 4.8 ± 0.9 | 5.1 ± 0.2 |
| 9-*cis* | 3.6 ± 0.6 | 2.5 ± 0.4 |
| 13-*trans* | 69.0 ± 2.3 | 72.1 ± 1.1 |

**Tab. 4** Retinal extraction and subsequent HPLC analysis of the Chrimson wild type at pH 5. Measurement conditions: 5 min red ($\lambda_{max}$ ~ 633 nm, *left*) or UV ($\lambda_{max}$ ~ 405 nm, *right*) illumination followed by 1 min in the dark. Equilibration was conducted at ambient temperature. Spectra were corrected for baseline drifts and bands were analyzed by fitting gaussians. Chromatograms are shown in Fig. S9.

To further support the hypothesis that the additional bands at 1185(-) and 1174(-) $cm^{-1}$ in the red light induced spectrum reflect a 13-*trans*,15-*anti*→13-*cis*,15-*syn* photoreaction, retinal extraction and HPLC experiments were conducted with the wild type at pH 5 after red and UV illumination, respectively (Tab. 4). Following UV illumination, Chrimson adopts roughly 72 % 13-*trans* retinal and 20 % 13-*cis*, while the contribution of 13-*cis* is increased to 23 % at the expense of 13-*trans* (69 %) after red illumination. This is in agreement with a photoreaction from 13-*trans*,15-*anti* to 13-*cis*,15-*syn* as the mechanism for D' formation. Nevertheless, the results have to be considered with great caution as the wavelength-dependent differences are very small. In any case, the retinal isomer analysis reveals that, although the retinal fingerprint pattern observed in the Chrimson difference spectra is quite different from *Cr*ChR2, *Ca*ChR1 or ReaChR, the isomeric composition of the dark state is similar.[51,99–101]

Fingerprint vibrations < 1000 $cm^{-1}$ in the K-like intermediates of most rhodopsins exhibit hydrogen out-of-plane (HOOP) vibrations. Positive HOOP bands formed after the initial photoreaction reflect a distortion of the chromophore.[144,146] This distortion was described to store energy from the photoreaction that is released to the protein as the chromophore relaxes in the ongoing photocycle.[203–205] In Chrimson, however, two negative bands at 969/68 and 958/57 $cm^{-1}$ are detected. H–D sensitivity of the band at 969/68(-) $cm^{-1}$ suggests its assignment to a $C_{15}$-HOOP vibration (with possible contributions of other C–H groups), as this vibration couples to vibrational modes of the $RSBH(D)^+$.[149] Presence of negative HOOP band(s) hint(s) at a distorted chromophore conformation in the Chrimson dark state that relaxes after photoisomerization. Although a distortion in the 11-*cis* retinal cofactor of the bovine rhodopsin dark state between $C_{10}$ and $C_{13}$ was reported[223], such a behavior was not described for any other microbial rhodopsin so far to the best of the author's knowledge.

In the amide I region (1700–1600 $cm^{-1}$) a negative band is present at 1632/30 $cm^{-1}$ in both the UV and red light induced spectrum that is affected by H–D exchange, which is a typical behavior of the υ(C=$NH^+$) vibration of the $RSBH^+$. In $D_2O$, two negative bands arise at 1616 and 1602/1599 $cm^{-1}$ that both might reflect the corresponding υ(C=$ND^+$) vibrations of the $RSBD^+$ in different dark states. The vibrational frequency of 1632/30(-) $cm^{-1}$ correlates well with the red absorption spectrum of the Chrimson dark state at pH 5 ($\lambda_{max}$ ≈ 590 nm) and is accordingly downshifted with respect to the corresponding vibrations in *Cr*ChR2 (1657 $cm^{-1}$)[99], *Ca*ChR1 (1646 $cm^{-1}$)[79] or BR (1640 $cm^{-1}$)[184]. While a downshift of the υ(C=$NH^+$) vibration in $D_2O$ by 14–16 $cm^{-1}$ would reflect a comparably weak N–H bond similar to BR[42], a downshift by 28–30 $cm^{-1}$ would be rather similar to the very strong N–H bonds observed in other ChRs[42,79,99].

The υ(C=O) region (> 1690 $cm^{-1}$) is indicative for changes involving glutamic and aspartic acids (see 2.2.1, p. 34). Here, significant differences exist between the spectra induced by UV and red illumination. At UV illumination, a single band pattern at 1726(-)/ 1716(+) $cm^{-1}$ is observed. The fact that both bands equally downshift in $D_2O$ to 1715(-)/ 1706(+) $cm^{-1}$ indicates that the band pattern reflects a light-induced hydrogen bond change of an aspartic or glutamic acid that is accessible to water (or $D_2O$) molecules. The frequency downshift corresponds with a strengthening of this hydrogen bond.[183] At red illumination, a similar pattern at 1726(-)/ 1718(+) $cm^{-1}$ is present along with two additional bands at 1742(-) and 1712(-) $cm^{-1}$. It might be due to these additional vibrational modes that the corresponding spectrum in $D_2O$ does not allow a clear assignment of H–D sensitive bands. Nevertheless, the spectral differences in the υ(C=O) region indicate that retinal double isomerization leading to formation of D′ involves protonation dynamics that are different to those occurring in the D→K transition.

## 3.3.3 Formation of the proton-conducting state

### 3.3.3.1 FTIR difference spectra at 240 K

K proceeds to the conducting L intermediate. To investigate the structural alterations occurring in the K→L transition, FTIR spectra were recorded at 240 K at which L is maximally accumulated according to UV-Vis spectra (see Fig. 3-31, p. 109, and Fig. 3-32, p. 110). In Fig. 3-34, the steady state spectra after green (*upper spectrum*) and red illumination *(lower spectrum)* and the averaged first 30 s of red illumination (*central spectrum*) are shown. The spectra obtained in the first 30 s of red illumination and the green light-induced steady state are similar to each other and different from the spectrum obtained after prolonged illumination with red light. Note that UV light induces similar changes as green light, albeit with

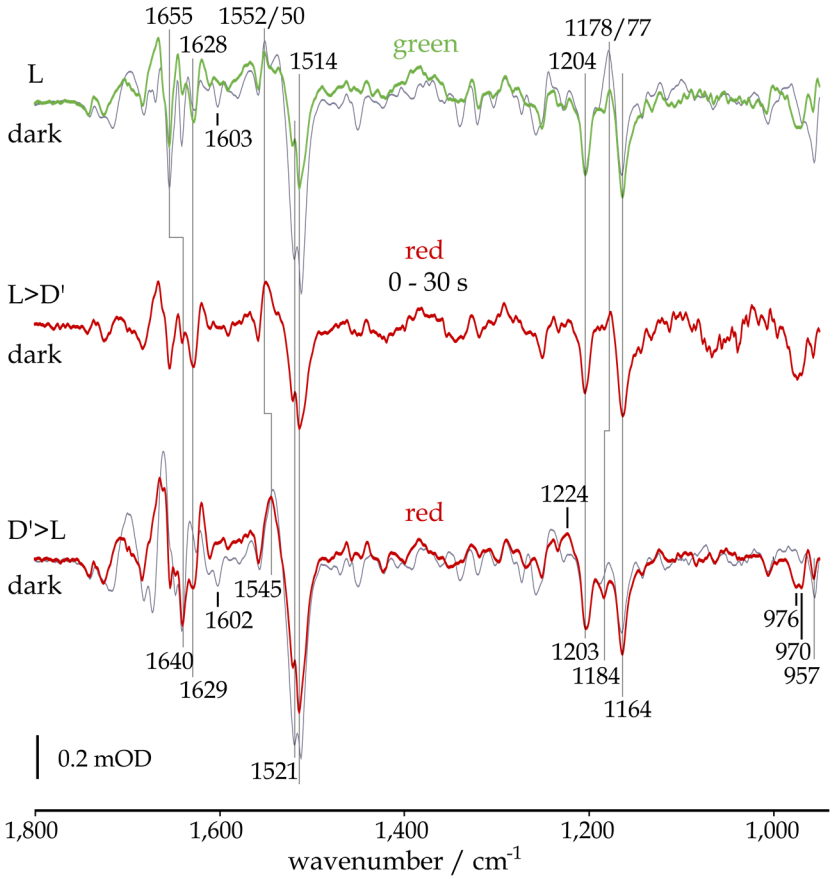


**Fig. 3-34** FTIR light – dark difference spectra of Chrimson-wt at pH 5 recorded at 240 K in $H_2O$ (*colored*) and $D_2O$ (*gray*). Illumination with green light ($\lambda_{max}$ ~ 523 nm) yields the proton-conducting L state (*upper spectrum*), while red light ($\lambda_{max}$ ~ 633 nm) induces parallel reactions that lead to (i) the formation of the L state, maximally populated in the initial phase of illumination (*central spectrum*), and (ii) the non-conducting D′ state that is maximally populated in the steady state (*lower spectrum*). Spectra were scaled to retinal fingerprint bands in the red light induced steady state in $H_2O$. Prior to illumination the sample was kept ≥ 5 min in the dark at ≥ 293 K.

reduced intensity (see Fig. S8). Bands at 1655(-), 1552/50(+) and 1178/77(+) $cm^{-1}$ are present in the green light induced spectrum and the spectrum obtained in the first 30 s of red illumination. Contrarily, bands at 1640(-), 1545(+) and 1184(-) $cm^{-1}$ are observed only in the red light induced steady state. The pattern at 1204/03(-)/ 1164(-)/ 1178/77(+) $cm^{-1}$ obtained after green illumination reflects 13-*trans*,15-*anti*→13-*cis*,15-*anti* isomerization.[160,224] In contrast, the H–D sensitive mode at 1184(-) $cm^{-1}$ yielded after red illumination most likely reflects depletion of a 13-*trans*,15-*anti* dark state by double isomerization to 13-*cis*,15-*syn* retinal[97,98] and was already observed at 80 K (see Fig. 3-33, p. 111). Thus, the red light induced steady state mainly represents formation of a state outside the 15-*anti* photocycle (as introduced in Fig. 1-10, p. 16). It is similar but not identical to the red light induced spectrum obtained at 80 K and thus could represent a later product of the D→D′ photoreaction. Alternatively, the difference could be due to contributions of the L intermediate to the red light induced spectrum at 240 K or to contributions of photoproducts of the D′ state.

The green light induced steady state and the spectrum obtained in the first 30 s of red illumination both reflect formation of the conducting L intermediate as explained in detail in 3.3.4 (p. 121). The pronounced υ(C=C) chromophore band at 1514(-) $cm^{-1}$ (with a shoulder at 1521(-) $cm^{-1}$) agrees well with depletion of the dark state, while bands at 1552/50(+) and 1545(+) $cm^{-1}$ probably reflect formation of the blue-shifted photoproducts L and D′. In both spectra the negative HOOP bands (< 1000 $cm^{-1}$) observed at 80 K are still present, indicating that the chromophore distortion in the dark is restored neither in L nor D′. In the following, the focus is set on formation of the open state, L, while formation of the D′ state is addressed in section 3.3.4 (p. 121).

### 3.3.3.2 Backbone changes in the D→L transition

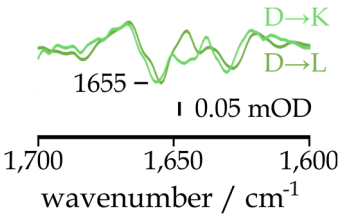


**Fig. 3-35** FTIR light – dark difference spectra of Chrimson-wt at pH 5 recorded at 80 K (D→K) and 240 K (D→L) after green illumination ($\lambda_{max}$ ~ 523 nm) following ≥ 5 min in the dark at ≥ 293 K. Spectra were scaled to retinal fingerprint bands in the spectrum at 240 K.

The amide I region is dominated by changes of the protein backbone (see Fig. 3-34, p. 116). Green illumination causes a negative band at 1655 $cm^{-1}$ that is insensitive to deuteration and thus assigned to an amide I mode. The υ(C=$NH^+$) vibration arises at 1629/28(-) $cm^{-1}$ as already seen at 80 K (see Fig. 3-33, p. 111). Based on the spectra obtained at 240 K, the corresponding υ(C=$ND^+$) vibration can be clearly assigned to the mode at 1603/02 $cm^{-1}$. The resulting 25–27 $cm^{-1}$ frequency downshift indicates strong hydrogen bonding of the $RSBH^+$ proton similar to other ChRs.[42,79,103] The frequency of the amide I mode (1655(-) $cm^{-1}$) is similar to the respective signals in other ChRs (1664–1658 $cm^{-1}$)[43,51,100,157] but the intensity is drastically reduced. Thus, the structural rearrangements required for formation of the ion conducting pathway are comparably small and rather reminiscent of the active states of proton pumps such as BR[160,161], PR[162,171,172] and Archaerhodopsin-3 (AR3)[225]. A comparison of the L intermediate with the steady state obtained by green illumination at 80 K (Fig. 3-35) shows that the structural changes are largely completed already in K, in contrast to the large backbone changes in *Cr*ChR2 that occur mainly in the M intermediate.[103,104,157]

### 3.3.3.3 Molecular determinants for the formation of L

As previously described, one of the factors for the bathochromic absorption of Chrimson is the protonation of Ci1 (see Fig. 1-5, p. 10) in the dark state. Along with further residues, E4, which is part of the extracellular gate (see Fig. 1-7, p. 13), has a surprisingly strong effect on the absorption maximum as its mutation to alanine resulted in a hypsochromic shift by ~ 70 nm.[39] In order to shed light on the mechanism by which E4 modulates the absorption spectrum and to elucidate the role of Ci1 and E4 for formation of the ion-conducting L state, mutant spectra were recorded (E165A and E139A). As it was not possible to conduct measurements of the Ci1 mutant E165A at pH 5 – presumably due to protein aggregation – the

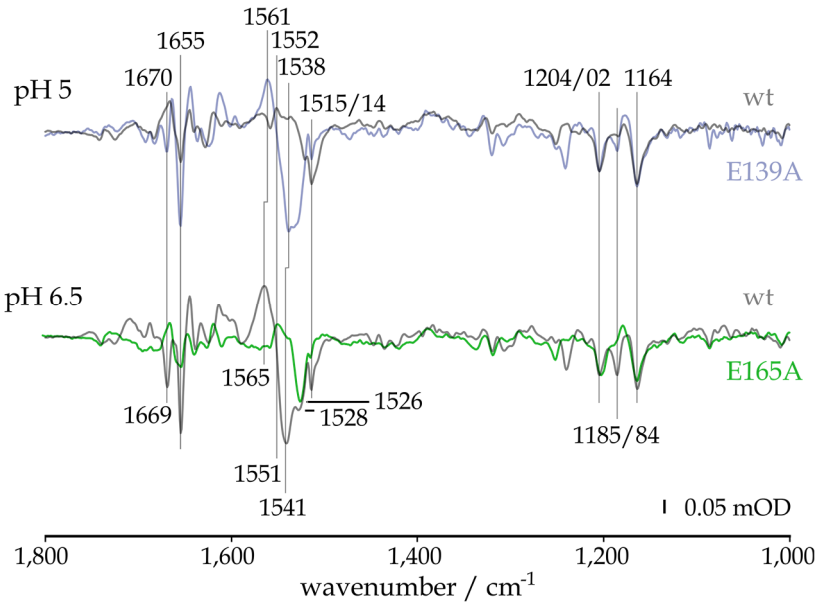


**Fig. 3-36** FTIR light – dark difference spectra of Chrimson-wt at pH 5 and pH 6.5, the E4 mutant E139A at pH 5 and the Ci1 mutant E165A at pH 6.5 recorded at 240 K. Illumination was conducted with green LEDs ($\lambda_{max}$ ~ 523 nm) following ≥ 5 min in the dark at ≥ 293 K. Spectra were scaled to retinal fingerprint bands in the wild type spectrum obtained at pH 5.

respective measurements were performed at pH 6.5 along with measurements of the wild type at the same pH value. At pH 6.5, the relative amount of deprotonated Ci1 is increased, given a p$K_a$ of Ci1 of 6.5 in detergent.[j] In Fig. 3-36, the green light induced steady states of the Chrimson wild type at pH 5 and pH 6.5 (*gray spectra*) as well as the E139A mutant at pH 5 and the E165A mutant at pH 6.5 are shown. The steady state of the wild type obtained at 240 K and pH 6.5 shows a negative amide I band at 1655 cm$^{-1}$ that is increased as compared to pH 5. Furthermore, an additional negative band arises at 1669 cm$^{-1}$. In the region of υ(C=C) vibrations of the chromophore, negative bands that reflect dark state depletion arise at 1541, 1526 and 1514 cm$^{-1}$ at pH 6.5 and at 1521 and 1514 cm$^{-1}$ at pH 5. Given the correlation of υ(C=C) modes with the absorption in the UV-Vis range[132,191], the additional band at 1541(-) cm$^{-1}$ reflects the fraction of the dark state whose absorption maximum is blue-shifted due to Ci1 deprotonation[39,54], while the vibrational bands at 1526(-) and 1514(-) cm$^{-1}$ reflect the red-shifted dark state with protonated Ci1. The band at 1565(+) cm$^{-1}$ observed in the wild type difference spectrum at pH 6.5 shows that the M intermediate is predominantly formed at

[j] Data from Johannes Vierock, Humboldt University Berlin. Included in: Kaufmann *et al.* A unique gating mechanism is responsible for the high proton selectivity of the red-absorbing channelrhodopsin Chrimson. Manuscript in preparation.

pH 6.5 as expected for the photocycle with deprotonated Ci1.[54] In contrast, L is the main photoproduct at pH 5 which is reflected by the band at 1552(+) $cm^{-1}$. In the retinal fingerprint region of the wild type spectrum at pH 6.5, the band at 1185/84(-) $cm^{-1}$ is observed that is assigned to the formation of 13-*cis*,15-*syn* retinal in the D→D′ reaction and is more pronounced as compared to pH 5, suggesting a pH effect on the efficiency of this photoreaction.

In the E165A mutant spectrum at pH 6.5, both the amide I and the υ(C=C) chromophore regions resemble those in the wild type spectrum at pH 5. As indicated by the band at 1551(+) $cm^{-1}$, the L intermediate is mainly formed which is in contrast to the wild type spectrum at pH 6.5. Thus, both mutation (E165A) and protonation of Ci1 (pH 5) reduce the light-induced backbone changes and block formation of the M intermediate. E4 mutation has the inverse effect: The difference spectrum of the E139A mutant at pH 5 resembles the spectrum of the wild type at pH 6.5. This is derived from the increased intensity of the band at 1655(-) $cm^{-1}$ as compared to the wild type at pH 5, as well as the additional band at 1669(-) $cm^{-1}$ and the vibrational modes in the υ(C=C) region at 1538(-) and 1561(+) $cm^{-1}$ that reflect formation of an M intermediate[k] by the photoreaction of a blue-shifted dark state. Notably, formation of the D′ state is impaired in both the Ci1 and E4 mutants as indicated by the lack of the marker band for the 13-*trans*,15-*anti*→13-*cis*,15-*syn* photoreaction[98] at ~ 1184(-) $cm^{-1}$.

Moreover, mutational effects on the υ(C=O) region reveal that E4 and Ci1 are involved in proton transfer processes that occur in the Chrimson photocycle (Fig. 3-37). In the wild type spectrum at pH 5, two negative bands arise in the D→L transition at 1742 and 1725 $cm^{-1}$ that are also observed at pH 6.5. A positive band is seen at 1703 $cm^{-1}$ at pH 5 and at 1710 $cm^{-1}$ at pH 6.5. The 1742(-) $cm^{-1}$ band is almost not affected by deuteration as opposed to the bands at 1725 and 1703 $cm^{-1}$, that gain intensity and are downshifted by 9 and 5 $cm^{-1}$, respectively. Sensitivity

[k] Confirmed by UV-Vis flash photolysis data from Benjamin Krause and Johannes Vierock, Humboldt University Berlin. Included in: Kaufmann *et al.* A unique gating mechanism is responsible for the high proton selectivity of the red-absorbing channelrhodopsin Chrimson. Manuscript in preparation.

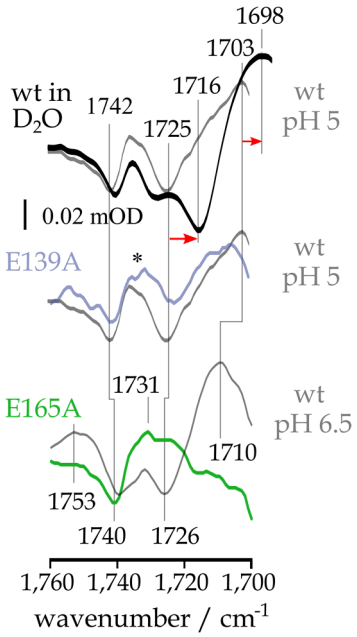


**Fig. 3-37** The υ(C=O) region of difference spectra of Chrimson wild type in $H_2O$ and $D_2O$ at pH 5 and pD 5.4, respectively, and at pH 6.5, the E139A mutant at pH 5 and the E165A mutant at pH 6.5 from Fig. 3-36 (p. 119) after illumination with green LEDs ($\lambda_{max}$ ~ 523 nm) following ≥ 5 min in the dark at ≥ 293 K. *1736 and 1732 $cm^{-1}$. *Red arrows* indicate shifts in $D_2O$.

to H–D exchange is indicative for aspartic and glutamic acids accessible by water (or $D_2O$) molecules. The downshift of a single negative (or positive) band in $D_2O$ without a positive (or negative) counterpart shifting in a similar fashion indicates that the respective band is caused by a proton transfer event rather than a hydrogen bond change (see Fig. 2-3, p. 37). Both mutants, E139A and E165A, cause significant alterations in the υ(C=O) region: In the E4 mutant (E139A) spectrum, the intensity of the band at 1725(-) $cm^{-1}$ is reduced and two positive bands arise at 1736 and 1732 $cm^{-1}$ (marked by *asterisk*). In the Ci1 mutant (E165A) spectrum, a vibrational band at 1726(-) $cm^{-1}$ is not observed. Furthermore, the band at 1710(+) $cm^{-1}$ is vanished in the mutant. Instead, a positive band arises peaking at 1731 $cm^{-1}$. Based on these observations, the band at 1725(-) $cm^{-1}$ is assigned to Ci1 that is protonated in the dark state and deprotonated in the illuminated state. At pH 6.5, Ci1 is only partially protonated and only the protonated fraction releases its proton after light activation. Mutation of E4 lowers the p$K_a$ of Ci1[39] so that the fraction of protonated Ci1 and thus the corresponding deprotonation band at 1725 $cm^{-1}$ is reduced.

## 3.3.4 Light adaptation

As mentioned in the beginning of section 3.3.3 (p. 116), formation of the proton-conducting L state, initiated by 13-*trans*,15-*anti*→13-*cis*,15-*anti* isomerization, is accompanied by formation of the more stable D′ intermediate that is preferably induced by red light (see Fig. 3-34, p. 116). L and D′ can be distinguished based on the marker bands at 1655 (L) and 1640 (D′) $cm^{-1}$. This assignment is supported by the kinetics of these marker bands at 240 K (Fig. 3-38): While the marker for L decays within seconds after light off, as expected from the fast recovery of the proton-conducting state[39,54], D′ even gains intensity, probably due to reduced

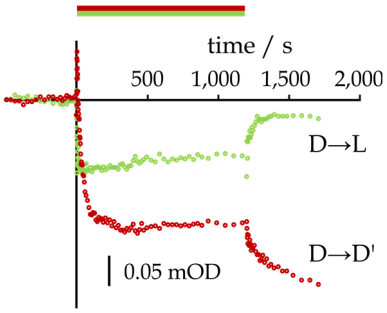


**Fig. 3-38** Kinetics of marker bands for L (1655(-) $cm^{-1}$) and D′ (1640(-) $cm^{-1}$) after activation with green ($\lambda_{max}$ ~ 523 nm) and red ($\lambda_{max}$ ~ 633 nm) LEDs (*colored bar*), following ≥ 5 min in the dark at ≥ 293 K. Measurement was conducted at 240 K.

overlap with L state-specific bands in the amide I region. The D′ marker at 1640(-) $cm^{-1}$ is insensitive to deuteration and thus assigned to an amide I mode (see Fig. 3-34, p. 116). Its appearance during formation of the D′ state hints at differences in the dark state configuration in the form of conformational substates that could be important for D′ formation. Given the inverse correlation of the amide I frequency with helical hydration[157] those substates that prefer light-induced D′ formation could involve more water molecules inside the protein as compared to the substates that favor light-induced K formation.

Light adaptation can be further investigated by application of a protocol with alternating illumination similar to Ritter *et al.* 2013[101]. Analysis of FTIR difference spectra obtained by alternating red and green illumination by SVD and rotational procedure (for details see 2.2.3.2, p. 41) reveals – among further components that are omitted for simplicity – a steady state component and a component strictly following the illumination protocol (Fig. 3-39). The steady state component comprises the L state marker bands at 1654(-) and 1177(+) $cm^{-1}$, while the alternating component exhibits the marker bands for the D′ state at 1640(-) and 1184(-) $cm^{-1}$. Additionally, a band is observed at 1237(+) $cm^{-1}$ that is more clearly pronounced than in the red light induced steady state spectrum (see Fig. 3-34, p. 116). This band could reflect a vibrational mode of the assumed 13-*cis*,15-*syn* photoproduct. A similar fingerprint pattern was observed in FTIR spectra of BR and PR at acidic pH and interpreted as light-induced 13-*trans*→9-*cis* reaction and concomitant thermal 13-*cis*,15-*syn*→13-*trans*,15-*anti* transition.[114] Considering the conflicting assignment of the 1184(-) $cm^{-1}$ band in BR (13-*cis*,15-*syn*) and *Cr*ChR2 (13-*trans*,15-*anti*), the alternating component provides additional strong evidence supporting its assignment to a 13-*trans*,15-*anti* vibration: the band at 1184(-) $cm^{-1}$ is temporally correlated with the bands at 1201(-) and 1165(-) $cm^{-1}$ that are typical for *trans*→*cis* isomerization.[160,224] The most straightforward explanation for this

correlation is a double isomerization event.[100] Furthermore, this experiment demonstrates that the thermally stable D′ state can bse photoconverted back to the dark state by a second light source of appropriate wavelength.[1]

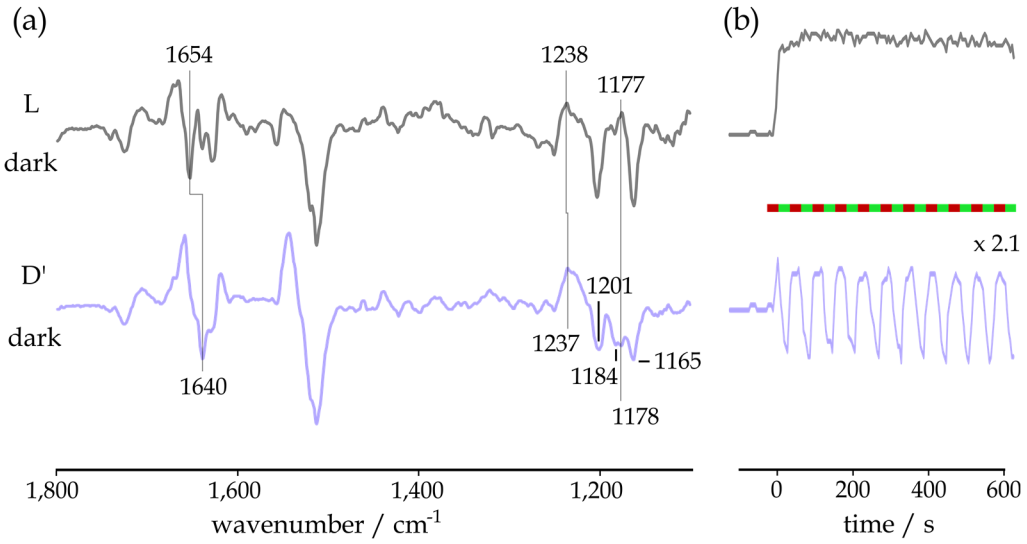


**Fig. 3-39** Alternating illumination of the Chrimson-wt at pH 5 and 240 K with red ($\lambda_{max}$ ~ 633 nm) and green ($\lambda_{max}$ ~ 523 nm) LEDs. Data evaluation was performed with SVD and rotational analysis. Shown are the steady state component (*upper lines*) and the component sensitive to alternating illumination (*lower lines*) with spectra **(a)** and corresponding kinetics **(b)**. Other components were omitted for simplicity. Absorbance is given in arbitrary units. Spectra were scaled to retinal fingerprint bands. Illumination was conducted following ≥ 5 min in the dark at ≥ 293 K.

[1] Confirmed by UV-Vis spectroscopic experiments conducted by Benjamin Krause and Johannes Vierock, Humboldt University Berlin. Included in: Vierock, Kaufmann *et al.* Light adaptation in the red shifted channelrhodopsin Chrimson involves unprecedented bistability of two dark states. Manuscript in preparation.

## 3.3.5 Discussion

### 3.3.5.1 Summary

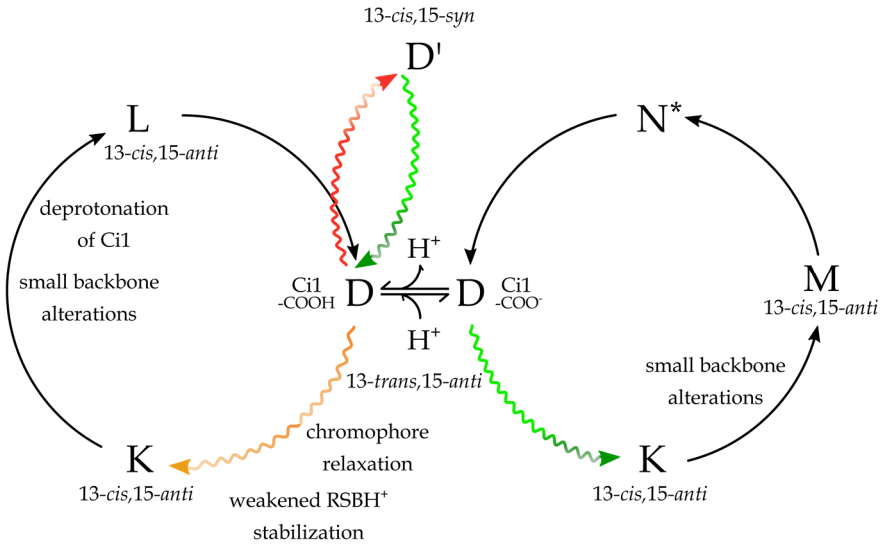


**Fig. 3-40** The photocycle dynamics of Chrimson, based on Urmann *et al.* 2017[54] and extended with respect to the experiments conducted in this thesis. Depending on the pH, two photocycles are induced by 13-*trans*,15-*anti*→13-*cis*,15-*anti* isomerization that differ with respect to the Ci1 protonation state (*left* and *right circles*). In a parallel reaction, the desensitized and thermally stable D′ state is formed by 13-*trans*,15-*anti*→13-*cis*,15-*syn* double isomerization. While this reaction takes place as well at alkaline pH, the illumination conditions are not known and thus it is omitted in the presented photocycle scheme. It is unknown whether a photocycle can be initiated from D′ by isomerization around the $C_{13}$=$C_{14}$ bond as described for *Cr*ChR2[96,98,101] and ReaChR[51]. *N could not be identified based on the υ(C=C) chromophore vibrations (see Fig. 3-36, p. 119).

The photocycle model (Fig. 3-40) of Chrimson exhibits a number of significant distinctions to other ChRs that are decisive for formation of the conducting pore, ion selectivity and light adaptation. The red-shift of the dark state at acidic pH with respect to other ChRs is caused by protonation of Ci1 along with a number of alterations in the retinal binding pocket. These alterations induce an unusual chromophore twist in the dark state that contributes to the bathochromic shift. The p$K_a$ of Ci1 depends on the protonation state of the extracellular gate residue E4 by a long-range interaction.

Starting from D, light-triggered 13-*trans*,15-*anti*→13-*cis*,15-*anti* photoisomerization leads to the formation of K. From K, the proton-conducting L intermediate is formed at pH 5. The blue-shift of L is caused by deprotonation of Ci1 along with relaxation of the distorted dark state chromophore. The structural rearrangements occurring upon light activation are significantly smaller than in other ChRs and largely occur already in the K intermediate.

Deprotonated Ci1 at more alkaline pH conditions establishes a blue-shifted dark state as compared to acidic pH. Light activation leads to formation of K, succeeded by M which is the conducting intermediate[54] (the N intermediate reported by Urmann *et al.* 2017[54] could not be characterized). The structural alterations leading to the conducting state are larger than in L.

Along with the 13-*trans*,15-*anti*→13-*cis*,15-*anti* photoreaction, a significant extent of 13-*trans*,15-*anti*→13-*cis*,15-*syn* retinal double isomerization is observed. D′ is thermally stable but can be photoconverted to the dark state with illumination at suitable wavelength.

#### 3.3.5.2 Bathochromic shift

A feature rendering Chrimson highly attractive for optogenetic applications is its bathochromically shifted absorption spectrum that allows the excitation of deeper layers of tissue as compared to other ChRs.[69,70] The absorption spectrum of Chrimson is > 40 nm red-shifted as compared to green-absorbing ChRs such as *Ca*ChR1[34] and ReaChR[51]. This study, along with previous investigations[39,54,73], suggests three factors for the bathochromic shift that are discussed in the following:

(1) the Ci1 protonation state
(2) the distorted chromophore geometry
(3) the water content near the active site

(1) Similar to other ChRs, Ci1 protonation contributes to the bathochromic shift by decreasing the energy difference between the electronic ground state and the excited state of the chromophore. This is due to a weakened electrostatic stabilization of the $RSBH^+$ that increases the attraction of the chromophore π-electrons as compared to the configuration with deprotonated Ci1 (see 1.2.5.2, p. 20). However, the strong spectral difference between *Ca*ChR1 ($\lambda_{max}$ = 520 nm[15]) and Chrimson ($\lambda_{max}$ = 585 nm[54]) shows that protonation of Ci1 can only partially account for the red-shifted absorption maximum of Chrimson, as Ci1 is protonated in the dark states of both proteins.[34,39,54,151] Thus, further distinctions in the

chromophore must be considered to explain the red-shifted absorption of Chrimson.

(2) In the retinal binding pocket, residues Ser169, Cys198 and Met201 are found instead of Thr127, Asp$^{DC}$ and Thr159 that together with Cys$^{DC}$ (which is conserved in Chrimson) span the chromophore from the $\beta$-ionone ring to the RSBH$^+$ in *Cr*ChR2.[46,72] Consequently, this interaction network found in the chromophore of blue-absorbing ChRs is disturbed by the exchanged residues in Chrimson. Most likely, these replacements contribute to the chromophore distortion in the Chrimson dark state. In particular, Oda *et al.* 2018[73] described an impact of Met201 on the torsion angle at the $C_6$-$C_7$ bond, which is in line with previous investigations on the homologous residue Thr198 in C1C2.[74] Additionally, the Chrimson crystal structure[73] reveals significant torsions around double bonds of the retinal polyene chain as compared to C1C2[41] (Fig. 3-41). This unusual chromophore distortion in the dark state is reflected by negative HOOP bands in FTIR light – dark difference spectra that are partially H–D sensitive (see Fig. 3-33, p. 111, and Fig. 3-34, p. 116). The deuteration-sensitive HOOP bands must originate from C–H (C–D) bonds located close to the RSBH$^+$ (most probably $C_{15}$–H) due to coupling to the N–H (N–D) vibration of the RSBH(D)$^+$,[149] in line with the distortions around the $C_{13}$=$C_{14}$ and $C_{15}$=N double bonds observed in the crystal structure (Fig. 3-41).

(a)

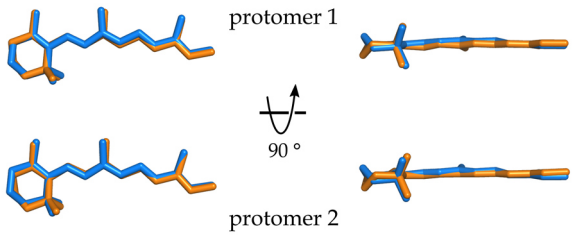


(b)

| | torsion angle | | | | |
|---|---|---|---|---|---|
| | $C_7$=$C_8$ | $C_9$=$C_{10}$ | $C_{11}$=$C_{12}$ | $C_{13}$=$C_{14}$ | $C_{15}$=N |
| C1C2 | -178 ° | -180 ° | 179 ° | -180 ° | -174 ° |
| Chrimson protomer 1 | -180 ° | -175 ° | -5 ° | -36 ° | 33 ° |
| Chrimson protomer 2 | -180 ° | -176 ° | -10 ° | -24 ° | 19 ° |

**Fig. 3-41** Chromophore distortion in the Chrimson dark state. **(a)** The dark state chromophore of C1C2 (*blue*) and Chrimson (*orange*) with side view (*left*) and top view (*right*) taken from the respective crystal structures (3UG9[41] and 5ZIH[73]). **(b)** Torsion angles for C=C and C=N bonds in the retinal polyene chains of C1C2 and the two protomers of Chrimson. Structure was visualized with PyMol (Version 2.1.1.).

To understand in which way chromophore distortion contributes to the bathochromic shift, a comparison with the K intermediates of rhodopsins is helpful. These red-shifted states are formed in most rhodopsins within ns after excitation and retain a distorted chromophore geometry that serves as storage for the photoreaction energy.[203–205] According to theoretical calculations on the K intermediate of bovine rhodopsin, the torsion around double bonds of the photoproduct 13-*trans*,15-*anti* retinal is mainly responsible for the red-shifted absorption.[133,134]

(3) Mutation of the access channel residue E4 led to an astonishing 60 nm blue-shift that cannot be solely explained by a decreased p$K_a$ of Ci1 because the pH induced shift accounts only for ~ 40 nm.[54] The long-range effect of E4 on the active site could result in further conformational alterations involving the influx of water molecules that could further stabilize the $RSBH^+$ and lead to a hypsochromic absorption shift as described for the primate blue-sensitive visual pigment.[128] An altered water content in the E139A mutant is in line with the larger backbone changes observed in FTIR difference spectra that suggest a higher conformational flexibility of the protein (see Fig. 3-36, p. 119).

#### 3.3.5.3 Light adaptation

As usual for ChRs, 13-*trans* retinal is the predominant isomer in the dark (see Tab. 4, p. 114). The main photoreaction pathway that involves formation of the ion-conducting L intermediate in the case of a dark state with protonated Ci1 and the M intermediate in the case of a dark state with deprotonated Ci1[54], is initiated by 13-*trans*,15-*anti*→13-*cis*,15-*anti* isomerization as in other ChRs. In a parallel reaction, D' is formed by 13-*trans*,15-*anti*→13-*cis*,15-*syn* retinal double isomerization similar to *Cr*ChR2 (see Fig. 3-40, p. 124).[97,98] In contrast to *Cr*ChR2 in which D recovers within tens of seconds from D'[97,98], D' is thermally stable and does not relax back to the 13-*trans*,15-*anti* dark state within the observation time (see Fig. 3-32, p. 110) but can be photoconverted to the 13-*trans*,15-*anti* dark state with light of suitable wavelength (see Fig. 3-39, p. 123).

What is the molecular determinant for the unusual stability of D′ in Chrimson? Thermal back isomerization requires simultaneous rotation around the $C_{13}$=$C_{14}$ and the $C_{15}$=N double bonds. Additionally, the distorted chromophore geometry needs to be restored during dark state recovery and reversal of the torsion around the double bonds close to the $RSBH^+$ (indicated by the H–D sensitive HOOP vibrations, see Fig. 3-33, p. 111, and Fig. 3-34, p. 116) could represent a significant barrier for back isomerization. Furthermore, the better electrostatic stabilization of the positive charge at the RSB by deprotonated Ci1, also evident in the significant blue-shift of D′ as compared to D (see Fig. 3-32, p. 110), increases the energy barrier for thermal back isomerization which can be deduced from the theoretical calculations by Tavan *et al.* 1985.[220] Accordingly, Ci1 reprotonation could become a critical step for thermal D′→D transition. Significant differences between L and D′ in the amide I region hint at structural deviations that could block efficient proton transfer pathways in the case of D′ (see Fig. 3-39, p. 123).

#### 3.3.5.4 Formation of the proton-conducting state

The structural changes in the Chrimson photocycle are significantly smaller than in C1C2 and other ChRs and rather reminiscent of microbial pumps.[160,161,162,171,172,225] Furthermore, the largest alterations occur in the early phototransition and only small additional changes are required for formation of the conducting state (see Fig. 3-35, p. 118). As described in 1.2.4.4 (p. 12), a water-filled half-channel spans from the extracellular site to the central gate in the *Cr*ChR2 dark state. In *Cr*ChR2, water molecules penetrate into the central gate during formation of the ion-conducting N state which leads to helical hydration causing the large backbone changes observed in the amide I region.[157] Instead, formation of the L intermediate in Chrimson does not involve a pronounced influx of water molecules. The electrophysiological investigation of Chrimson already suggested that channel gating is more delocalized over the entire ion-conducting pore, involving E1 and E2 at the intracellular site, and E4 and E5 at the extracellular site (see Fig. 1-6, p. 12).[39] At acidic pH, these gates appear to block water molecules from entering the ion channel after light activation. In the E139A mutant as well as at higher pH, the light-induced structural changes are increased as compared to pH 5 (see Fig. 3-36, p. 119). This indicates that the extracellular gate involves a hydrogen

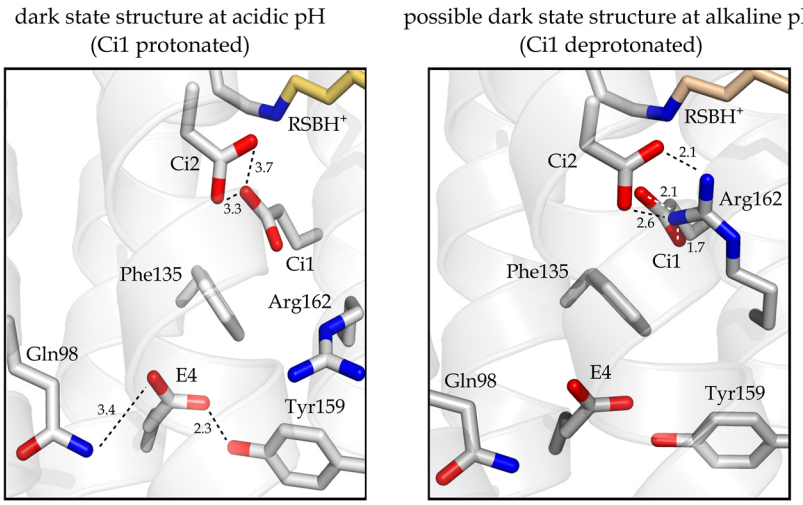


**Fig. 3-42** Putative long-range interaction between Ci1 and E4 mediated by Arg162. In the dark state at acidic pH (*left*), Arg162 is oriented toward E4. In the dark state at alkaline pH (*right*), it might reorient toward Ci1 instead and stabilize its deprotonated form. Thereby, this rotation could mediate the long-range interaction between E4 and Ci1 implied by FTIR (see Fig. 3-37, p. 121) and electrophysiological data.[39] The rotamer was introduced using the Mutagenesis tool provided by the PyMol software package while other residues were not changed. The structure was visualized with PyMol (Version 2.1.1.).

bond of protonated E4. If protonated (pH 5), E4 forms a restriction site that prevents water influx. The hydrogen bonding partner is Tyr159 whose aromatic ring creates a steric hindrance at the access channel.[73] If E4 is deprotonated (or mutated) this barrier is comparably weakened – presumably due to reorientation of the tyrosine ring – which facilitates the influx of water molecules. The fact that E4 mutation as well as pH increase shift the ion selectivity of the channel from $H^+$ to $Na^+$[39] allows the conclusion that the restriction site formed by protonated E4 and Tyr159 is crucial for the unusually high $H^+$ selectivity of Chrimson as compared to other ChRs, as hydrated cations are blocked from entering the channel from the extracellular site, while dehydrated protons are efficiently guided through the gates.

The p$K_a$ values of E4 and Ci1 are coupled by a long-range interaction. This can be derived from the observation that Ci1 is mainly deprotonated in the E139A mutant (see Fig. 3-37, p. 121). Although the accurate coupling mechanism could not be resolved in this study, the crystal structure suggests a critical role of Arg162 (Fig. 3-42).[73] While Arg162 is oriented towards the extracellular site in the Chrimson dark state structure obtained at acidic pH (with Ci1 and presumably E4 being protonated)[73], it might flip if the interaction between Tyr159 and E4 is altered

at higher pH (with Ci1 and E4 being deprotonated) as well as in the E139A mutant. A movement of Arg162 toward the active site could compensate for the stabilizing effect of $Phe^{CI}$ (Phe135) on the protonated form of Ci1 and, accordingly, could drive deprotonation of Ci1. Additionally, deprotonated E4 might form a stronger hydrogen bond to the $NH_2$ side group of the neighboring Gln98 as compared to the dark state at acidic pH (with a minimum distance of 3.4 Å, see Fig. 3-42). This could weaken the interaction between E4 and Tyr159 and result in a reorientation of the tyrosine ring facilitating the influx of water molecules and larger cations.

Light activation of the orange-absorbing dark state at acidic pH induces deprotonation of Ci1. This deprotonation event – along with chromophore relaxation – explains formation of the blue-shifted L intermediate that is achieved by a better electrostatic stabilization of the positive charge residing at the $RSBH^+$. An M intermediate formed by deprotonation of the $RSBH^+$ is not observed at pH 5[54], suggesting that the additional negative charge that is provided to the active site by deprotonation of Ci1 stabilizes the protonated $RSBH^+$. Contrarily, light activation of the green-absorbing dark state at alkaline pH, in which Ci1 is already deprotonated, leads to formation of an M intermediate[54] that – in analogy to other ChRs – involves protonation of the counter-ion complex.[47,104] If the above-mentioned concept held true that the long-range effect between E4 and Ci1 is mediated by the pH dependent orientation of Arg162, it would appear reasonable that reorientation of Arg162 could be initiated by illumination as well. According to this concept, light-induced deprotonation of Ci1 could be due to formation of a salt bridge to reoriented Arg162 as illustrated in Fig. 3-42 (*right panel*). The formation of strong salt bridges in the middle of the pore by such a Arg162-Ci1 interaction and/ or strengthening of the $RSBH^+$-counter-ion interaction could serve the efficient guidance of protons through the channel and simultaneously block the passage of larger ions by creating a restriction site in the middle of the pore. The key function of Ci1 for ion conductivity of Chrimson is reflected by the significant reduction of photocurrents[39] which is in stark contrast to the negligible effects observed in other ChRs[41,51,226].

# 4 General discussion

## 4.1 Introduction

Since their discovery in 2002, numerous biophysical studies have elucidated important functional determinants of various members of the ChR family. The ChR photocurrents raise a number of questions such as:

- What are the factors for dark state absorption that determine the excitation wavelength?
- How are the ion-conducting states formed and what are the determinants for channel closure?
- What are the factors determining ion selectivity?
- Which parallel photoreactions exist and how are they modulated?

Finding answers to these questions is not only meaningful in order to design more suitable optogenetic tools or to achieve a more substantial understanding of the photoreception of single-cell algae but is also relevant for extending the existing knowledge about light-sensing and ion-conducting proteins in general. Moreover, the role of protonation changes for the modulation of reaction pathways hints at generic principles of protein function.

In this thesis, three different ChRs were investigated and the important mechanistic aspects of their photocycles were discussed in detail in the respective sections (3.1–3.3). The scope of the general discussion is to compare these ChRs with each other with respect to the most outstanding features revealed in this thesis: (i) energy storage and energy transfer from the chromophore to the protein following photoisomerization, (ii) formation of the ion-conducting states and ion selectivity and (iii) molecular determinants of parallel photoreactions.

## 4.2 Energy transfer from chromophore to protein

ChRs are optimized to convert the energy of photons into kinetic energy of the protein in order to form the ion-conducting pore. In the K intermediate that is formed within $10^{-12}$–$10^{-8}$ s after photoisomerization[31,44,92,122], a substantial fraction of the photon energy is stored by (i) chromophore distortion and/or (ii) reduced electrostatic stabilization of the $RSBH^+$ by increased distance to its counter-ions (Fig. 4-1c).[135,137,142,143] Both factors contribute to the bathochromic shift that is a common feature of the K intermediate in rhodopsins and that is observed in C1C2, ReaChR and Chrimson as well.[44,51,54]

Although further investigations are required to obtain quantitative measures for the relative contributions of (i) and (ii) to energy storage, the significant distinctions observed in FTIR spectra suggest crucial differences among the three ChRs: The strong HOOP bands observed in the FTIR spectra of ReaChR, in particular in the acidic and physiological pH range, indicate that with protonated Ci1 the energy storage is largely achieved by chromophore distortion (Fig. 4-1a) while with deprotonated Ci1 the contribution of chromophore distortion to energy storage is comparably smaller. In contrast, pronounced HOOP bands were not observed in the C1C2 chimera, regardless of the Ci1 protonation state (pH 4 vs. pH 8). Similarly, chromophore distortion was not observed in the K intermediate of *Cr*ChR2 (with deprotonated Ci1)[31,103,104] and *Ca*ChR1 (with protonated Ci1)[151]. Therefore, energy storage in these ChRs is carried instead by charge separation in the active site.

In the more distantly related Chrimson, the chromophore is distorted in the dark state and relaxes after light activation. Distortion of the chromophore in the dark most likely is a key mechanism for the unprecedented bathochromic shift of Chrimson, in agreement with quantum mechanical calculations performed on the K-like intermediate bathorhodopsin in the photocycle of bovine rhodopsin.[133,134] The light-triggered release of this strain energy contributes to the formation of the blue-shifted proton-conducting L intermediate (along with deprotonation of Ci1). Prior to formation of L, the absorption spectrum of Chrimson is red-shifted as compared to the dark state[54], although the corresponding FTIR difference spectra

exhibit negative HOOP bands as markers for chromophore relaxation (see Fig. 3-33, p. 111). This means that the hypsochromic effect of light-induced chromophore relaxation must be more than compensated by the bathochromic effect of displacement of the RSBH⁺-counter-ion charges which accordingly is the main mechanism of energy storage in Chrimson.

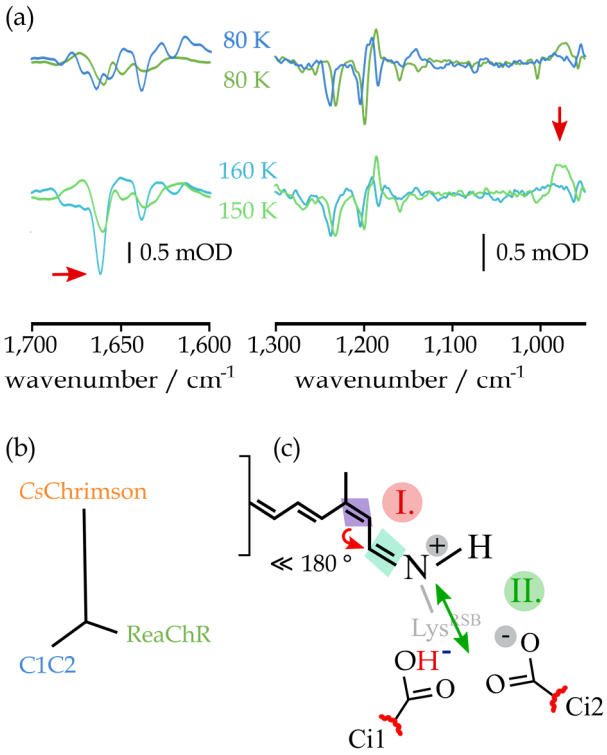


**Fig. 4-1** Storage and transfer of photon energy in ChRs. **(a)** FTIR light – dark difference spectra of C1C2 at pH 4 (*blue*) and ReaChR at pH 5 (*green*) after blue ($\lambda_{max}$ ~ 471 nm) and green ($\lambda_{max}$ ~ 529 nm) illumination, respectively. In ReaChR, a larger fraction of photon energy is stored as strain energy as compared to C1C2 as indicated by the more intense HOOP bands (*right red arrow*). The backbone rearrangements (*left red arrow*) are the result of energy transfer from the chromophore to the protein. The spectra were scaled to retinal fingerprint bands in the ReaChR spectrum at 80 K. The Chrimson spectra that indicated chromophore relaxation in the D→K transition (see Fig. 3-33, p. 111) were omitted because no spectra were recorded at ~ 150–160 K. **(b)** Phylogenetic tree of the ChRs investigated in this thesis calculated with Clustal Omega and the Simple Phylogeny tool provided by EMBL-EBI[227] and visualized with the Phylodendron server (version 0.8d). **(c)** Scheme for the mechanism of energy storage in ChRs. Energy can be stored in the chromophore by distortion of the retinal cofactor (*I.*) and charge separation of the RSBH⁺ and its counter-ions in the active site (*II.*). Ci1 is either protonated (*red hydrogen*) or deprotonated (*blue negative charge*).

## 4.3 Formation of the ion-conducting state

The energy from the photoreaction that is transferred to the protein following the K intermediate eventually leads to the formation of an ion-conducting pore. Although an open state structure is lacking to date, FTIR spectroscopic studies[157] as well as EPR measurements[77] and cryo-EM[165] have shed light on formation of the ion-conducting channel. These studies which are based on *Cr*ChR2 suggest that upon light activation the extracellular water-filled half-channel present in the crystal structure[72] is extended toward the intracellular site by light-induced alterations near the active site. Helical movements initiated within the active site drive the opening of the intracellular gates establishing the conductive pore. Kuhne *et al.* 2015[47] proposed the so-called EHT model, postulating that E3 deprotonation plays a crucial role in this helical movement. This model created a direct link between light-induced p$K_a$ changes near the active site and the process of channel formation. The MD calculations used for the development of this concept were conducted with a homology model of *Cr*ChR2 based on the C1C2 crystal structure by Kato *et al.* 2012.[41] The subsequently released *Cr*ChR2 crystal structure by Volkov *et al.* 2017[72] challenged this activation model, since it revealed that *Cr*ChR2 and C1C2 differ with respect to the orientation of E3 (see Fig. 1-5, p. 10). More recently, Kuhne *et al.* 2019[98] proposed that E3 is exclusively deprotonated in the 15-*syn* cycle and remains protonated during the entire 15-*anti* cycle. According to this interpretation, E3 deprotonation was assigned to occur after the 13-*trans*,15-*anti*→13-*cis*,15-*syn* retinal double isomerization reaction and characterized as being crucial for formation of the proton-selective open state of the 15-*syn* cycle. While this concept is backed up by convincing electrophysiological experiments[98], comparable experiments are not available for C1C2 and ReaChR to the best of the author's knowledge. However, several observations from FTIR spectropscopy and electrophysiology raise doubts about the applicability of this concept to both C1C2 and ReaChR (see detailed discussions in 3.1.4.2, p. 57, and 3.2.5.3, p. 97) and implied that instead E3 is also deprotonated in the 15-*anti* cycles of both ChRs.

Photon absorption provides the energy for charge separation in the active site which along with chromophore distortion causes the bathochromic shift of the K

intermediate. This alteration of the active site structure is likely to affect the hydrogen bonding of E3 in the downward orientation found in the crystal structure of *Cr*ChR2[72] but could also be the result of a light-induced downward movement of an upward oriented E3 as observed in the C1C2 crystal structure[41] and postulated by the EHT model[47]. A weakening of the strength of hydrogen bonding involving E3 could not be unambiguously proven in previous studies on *Cr*ChR2[31,103] and C1C2[42], similar to the examination of C1C2 in this thesis (see Fig. 3-2, p. 49). For ReaChR, however, the altered hydrogen bonding of E3 in the D→K transition was clearly resolved (see Fig. 3-10, p. 66). The weakened hydrogen bonding is the prerequisite for the subsequent deprotonation of E3 in the K→L transition. An L intermediate was not observed in *Cr*ChR2 but recently reported for C1C2.[44] Likely, the formation of this blue-shifted intermediate is due to the increased electrostatic stabilization of the $RBSH^+$ by the additional negative charge provided by E3. Deprotonation of E3 is not essential for ion channel function but is an important factor for the ion selectivity of ChRs.[41,52,219] Notably, electrophysiological measurements on C1C2 imply that the assumed salt bridge formed by deprotonated E3 leads to a widening of the restriction site that favors the transport of $Ca^{2+}$ ions[41], while leading to a narrower pore geometry in ReaChR and *Cr*ChR2, resulting in an increased proton selectivity in these ChRs[52,87,88].

Formation of the L and M intermediates is associated with large backbone alterations mainly due to the influx of water molecules.[157] This is reflected by strong changes in the amide I region in the case of C1C2 and ReaChR. From experiments on ReaChR with incorporated *p*-azido-L-phenylalanine labels, it could be derived that the light-induced hydration changes are particularly large in the inner gate (see Fig. 3-19, p. 80). In Chrimson, the light-induced backbone changes are drastically reduced as compared to C1C2 and ReaChR and are largely achieved already in the D→K transition (Fig. 4-2a). This deviation hints at a negative correlation between proton selectivity and the extent of backbone changes: a narrower pore exhibits higher selectivity for protons because it creates a barrier against the passage of large hydrated cations (Fig. 4-2b–c). In agreement with this assumed correlation, a higher pH in Chrimson, at which the proton selectivity is comparably reduced, resulted in larger backbone changes (see Fig. 3-36, p. 119).

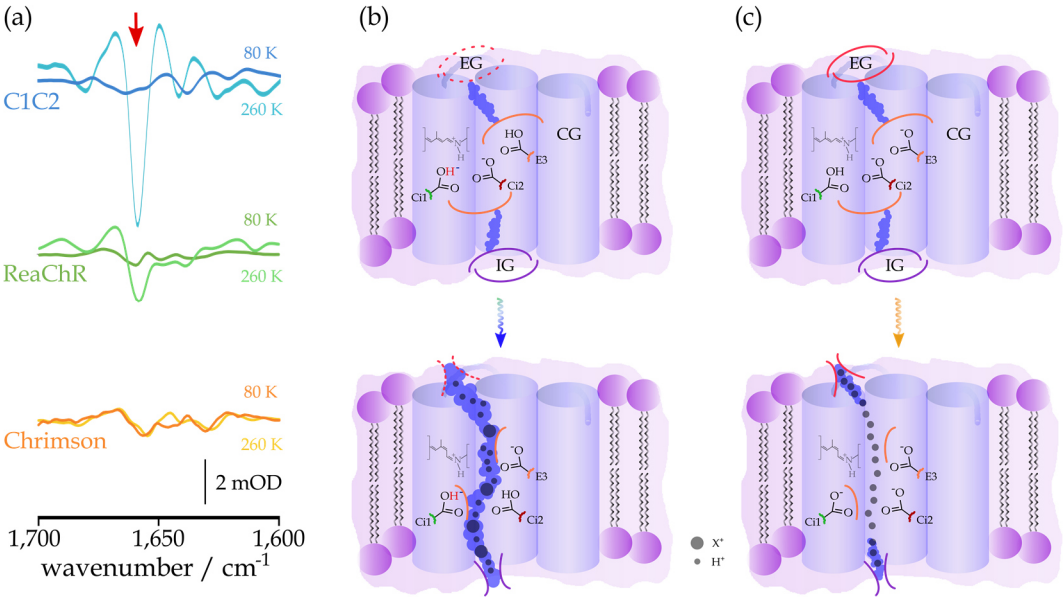


**Fig. 4-2** Formation of the ion-conducting pore. **(a)** FTIR light – dark difference spectra of C1C2 at pH 4, ReaChR at pH 5 and Chrimson at pH 5 induced by blue ($\lambda_{max}$ ~ 471 nm), green ($\lambda_{max}$ ~ 529 nm) and orange ($\lambda_{max}$ ~ 594 nm) illumination, respectively. The backbone changes (*red arrow*) are most pronounced in C1C2 and least pronounced in Chrimson. While the large backbone changes occur in the transition to the assumed conducting state in both C1C2 and ReaChR, the backbone changes in Chrimson largely occur already in the D→K transition. **(b)** Scheme for the probable ion conduction mechanism of C1C2 and ReaChR. Formation of the ion-conducting pathway involves deprotonation of E3 and protonation of Ci2 leading to a continuous water-filled pore that allows the efficient guidance of $H^+$ and larger cations, $X^+$. **(c)** Scheme for the likely ion conduction mechanism of Chrimson at acidic pH. The salt bridge between the $RSBH^+$ and Ci2 is maintained in the conducting state, presumably due to deprotonation of Ci1. This salt bridge – as well as the restriction site formed by E4 and Tyr159 at the extracellular gate (see Fig. 1-7, p. 13) – favors the transport of $H^+$ over larger cations. The protonation state of E3 in Chrimson is unclear.

The same tendency is observed in C1C2 and ReaChR: While at alkaline pH the photoreaction leads to a frequency downshift of amide I bands due to helix hydration during pore formation[157], a light-induced frequency upshift is observed at acidic pH and the changes in the amide I region are comparably reduced (see Fig. 3-3, p. 51, and Fig. 3-16, p. 75). This indicates a reduced water influx at acidic pH due to a narrower pore that likely leads to increased proton selectivity.

The high proton selectivity of Chrimson as compared to other ChRs is also the result of an altered structure of the gates.[39] The extracellular gate residue E4 acts as a pH sensor that in its protonated state forms a hydrogen bond to Tyr159[73] that serves as a barrier against the influx of larger cations and is considered an important determinant for the high proton selectivity.[39] At this position, a valine is found in C1C2 and ReaChR (see Fig. S1). The proton selectivity is furthermore determined by alterations in the active site and the central gate with the interaction between Ci1 and Phe[CI] being particularly relevant, as mutations of both residues

decisively reduce the photocurrents.[39] This is in stark contrast to both C1C2 and ReaChR in which Ci1 mutation has a negligible effect on the photocurrent amplitudes.[41,52] This difference is likely related to the fact that Ci1 is not directly involved in proton transfers in C1C2, ReaChR or *Cr*ChR2, but deprotonates in the photocycle of Chrimson. This deprotonation event presumably serves two purposes: (i) deprotonated Ci1 prevents deprotonation of the $RSBH^+$ and thus retains a strong electrostatic interaction in the active site (deprotonated Ci1 and Ci2 and the $RSBH^+$) that acts as a barrier against the passage of larger cations, and (ii) mediates structural changes at the extracellular (and potentially the intracellular) gate that are essential to channel opening.

## 4.4 Parallel photoreactions

The reduction of the photocurrents at continuous illumination conditions is a typical feature of most ChRs and reflects partial inactivation of the photocurrent due to formation of an equilibrium between open and closed states. Several ideas have been discussed over the past decades to explain this phenomenon (see 1.2.5.1, p. 15). The photocycle model for *Cr*ChR2 introduced by Ritter *et al.* 2013[101] and Bruun *et al.* 2015[96] and recently extended by Kuhne *et al.* 2019[98] comprises a 15-*anti* and a 15-*syn* cycle with the retinal of the dark state of the main branch (D) in 13-*trans*,15-*anti* conformation and the retinal of the dark state of the side branch (D') in 13-*cis*,15-*syn* conformation. According to this concept, partial photocurrent inactivation at extended illumination is mainly explained by accumulation of D' and its 15-*syn* retinal photoproducts. Given the presence of ~ 20 % 13-*cis* along with 13-*trans* retinal in the apparent dark state of C1C2, ReaChR and Chrimson as revealed by HPLC analysis of extracted retinals (see Tab. 1, p. 48, Tab. 3, p. 84, and Tab. 4, p. 114), D and D' are presumably present in all of the ChRs investigated in this thesis and parallel photoreactions must be taken into consideration to appropriately describe their photocurrents.

Although previous investigations on BR revealed a significant influence of the $RSBH^+$ counter-ions on the efficiency of the photoreaction[129,222], an effect on the stereoselectivity was not described to the best of the author's knowledge. Such an effect, however, was clearly indicated by the FTIR spectroscopic investigation of

the ChRs ReaChR and Chrimson. In both variants, deprotonated Ci1 enhances the 13-*trans*,15-*anti*→13-*cis*,15-*syn* double isomerization as compared to protonated Ci1 as could be deduced from the respective marker bands (see Fig. 3-21, p. 83, and Fig. 3-36, p. 119). In both cases, the additional negative charge of deprotonated Ci1 appears to have a catalytic effect on the D→D′ reaction given the impairment of this transition in the Ci1 mutants ReaChR-E163T and Chrimson-E165A (see Fig. 3-21, p. 83, and Fig. 3-36, p. 119).

A notable difference between the more closely related ChRs, C1C2 and ReaChR, on the one hand and Chrimson on the other hand with respect to the 13-*trans*,15-*anti*→13-*cis*,15-*syn* double isomerization reaction lies in the unusually high thermal stability of the D′ state in Chrimson (see Fig. 3-32, p. 110). This is presumably due to a stabilizing effect of deprotonated Ci1 on the 13-*cis*,15-*syn* conformation by an impairment of the thermal back reaction to D (13-*trans*,15-*anti*) which is in line with theoretical calculations on the effect of electrostatic interactions in the active site on barriers for thermal retinal isomerization.[220]

In addition to Ci1, $Asp^{DC}$ had a strong effect on the isomeric composition of the apparent dark state in both C1C2 and ReaChR (but not in Chrimson, as a cysteine is found at this location), as mutation to asparagine reduced the contribution of 13-*trans* to ~ 50 % and gave increase to 13-*cis*, 11-*cis* and 9-*cis* retinal isomers (see Tab. 1, p. 48, and Tab. 3, p. 84). This hints at a critical role of this residue for maintaining a binding pocket that is largely selective for 13-*trans*,15-*anti* in the dark. The reduced stereoselectivity in the asparagine mutants of $Asp^{DC}$ could explain the lack of photocurrent inactivation previously observed in ReaChR[52] and *Cr*ChR2[82]. Based on electrophysiological studies, the transient current that is typically observed in wild type photocurrents (see Fig. 1-10a, p. 16) is mainly due to formation of the open state of the 15-*anti* cycle[98] and could thus be abolished by reduction of the 15-*anti* dark state in the $Asp^{DC}$ mutants. Additionally, the quantum efficiencies for photoreactions other than 13-*trans*,15-*anti*→13-*cis*,15-*anti* could be increased in the $Asp^{DC}$ mutants so that an equilibrium between the competing photoreactions would be more rapidly achieved in comparison to the wild types. Given that Ritter *et al.* 2013[101] reported on a similar effect of the $Cys^{DC}$

mutant C128T in *Cr*ChR2 on the isomeric composition of the retinal binding pocket, a crucial role of the DC pair for the stereoselectivity can be assumed. While MD calculations[45] and the crystal structure of *Cr*ChR2[72] showed that Asp$^{DC}$ and Cys$^{DC}$ are connected via a water molecule, such an interaction was not observed in the structure of the C1C2 wild type (see Fig. 1-5, p. 10).[41] However, an interaction of these residues also in C1C2 is implied by FTIR spectra as Cys$^{DC}$ mutation (C167S) drastically altered the υ(C=O) mode associated with deprotonation of Asp$^{DC}$,[43] similar to previous observations for *Cr*ChR2[81,103]. In ReaChR, Cys$^{DC}$ mutation (C168S) completely abolished the marker band for deprotonation of Asp$^{DC}$ (see Fig. 3-25, p. 91) which implies an interaction of these residues. However, the respective band that reflects deprotonation of Asp$^{DC}$ (1753 cm$^{-1}$) is decisively upshifted as compared to C1C2 and *Cr*ChR2 (~ 1738 cm$^{-1}$)[81,103], indicating a relatively weakened interaction of the DC pair residues in ReaChR[183]. Berndt *et al.* 2009[83] argued based on electrophysiological experiments on Cys$^{DC}$ mutants of *Cr*ChR2 that the sulfur might accelerate retinal back isomerization by interacting with the retinal polyene chain. Accordingly, the drastic life-time prolongation of the ion conducting state in Cys$^{DC}$ mutants[82–84] could be explained by impairment of the back isomerization reaction, and the similar observations on the Asp$^{DC}$ mutants[82,84,85] could be due to an altered interaction between the Cys$^{DC}$ sulfur and the retinal polyene chain. Following this hypothesis, pathways for retinal isomerization to isomers other than 13-*trans*,15-*anti* could be relatively favored in the DC pair mutants which would explain the altered isomeric composition observed for C1C2-D195N and ReaChR-D196N in this thesis and for the *Cr*ChR2-C128T mutant[101]. Notably, the catalytic effect of the DC pair on the thermal back reaction of the retinal could also be due to the deprotonation of Asp$^{DC}$ in a more direct fashion as this provides an additional negative charge to the binding pocket that could guide transient translocation of the positive charge residing at the RSBH$^+$ toward the $C_{13}$=$C_{14}$ bond and thereby catalyze retinal isomerization.

## 4.5 Conclusion and outlook

The comparative investigation of selected ChR variants revealed the presence of several mechanistic modules (*e.g.* $Asp^{DC}$, Ci1 and E3 and their vicinity) within the ChR family that are crucial for a variety of properties such as ion selectivity, the absorption spectrum and the stereoselectivity of the photoreaction. More generally, this study emphasizes the relevance of proton dynamics for the mechanism of proteins by providing examples for molecular switches that control the dynamics of reaction pathways in dependence of their protonation state. The presence of these molecular switches increases the plasticity of the protein and enhances its susceptibility to altered environmental conditions which is of particular relevance for ChRs as they combine the light-sensing function with the generation of functional output in a compact fashion.

A number of additional experiments would help to further characterize the main findings of this thesis:

- Usage of a He- or dry cryostat that allows measurement of temperatures << 77 K would help to further characterize the processes of energy storage and transfer and identify intermediate steps.
- Femtosecond pump-probe FTIR spectroscopic investigation of the photoreaction of ReaChR in dependence of the Ci1 protonation state could verify/ falsify the proposed model for double isomerization of the retinal cofactor (see Fig. 3-30, p. 107).
- The application of complex illumination protocols to Chrimson, including laser excitation, could help to characterize possible photointermediates of the D' state.

In addition to the main findings of this thesis, the following aspects concerning the photocycles of ChRs are of particular interest:

- The actual gating mechanism at the intracellular gate that establishes the ion-conducting pore. Therefore, mutations and/ or isotopically labelled side chains of the intracellular gate would be required.

- The cooperativity between the ChR dimers that is largely neglected in present considerations. Dimer-dimer interaction could be modified by mutants or altered salt conditions.
- The long-term inactivation of ChR proteins that is observed in addition to the photocurrent inactivation and affects a large fraction of ChRs. This phenomenon is addressed neither in functional nor in mechanistic studies to the best of the author's knowledge. Functional measurements in algae would be required that involve long dark adaptation periods. These should be complemented with mechanistic studies, *e.g.* by FTIR measurements.

# 5 References


1. Spudich, J. L., Yang, C.-S., Jung, K.-H. & Spudich, E. N. Retinylidene Proteins: Structures and Functions from Archaea to Humans. *Annu. Rev. Cell Dev. Biol.* **16**, 365–392 (2000).
2. Hofmann, K. P. *et al.* A G protein-coupled receptor at work: the rhodopsin model. *Trends Biochem. Sci.* **34**, 540–552 (2009).
3. Arendt, D., Tessmar-Raible, K., Snyman, H., Dorresteijn, A. W. & Wittbrodt, J. Ciliary Photoreceptors with a Vertebrate-Type Opsin in an Invertebrate Brain. *Science* **306**, 869–871 (2004).
4. Spudich, J. L. & Bogomolni, R. A. Mechanism of colour discrimination by a bacterial sensory rhodopsin. *Nature* **312**, 509–513 (1984).
5. Oesterhelt, D. & Stoeckenius, W. Rhodopsin-like protein from the purple membrane of *Halobacterium halobium*. *Nat. New. Biol.* **233**, 149–152
6. Matsuno-Yagi, A. & Mukohata, Y. Two possible roles of bacteriorhodopsin; a comparative study of strains of *Halobacterium halobium* differing in pigmentation. *Biochem. Biophys. Res. Commun.* **78**, 237–243 (1977).
7. Nagel, G., Ollig, D., Fuhrmann, M., Kateriya, S., Musti, A. M., Bamberg, E., and Hegemann, P. Channelrhodopsin-1: A Light-Gated Proton Channel in Green Algae. *Science* **296**, 2395–2398 (2002).
8. Nagel, G. *et al.* Channelrhodopsin-2, a directly light-gated cation-selective membrane channel. *Proc. Natl. Acad. Sci. U. S. A.* **100**, 13940–13945 (2003).
9. Boll, F. Zur Anatomie und Physiologie der Retina. *Monatsberichte der Königlichen Preußischen Akad. der Wissenschaften zu Berlin* 783–787 (1876).
10. Kühne, W. Über den Sehpurpur. *Untersuchungen aus dem Physiol. Inst. der Univ. Heidelb.* 15–113 (1878).
11. Costanzi, S., Siegel, J., Tikhonova, I. G. & Jacobson, K. A. Rhodopsin and the others: a historical perspective on structural studies of G protein-coupled receptors. *Curr. Pharm. Des.* **15**, 3994–4002 (2009).
12. Insel, P. A., Tang, C.-M., Hahntow, I. & Michel, M. C. Impact of GPCRs in clinical medicine: genetic variants and drug targets. *Biochim. Biophys. Acta* **1768**, 994–1005 (2008).
13. Stoeckenius, W. & Rowen, R. A morphological study of *Halobacterium halobium* and its lysis in media of low salt concentration. *J. Cell Biol.* **34**, 365–393 (1967).
14. Oesterhelt, D. & Stoeckenius, W. Rhodopsin-like Protein from the purple membrane of *Halobacterium halobium*. *Nat. New Biol.* **233**, 149–152 (1971).
15. Hou, S.-Y. *et al.* Diversity of *Chlamydomonas* Channelrhodopsins. *Photochem. Photobiol.* **88**, 119–128 (2012).
16. Zhang, F. *et al.* The microbial opsin family of optogenetic tools. *Cell* **147**, 1446–1457 (2011).
17. Govorunova, E. G., Spudich, E. N., Lane, C. E., Sineshchekov, O. A. & Spudich, J. L. New Channelrhodopsin with a Red-Shifted Spectrum and Rapid Kinetics from *Mesostigma viride*. *MBio* **2**, 1–9 (2011).
18. Govorunova, E. G., Sineshchekov, O. A., Li, H., Janz, R. & Spudich, J. L. Characterization of a Highly Efficient Blue-shifted Channelrhodopsin from the Marine Alga *Platymonas subcordiformis*. *J. Biol. Chem.* **288**, 29911–29922 (2013).
19. Stavis, R. L. & Hirschberg, R. Phototaxis in *Chlamydomonas reinhardtii*. *J. Cell Biol.* **59**, 367–377 (1973).

20. Stavis, R. L. The Effect of Azide on Phototaxis in *Chlamydomonas reinhardi*. *Proc. Natl. Acad. Sci. U. S. A.* **71**, 1824–1827 (1974).
21. Hirschberg, R. & Stavis, R. Phototaxis mutants of *Chlamydomonas reinhardtii*. *J. Bacteriol.* **129**, 803–808 (1977).
22. Schneider, F., Grimm, C. & Hegemann, P. Biophysics of Channelrhodopsin. *Annu. Rev. Biophys.* **44**, 167–86 (2015).
23. Foster, K. W. & Smyth, R. D. Light Antennas in phototactic algae. *Microbiol. Rev.* **44**, 572–630 (1980).
24. Tsunoda, S. P. & and Hegemann, P. Glu 87 of Channelrhodopsin-1 Causes pH-dependent Color Tuning and Fast Photocurrent Inactivation. *Photochem. Photobiol.* **85**, 564–569 (2008).
25. Berthold, P. *et al.* Channelrhodopsin-1 Initiates Phototaxis and Photophobic Responses in *Chlamydomonas* by Immediate Light-Induced Depolarization. *Plant Cell* **20**, 1665–1677 (2008).
26. Sineshchekov, O. A. & Govorunova, E. G. Rhodopsin-mediated photosensing in green flagellated algae. *Trends Plant Sci.* **4**, 58–63 (1999).
27. Harz, H., and Hegemann, P. Rhodopsin-regulated calcium currents in *Chlamydomonas*. *Nature* **351**, 489–491 (1991).
28. Beckmann, M. & Hegemann, P. In Vitro Identification of Rhodopsin in the Green Alga *Chlamydomonas*. *Biochemistry* **30**, 3692–3697 (1991).
29. Harz, H., Nonnengässer, C. & Hegemann, P. The photoreceptor current of the green alga *Chlamydomonas*. *Philos. Trans. R. Soc. B Biol. Sci.* **338**, 39–52 (1992).
30. Hegemann, P. Algal Sensory Photoreceptors. *Annu. Rev. Plant Biol* **59**, 167–189 (2008).
31. Ritter, E., Stehfest, K., Berndt, A., Hegemann, P. & Bartl, F. J. Monitoring Light-induced Structural Changes of Channelrhodopsin-2 by UV-visible and Fourier Transform Infrared Spectroscopy. *J. Biol. Chem.* **283**, 35033–35041 (2008).
32. Zhang, F. *et al.* Red-shifted optogenetic excitation: a tool for fast neural control derived from *Volvox carteri*. *Nat. Neurosci.* **11**, 631–633 (2008).
33. Prigge, M. *et al.* Color-tuned channelrhodopsins for multiwavelength optogenetics. *J. Biol. Chem.* **287**, 31804–31812 (2012).
34. Li, H., Govorunova, E. G., Sineshchekov, O. A. & Spudich, J. L. Role of a Helix B Lysine Residue in the Photoactive Site in Channelrhodopsins. *Biophys. J.* **106**, 1607–1617 (2014).
35. Sineshchekov, O. A., Govorunova, E. G., Wang, J., Li, H. & Spudich, J. L. Intramolecular proton transfer in channelrhodopsins. *Biophys. J.* **104**, 807–817 (2013).
36. Feldbauer, K. *et al.* Channelrhodopsin-2 is a leaky proton pump. *Proc. Natl. Acad. Sci. U. S. A.* **106**, 12317–22 (2009).
37. Nack, M. *et al.* Kinetics of proton release and uptake by channelrhodopsin-2. *FEBS Lett.* **586**, 1344–1348 (2012).
38. Klapoetke, N. C. *et al.* Independent optical excitation of distinct neural populations. *Nat. Methods* **11**, 338–46 (2014).
39. Vierock, J., Grimm, C., Nitzan, N. & Hegemann, P. Molecular determinants of proton selectivity and gating in the red-light activated channelrhodopsin Chrimson. *Sci. Rep.* **7**, 1–15 (2017).
40. Govorunova, E. G., Sineshchekov, O. A., Janz, R., Liu, X. & Spudich, J. L. Natural light-gated anion channels: A family of microbial rhodopsins for

advanced optogenetics. *Science* **349**, 647–650 (2015).
41. Kato, H. E. *et al.* Crystal structure of the channelrhodopsin light-gated cation channel. *Nature* **482**, 369–374 (2012).
42. Ito, S. *et al.* Water-containing hydrogen-bonding network in the active center of channelrhodopsin. *J. Am. Chem. Soc.* **136**, 3475–3482 (2014).
43. Inaguma, A. *et al.* Chimeras of channelrhodopsin-1 and -2 from *Chlamydomonas reinhardtii* exhibit distinctive light-induced structural changes from channelrhodopsin-2. *J. Biol. Chem.* **290**, 11623–11634 (2015).
44. Hontani, Y. *et al.* Reaction dynamics of the chimeric channelrhodopsin C1C2. *Sci. Rep.* **7**, 1–12 (2017).
45. Watanabe, H. C., Welke, K., Sindhikara, D. J., Hegemann, P. & Elstner, M. Towards an Understanding of Channelrhodopsin Function: Simulations Lead to Novel Insights of the Channel Mechanism. *J. Mol. Biol.* **425**, 1795–1814 (2013).
46. Welke, K., Watanabe, H. C., Wolter, T., Gaus, M. & Elstner, M. QM/MM simulations of vibrational spectra of bacteriorhodopsin and channelrhodopsin-2. *Phys. Chem. Chem. Phys.* **15**, 6651–9 (2013).
47. Kuhne, J. *et al.* Early Formation of the Ion-Conducting Pore in Channelrhodopsin-2. *Angew. Chem. Int. Ed. Engl.* **54**, 4953–4957 (2015).
48. Guo, Y. *et al.* Active site structure and absorption spectrum of channelrhodopsin-2 wild-type and C128T mutant. *Chem. Sci.* **7**, 3879–3891 (2016).
49. Lin, J. Y., Knutsen, P. M., Muller, A., Kleinfeld, D. & Tsien, R. Y. ReaChR: a red-shifted variant of channelrhodopsin enables deep transcranial optogenetic excitation. *Nat. Neurosci.* **16**, 1499–1508 (2013).
50. Lin, J. Y., Lin, M. Z., Steinbach, P. & Tsien, R. Y. Characterization of engineered channelrhodopsin variants with improved properties and kinetics. *Biophys. J.* **96**, 1803–1814 (2009).
51. Krause, B. S. *et al.* Complex Photochemistry within the Green-Absorbing Channelrhodopsin ReaChR. *Biophys. J.* **112**, 1166–1175 (2017).
52. Kaufmann, J. C. D. *et al.* Proton transfer reactions in the red light-activatable channelrhodopsin variant ReaChR and their relevance for its function. *J. Biol. Chem.* **292**, 14205–14216 (2017).
53. Krause, B. S. *et al.* Tracking Pore Hydration in Channelrhodopsin by Site-Directed Infrared-Active Azido Probes. *Biochemistry* **58**, 1275–1286 (2019).
54. Urmann, D. *et al.* Photochemical Properties of the Red-shifted Channelrhodopsin Chrimson. *Photochem. Photobiol.* **93**, 782–795 (2017).
55. Ishizuka, T., Kakuda, M., Araki, R. & Yawo, H. Kinetic evaluation of photosensitivity in genetically engineered neurons expressing green algae light-gated channels. *Neurosci. Res.* **54**, 85–94 (2006).
56. Boyden, E. S., Zhang, F., Bamberg, E., Nagel, G. & Deisseroth, K. Millisecond-timescale, genetically targeted optical control of neural activity. *Nat. Neurosci.* **8**, 1263–1268 (2005).
57. Grosenick, L., Marshel, J. H. & Deisseroth, K. Closed-Loop and Activity-Guided Optogenetic Control. *Neuron* **86**, 106–139 (2015).
58. Bi, A. *et al.* Ectopic Expression of a Microbial-Type Rhodopsin Restores Visual Responses in Mice with Photoreceptor Degeneration. *Neuron* **50**, 23–33 (2006).
59. Inagaki, H. K. *et al.* Optogenetic control of *Drosophila* using a red-shifted channelrhodopsin reveals experience-dependent influences on courtship.

*Nat. Methods* **11**, 325–332 (2014).
60. Nagel, G. *et al.* Channelrhodopsins: directly light-gated cation channels. *Biochem. Soc. Trans.* **33**, 863–866 (2005).
61. Sengupta, A. *et al.* Red-shifted channelrhodopsin stimulation restores light responses in blind mice, macaque retina, and human retina. *EMBO Mol. Med.* **8**, 1248–1264 (2016).
62. Li, X. *et al.* Fast noninvasive activation and inhibition of neural and network activity by vertebrate rhodopsin and green algae channelrhodopsin. *Proc. Natl. Acad. Sci. U. S. A.* **102**, 17816–17821 (2005).
63. Nyns, E. C. A. *et al.* Optogenetic termination of ventricular arrhythmias in the whole heart: towards biological cardiac rhythm management. *Eur. Heart J.* **38**, 2132–2136 (2017).
64. Yizhar, O., Fenno, L. E., Davidson, T. J., Mogri, M. & Deisseroth, K. Optogenetics in Neural Systems. *Neuron* **71**, 9–34 (2011).
65. Schneider, F., Gradmann, D. & Hegemann, P. Ion Selectivity and Competition in Channelrhodopsins. *Biophys. J.* **105**, 91–100 (2013).
66. Berndt, A., Lee, S. Y., Ramakrishnan, C. & Deisseroth, K. Structure-Guided Transformation of Channelrhodopsin into a Light-Activated Chloride Channel. *Science* **344**, 420–424 (2014).
67. Wietek, J. *et al.* Conversion of Channelrhodopsin into a Light-Gated Chloride Channel. *Science* **344**, 409–412 (2014).
68. Wietek, J., Broser, M., Krause, B. S. & Hegemann, P. Identification of a Natural Green Light Absorbing Chloride Conducting Channelrhodopsin from *Proteomonas sulcata*. *J. Biol. Chem.* **291**, 4121–4127 (2016).
69. Tromberg, B. J. *et al.* Non-Invasive *In Vivo* Characterization of Breast Tumors Using Photon Migration Spectroscopy. *Neoplasia* **2**, 26–40 (2000).
70. Marblestone, A. H. *et al.* Physical principles for scalable neural recording. *Front. Comput. Neurosci.* **7**, 1–34 (2013).
71. Hooks, B. M., Lin, J. Y., Guo, C. & Svoboda, K. Dual-Channel Circuit Mapping Reveals Sensorimotor Convergence in the Primary Motor Cortex. *J. Neurosci.* **35**, 4418–4426 (2015).
72. Volkov, O. *et al.* Structural insights into ion conduction by channelrhodopsin 2. *Science* **358**, 1–8 (2017).
73. Oda, K. *et al.* Crystal structure of the red light-activated channelrhodopsin Chrimson. *Nat. Commun.* **9**, 3949 (2018).
74. Kato, H. E. *et al.* Atomistic design of microbial opsin-based blue-shifted optogenetics tools. *Nat. Commun.* **6**, 1–10 (2015).
75. Kim, Y. S. *et al.* Crystal structure of the natural anion-conducting channelrhodopsin *Gt*ACR1. *Nature* **561**, 343–348 (2018).
76. Sattig, T., Rickert, C., Bamberg, E., Steinhoff, H. & Bamann, C. Light-Induced Movement of the Transmembrane Helix B in Channelrhodopsin-2. *Angew. Chem. Int. Ed. Engl.* **52**, 9705–9708 (2013).
77. Krause, N., Engelhard, C., Heberle, J., Schlesinger, R. & Bittl, R. Structural differences between the closed and open states of channelrhodopsin-2 as observed by EPR spectroscopy. *FEBS Lett.* **587**, 3309–3313 (2013).
78. Luecke, H., Schobert, B., Richter, H.-T., Cartailler, J.-P. & Lanyi, J. K. Structure of Bacteriorhodopsin at 1.55 Å Resolution. *J. Mol. Biol.* **291**, 899–911 (1999).
79. Ogren, J. I. *et al.* Retinal Chromophore Structure and Schiff Base Interactions in Red-Shifted Channelrhodopsin-1 from *Chlamydomonas augustae*.

*Biochemistry* **53**, 3961–3970 (2014).
80. Watanabe, H. C. *et al.* Structural Model of Channelrhodopsin. *J. Biol. Chem.* **287**, 7456–7466 (2012).
81. Nack, M. *et al.* The DC gate in Channelrhodopsin-2: crucial hydrogen bonding interaction between C128 and D156. *Photochem. Photobiol. Sci.* **9**, 194–198 (2010).
82. Bamann, C., Gueta, R., Kleinlogel, S., Nagel, G. & Bamberg, E. Structural Guidance of the Photocycle of Channelrhodopsin-2 by an Interhelical Hydrogen Bond. *Biochemistry* **49**, 267–278 (2010).
83. Berndt, A., Yizhar, O., Gunaydin, L. A., Hegemann, P. & Deisseroth, K. Bi-stable neural state switches. *Nat. Neurosci.* **12**, 229–234 (2009).
84. Yizhar, O. *et al.* Neocortical excitation/inhibition balance in information processing and social dysfunction. *Nature* **477**, 171–178 (2011).
85. Dawydow, A. *et al.* Channelrhodopsin-2-XXL, a powerful optogenetic tool for low-light applications. *Proc. Natl. Acad. Sci. U. S. A.* **111**, 13972–13977 (2014).
86. Plazzo, A. P. *et al.* Bioinformatic and mutational analysis of channelrhodopsin-2 protein cation-conducting pathway. *J. Biol. Chem.* **287**, 4818–4825 (2012).
87. Ruffert, K. *et al.* Glutamate residue 90 in the predicted transmembrane domain 2 is crucial for cation flux through channelrhodopsin 2. *Biochem. Biophys. Res. Commun.* **410**, 737–743 (2011).
88. Eisenhauer, K. *et al.* In Channelrhodopsin-2 Glu-90 Is Crucial for Ion Selectivity and Is Deprotonated during the Photocycle. *J. Biol. Chem.* **287**, 6904–6911 (2012).
89. Takemoto, M. *et al.* Molecular Dynamics of Channelrhodopsin at the Early Stages of Channel Opening. *PLoS One* **10**, e0131094 (2015).
90. Gradmann, D., Berndt, A., Schneider, F. & Hegemann, P. Rectification of the channelrhodopsin early conductance. *Biophys. J.* **101**, 1057–1068 (2011).
91. Sugiyama, Y. *et al.* Photocurrent attenuation by a single polar-to-nonpolar point mutation of channelrhodopsin-2. *Photochem. Photobiol. Sci.* **8**, 328–336 (2009).
92. Ernst, O. P. *et al.* Photoactivation of channelrhodopsin. *J. Biol. Chem.* **283**, 1637–1643 (2008).
93. Hegemann, P., Ehlenbeck, S. & Gradmann, D. Multiple Photocycles of Channelrhodopsin. *Biophys. J.* **89**, 3911–3918 (2005).
94. Nikolic, K. *et al.* Photocycles of Channelrhodopsin-2. *Photochem. Photobiol.* **85**, 400–411 (2009).
95. Berndt, A., Prigge, M., Gradmann, D. & Hegemann, P. Two Open States with Progressive Proton Selectivities in the Branched Channelrhodopsin-2 Photocycle. *Biophys. J.* **98**, 753–761 (2010).
96. Bruun, S. *et al.* Light-Dark Adaptation of Channelrhodopsin Involves Photoconversion between the all-*trans* and 13-*cis* Retinal Isomers. *Biochemistry* **54**, 5389–5400 (2015).
97. Kuhne, J. Schwingungsspektroskopische Untersuchungen an Channelrhodopsin-2 mithilfe von zeitaufgelöster FTIR- und Raman-Spektroskopie. Ph.D. dissertation. *Ruhr Univ. Bochum* (2016).
98. Kuhne, J. *et al.* A unifying photocycle model for light adaptation and temporal evolution of cation conductance in channelrhodopsin-2. *Proc. Natl. Acad. Sci. U. S. A.* **116**, 9380–9389 (2019).

99. Nack, M., Radu, I., Bamann, C., Bamberg, E. & Heberle, J. The retinal structure of channelrhodopsin-2 assessed by resonance Raman spectroscopy. *FEBS Lett.* **583**, 3676–3680 (2009).
100. Muders, V. *et al.* Resonance Raman and FTIR spectroscopic characterization of the closed and open states of channelrhodopsin-1. *FEBS Lett.* **588**, 2301–2306 (2014).
101. Ritter, E., Piwowarski, P., Hegemann, P. & Bartl, F. J. Light-dark Adaptation of Channelrhodopsin C128T Mutant. *J. Biol. Chem.* **288**, 10451–10458 (2013).
102. Becker-Baldus, J. *et al.* Enlightening the photoactive site of channelrhodopsin-2 by DNP-enhanced solid-state NMR spectroscopy. *Proc. Natl. Acad. Sci. U. S. A.* **112**, 9896–9901 (2015).
103. Radu, I. *et al.* Conformational Changes of Channelrhodopsin-2. *J. Am. Chem. Soc.* **446**, 7313–7319 (2009).
104. Lórenz-Fonfría, V. A. *et al.* Transient protonation changes in channelrhodopsin-2 and their relevance to channel gating. *Proc. Natl. Acad. Sci. U. S. A.* **110**, E1273–E1281 (2013).
105. Lórenz-Fónfria, V. A. *et al.* Pre-Gating Conformational Changes in the ChETA Variant of Channelrhodopsin-2 Monitored by Nanosecond IR Spectroscopy. *J. Am. Chem. Soc.* **137**, 1850–1861 (2015).
106. Oesterhelt, D., Meentzen, M. & Schuhmann, L. Reversible Dissociation of the Purple Complex in Bacteriorhodopsin and Identification of 13-*cis* and all-*trans*-Retinal as its Chromophores. *European Journal of Biochemistry* **40**, 453–463 (1973).
107. Pettei, M. J., Yudd, A. P., Nakanishi, K., Henselman, R. & Stoeckenius, W. Identification of Retinal Isomers Isolated from Bacteriorhodopsin. *Biochemistry* **16**, 1955–1959 (1977).
108. Harbison, G. S. *et al.* Dark-adapted bacteriorhodopsin contains 13-*cis*, 15-*syn* and all-*trans*, 15-*anti* retinal Schiff bases. *Proc. Natl. Acad. Sci. U. S. A.* **81**, 1706–1709 (1984).
109. Smith, S. O., Pardoen, J. A., Lugtenburg, J. & Mathies, R. A. Vibrational Analysis of the 13-*cis*-Retinal Chromophore in Dark-Adapted Bacteriorhodopsin. *J. Phys. Chem.* **91**, 804–819 (1987).
110. Roepe, P. D., Ahl, P. L., Herzfeld, J., Lugtenburg, J. & Rothschild, K. J. Tyrosine Protonation Changes in Bacteriorhodopsin. *J. Biol. Chem.* **263**, 5110–5117 (1988).
111. Kawanabe, A. & Kandori, H. Photoreactions and Structural Changes of *Anabaena* Sensory Rhodopsin. *Sensors* **9**, 9741–9804 (2009).
112. Enami, N. *et al.* Crystal Structures of Archaerhodopsin-1 and -2: Common Structural Motif in Archaeal Light-driven Proton Pumps. *J. Mol. Biol.* **358**, 675–685 (2006).
113. Kato, H. E. *et al.* Structural basis for $Na^+$ transport mechanism by a light-driven $Na^+$ pump. *Nature* **521**, 48–53 (2015).
114. Imasheva, E. S., Balashov, S. P., Wang, J. M., Dioumaev, A. K. & Lanyi, J. K. Selectivity of Retinal Photoisomerization in Proteorhodopsin Is Controlled by Aspartic Acid 227. *Biochemistry* **43**, 1648–1655 (2004).
115. Patzelt, H. *et al.* The structures of the active center in dark-adapted bacteriorhodopsin by solution-state NMR spectroscopy. *Proc. Natl. Acad. Sci. U. S. A.* **99**, 9765–70 (2002).
116. Kalisky, O., Goldschmidt, C. R. & Ottolenghi, M. On the photocycle and light adaptation of dark-adapted bacteriorhodopsin. *Biophys. J.* **19**, 185–189

(1977).
117. Ihara, K., Amemiya, T., Miyashita, Y. & Mukohata, and Y. Met-145 Is a Key Residue in the Dark Adaptation of Bacteriorhodopsin Homologs. *Biophys. J.* **67**, 1187–1191 (1994).
118. Ding, X. *et al.* Mediation mechanism of tyrosine 185 on the retinal isomerization equilibrium and the proton release channel in the seven-transmembrane receptor bacteriorhodopsin. *Biochim. Biophys. Acta - Bioenerg.* **1857**, 1786–1795 (2016).
119. Stensitzki, T., Muders, V., Schlesinger, R., Heberle, J. & Heyne, K. The primary photoreaction of channelrhodopsin-1: wavelength dependent photoreactions induced by ground-state heterogeneity. *Front. Mol. Biosci.* **2**, 1–10 (2015).
120. Schnedermann, C. *et al.* Vibronic Dynamics of the Ultrafast all-*trans* to 13-*cis* Photoisomerization of Retinal in Channelrhodopsin-1. *J. Am. Chem. Soc.* **138**, 4757–4762 (2016).
121. Scholz, F., Bamberg, E., Bamann, C. & Wachtveitl, J. Tuning the primary reaction of channelrhodopsin-2 by imidazole, pH, and site-specific mutations. *Biophys. J.* **102**, 2649–2657 (2012).
122. Verhoefen, M.-K. *et al.* The Photocycle of Channelrhodopsin-2: Ultrafast Reaction Dynamics and Subsequent Reaction Steps. *ChemPhysChem* **11**, 3113–3122 (2010).
123. Bamann, C., Kirsch, T., Nagel, G. & Bamberg, E. Spectral Characteristics of the Photocycle of Channelrhodopsin-2 and Its Implication for Channel Function. *J. Mol. Biol.* **375**, 686–694 (2008).
124. Dioumaev, A. K. & Lanyi, J. K. Bacteriorhodopsin photocycle at cryogenic temperatures reveals distributed barriers of conformational substates. *Proc. Natl. Acad. Sci. U. S. A.* **104**, 9621–6 (2007).
125. Horwitz, J. & Heller, J. Interactions of All-*trans*, 9-, 11-, and 13-*cis*-retinal, All-*trans*-retinyl Acetate, and Retinoic Acid with Human Retinol-binding Protein and Prealbumin. *J. Biol. Chem.* **248**, 6317–6324 (1973).
126. Ernst, O. P. *et al.* Microbial and animal rhodopsins: Structures, functions, and molecular mechanisms. *Chem. Rev.* **114**, 126–163 (2014).
127. Gunaydin, L. A. *et al.* Ultrafast optogenetic control. *Nat. Neurosci.* **13**, 387–392 (2010).
128. Katayama, K., Nonaka, Y., Tsutsui, K., Imai, H. & Kandori, H. Spectral Tuning Mechanism of Primate Blue-sensitive Visual Pigment Elucidated by FTIR Spectroscopy. *Sci. Rep.* **7**, 1–10 (2017).
129. Song, L., El-Sayed, M. A. & Lanyi, J. K. Protein Catalysis of the Retinal Subpicosecond Photoisomerization in the Primary Process of Bacteriorhodopsin Photosynthesis. *Science* **261**, 891–894 (1993).
130. González-Luque, R. *et al.* Computational evidence in favor of a two-state, two-mode model of the retinal chromophore photoisomerization. *Proc. Natl. Acad. Sci. U. S. A.* **97**, 9379–9384 (2000).
131. Schenkl, S., Van Mourik, F., Van Der Zwan, G., Haacke, S. & Chergui, M. Chemistry: Probing the Ultrafast Charge Translocation of Photoexcited Retinal in Bacteriorhodopsin. *Science* **309**, 917–920 (2005).
132. Neumann-Verhoefen, M.-K. *et al.* Ultrafast Infrared Spectroscopy on Channelrhodopsin-2 Reveals Efficient Energy Transfer from the Retinal Chromophore to the Protein. *J. Am. Chem. Soc.* **135**, 6968–6976 (2013).
133. Schreiber, M. & Buss, V. Origin of the Bathochromic Shift in the Early

Photointermediates of the Rhodopsin Visual Cycle: A CASSCF/CASPT2 Study. *Int. J. Quantum Chem.* **95**, 882–889 (2003).
134. Schreiber, M., Sugihara, M., Okada, T. & Buss, V. Quantum Mechanical Studies on the Crystallographic Model of Bathorhodopsin. *Angew. Chem. Int. Ed. Engl.* **45**, 4274–4277 (2006).
135. Sekharan, S. & Morokuma, K. QM/MM Study of the Structure, Energy Storage, and Origin of the Bathochromic Shift in Vertebrate and Invertebrate Bathorhodopsins. *J. Am. Chem. Soc.* **133**, 4734–4737 (2011).
136. Schobert, B., Cupp-Vickery, J., Hornak, V., Smith, S. O. & Lanyi, J. K. Crystallographic Structure of the K Intermediate of Bacteriorhodopsin: Conservation of Free Energy after Photoisomerization of the Retinal. *J. Mol. Biol.* **321**, 715–726 (2002).
137. Hayashi, S., Tajkhorshid, E., Kandori, H. & Schulten, K. Role of Hydrogen-Bond Network in Energy Storage of Bacteriorhodopsin's Light-Driven Proton Pump Revealed by ab Initio Normal-Mode Analysis. *J. Am. Chem. Soc.* **126**, 10516–10517 (2004).
138. Cooper, A. Energy uptake in the first step of visual excitation. *Nature* **282**, 531–533 (1979).
139. Birge, R. R. & Cooper, T. M. Energy storage in the primary step of the photocycle of bacteriorhodopsin. *Biophys. J.* **42**, 61–69 (1983).
140. Gascon, J. A. & Batista, V. S. QM/MM Study of Energy Storage and Molecular Rearrangements Due to the Primary Event in Vision. *Biophys. J.* **87**, 2931–2941 (2004).
141. Andruniów, T., Ferré, N. & Olivucci, M. Structure, initial excited-state relaxation, and energy storage of rhodopsin resolved at the multiconfigurational perturbation theory level. *Proc. Natl. Acad. Sci. U. S. A.* **101**, 17908–17913 (2004).
142. Birge, R. R., Einterz, C. M., Knapp, H. M. & Murray, L. P. The nature of the primary photochemical events in rhodopsin and isorhodopsin. *Biophys. J.* **53**, 367–385 (1988).
143. Hayashi, S., Tajkhorshid, E. & Schulten, K. Structural Changes during the Formation of Early Intermediates in the Bacteriorhodopsin Photocycle. *Biophys. J.* **83**, 1281–1297 (2002).
144. Smith, S. O., Lugtenburg, J. & Mathies, R. A. Determination of Retinal Chromophore Structure in Bacteriorhodopsin with Resonance Raman Spectroscopy. *J. Membr. Biol.* **85**, 95–109 (1985).
145. Yamauchi, Y. *et al.* Molecular properties of a DTD channelrhodopsin from *Guillardia theta*. *Biophys. Physicobiology* **14**, 57–66 (2017).
146. Eyring, G., Curry, B., Broek, A., Lugtenburg, J. & Mathies, R. Assignment and Interpretation of Hydrogen Out-of-Plane Vibrations in the Resonance Raman Spectra of Rhodopsin and Bathorhodopsin. *Biochemistry* **21**, 384–393 (1982).
147. Dioumaev, A. K., Wang, J. M. & Lanyi, J. K. Low-Temperature FTIR Study of Multiple K Intermediates in the Photocycles of Bacteriorhodopsin and Xanthorhodopsin. *J. Phys. Chem. B* **114**, 1–24 (2010).
148. Ikeda, D., Furutani, Y. & Kandori, H. FTIR study of the retinal Schiff base and internal water molecules of proteorhodopsin. *Biochemistry* **46**, 5365–5373 (2007).
149. Furutani, Y. *et al.* Assignment of the Hydrogen-Out-Of-Plane and -in-Plane Vibrations of the Retinal Chromophore in the K Intermediate of *pharaonis*

Phoborhodopsin. *Biochemistry* **45**, 11836–11843 (2006).
150. Dioumaev, A. K. *et al.* Photocycle of *Exiguobacterium sibiricum* Rhodopsin Characterized by Low-Temperature Trapping in the IR and Time-resolved Studies in the Visible. *J. Phys Chem. B* **117**, 7235–7253 (2013).
151. Ogren, J. I. *et al.* Comparison of the Structural Changes Occurring during the Primary Phototransition of Two Different Channelrhodopsins from *Chlamydomonas* Algae. *Biochemistry* **54**, 377–388 (2015).
152. Lanyi, J. K. & Schobert, B. Mechanism of Proton Transport in Bacteriorhodopsin from Crystallographic Structures of the K, L, $M_1$, $M_2$, and $M_2'$ Intermediates of the Photocycle. *J. Mol. Biol.* **328**, 439–450 (2003).
153. Schobert, B., Brown, L. S. & Lanyi, J. K. Crystallographic Structures of the M and N Intermediates of Bacteriorhodopsin: Assembly of a Hydrogen-bonded Chain of Water Molecules Between Asp-96 and the Retinal Schiff Base. *J. Mol. Biol.* **330**, 553–570 (2003).
154. Neutze, R. *et al.* Bacteriorhodopsin: A high-resolution structural view of vectorial proton transport. *Biochim. Biophys. Acta - Biomembr.* **1565**, 144–167 (2002).
155. Smith, S. O. *et al.* Determination of retinal Schiff base configuration in bacteriorhodopsin. *Proc. Natl. Acad. Sci. U. S. A.* **81**, 2055–2059 (1984).
156. Stehfest, K., Ritter, E., Berndt, A., Bartl, F. & Hegemann, P. The branched photocycle of the slow-cycling channelrhodopsin-2 mutant C128T. *J. Mol. Biol.* **398**, 690–702 (2010).
157. Lórenz-Fonfría, V. A. *et al.* Temporal evolution of helix hydration in a light-gated ion channel correlates with ion conductance. *Proc. Natl. Acad. Sci. U. S. A.* **112**, E5796–E5804 (2015).
158. Ogren, J. I. *et al.* Proton Transfers in a Channelrhodopsin-1 Studied by Fourier Transform Infrared (FTIR) Difference Spectroscopy and Site-directed Mutagenesis. *J. Biol. Chem.* **290**, 12719–12730 (2015).
159. Lórenz-Fonfría, V. A., Muders, V., Schlesinger, R. & Heberle, J. Changes in the hydrogen-bonding strength of internal water molecules and cysteine residues in the conductive state of channelrhodopsin-1. *J. Chem. Phys.* **141**, 0–12 (2014).
160. Braiman, M. S., Bousché, O. & Rothschild, K. J. Protein dynamics in the bacteriorhodopsin photocycle: submillisecond Fourier transform infrared spectra of the L, M, and N photointermediates. *Proc. Natl. Acad. Sci. U. S. A.* **88**, 2388–92 (1991).
161. Hendrickson, F. M., Burkard, F. & Glaeser, R. M. Structural characterization of the L-to-M transition of the bacteriorhodopsin photocycle. *Biophys. J.* **75**, 1446–54 (1998).
162. Xiao, Y., Partha, R., Krebs, R. & Braiman, M. Time-Resolved FTIR Spectroscopy of the Photointermediates Involved in Fast Transient $H^+$ Release by Proteorhodopsin. *J. Phys. Chem. B* **109**, 634–641 (2005).
163. Verhoefen, M. K. *et al.* Low temperature FTIR spectroscopy provides new insights in the pH-dependent proton pathway of proteorhodopsin. *Biochim. Biophys. Acta - Bioenerg.* **1807**, 1583–1590 (2011).
164. Miranda, M. R. M. *et al.* The Photocycle and Proton Translocation Pathway in a Cyanobacterial Ion-Pumping Rhodopsin. *Biophys. J.* **96**, 1471–1481 (2009).
165. Müller, M., Bamann, C., Bamberg, E. & Kühlbrandt, W. Light-Induced Helix Movements in Channelrhodopsin-2. *J. Mol. Biol.* **427**, 341–349 (2015).

166. Szundi, I. *et al. Platymonas subcordiformis* Channelrhodopsin-2 Function. I. The photochemical reaction cycle. *J. Biol. Chem.* **290**, 16573–16584 (2015).
167. Szundi, I., Bogomolni, R. & Kliger, D. S. *Platymonas subcordiformis* Channelrhodopsin-2 (*Ps*ChR2) Function. II. Relationship of the photochemical reaction cycle to channel currents. *J. Biol. Chem.* **290**, 16585–16594 (2015).
168. Ardevol, A. & Hummer, G. Retinal isomerization and water-pore formation in channelrhodopsin-2. *Proc. Natl. Acad. Sci. U. S. A.* **115**, 3557–3562 (2018).
169. Hososhima, S., Sakai, S., Ishizuka, T. & Yawo, H. Kinetic evaluation of photosensitivity in Bi-stable variants of chimeric channelrhodopsins. *PLoS One* **10**, 1–14 (2015).
170. Khorana, H. G. Bacteriorhodopsin, a Membrane Protein That Uses Light to Translocate Protons. *J. Biol. Chem.* **263**, 7439–7442 (1988).
171. Friedrich, T. *et al.* Proteorhodopsin is a Light-driven Proton Pump with Variable Vectoriality. *J. Mol. Biol.* **321**, 821–838 (2002).
172. Dioumaev, A. K. *et al.* Proton transfers in the photochemical reaction cycle of proteorhodopsin. *Biochemistry* **41**, 5348–5358 (2002).
173. Lakatos, M. & Váró, G. The influence of water on the photochemical reaction cycle of proteorhodopsin at low and high pH. *J. Photochem. Photobiol. B Biol.* **73**, 177–182 (2004).
174. Balashov, S. P. *et al.* Xanthorhodopsin: A Proton Pump with a Light-Harvesting Carotenoid Antenna. *Science* **309**, 2061–2064 (2005).
175. Nakamura, S. *et al.* Photochemical characterization of actinorhodopsin and its functional existence in the natural host. *Biochim. Biophys. Acta - Bioenerg.* **1857**, 1900–1908 (2016).
176. Saita, M. *et al.* Photoexcitation of the $P_4^{480}$ State Induces a Secondary Photocycle That Potentially Desensitizes Channelrhodopsin-2. *J. Am. Chem. Soc.* **140**, 9899–9903 (2018).
177. Bruun, S. *et al.* The chromophore structure of the long-lived intermediate of the C128T channelrhodopsin-2 variant. *FEBS Lett.* **585**, 3998–4001 (2011).
178. Nydegger, M. W., Dutta, S. & Cheatum, C. M. Two-dimensional infrared study of 3-azidopyridine as a potential spectroscopic reporter of protonation state. *J. Chem. Phys.* **133**, (2010).
179. Dyall, L. K. & Kemp, J. E. The infrared spectra of aryl azides. *Aust. J. Chem.* **20**, 1395–1402 (1967).
180. Barth, A. Infrared spectroscopy of proteins. *Biochim. Biophys. Acta - Bioenerg.* **1767**, 1073–1101 (2007).
181. Krimm, S. & Bandekar, J. Vibrational spectroscopy and conformation of peptides, polypeptides, and proteins. *Adv. Protein Chem.* **38**, 181–364 (1986).
182. Barth, A. The infrared absorption of amino acid side chains. *Prog. Biophys. Mol. Biol.* **74**, 141–173 (2000).
183. Nie, B., Stutzman, J. & Xie, A. A Vibrational Spectral Maker for Probing the Hydrogen-Bonding Status of Protonated Asp and Glu Residues. *Biophys. J.* **88**, 2833–2847 (2005).
184. Smith, S. O. *et al.* Vibrational analysis of the all-*trans* retinal protonated Schiff base. *Biophys. J.* **47**, 653–664 (1985).
185. Hesse, M., Meier, H. & Zeeh, B. Spektroskopische Methoden in der organischen Chemie. *Georg Thieme Verlag Stuttgart* (2005).
186. Elgeti, M., Ritter, E. & Bartl, F. J. New Insights into Light-Induced Deactivation of Active Rhodopsin by SVD and Global Analysis of Time-

Resolved UV/Vis- and FTIR-Data. *Zeitschrift für Phys. Chemie* **222**, 1117–1129 (2008).
187. Henry, E. R. & Hofrichter, J. Singular Value Decomposition: Application to Analysis of Experimental Data. *Methods Enzymol.* **210**, 129–192 (1992).
188. Austin, R. H., Beeson, K., L, E., Frauenfelder, H. & I, G. Ligand binding to myoglobin. *Biochemistry* **14**, 5355–5373 (1975).
189. Krężel, A. & Bal, W. A formula for correlating pKa values determined in $D_2O$ and $H_2O$. *J. Inorg. Biochem.* **98**, 161–166 (2004).
190. Covington, A. K., Paabo, M., Robinson, R. A. & Bates, R. G. Use of the glass electrode in deuterium oxide and the relation between the standardized pD ($pa_D$) scale and the operational pH in heavy water. *Anal. Chem.* **40**, 700–706 (1968).
191. Aton, B., Doukas, A. G., Callender, R. H., Becher, B. & Ebrey, T. G. Resonance Raman studies of the purple membrane. *Biochemistry* **16**, 2995–2999 (1977).
192. Resler, T., Schultz, B.-J., Lórenz-Fonfría, V. A., Schlesinger, R. & Heberle, J. Kinetic and Vibrational Isotope Effects of Proton Transfer Reactions in Channelrhodopsin-2. *Biophys. J.* **109**, 287–297 (2015).
193. Wietek, J. *et al.* Anion-conducting channelrhodopsins with tuned spectra and modified kinetics engineered for optogenetic manipulation of behavior. *Sci. Rep.* **7**, 1–18 (2017).
194. Krause, B. S. Spektroskopische Charakterisierung der grün-absorbierenden Kanalrhodopsin-Chimäre ReaChR. Ph.D. dissertation. *Humboldt Univ.* (2017).
195. Ames, J. B. & Mathies, R. A. The Role of Back-Reactions and Proton Uptake during the N → O Transition in Bacteriorhodopsin's Photocycle: A Kinetic Resonance Raman Study. *Biochemistry* **29**, 7181–7190 (1990).
196. Eyring, G., Curry, B., Broek, A., Lugtenburg, J. & Mathies, R. Assignment and Interpretation of Hydrogen Out-of-Plane Vibrations in the Resonance Raman Spectra of Rhodopsin and Bathorhodopsin. *Biochemistry* **21**, 384–393 (1982).
197. Furutani, Y. *et al.* FTIR Spectroscopy of the K Photointermediate of *Neurospora* Rhodopsin: Structural Changes of the Retinal, Protein, and Water Molecules after Photoisomerization. *Biochemistry* **43**, 9636–9646 (2004).
198. Hashimoto, K., Choi, A. R., Furutani, Y., Jung, K. H. & Kandori, H. Low-temperature FTIR Study of *Gloeobacter* Rhodopsin: Presence of Strongly Hydrogen-Bonded Water and Long-Range Structural Protein Perturbation upon Retinal Photoisomerization. *Biochemistry* **49**, 3343–3350 (2010).
199. Rothschild, K. J., Roepe, P., Lugtenburg, J. & Pardoen, J. A. Fourier Transform Infrared Evidence for Schiff Base Alteration in the First Step of the Bacteriorhodopsin Photocycle. *Biochemistry* **23**, 6103–6109 (1984).
200. Wang, H. *et al.* Molecular determinants differentiating photocurrent properties of two channelrhodopsins from *Chlamydomonas*. *J. Biol. Chem.* **284**, 5685–5696 (2009).
201. Heyde, M. E., Gill, D., Kilponen, R. G. & Rimai, L. Raman Spectra of Schiff Bases of Retinal (Models of Visual Photoreceptors). *J. Am. Chem. Soc.* **93**, 6776–6780 (1971).
202. Maeda, A., Sasaki, J., Pfefferlé, J.-M., Shichida, Y. & Yoshizawa, T. Fourier transform infrared spectral studies on the Schiff base mode of all-*trans*

bacteriorhodopsin and its photointermediates, K and L. *Photochem. Photobiol.* **54**, 911–921 (1991).
203. Warshel, A. & Barboy, N. Energy Storage and Reaction Pathways in the First Step of the Vision Process. *J. Am. Chem. Soc.* **104**, 1469–1476 (1982).
204. Palings, I. *et al.* Assignment of Fingerprint Vibrations in the Resonance Raman Spectra of Rhodopsin, Isorhodopsin, and Bathorhodopsin: Implications for Chromophore Structure and Environment. *Biochemistry* **26**, 2544–2556 (1987).
205. Yan, E. C. Y. *et al.* Resonance Raman Analysis of the Mechanism of Energy Storage and Chromophore Distortion in the Primary Visual Photoproduct. *Biochemistry* **43**, 10867–10876 (2004).
206. Ringe, D. & Petsko, G. A. The 'glass transition' in protein dynamics: what it is, why it occurs, and how to exploit it. *Biophys. Chem.* **105**, 667–680 (2003).
207. Doster, W. The protein-solvent glass transition. *Biochim. Biophys. Acta - Proteins Proteomics* **1804**, 3–14 (2010).
208. Oh, K.-I., Lee, J.-H., Joo, C., Han, H. & Cho, M. *ß*-Azidoalanine as an IR Probe: Application to Amyloid A*ß*(16-22) Aggregation. *J. Phys. Chem. B* **112**, 10352–10357 (2008).
209. Ye, S., Huber, T., Vogel, R. & Sakmar, T. P. FTIR analysis of GPCR activation using azido probes. *Nat. Chem. Biol.* **5**, 397–399 (2009).
210. Ye, S. *et al.* Tracking G-protein-coupled receptor activation using genetically encoded infrared probes. *Nature* **464**, 1386–1389 (2010).
211. Farrar, M. R. *et al.* Solid State NMR Study of [ε-$^{13}$C]Lys-bacteriorhodopsin: Schiff Base Photoisomerization. *Biophys. J.* **65**, 310–315 (1993).
212. Oshima, K. *et al.* Characterization of photo-intermediates in the photo-reaction pathways of a bacteriorhodopsin Y185F mutant using *in situ* photo-irradiation solid-state NMR spectroscopy. *Photochem. Photobiol. Sci.* **14**, 1694–1702 (2015).
213. Oppermann, J. *et al.* MerMAIDs: a family of metagenomically discovered marine anion-conducting and intensely desensitizing channelrhodopsins. *Nat. Commun.* **10**, 3315–3327 (2019).
214. Huang, X. & Miller, W. A Time-Efficient, Linear-Space Local Similarity Algorithm. *Adv. Appl. Math.* **12**, 337–357 (1991).
215. Köhler, T., Weber, I., Glaubitz, C. & Wachtveitl, J. Proteorhodopsin Photocycle Kinetics Between pH 5 and pH 9. *Photochem. Photobiol.* **93**, 762–771 (2017).
216. Dioumaev, A. K., Wang, J. M., Bálint, Z., Váró, G. & Lanyi, J. K. Proton transport by proteorhodopsin requires that the retinal Schiff base counterion Asp-97 be anionic. *Biochemistry* **42**, 6582–6587 (2003).
217. Suydam, I. T. & Boxer, S. G. Vibrational Stark Effects Calibrate the Sensitivity of Vibrational Probes for Electric Fields in Proteins. *Biochemistry* **42**, 12050–12055 (2003).
218. Silverman, L. N., Pitzer, M. E., Ankomah, P. O., Boxer, S. G. & Fenlon, E. E. Vibrational Stark Effect Probes for Nucleic Acids. *J. Phys. Chem. B* **111**, 11611–11613 (2007).
219. Eisenhauer, K. *et al.* In Channelrhodopsin-2 Glu-90 Is Crucial for Ion Selectivity and Is Deprotonated during the Photocycle. *J. Biol. Chem.* **287**, 6904–6911 (2012).
220. Tavan, P., Schulten, K. & Oesterhelt, D. The Effect of Protonation and Electrical Interactions on the Stereochemistry of Retinal Schiff Bases.

*Biophys. J.* **47**, 415–430 (1985).
221. Nogly, P. *et al.* Retinal isomerization in bacteriorhodopsin captured by a femtosecond x-ray laser. *Science* **361**, 1–15 (2018).
222. Sobotta, C., Braun, M., Tittor, J., Oesterhelt, D. & Zinth, W. Influence of the Charge at D85 on the Initial Steps in the Photocycle of Bacteriorhodopsin. *Biophys. J.* **97**, 267–276 (2009).
223. Struts, A. V. *et al.* Structural Analysis and Dynamics of Retinal Chromophore in Dark and Meta I States of Rhodopsin from $^{2}$H NMR of Aligned Membranes. *J. Mol. Biol.* **372**, 50–66 (2007).
224. Bousché, O. *et al.* Vibrational Spectroscopy of Bacteriorhodopsin Mutants. *J. Biol. Chem.* **266**, 11063–11067 (1991).
225. Saint Clair, E. C., Ogren, J. I., Mamaev, S., Kralj, J. M. & Rothschild, K. J. Conformational changes in the archaerhodopsin-3 proton pump: detection of conserved strongly hydrogen bonded water networks. *J. Biol. Phys.* **38**, 153–168 (2012).
226. Lin, J. Y. A user's guide to channelrhodopsin variants: features, limitations and future developments. *Exp. Physiol.* **96**, 19–25 (2011).
227. Sievers, F. *et al.* Fast, scalable generation of high-quality protein multiple sequence alignments using Clustal Omega. *Mol. Syst. Biol.* **7**, 1–6 (2011).

# 6 Appendix

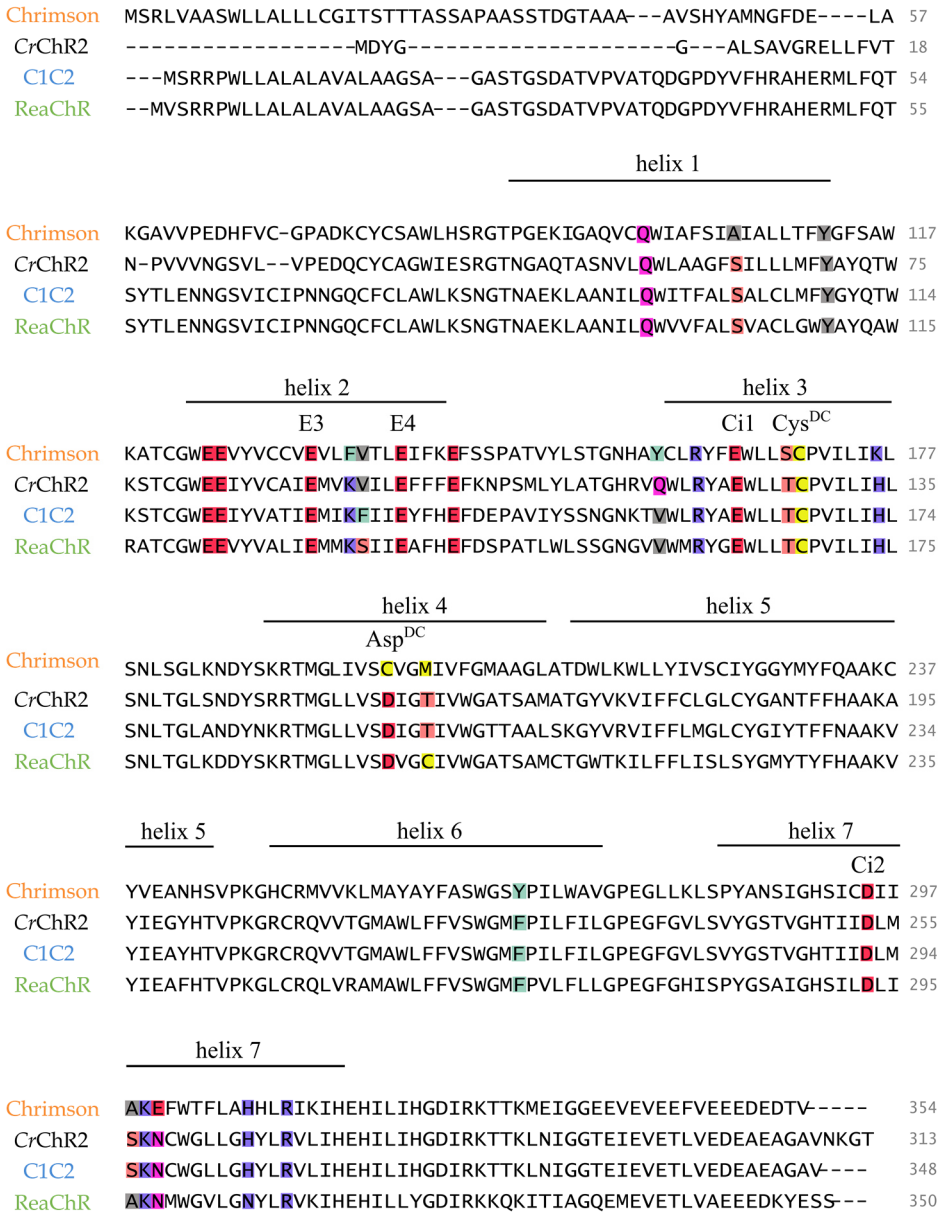


**Fig. S1** Multiple sequence alignment of several ChR sequences performed with Clustal Omega.[227] Residues discussed in this thesis are highlighted and the residues that were investigated are labelled *above the line*. Assignment of helices is according to the C1C2 crystal structure (3UG9).

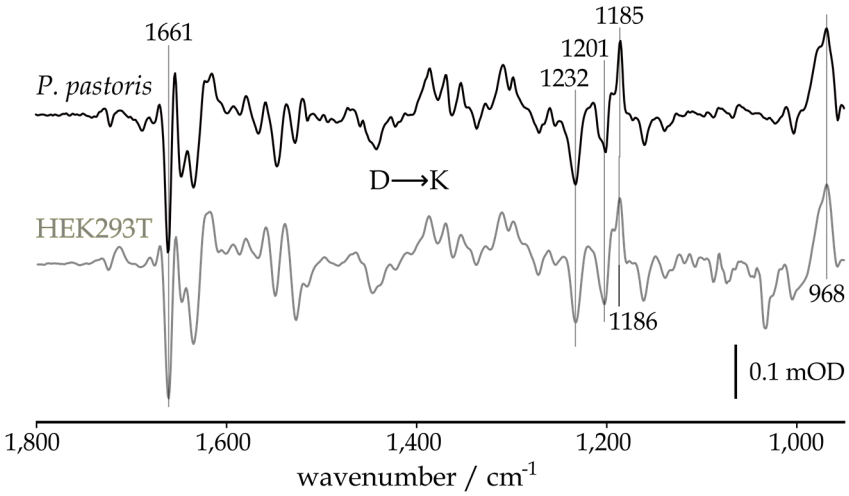


**Fig. S2** FTIR light – dark difference spectra of ReaChR wild type expressed in *P. pastoris* and HEK293T cells at pH 7.4 and 150 K. Illumination was conducted with green LEDs ($\lambda_{max}$ ~ 529 nm) following ≥ 30 min in the dark at ≥ 293 K. Spectra were scaled to retinal fingerprint bands in the spectrum of ReaChR from HEK293T cells.

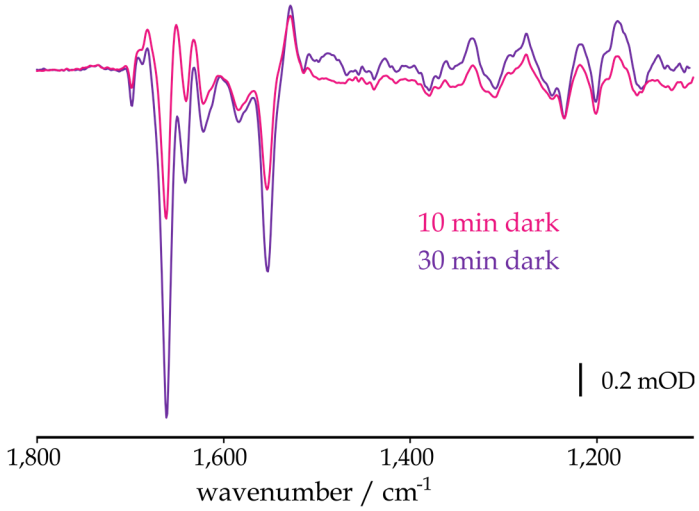


**Fig. S3** FTIR light – dark difference spectra of the Asp$^{DC}$ mutant D195N at 293 K following 10 min and 30 min in the dark, respectively. Illumination was conducted with blue LEDs ($\lambda_{max}$ ~ 471 nm). Spectra were scaled to retinal fingerprint bands in the difference spectrum obtained after 10 min in the dark.

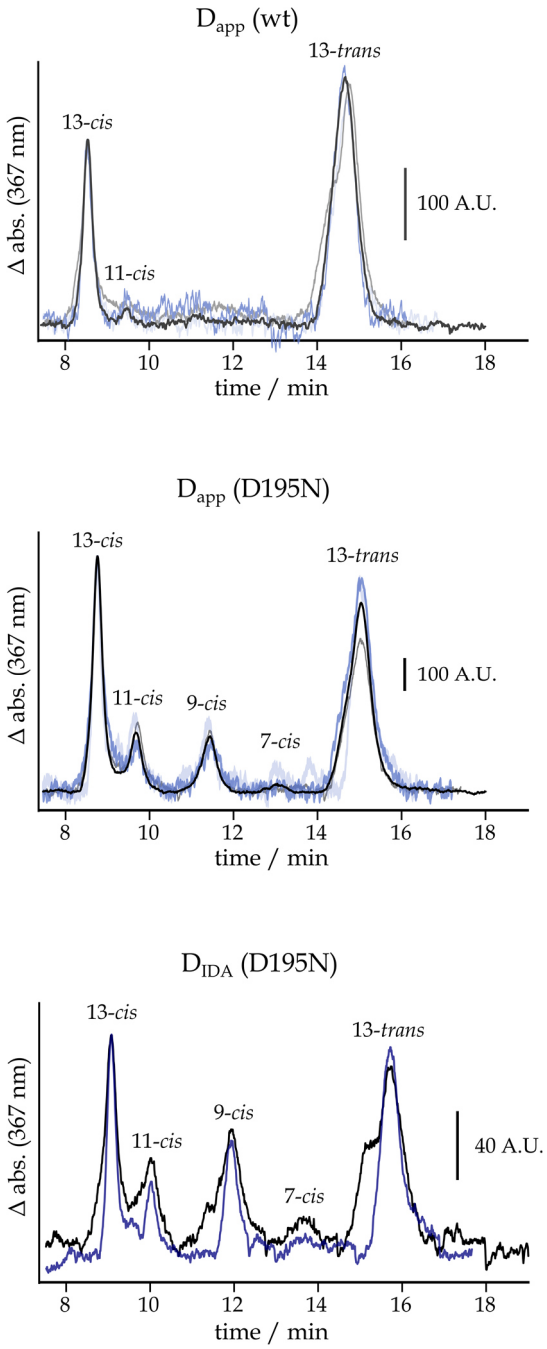


**Fig. S4** HPLC chromatograms of C1C2 wild type and the D195N mutant. Protocol to obtain $D_{app}$: 10 min blue illumination ($\lambda_{max}$ ~ 471 nm), 30 min dark. Protocol to obtain $D_{IDA}$: 10 min blue illumination ($\lambda_{max}$ ~ 471 nm), overnight in the dark. Chromatograms were baseline-corrected and scaled to the maximum intensity of the 13-*cis* band of the *black* chromatogram.

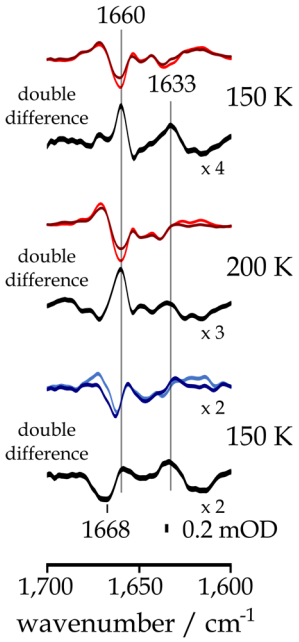


**Fig. S5** The amide I region of light – dark difference spectra of ReaChR wt at pH 5 and 9 recorded during (*light lines*) and after (*dark lines*) illumination with green LEDs and the respective double difference spectra (*black lines*, relaxed state– illuminated state).

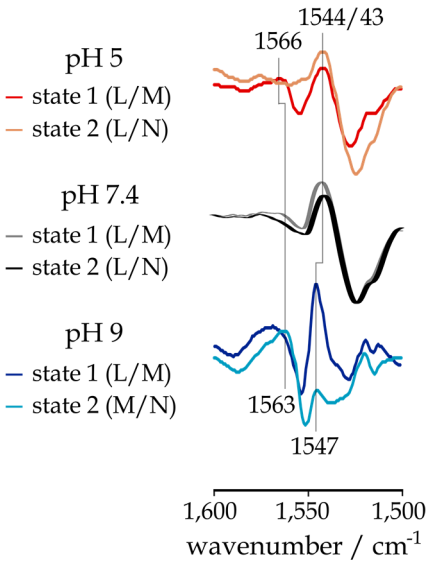


**Fig. S6** The υ(C=C) region of FTIR light – dark difference spectra of ReaChR wild type at pH 5, 7.4 and 9. Illumination was conducted with green LEDs ($\lambda_{max}$ ~ 529 nm) following ≥ 30 min in the dark at ≥ 293 K. Spectra were scaled to retinal fingerprint bands in the state 1 difference spectrum at pH 9 (see Fig. 3-16, p. 75).

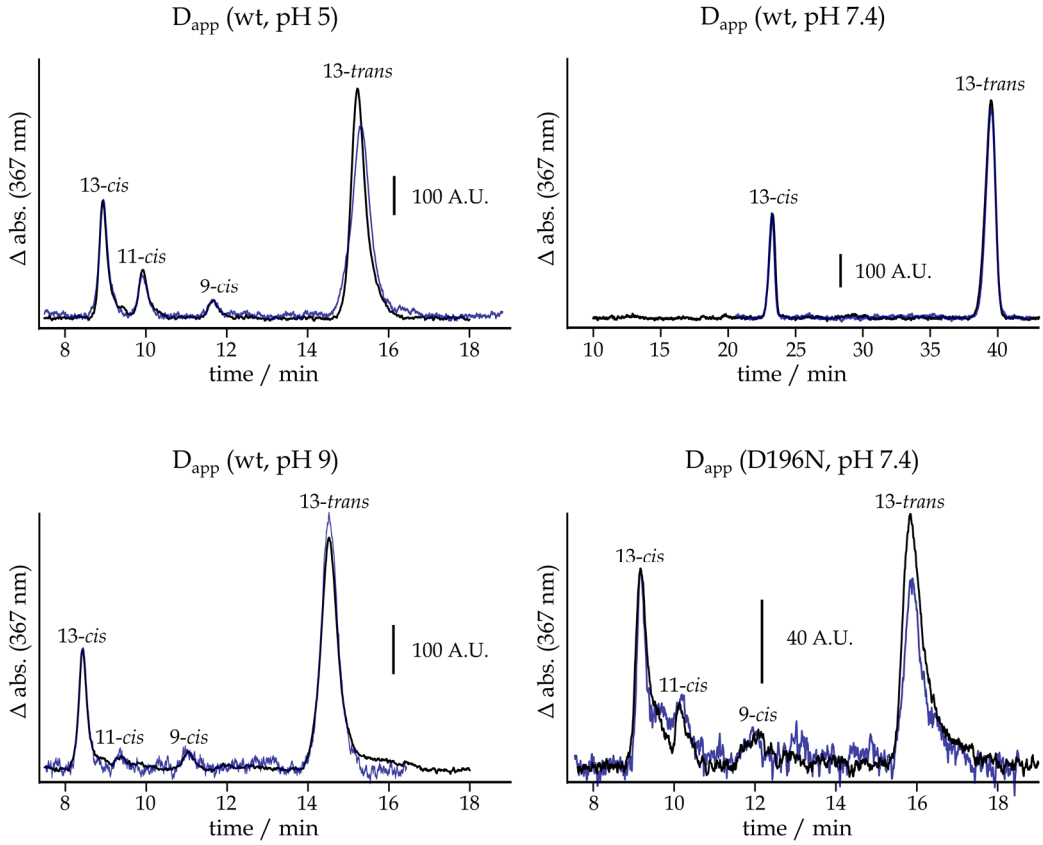


**Fig. S7** HPLC chromatograms of ReaChR wild type and the D196N mutant. Protocol to obtain $D_{app}$: 10 min green illumination ($\lambda_{max}$ ~ 529 nm), 30 min dark. In the case of the wild type at pH 7.4 only 10 min dark. Chromatograms were baseline-corrected and scaled to the maximum intensity of the 13-*cis* band of the *black* chromatogram.

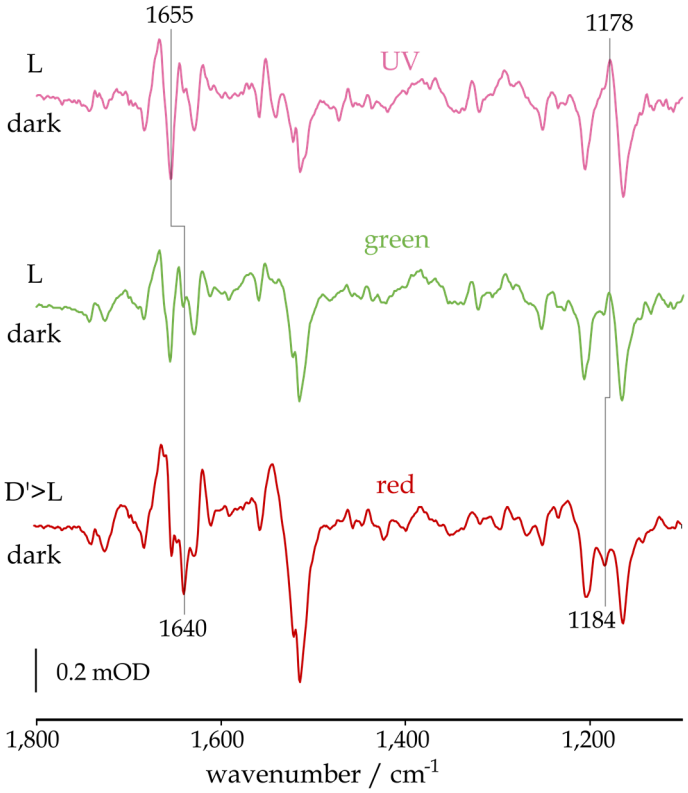


**Fig. S8** Light – dark FTIR difference spectra of Chrimson-wt at pH 5 recorded at 240 K. Illumination with both green ($\lambda_{max}$ ~ 523 nm) and UV ($\lambda_{max}$ ~ 405 nm) LEDs following ≥ 5 min in the dark at ≥ 293 K mainly yields the proton-conducting L state (*upper* and *central spectrum*), while extended illumination with red light ($\lambda_{max}$ ~ 633 nm) mainly induces the non-conducting long lived D′ intermediate (*lower spectrum*). Spectra were scaled to retinal fingerprint bands in the difference spectrum obtained with red illumination.

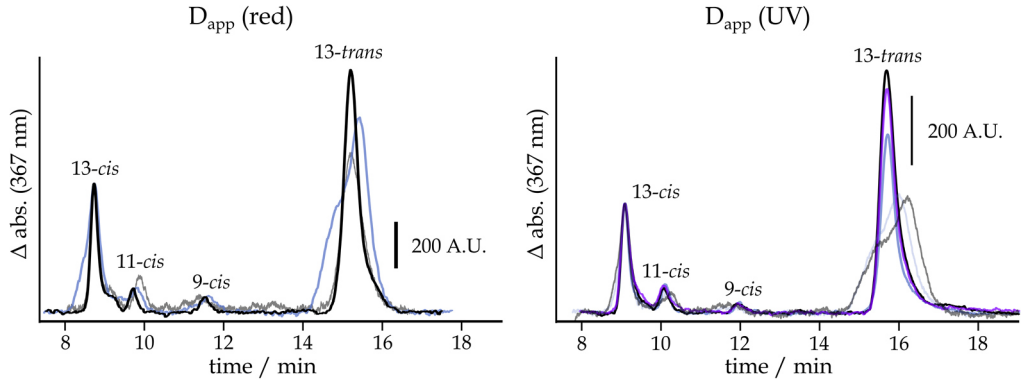


**Fig. S9** HPLC chromatograms of Chrimson after red ($\lambda_{max}$ ~ 633 nm) and UV ($\lambda_{max}$ ~ 405 nm) illumination, respectively. Protocol to obtain $D_{app}$: 1 min illumination, 5 min dark. Chromatograms were baseline-corrected and scaled to the maximum intensity of the 13-*cis* band of the *black* chromatogram.

# 7 Danksagung

Meine zurückliegenden Jahre waren geprägt von der Arbeit, die hier nun in Teilen niedergeschrieben ist. Ich habe Frustierendes und Erfreuliches durchlebt; vor allem aber habe ich über die Jahre eine große Freude entwickelt, mich dem Verstehen der Dinge anzunähern und – vielleicht noch wichtiger – die Grenzen meines Verständnisvermögens auszuloten. Widersprüchlichkeiten, Uneindeutigkeiten, Nuancen, ja, die Unzulänglichkeit des eigenen Verstandes zu erkennen und als unabdingbares Prinzip des Lebens wie des Forschens hinzunehmen, ist von großer Bedeutung. Ferner einzusehen, dass in das Wesen der Dinge zu dringen, zuallererst an sich von Wert ist, weil es Verbindung schafft und Vergnügen bereitet. Obwohl unsere zivilisatorische Fassade dieser Zeit Risse zeigt und gleichsam die herbeigesehnten Werte von Menschlichkeit zu zerreißen drohen, gelingt es unserer Gesellschaft noch, Verstehen zu ermöglichen, können sich Menschen ohne allzu großen ökonomischen Druck dem wunderbaren Irrsinn der reinen Wissenschaft widmen. Für das große Privileg, dass ich in den letzten Jahren mit großer persönlicher Freiheit dem Wunsch nach Verstehen nachgehen konnte, möchte ich mich bedanken; ich danke der so unfertigen, zart gebauten Gesellschaft, die mir dieses Privileg eingeräumt hat, welches so vielen verwehrt bleibt.

Die persönliche Freiheit, die es mir erlaubte, meinen eigenen Weg des Verstehens zu suchen, ist keine Selbstverständlichkeit in der Wissenschaft, obschon sie vielleicht ihre Voraussetzung ist. Prof. Dr. Franz Bartl hat mir stets vertrauensvoll große Freiheiten eingeräumt und ein Arbeitsumfeld mit flacher Hierarchie geschaffen, wofür ich ihm großen Dank und Respekt aussprechen möchte. Ferner möchte ich mich für die vielen wissenschaftlichen Diskussionen bedanken, in diesem Zusammenhang auch bei unserem Kooperationspartner Prof. Dr. Peter Hegemann, insbesondere für die kritische Auseinandersetzung mit den Erzeugnissen meiner Arbeit. Herzlich danken möchte ich auch Prof. Dr. Peter Hildebrandt für seine Bereitschaft, als externer Gutachter zu fungieren, sowie Prof. Dr. Enrico Klotzsch und Prof. Dr. Holger Dobbek für ihre Teilnahme an der Prüfungskommission.

Ferner möchte ich meinen langjährigen Kollegen danken, von denen einige noch an unsere Arbeitsgruppe gebunden und andere schon weitergezogen sind; ich danke Dr. Eglof Ritter, Dr. Patrick Piwowarski, Paul Fischer, Dr. Roman Kazmin, Żaneta Nogacz und Anna Digilova für die gute kollegiale Athmosphäre und die gegenseitige Unterstützung im wissenschaftlichen Alltag und darüber hinaus. Dr. Eglof Ritter gilt ferner besonderer Dank für die Bereitstellung seiner „spoc"-Software, ohne welche die Datenauswertung ein weitaus schwierigeres Unterfangen gewesen wäre, sowie für die stetige Unterstützung bei technischen oder interpretatorischen Fragen. Paul Fischer und Dr. Patrick Piwowarski möchte ich danken für ihren immensen Einsatz beim Aufbau des neuen Spektrometers, das ich bereits zum Aufnehmen neuer Daten nutzen konnte. Es darf an dieser Stelle nicht verschwiegen werden, dass ich auch unsere lebhaften und wertvollen Nebengespräche besonders schätze.

Beim Anfertigen der veröffentlichten und geplanten Publikationen habe ich mit einigen Menschen kooperiert, denen ich großen Dank aussprechen möchte für die konstruktive Zusammenarbeit: Dr. Benjamin Krause, Dr. Christiane Grimm, Johannes Vierock und Dr. Katja Stehfest. Besonders hervorzuheben ist Dr. Benjamin Krause, mit dem viele Projekte realisiert werden konnten und auf dessen freundliche und kompetente Arbeitsweise stets Verlass war. Für die Bereitstellung von Proteinproben geht außerdem mein Dank an Brian Bauer, Anja Koch, Thi Bich Thao Nguyen und Christina Schnick. In Anbetracht dessen, dass die dieser Arbeit zugrundeliegende experimentelle Arbeit fast ausschließlich am Institut für Medizinische Physik und Biophysik der Charité angefertigt wurde, möchte ich allen Mitarbeiterinnen und Mitarbeitern des Instituts für die gute Arbeitsathmosphäre danken. Neben Brian Bauer und Anja Koch möchte ich Birgit Schroeer hervorheben, die mich bei allgemeinen Fragen zur Laborarbeit immerzu auf ihre freundliche Art unterstützt hat. Außerdem danke ich Julius Naujoks für die Einarbeitung in die HPLC-Methode auf seine kompetente und überaus hilfsbereite Weise. Dr. Ciara Lally danke ich für das Überprüfen meines Ausdrucksvermögens im Englischen.

Es ist nicht unüblich, Dissertationen einzelnen geliebten Menschen zu widmen. Ich habe mich gegen eine solche persönliche Widmung entschieden, weil ich mich so vieler geliebter Menschen in meinem Umfeld erfreue, dass eine Auswahl schwerfiele. Daher ein paar allgemeinere Worte: Danke für eure Zuneigung, euer Verständnis und eure tatkräftige Unterstützung in schwierigen Zeiten. Seid euch meiner Liebe und Verbundenheit gewiss! Besonders hervorheben möchte ich meine Eltern, die mir auf ihre besondere Weise immer das Gefühl gegeben haben und geben, nichts werden zu müssen, da ich schon bin. Ferner möchte ich meiner Freundin Nadia für ihre Herzlichkeit und Fürsorglichkeit danken, mit der sie in den letzten Jahren meinen Weg begleitet hat.

Bei alledem bleibt die vage und doch so tiefe Einsicht, dass dem Vergehen aller akademischen und sonstigen Belohnungen dieser Welt eine göttliche Verbundenheit trotzen wird, die alles eint.

# Eigenständigkeitserklärung

Hiermit erkläre ich, dass ich die vorliegende Dissertationsschrift eigenständig und alleinig unter Zuhilfenahme der angegebenen Quellen, Mitteilungen und Hilfsmitteln angefertigt habe.

Berlin, den 14. August 2019

Joel Kaufmann